A Climatology and Synoptic-Dynamic Basis for Distinguishing Cool-Season Precipitation Events at St. John's, Newfoundland

Shawn M. Milrad

Doctor of Philosophy

Department of Atmospheric and Oceanic Sciences

McGill University

Montreal, Quebec, Canada

January 2010

A thesis submitted to the Faculty of Graduate Studies and Research in partial fulfillment of the requirements for the degree of Doctor of Philosophy

© Shawn M. Milrad 2010

Abstract

For St. John's, Newfoundland, at the confluence of several North American storm tracks, we identify synoptic-scale characteristics and precursors of various classes of cool-season precipitation events.

Such events, based upon a climatology for 1979-2005, are separated into three categories based on precipitation amount. We find that the storm systems responsible for extreme precipitation events originate farther south and east than corresponding features in moderate and light events. A wind climatology shows that extreme precipitation events at St. John's are characterized almost exclusively by easterly surface and 925 hPa geostrophic winds, and that both the surface and 925 hPa geostrophic winds rotate clockwise with decreasing precipitation amount.

Focusing on extreme events, we utilize two methods of manual synoptic typing to further partition events. The first method uses backward air parcel trajectories to separate events by air parcel source region. One subset of events ("west") is characterized by strong upper-level dynamics and high precipitable water values in the central United States, which helps to produce a strong cyclone upon reaching the Atlantic Ocean; this is not seen for "west" events outside the extreme category. The second method of synoptic typing utilizes time series of three ascent-forcing quasi-geostrophic (QG) variables. While most events are characterized by a strong upstream sea-level cyclone originating from the Gulf of

Mexico ("cyclone"), a subset are dominated by strong low-level frontogenesis, in the absence of a substantial upstream cyclone ("frontal").

Finally, a dynamic and thermodynamic analysis, and forecast model evaluation is completed for consecutive extreme events in December 2008, which produced over 125 mm of precipitation over six days. The first event is a "cyclone", and is marked by strong QG forcing for ascent in the presence of low static stability and high values of subtropical moisture. The second event is a "frontal" event, and is associated with a persistent quasi-stationary baroclinic zone in the presence of moderately stable air and large values of low-level frontogenesis, in the absence of substantial temperature and vorticity advection. These two events highlight rather disparate means by which an extreme precipitation event can occur at St. John's.

Résumé

Pour St. John's, Terre-Neuve, à la confluence de plusieurs trajectoires de tempêtes nord-américaines, nous identifions des caractéristiques à l'échelle synoptique et des précurseurs d'une variété de type d'événements de précipitation de la saison froide.

Ces événements, basés sur une climatologie allant de 1979-2005, sont séparés en trois catégories basées sur la quantité de précipitation. Nous trouvons que les systèmes de tempêtes responsables des événements de précipitation extrêmes débutent plus au sud et à l'est que les événements correspondants avec précipitation modérée ou faible. Une climatologie des vents montre que les événements de précipitation extrêmes à St. John's sont caractérisés presque exclusivement par des vents de surface et géostrophique à 925 hPa provenant de l'est, et tournant dans le sens des aiguilles d'une montre avec une diminution de la quantité de précipitation.

En se concentrant sur les événements extrêmes, nous utilisons deux méthodes de classification synoptique manuelle pour séparer davantage les événements. La première méthode utilise une trajectoire renversée des parcelles d'air pour séparer les événements en fonction de leur région d'origine. Un sousensemble des événements ("ouest") est caractérisé par une forte dynamique dans les niveaux supérieurs et des valeurs d'eau précipitable élevées dans le centre des États-Unis, ce qui aide à produire un puissant cyclone lorsque l'océan Atlantique

est atteint; ceci n'est pas observé pour les événements "ouest" en dehors de la catégorie des extrêmes. La seconde méthode utilise des séries temporelles de trois variables quasi-géostrophiques (QG) forçant l'ascension. Bien que la plupart des événements sont caractérisés par un puissant cyclone au niveau de la mer en amont qui origine du Golfe du Mexique ("cyclone"), un sous-ensemble est dominé par une forte frontogenèse dans les niveaux inférieurs, en l'absence substantielle de cyclone en amont ("frontal").

Finalement, une analyse dynamique et thermodynamique, ainsi qu'une évaluation de modèle de prévision est complétée pour des événements extrêmes consécutifs en décembre 2008, qui produisent plus de 125 mm de précipitation sur une période de six jours. Le premier événement est du type "cyclone", et est marqué par un puissant forçage QG d'ascension en présence de faible stabilité statique et de hautes valeurs d'humidité subtropicale. Le deuxième événement est de type "frontal", et est associé à une zone barocline persistante d'air modérément stable et de hautes valeurs de frontogenèse dans les niveaux inférieurs en absence d'advection de température et de vorticité substantielle. Ces deux événements mettent en valeur des manières plutôt différentes par lesquelles un événement de précipitation extrême peut se produire à St. John's.

Contributions of Authors

Chapters 2 and 3 of this thesis consist of articles published in the peer-reivewed journal *Weather and Forecasting*. Chapter 4 is a manuscript that has been submitted for publication in *Weather and Forecasting*. As the lead author for each of the three articles, the candidate is responsible for the overwhelming majority of research and content presented therein. Dr. John R. Gyakum and Dr. Eyad H. Atallah are co-authors on all three papers and assisted in the editing of the manuscripts and in the organization of the project, as is expected of their supervisory stature.

Statement of Originality

The contributions of this dissertation to original knowledge are as follows:

- It is established that Atlantic Canada, and more specifically St. John's,
 Newfoundland, is prone to frequent and extreme precipitation events,
 particularly in the cool season. This is due at least in part to its location at the confluence of several North American storm tracks and two contrasting ocean currents. Consequently, a cool-season precipitation event climatology is established for 1979-2005.
- Statistically significant, precursor synoptic-scale signals are identified and contrasted for extreme, moderate, and light events, respectively, at times up to 72 hours prior to the onset of the heaviest precipitation at St. John's.
- Composite synoptic analyses indicate that the storm systems responsible for extreme precipitation events originate farther south and east than corresponding features in moderate and light events.
- It is established that downstream development due to Rossby wave propagation, associated with the aforementioned synoptic-scale precursors, is more prevalent in the extreme and moderate cases than in the light cases. This contributes to the intensity of the precipitation-causing storm system (i.e. cyclone) at St. John's. It is believed that the main difference between the extreme and moderate composites is in storm

track and moisture source region, and not in intensity of synoptic-scale features.

- A wind climatology is developed for St. John's, for both the near-surface (925 hPa) geostrophic and 10 m observed winds. Extreme events are characterized almost exclusively by easterly winds, which in the overall climatology is the least favored wind direction at St. John's. In addition, it is found that there is a clockwise rotation of both the 925 hPa geostrophic and 10 m observed winds with decreasing precipitation amount.
- Two methodologies of manual synoptic typing are used to further partition the fifty median cases in each precipitation event intensity category, with a focus on the extreme events. The second methodology develops a new classification system that partitions events using time series of three dynamically and operationally relevant quasi-geostrophic (QG) forcing parameters and establishes two types (cyclone and frontal).
- Composite plots are created for all synoptic types and are used to show the disparate dynamic and thermodynamic structures responsible for an extreme precipitation event at St. John's. Using the first methodology, it is found, among other results, that extreme cases of west trajectory events contain a precursor signal of anomalously high precipitable water values in the central United States. Using the second methodology, it is found, among other results, that cyclone events are associated with a rapidly intensifying sea-level cyclone and associated upper-level trough, while frontal events are marked by a downstream sea-level anticyclone and

- associated upper-level ridge. Frontal events are also associated with a quasi-stationary baroclinic zone situated near St. John's and occur in a substantially more benign synoptic-scale environment.
- Case studies are completed for consecutive extreme precipitation events at St. John's in December 2008. Among other results, it is found that the two events are produced by entirely different synoptic structures and ascent-forcing mechanisms, in the presence of low static stability and high values of subtropical moisture.
- with respect to the aforementioned case studies, an assessment of two independent operational forecasts is performed using 1) the National Centers for Environmental Prediction (NCEP) Global Forecast System (GFS) half-degree model forecasts and 2) the operational forecasts issued for St. John's by Environment Canada as a proxy for the Environment Canada Global Environment Multiscale (GEM) model forecasts. Among other results, it is found that both models underforecast the precipitable water and precipitation at St. John's at all but the shortest lead times (e.g. 12-24 hours), particularly with respect to the first event. This is due to a combination of inaccurate representation of synoptic-scale features, both in intensity and position, as well as poor handling of diabatic impacts of precipitation during the early stages of each event. This latter point is particularly evident in the first case.

Acknowledgments

There are numerous people who have greatly contributed to the completion of this thesis and to whom I am deeply indebted to.

First, to my supervisor, Dr. John Gyakum, many thanks are due for his guidance, meteorological knowledge, patience, and unrelenting belief in my abilities to complete this work. Our weekly group meetings, numerous individual meetings, and regular weather discussions have given me insights into my work that I would not otherwise have had. In particular, I greatly appreciate his support during the early years of this process when things did not always look so rosy.

Secondly, to my co-author, officemate and good friend, Dr. Eyad Atallah, many thanks for countless pearls of meteorological wisdom, programming and technical advice, paper editing, extraordinary patience, and friendship that he has provided throughout my 6+ years at McGill.

Thanks to all the students, collaborators, and post-doctorate fellows who have been part of Dr. John Gyakum's synoptic group during my time at McGill, for listening to my presentations, providing me with ideas and constructive criticism, and for all of their support during this process. A special note of thanks is due to St. John's, Newfoundland, for being such a great place for extreme weather.

Many other people have been influential and important to me during my time at McGill, including all the great friends I have made in the past six years. Special thanks are due to Clare Salustro and Briana Gordon, for providing friendship and guidance along the way, in times both good and bad, despite living far from Montreal.

Last, but by no means least, thanks to the people closest to me, including my parents Jan West and Martin Milrad, and my brother Jared Milrad, all of whom believed in my abilities from the beginning and continue to do so. Finally, but most importantly, thanks to my girlfriend Jennifer Smith, whose love, friendship, patience, belief, and understanding has helped bring me to this point, and without whom I would not have been able to accomplish all of this.

This research has been funded by grants from the Natural Sciences and Engineering Research Council of Canada and the Canadian Foundation for Climate and Atmospheric Sciences. Thanks to the National Centers for Environmental Prediction (NCEP) and the National Climatic Data Center (NCDC) for providing access to the Global Forecast System (GFS) analyses, North American Regional Reanalysis (NARR), and National Centers for Environmental Prediction (NCEP) Global Reanalysis. Finally, thanks to Gerard Morin at the Atlantic Climate Centre of Environment Canada for providing the six hourly precipitation data and the Holyrood, Newfoundland radar imagery.

Contents

Ab	stract	t		i
Re	sumé			iii
Co	ntrib	utions o	f Authors	v
Sta	ateme	nt of Or	riginality	vi
Ac	know	ledgmei	nts	ix
Co	ontent	s		xi
Lis	st of F	igures		xvii
Lis	st of T	ables		xxvi
1	Intr	oductio	n	1
	1.1	Motiv	ation	1
		1.1.1	Quantitative Precipitation Forecasting (QPF)	1
		1.1.2	Atlantic Canada	4
		1.1.3	Extreme Precipitation Events	6
	1.2	Object	tives and Manuscript Outline	9
2	Clin	natology	and Synoptic-Scale Characteristics of Cool-	
	Seas	son Prec	cipitation Events at St. John's, Newfoundland, 1979-200	05 17

2.1	Introdu	iction		20
	2.1.1	Motivati	on	20
	2.1.2	Objectiv	es and Methodology	22
2.2	Data			24
2.3	Precip	itation Cli	matology	25
2.4	Compo	osite Resu	lts	27
	2.4.1	Methodo	ology	28
	2.4.2	Sea-leve	l Pressure (SLP)	29
		2.4.2.1	Extreme Precipitation Cases	29
		2.4.2.2	Moderate Precipitation Cases	30
		2.4.2.3	Light Precipitation Cases	30
	2.4.3	500 hPa	Height	31
		2.4.3.1	Extreme Precipitation Cases	31
		2.4.3.2	Moderate Precipitation Cases	33
		2.4.3.3	Light Precipitation Cases	34
	2.4.4	Precipita	able Water	36
		2.4.3.1	Extreme Precipitation Cases	36

			2.4.3.2 Moderate Precipitation Cases	36
			2.4.3.3 Light Precipitation Cases	37
	2.5	Wind A	Analysis	38
		2.5.1	Background and Climatology	38
		2.5.2	Wind Roses during Precipitation Events	39
	2.6	Conclu	Iding Discussion and Future Work	41
3	Syno	ptic Ty _l	ping of Extreme Cool-Season Precipitation Events at St.	
	John	's, New	foundland, 1979-2005	70
	3.1	Introdu	action	73
	3.2	Method	dology and Data	75
		3.2.1	Methodology	75
			3.2.1.1 Backward Trajectory Analysis	75
			3.2.1.2 Quasi-Geostrophic Forcing	77
		3.2.2	Data	79
	3.3	Synopt	ic Typing I: Backward Trajectory Analysis	80
		3.3.1	Partitioning Methodology	80
		3.3.2	Composite Results	81

			3.3.2.1	South Trajectory Composites	82
			3.3.2.2	Southwest Trajectory Composites	84
			3.3.2.3	West Trajectory Composites	86
	3.4	Synopt	tic Typing	II: Using Quasi-Geostrophic Forcing Parameters	88
		3.4.1	Partition	ing Methodology	88
		3.4.2	Composi	ite Results	91
			3.4.2.1	Cyclone Composites	91
			3.4.2.2	Frontal Composites	92
	3.5	Conclu	ıding Disc	ussion and Future Work	94
4	A Di	agnostic	e Examina	ation of Consecutive Extreme Cool-Season	
	Prec	ipitatio	n Events a	at St. John's, Newfoundland in December 2008	128
	4.1	Introdu	action		132
	4.2	Data a	nd Method	dology	136
		4.2.1	Data		136
		4.2.2	Methodo	ology	138
	4.3	MAG	1: Decem	ber 8 th , 2008	139
		4.3.1	Overviev	w and Synoptic Typing	139

		4.3.2 Synoptic-Dynamic Analysis
	4.4	MAG 2: December 11 th , 2008
		4.4.1 Overview and Synoptic Typing
		4.4.2 Synoptic-Dynamic Analysis
	4.5	Concluding Discussion and Future Work
5	Eval	luation of Two Independent Operational Forecasts during
	Con	secutive Extreme Cool-Season Precipitation Events at St. John's,
	New	foundland in December 2008 182
	5.1	Introduction
	5.2	Forecasts for MAG 1
		5.2.1 GFS Half-Degree Model Forecasts
		5.2.2 Environment Canada Operational Forecasts
	5.3	Forecasts for MAG 2
		5.3.1 GFS Half-Degree Model Forecasts
		5.3.2 Environment Canada Operational Forecasts
	5.4	Summary and Discussion
6	Sum	amary, Discussion, and Future Research 215

6.1	Climatology and Synoptic-Scale Characteristics of Cool-Season
	Precipitation Events at St. John's, Newfoundland, 1979-2005 215
6.2	Synoptic Typing of Extreme Cool-Season Precipitation Events at St.
	John's, Newfoundland, 1979-2005
6.3	A Diagnostic Examination of Consecutive Extreme Cool-Season
	Precipitation Events at St. John's, Newfoundland in December 2008
6.4	Evaluation of Two Independent Operational Forecasts during
	Consecutive Extreme Cool-Season Precipitation Events at St. John's,
	Newfoundland in December 2008
6.5	General Conclusions
66	Future Research Directions 228

List of Figures

1.1	From Fritsch and Carbone (2004): Annual threat scores for the National Oceanic Atmospheric Administration (NOAA) Hydrometeorological Prediction Center (HPC) for 24-h forecasts of ≥ 1.00 in. or more of precipitation, showing that QPF improves over the fifty year period of 1961-2001
1.2	From Olson et al. (1995): Monthly threat scores for 24-h forecasts of \geq 1.00 in. or more of precipitation, for 1991-1994 comparing day one and day two subjective human forecasts issued by the NOAA Forecast Bureau (FB) with the Regional Area Forecast System (RAFS) model used operationally in the U.S. in the early 1990's
1.3	From Reynolds (2003): Human forecast improvement (bars) in percent versus the main National Centers for Environmental Prediction (NCEP) operational forecast models from 1993-2001
1.4	From the British Society for Geomorphology (2009): A schematic of ocean currents that impact Atlantic Canada, in particular the confluence of the cold Labrador and warm Gulf Stream current near the coast of Newfoundland and Labrador
2.1	The geography of Atlantic Canada, with the capital city of each province identified, and scale as shown
2.2	October-April 30-year (1971-2000) climatological frequency of 500 hPa absolute vorticity centers, calculated by counting the number of absolute vorticity maxima in the region shown; this roughly depicts the mean North American storm tracks and their importance to Atlantic Canada. The units are number of events per 5 degree by 5 degree area (approximately 500 sq. km) and calculations are completed using the NCEP global reanalysis. 51
2.3	The precipitation event distribution histogram, depicting bins every 5 mm, and with the median of each precipitation category indicated 52
2.4	Sea-level pressure (SLP) anomalies every 2 hPa, heavy dashed for negative values and heavy solid for positive values, with respect to climatology, for the extreme cases at (a) -48, (b) -36, (c) -24, (d) -12, (e) 0, and (f) +12 h. Light solid contours represent full composite SLP field, every 4 hPa. Shading represents statistical significance of the anomalies at the 95% (darker shading) and 99% (lighter shading) confidence levels, according to the Student's <i>t</i> test. All fields are derived from the NCEP global reanalysis

2.5	As in Fig. 2.4, but for the moderate cases
2.6	As in Fig. 2.4, but for the light cases
2.7	500 hPa height anomalies every 3 dam, heavy dashed for negative values and heavy solid for positive values, with respect to climatology for the composite of the extreme cases at (a) -72, (b) -60, (c) -48, (d) -36, (e) -24, (f) -12, (g) 0, (h) +12, and (i) +24 h. Light solid contours represent full composite 500 hPa field, every 6 dam. Shading represents statistical significance of the anomalies at the 95% (lighter shading) and 99% (darker shading) confidence levels, according to the Student's <i>t</i> test. All fields are derived from the NCEP global reanalysis
2.8	Time-longitude plot of the 500 hPa meridional (v) component of the wind anomalies relative to climatology at latitude 40° North (every 3 m s ⁻¹ , shaded warm colors for positive and cool colors for negative) for the extreme cases from t=-72 h to t=+24 h. All fields are derived from the NCEP global reanalysis.
2.9	As in Fig. 2.7, but for the moderate cases
2.10	As in Fig. 2.8, but at latitiude 45° and for the moderate cases 59
2.11	As in Fig. 2.7, but for the light cases
2.12	As in Fig. 2.8, but at latitiude 45° and for the light cases 61
2.13	Precipitable water anomalies every 2 mm, heavy dashed for negative values and heavy solid for positive values, with respect to climatology, for the extreme cases at (a) -48, (b) -36, (c) -24, (d) -12, (e) 0, and (f) +12 h. Light solid contours represent full composite precipitable water field, every 6 mm. Shading represents statistical significance of the anomalies at the 95% (lighter shading) and 99% (darker shading) confidence levels, according to the Student's <i>t</i> test. All fields are derived from the NCEP global reanalysis
2.14	As in Fig. 2.13, but for the moderate cases 63
2.15	As in Fig. 2.13, but for the light cases
2.16	Wind rose climatology for the period from 1979-2005, all months inclusive, at St. John's (YYT) (a) 925 hPa geostrophic wind derived from the NCEP global reanalysis and (b) 10 m observed wind, from station data. Wind classes are as follows: 1-4 knots (black), 4-7 knots (yellow), 7-11 knots (red), 11-17 knots (blue), 17-21 knots (green), and greater than 22 knots (turquoise)
2.17	As in Fig. 2.16, but for 1979-2005, October-April only

2.18	As in Fig. 2.16, but for the fifty extreme precipitation cases, at $t=0$ h. 67
2.19	As in Fig. 2.16, but for the fifty moderate precipitation cases, at $t = 0$ h. 68
2.20	As in Fig. 2.16, but for the fifty light precipitation cases, at $t = 0 h69$
3.1	Twenty-seven backward trajectories with the origin being five days earlier and the ending points at 300, 500, and 700 hPa at 0600 UTC October 18 th , 1986. Ending points are distributed within a box whose corners are 48.4°N 53.5°W and 46.4°N 51.5°W. This is an example of a 'south' event.
	a) The tracer used is pressure (hPa) where warm colors indicate closer to the surface.
	b) Tracer used is relative humidity (%) where warm colors indicate values closer to 100% .
	c) Tracer used is θ_e (k) where warm colors indicate greater values of θ_e
3.2	Twenty-seven backward trajectories with the origin being five days earlier and the ending points at 300, 500, and 700 hPa at 0000 UTC April 21 st , 1988. Ending points are distributed within a box whose corners are 48.4°N 53.5°W and 46.4°N 51.5°W. This is an example of a 'southwest' event.
	a) The tracer used is pressure (hPa) where warm colors indicate closer to the surface.
	b) Tracer used is relative humidity (%) where warm colors indicate values closer to 100% .
	c) Tracer used is θ_e (k) where warm colors indicate greater values of θ_e
3.3	Twenty-seven backward trajectories with the origin being five days earlier and the ending points at 300, 500, and 700 hPa at 0000 UTC December 8 th , 2000. Ending points are distributed within a box whose corners are 48.4°N 53.5°W and 46.4°N 51.5°W. This is an example of a 'west' event.
	a) The tracer used is pressure (hPa) where warm colors indicate closer to the surface.
	b) Tracer used is relative humidity (%) where warm colors indicate values closer to 100% .
	c) Tracer used is $\theta_e\left(k\right)$ where warm colors indicate greater values of $\theta_e.$
	111
3.4	Sea-level pressure (SLP) anomalies every 2 hPa, heavy dashed for negative values and heavy solid for positive values, with respect to

	climatology, for the south cases at (a) -48, (b) -36, (c) -24, (d) -12, (e) 0, and (f) +12 h. Light solid contours represent full composite SLP field, every 4 hPa. Shading represents statistical significance of the anomalies at the 95% (darker shading) and 99% (lighter shading) confidence levels, according to the Student's <i>t</i> test
3.5	500 hPa height anomalies every 3 dam, heavy dashed for negative values and heavy solid for positive values, with respect to climatology for the composite of the south cases at (a) -72, (b) -60, (c) -48, (d) -36, (e) -24, (f) -12, (g) 0, (h) +12, and (i) +24 h. Light solid contours represent full composite 500 hPa field, every 6 dam. Shading represents statistical significance of the anomalies at the 95% (lighter shading) and 99% (darker shading) confidence levels, according to the Student's t test 113
3.6	Precipitable water anomalies every 2 mm, heavy dashed for negative values and heavy solid for positive values, with respect to climatology, for the south cases at (a) -48, (b) -36, (c) -24, (d) -12, (e) 0, and (f) +12 h. Light solid contours represent full composite PW field, every 6 mm. Shading represents statistical significance of the anomalies at the 95% (lighter shading) and 99% (darker shading) confidence levels, according to the Student's <i>t</i> test
3.7	As in Fig. 3.4, but for the southwest cases
3.8	As in Fig. 3.5, but for the southwest cases
3.9	As in Fig. 3.6, but for the southwest cases
3.10	As in Fig. 3.4, but for the west cases
3.11	As in Fig. 3.5, but for the west cases
3.12	As in Fig. 3.6, but for the west cases
3.13	Time series during which precipitation was recorded at St. John's of NCEP Global Reanalysis 700-400 hPa layer-averaged relative vorticity advection $\times 10^{-10}$ s ⁻² (green), 1000-700 hPa layer-averaged horizontal temperature advection $\times 10^{-5}$ Ks ⁻¹ (blue), and 1000-700 hPa layer-averaged frontogenesis $\times 10^{-2}$ K/100 m/3 hr (red) for (a) a cyclone case and (b) a frontal case. Time on the horizontal axis is every six hours, with time "4" being t=0 h
3.14	Sea-level pressure (SLP) anomalies every 2 hPa, heavy dashed for negative values and heavy solid for positive values, with respect to climatology, for the cyclone cases at (a) -48, (b) -36, (c) -24, (d) -12, (e) 0, and (f) +12 h. Light solid contours represent full composite SLP field, every 4 hPa. Shading represents statistical significance of the anomalies at

	according to the Student's t test
3.15	500 hPa height anomalies every 3 dam, heavy dashed for negative values and heavy solid for positive values, with respect to climatology for the composite of the cyclone cases at (a) -72, (b) -60, (c) -48, (d) -36, (e) -24, (f) -12, (g) 0, (h) +12, and (i) +24 h. Light solid contours represent full composite 500 hPa field, every 6 dam. Shading represents statistical significance of the anomalies at the 95% (lighter shading) and 99% (darker shading) confidence levels, according to the Student's <i>t</i> test 123
3.16	Precipitable water anomalies every 2 mm, heavy dashed for negative values and heavy solid for positive values, with respect to climatology, for the cyclone cases at (a) -48, (b) -36, (c) -24, (d) -12, (e) 0, and (f) +12 h. Light solid contours represent full composite PW field, every 6 mm. Shading represents statistical significance of the anomalies at the 95% (lighter shading) and 99% (darker shading) confidence levels, according to the Student's <i>t</i> test
3.17	As in Fig. 3.14, but for the frontal cases
3.18	As in Fig. 3.15, but for the frontal cases
3.19	As in Fig. 3.16, but for the frontal cases
4.1	Meteograms for the entire period of precipitation at St. John's (CYYT) for MAG 1. In the top panel of (a) December 7 th , 2008, (b) December 8 th , 2008, and (c) December 9 th , 2008, temperature (dewpoint) is plotted in red (green). In the bottom panel of (a), (b), and (c), time on the horizontal axis is in UTC, visibility on the vertical axis is plotted in blue, wind (in knots) is represented by barbs, and 6-hour precipitation amounts are bold.
4.0	
4.2	Time series of infared (IR) satellite imagery for MAG 1. Images are presented for (a) t=-72 h, (b) t=-48 h, (c) t=-36 h, (d) t=-24 h, (e) t=-12 h, (f) t=-6 h, (g) t=0 h, (h) t=+6 h, and (i) t=+12 h, where t=0 h is 0600 UTC 8 December, 2008. A blue star is placed in each panel at the approximate location of St. John's and the area of interest explored in Fig. 4.11 (cross section) is outlined with a black line in panel (a)
4.3	Time series of radar imagery for MAG 1, from the Environment Canada radar located in Holyrood, Newfoundland. Radar imagery is shown for (a) t=-18 h, (b) t=-12 h, (c) t=-6 h, (d) t=0 h, (e) t=+6 h, and (f) t=+12 h, where t=0 h is 0600 UTC 8 December, 2008. A red star is placed at the approximate location of the St. John's international airport (CYYT) 162
4.4	Twenty-seven backward trajectories derived from the NCEP GFS 0.5 degree analysis, with the origin being five days earlier and the ending

	points at 300, 500, and 700 hPa at 0600 UTC December 8 th , 2008. Ending points are distributed within a box whose corners are 48.4°N 53.5°W and 46.4°N 51.5°W. This is for MAG 1
4.5	Time series for MAG 1 during the period of precipitation at St. John's (t=-18 h, 1200 UTC 7 December to t=+24 h, 0600 UTC 9 December), of GFS half-degree analysis for (a) 700-400 hPa layer-averaged relative vorticity advection $\times 10^{-10}$ s ⁻² (green), 1000-700 hPa layer-averaged horizontal temperature advection $\times 10^{-5}$ K s ⁻¹ (blue), and 1000-700 hPa layer-averaged frontogenesis $\times 10^{-2}$ K (100 km) ⁻¹ (3 hr) ⁻¹ (red), and 1000-700 hPa layer-averaged geostrophic frontogenesis $\times 10^{-2}$ K (100 km) ⁻¹ (3 hr) ⁻¹ (purple) and (b) column precipitable water (mm, blue) and 700 hPa omega (cm s ⁻¹ , red)
4.6	Time series of GFS half-degree analyses sea-level pressure (SLP, solid) contoured every 4 hPa, 1000-500 hPa thickness (dashed) contoured every 6 dam, and 6-hourly precipitation totals (shaded) in mm, for MAG 1. Results are shown for (a) t=-72 h, (b) t=-48 h, (c) t=-36 h, (d) t=-24 h, (e) t=-12 h, (f) t=-6 h, (g) t=0 h, (h) t=+6 h, and (i) t=+12 h, where t=0 h is 0600 UTC 8 December, 2008
4.7	As in Fig. 4.6, but for SLP (solid, every 4 hPa) and potential temperature (K) on the Dynamic Tropopause (shaded)
4.8	As in Fig. 4.6, but for 850 hPa equivalent potential temperature (K, shaded), and Coupling Index (K, solid, every 4 K from 0 to +16) 167
4.9	As in Fig. 4.6, but for SLP (solid, every 4 hPa), 1000-700 hPa moisture flux convergence (kg m ⁻² s ⁻¹ , shaded), and 1000-700 hPa moisture transport vectors (red)
4.10	Time series of observed soundings at St. John's (CYYT) for MAG 1. Soundings are shown for (a) t =-30 h, (b) t=-18 h, (c) t=-6 h, (d) t=+6 h, (e) t=+18 h, and (f) t=+30 h, where t=0 h is 0600 UTC 8 December 2008.
4.11	Time series of cross-section plots along latitude 47.37 N, from -62.4 W to -42.4 W, for MAG 1. Relative humidity (%, shaded), equivalent potential temperature (K, red solid lines), momentum (M) surfaces (m/s, black dashed) and winds (barbs) shown for (a) t =-24 h, (b) t=-12 h, (c) t=-6 h, (d) t=0 h, (e) t=+6 h, and (f) t=+12 h, where t=0 h is 0600 UTC 8 December 2008. The 2 PVU surface is also contoured (bold black), when present
4.12	Meteograms for the entire period of precipitation at St. John's (CYYT) for MAG 2. As in Fig. 4.1, but for (a) December 11 th , 2008, and (b) December 12 th , 2008

4.13	presented for (a) t=-72 h, (b) t=-48 h, (c) t=-36 h, (d) t=-24 h, (e) t=-12 h, (f) t=-6 h, (g) t=0 h, (h) t=+6 h, and (i) t=+12 h, where t=0 h is 0600 UTC 11 December, 2008. A blue star is placed in each panel at the approximate location of St. John's and the area of interest explored in Fig. 4.21 (cross section) is outlined with a black line in panel (a)
4.14	Time series of radar imagery for MAG 2, from the Environment Canada radar located in Holyrood, Newfoundland. Radar imagery is shown for (a) $t=-10\ h$, (b) $t=+12\ h$, (c) $t=+15\ h$, (d) $t=+18\ h$, (e) $t=+24\ h$, and (f) $t=+30\ h$, where $t=0\ h$ is $0600\ UTC\ 11\ December,\ 2008$. A red star is placed at the approximate location of the St. John's international airport (CYYT) 173
4.15	Twenty-seven backward trajectories derived from the NCEP GFS 0.5 degree analysis, with the origin being five days earlier and the ending points at 300, 500, and 700 hPa at 0600 UTC December 11 th , 2008. Ending points are distributed within a box whose corners are 48.4°N 53.5°W and 46.4°N 51.5°W. This is for MAG 2 174
4.16	Time series for MAG 2 during the period of precipitation at St. John's (t=-6 h, 0000 UTC 11 December to t=+36 h, 1800 UTC 12 December), of GFS half-degree analysis for (a) 700-400 hPa layer-averaged relative vorticity advection $\times 10^{-10}$ s ⁻² (green), 1000-700 hPa layer-averaged horizontal temperature advection $\times 10^{-5}$ K s ⁻¹ (blue), and 1000-700 hPa layer-averaged frontogenesis $\times 10^{-2}$ K (100 km) ⁻¹ (3 hr) ⁻¹ (red), and 1000-700 hPa layer-averaged geostrophic frontogenesis $\times 10^{-2}$ K (100 km) ⁻¹ (3 hr) ⁻¹ (purple) and (b) column precipitable water (mm, blue) and 700 hPa omega (cm s ⁻¹ , red)
4.17	Time series of GFS half-degree analysis sea-level pressure (SLP, solid) contoured every 4 hPa, 1000-500 hPa thickness (dashed) contoured every 6 dam, and 6-hourly precipitation totals (shaded) in mm, for the second case in this study. Results are shown for (a) t=-72 h, (b) t=-48 h, (c) t=-36 h, (d) t=-24 h, (e) t=-12 h, (f) t=-6 h, (g) t=0 h, (h) t=+6 h, and (i) t=+12 h, where t=0 h is 0600 UTC 11 December, 2008
4.18	As in Fig. 4.17, but for SLP (solid, every 4 hPa) and potential temperature (K) on the Dynamic Tropopause (shaded)
4.19	As in Fig. 4.17, but for 850 hPa equivalent potential temperature (K, shaded), and Coupling Index (K, solid, every 4 K from 0 to +16) 178
4.20	As in Fig. 4.17, but for SLP (solid, every 4 hPa), 1000-700 hPa moisture flux convergence (kg m ⁻² s ⁻¹ , shaded), and 1000-700 hPa moisture transport vectors (red)
4.21	Time series of observed soundings at St. John's (CYYT) for MAG 2. Soundings are shown for (a) t =-30 h, (b) t=-18 h, (c) t=-6 h, (d) t=+6 h,

	(e) t=+30 h, and (f) t=+42 h, where t=0 h is 0600 UTC 11 December 2008. The sounding from t=+18 h is missing in the dataset
4.22	Time series of northwest-southeast cross-section plots from 52.37 N, -62.4 W to 42.37 N, -42.4 W, for MAG 2. Relative humidity (%, shaded), equivalent potential temperature (K, red solid lines), momentum (M) surfaces (m/s, black dashed) and winds (barbs) shown for (a) t =-24 h, (b) t=-12 h, (c) t=-6 h, (d) t=0 h, (e) t=+6 h, and (f) t=+12 h, where t=0 h is 0600 UTC 11 December 2008
5.1	Time series for MAG 1 of GFS half-degree forecasts for precipitable water (mm). Each line is a different initialization time, with forecasts for every six hours (horizontal axis) during the period of precipitation at St. John's, which is t=-18 h (1200 UTC 7 December 2008) to t=+24 h (0600 UTC 9 December 2008). The GFS half-degree analysis is represented by a bold black line
5.2:	Time series for MAG 1 of GFS half-degree forecasts for precipitation (mm) for six hour periods beginning at each verification time (horizontal axis). Each line is a different initialization time, with forecasts for every six hours (horizontal axis) during the period of precipitation at St. John's, which is t=-18 h (1200 UTC 7 December 2008) to t=+24 h (0600 UTC 9 December 2008). The GFS half-degree analysis is represented by a bold black line
5.3	Time series of GFS half-degree analyses sea-level pressure (SLP, solid) contoured every 4 hPa, 1000-500 hPa thickness (dashed) contoured every 6 dam, and 6-hourly precipitation totals (shaded) in mm, for MAG 1, all validating at t=0 h, 0600 UTC 8 December 2008. Results are displayed for forecast lead times of (a) t=96 h, (b) t=84 h, (c) t=72 h, (d) t=60h, (e) t=48 h, (f) t=36 h, (g) t=24 h, (h) t=12 h, and (i) t=0 h 205
5.4	As in Fig. 5.3, but for SLP (solid, every 4 hPa) and potential temperature (K) on the Dynamic Tropopause (shaded)
5.5	As in Fig. 5.3, but for 850 hPa equivalent potential temperature (K, shaded), and Coupling Index (K, solid, every 4 K from 0 to +16) 207
5.6	As in Fig. 5.3, but for GFS forecast soundings at St. John's (CYYT) with temperature (°C, red) and dewpoint (°C, green)
5.7	Time series for MAG 2 of GFS half-degree forecasts for precipitable water (mm). Each line is a different initialization time, with forecasts for every six hours (horizontal axis) during the period of precipitation at St. John's, which is t=-6 h (0000 UTC 11 December 2008) to t=+36 h (1800 UTC 12 December 2008). The GFS half-degree analysis is represented by a bold black line

5.8:	Time series for MAG 2 of GFS half-degree forecasts for precipitation (mm) for six hour periods beginning at each verification time (horizontal axis). Each line is a different initialization time, with forecasts for every six hours (horizontal axis) during the period of precipitation at St. John's, which is t=-6 h (0000 UTC 11 December 2008) to t=+36 h (1800 UTC 12 December 2008). The GFS half-degree analysis is represented by a bold black line
5.9	Time series of GFS half-degree analyses sea-level pressure (SLP, solid) contoured every 4 hPa, 1000-500 hPa thickness (dashed) contoured every 6 dam, and 6-hourly precipitation totals (shaded) in mm, for MAG 2, all validating at t=0 h, 0600 UTC 11 December 2008. Results are displayed for forecast lead times of (a) t=96 h, (b) t=84 h, (c) t=72 h, (d) t=60h, (e) t=48 h, (f) t=36 h, (g) t=24 h, (h) t=12 h, and (i) t=0 h
5.10	As in Fig. 5.9, but for SLP (solid, every 4 hPa) and potential temperature (K) on the Dynamic Tropopause (shaded)
5.11	As in Fig. 5.9, but for 850 hPa equivalent potential temperature (K, shaded), and Coupling Index (K, solid, every 4 K from 0 to +16) 213
5.12	As in Fig. 5.9, but for GFS forecast soundings at St. John's (CYYT) with temperature (°C, red) and dewpoint (°C, green)

List of Tables

2.1	The number of cool-season (October-April) measurable precipitation events at four selected station in Atlantic Canada
2.2	Mean monthly precipitation amounts for the four capital cities in Atlantic Canada during the cool season (October-April)
3.1	The fifty extreme cases broken down by methodology and synoptic typing
3.2	Average event precipitation and synoptic characteristics associated with each trajectory type, for the fifty extreme precipitation cases 103
3.3	Average event precipitation and synoptic characteristics associated with each quasi-geostrophic forcing type
3.4	The fifty cases from each precipitation amount group defined in Milrad et al. (2009), listed by trajectory classification
3.5	The fifty cases from each precipitation amount group defined in Milrad et al. (2009), listed by Quasi-Geostrophic forcing classification 106
3.6	Important synoptic-scale structures and precursors associated with each trajectory composite group, among the three precipitation amount categories defined in Milrad et al. (2009)
3.7	Important synoptic-scale structures and precursors associated with each Quasi-Geostrophic (QG) forcing composite group, among the three precipitation amount categories defined in Milrad et al. (2009) 108
5.1	Environment Canada operational forecasts issued by the Newfoundland Weather Office, for St. John's, before and during the first part of MAG 1 (Saturday 6 December 2008 and Sunday 7 December 2008) 199
5.2	Environment Canada operational forecasts issued by the Newfoundland Weather Office, for St. John's, during the latter part of MAG 1 (Monday 8 December 2008 and Tuesday 9 December 2008)
5.3	Environment Canada operational forecasts issued by the Newfoundland Weather Office, for St. John's, before the first part of MAG 2 (Tuesday 9 December 2008 and Wednesday 10 December 2008)
5.4	Environment Canada operational forecasts issued by the Newfoundland Weather Office, for St. John's, during MAG 2 (Thursday 11 December 2008)

Chapter 1

Introduction

1.1 Motivation

1.1.1 Quantitative Precipitation Forecasting (QPF)

Quantitative precipitation forecasting (QPF) is a crucially important and difficult challenge in operational meteorology. Fritsch et al. (1998) point out that "what people need to know most about the weather is, will it rain or snow, and if so, how much?" The intensity and characteristics of the precipitation can have a large impact on public safety, property, and commercial operations and can greatly affect daily governmental and business decisions (Fritsch et al. 1998). This is particularly true in the case of intense or extreme precipitation events where a large amount of precipitation can result in losses of life and property, in addition to severely damaging local and regional economies (Olson et al. 1995). Therefore, as Doswell et al. (1996) state, "the task is not just to forecast the occurrence of an event...but to anticipate the magnitude...It is the amount of precipitation that transforms an otherwise ordinary rainfall into an extraordinary, life-threatening situation."

The difficulties associated with QPF are not new and are well documented in the atmospheric science literature. In the late 1950's, Estoque (1957) employed

a two-level prediction model to show that a 24-hour QPF could be calculated for North America over the span of two hours. In the 1960's, Harley (1965) used calculations of vertical velocities to create an operational method for predicting rainfall amounts.

In more recent years, the accuracy of QPF has improved somewhat, particularly at shorter lead times, as shown for the United States (U.S.) by Fritsch and Carbone (2004), and shown in Fig. 1.1. However, while progress has been made in the last thirty to forty years, particularly due to improvements in numerical weather prediction (NWP) models, the level of progress pales in comparison to advancements in the forecasts of atmospheric mass fields, such as sea-level pressure (SLP), upper- and mid-tropospheric heights, wind, and moisture. This trend was noticed as early as 1980, when Bosart (1980) assessed the main U.S. operational model at the time, the Limited Fine Mesh (LFM) model, and concluded that while synoptic-scale mass field forecasts had substantially improved, "corresponding progress (in QPF) has been stubborn, slow and disappointing." In later studies, Bosart (1981), Gyakum and Samuels (1987), Olson et al. (1995), Roebber and Bosart (1998), and Sisson and Gyakum (2004) come to similar conclusions regarding the lag in improvements between mass fields and QPF.

Given the aforementioned limitations in computational advances in QPF compared with the mass fields, the importance of the human forecaster becomes magnified, especially in reference to intense and extreme precipitation events.

Furthermore, the individual forecaster can effectively utilize the advances in mass field forecasts to help identify synoptic-scale patterns and structures typically associated with these types of events (Funk 1991). Durran and Snellman (1987) support this assertion by claiming that "good" forecasters do not rely exclusively on numerical weather prediction models and instead "examine the developing weather patterns and attempt to understand the factors which are likely to be responsible for the current and next day's weather." To that end, previous research indicates that subjective human forecasts (which, of course, incorporate numerical model guidance) are typically more accurate than pure model-based guidance, as is shown for older U.S. operational models in Fig. 1.2 and more recent models in Fig. 1.3. Funk (1991) also relates this assertion to QPF, stating that if good pattern-recognition and forecasting techniques are employed by the human forecaster, manual QPF will likely prove to be substantially more accurate than purely model-based OPF.

As Reynolds (2003) points out, in order for subjective QPF to actually be an improvement over model QPF, the forecaster must use his/her knowledge of the underlying physical characteristics and processes of the atmosphere in combination with a complete understanding of numerical model guidance. The research community can be useful in this regard by contributing valuable knowledge regarding synoptic-scale patterns and characteristics of a particular geographical region to the operational forecasters. This is particularly important in a region prone to intense and extreme precipitation events, where risks to life and property are inherently higher, particularly in more densely populated areas.

1.1.2 Atlantic Canada

Ralph et al. (2005) state that despite the focus on QPF in U.S. literature, there is also a substantial amount of cool-season, high-impact weather in eastern Canada, which indicates a significant risk to life and property in this region. This is especially true in Atlantic Canada, which consists of four provinces: New Brunswick, Prince Edward Island, Nova Scotia, and Newfoundland and Labrador. The geography of the region, with the capital city of each province labeled, is shown in Fig. 2.1. As is clear from Fig. 2.1, the proximity of Atlantic Canada to the Atlantic Ocean plays a large role in the weather of the region.

However, it is more than just the proximity of Atlantic Canada to the ocean that makes it a region of interest. As shown in Fig. 2.2, and detailed in Chapter 2, the region is located at the confluence of several typical North American storm tracks, as also found by Zishka and Smith (1980). This is especially true for the Avalon Penninsula in southeastern Newfoundland and Labrador, where the provincial capital of St. John's (CYYT) is located.

Moreover, Atlantic Canada, and particularly southeastern Newfoundland, is located near the confluence of two major ocean currents, the southward-flowing cold Labrador current and the northward-flowing warm Gulf Stream current (Fig. 1.4). Regions around the world (e.g. the east coast of Japan) that are located at the confluence of contrasting ocean currents can be quite prone to intense and extreme precipitation events, frequently due to intense cyclogenesis that is

enhanced by certain factors (e.g. heat fluxes, moisture availability, sea-surface temperature, etc.) (Aguado and Burt 2007).

With the above factors in mind, Stewart et al. (1987) argue that Atlantic Canada, including St. John's and the Avalon Peninsula, is a region prone to extreme precipitation events, particularly in the cool season. Given the Arctic air masses often present in the cool season at the latitudes of Atlantic Canada (i.e. 45-50° N), the effects of these storms can include heavy snow or rain, strong winds, storm surges, and blizzard or near-blizzard conditions (Stewart et al. 1987). The impacts of such events are felt widely throughout the region, and can severely impact human and commercial interests (e.g. fishing, shipping, etc.).

In addition to the need for a comprehensive study of precipitation events in a region prone to such frequent and extreme events, the relative lack of meteorological research centered on Atlantic Canada, particularly on the synoptic scale, is a major motivation for this work. Most, if not all of the literature revolves around two field experiments conducted in the winters of 1987 of 1992, phase I and II, respectively, of the Canadian Atlantic Storms Program (CASP), as detailed by Stewart et al. (1987) and Stewart et al. (1991). While the majority of the work in CASP I and II focuses on mesoscale structures such as heavy precipitation bands and rain-snow boundaries within east coast cyclones (e.g. Stewart et al. 1990; Reuter and Yau 1990), a few are detailed case studies of intense cyclogenesis in the region (Yau and Jean 1989; Stewart and Donaldson 1989; Gyakum et al. 1996; Gyakum and Stewart 1996; Huo et al. 1996).

Gyakum et al. (1996) addresses climatological characteristics of cyclogenesis and storms tracks that affect Atlantic Canada; specifically, Gyakum et al. (1996) state that the formative regions for intense cyclones that affect Atlantic Canada are often located far upstream of these storms and that proper analysis of these features at early lead times is necessary in order to provide accurate forecasts for Atlantic Canada.

In summary, Atlantic Canada is a region that is located at the confluence of several North American storm tracks and two contrasting ocean currents, and has been largely ignored in the literature, particularly with regard to synoptic meteorology. It is evident that a comprehensive climatology and synoptic-scale study of cool-season precipitation events, with a focus on extreme events, would prove quite useful to forecasters in the area.

1.1.3 Extreme Precipitation Events

Stewart et al. (1987) point out that Atlantic Canada is a region prone to extreme precipitation events, particularly in the cool season. In addition, Sisson and Gyakum (2004) state that in regions prone to extreme events, the challenge presented by QPF becomes even more daunting. As a result, and as is outlined in Section 1.2, the majority of this work is centered around a detailed synoptic-scale (dynamic and thermodynamic) analysis of extreme precipitation events at St. John's, Newfoundland and Labrador.

Studies of extreme or intense precipitation events are not new in atmospheric science literature. Over the past century, many case studies of extreme, and in some cases, infamous precipitation events have been published. More often than not, these studies focus on cases of intense cool-season or wintertime cyclogenesis that impact major population centers throughout North America.

One of the most researched cases of intense and destructive cool-season cyclones is the Presidents' Day snowstorm of 18-19 February 1979. This storm is discussed by Bosart (1981), Bosart and Lin (1984), Uccellini et al. (1984, 1985), and Whitaker et al. (1988). All of these studies focus on various synoptic- and meso-scale characteristics of the storm. Specifially, Bosart and Lin (1984) and Uccellini et al. (1985) argue that a tropopause fold and accompanying stratospheric air extrusion are present to the west of the surface cyclone, while Uccellini et al. (1984) find that three separate upper-level jet streaks play a crucial role in the rapid intensification of the cyclone. Finally, Whitaker et al. (1988) utilize a backward trajectory analysis to identify air parcels with substantially different origins that converge in the region of cyclogenesis.

Another infamous case is the Superstorm of 12-14 March 1993, the synoptic and destructive characteristics of which Kocin et al. (1995) comprehensively discuss. Bosart et al. (1996) and Dickinson et al. (1997) support the analysis of Kocin et al. (1995) with examinations of precursor planetary-scale structures and upper-tropospheric dynamics, respectively. Bosart et al. (1996)

find that downstream Rossby wave development plays a role in the cyclogenesis of the Superstorm, while Dickinson et al. (1997) utilize potential vorticity (PV) analyses to illustrate the impact of latent heat release as a result of heavy precipitation. Finally, Huo et al. (1995) focus on the static stability of the atmosphere prior to and during the rapid formation stage of the Superstorm.

The two cases outlined above are just the tip of the iceberg in terms of historical case studies of intense precipitation events. Other examples include, but are not limited to: the "surprise" snowstorm in the mid-Atlantic region of the U.S. in 2000 (Zhang et al. 2002; Brennan and Lackmann 2006), the Queen Elizabeth II cyclone of September 1978 (Uccellini 1986; Gyakum 1991), the destructive ice storm of northern New England and southeastern Canada in January 1998 (Gyakum and Roebber 2001; Roebber and Gyakum 2003), intense cyclogenesis events in Atlantic Canada during the aforementioned CASP I and II field projects (Yau and Jean 1989; Stewart and Donaldson 1989; Gyakum et al. 1996; Gyakum and Stewart 1996; Huo et al. 1996), and the 1999 winter storm in Europe, dubbed "Lothar" (Wernli et al. 2002).

Prior cases of intense or extreme cool-season precipitation are important to this study because they provide a basis for the types of synoptic analyses that are presented in the later part of the manuscript. It is important to fully understand the lessons learned from other remarkable precipitation events before determining those that result from the extreme precipitation events discussed in this study.

These lessons result from diagnostics that range from upper-tropospheric and jet

streak structures (e.g. Bosart and Lin (1984), Uccellini et al. (1985), Uccellini et al. (1984), in the case of the Presidents' Day cyclone) to analyses of low-level moisture convergence and moisture sources (e.g. Gyakum and Roebber 2001, in the case of the 1998 ice storm). Finally, with the important exception of the 1998 ice storm (Gyakum and Roebber 2001; Roebber and Gyakum 2003), the overwhelming majority of historical cool-season precipitation events analyzed in the literature result from instances of rapid and intense cyclogenesis. Therefore, the latter part of this thesis aims to go beyond this threshold and provide a synoptic-scale analysis of extreme precipitation events at St. John's, regardless of whether an intense or rapidly developing cyclone is involved.

1.2 Objectives and Manuscript Outline

The primary goal of this thesis is to provide a detailed synoptic analysis of precipitation events at St. John's, Newfoundland and Labrador during the past three decades, and identify dynamically and thermodynamically relevant patterns and structures that can aid the local forecaster in predicting such events. This is accomplished in stages, as detailed below.

Chapter 2 presents a working definition of a cool-season (October-April) precipitation event at St. John's, Newfoundland and Labrador. As is shown in Chapters 1 and 2, St. John's is chosen over other cities in Atlantic Canada (Fig. 2.1) because of its location near the confluence of several North American storm tracks (Fig. 2.2) and two contrasting ocean currents (Fig. 1.4), and its propensity for receiving more precipitation on average than other stations in the region,

during every month in the cool season (Table 2.2). Consequently, a precipitation event climatology is developed for 1979-2005. Using the calculated statistics of the climatology, three categories of precipitation events (extreme, moderate, light) are created based on the amount of precipitation recorded during a particular event. Next, a representative subset of fifty events is chosen from each precipitation amount category and subjected to a composite analysis of dynamically important variables such as sea-level pressure (SLP), 500 hPa height, and precipitable water (PW). Composite plots of each precipitation amount category show distinct synoptic-scale precursors and characteristics associated with each event category, which the local forecaster can use to help predict the potential amount of precipitation for a particular event. Finally, a climatology and compositing of near-surface (925 hPa) geostrophic and 10 m observed winds is completed for St. John's; this process identifies structures in the wind field that are unique to or prevalent in a particular category of precipitation event.

Chapter 3 builds on the results shown in Chapter 2 by further analyzing subsets of events described in Chapter 2, with a primary focus on extreme events. Understanding extreme events can only be accomplished with a systematic comparison with more ordinary events; it is for this reason that the fifty median events in each precipitation event category established in Chapter 2 are further partitioned, utilizing two separate methodologies of manual synoptic typing. The first methodology is based on a backward air parcel trajectory analysis, which partitions events by air parcel origin five days prior to the heaviest precipitation at St. John's. The second methodology separates events using time series of three

commonly used quasi-geostrophic (QG) forcing mechanisms for ascent, namely mid-tropospheric (700-400 hPa) vorticity advection, low-tropospheric (1000-700 hPa) temperature advection, and low-tropospheric (1000-700 hPa) frontogenesis. Time series of these three variables can help in the analysis of the synoptic structures responsible for a particular precipitation event at St. John's. For example, one would associate high positive values of mid-level vorticity advection with a strong mid-tropospheric trough and a likely associated sea-level cyclone, while near-zero values of mid-level vorticity advection over the course of the precipitation event would suggest a lack of the aforementioned mid-tropospheric trough.

As a result of the first methodology, three categories of events (south, southwest, west) are established and two subsets of events (cyclone, frontal) result from the second methodology. Composite analyses are shown for each subset of events in Chapter 3, using the same dynamically relevant parameters presented in Chapter 2. Composite plots in Chapter 3 will show that vastly diverse synoptic regimes can cause extreme precipitation events at St. John's. Additionally, it is shown that certain subsets of extreme events exhibit precursor synoptic-scale signals that are not present in the corresponding subsets of smaller precipitation events. These findings are an example of the material in this study that can be employed by operational forecasters in the future, in order to more accurately predict OPF at St. John's and similar stations.

Chapters 4 and 5 present an overview and analysis of consecutive extreme cool-season precipitation events that affected St. John's in December 2008.

Combined, these two events produced over 125 mm of precipitation in six days.

Applying the manual synoptic typing outlined in Chapter 3, and utilizing a detailed dynamic and thermodynamic analysis (e.g. upper-tropospheric heights and vorticity, lower-tropospheric moisture, vertical atmospheric profiles), Chapter 4 illustrates the very disparate means of producing extreme precipitation events at St. John's. Finally, Chapter 5 presents a preliminary evaluation of two separate operational forecasting systems during these two extreme events, highlighting specific forecast successes and difficulties.

Chapter 6 presents important conclusions derived from this work, including how it can be useful to the operational forecaster in Atlantic Canada and how a transfer of knowledge could be best accomplished. Additionally, arguments are made for future research directions, including but not limited to a) extending the methodology to other stations in the region and across Canada, and b) undertaking a similar study for the warm season.

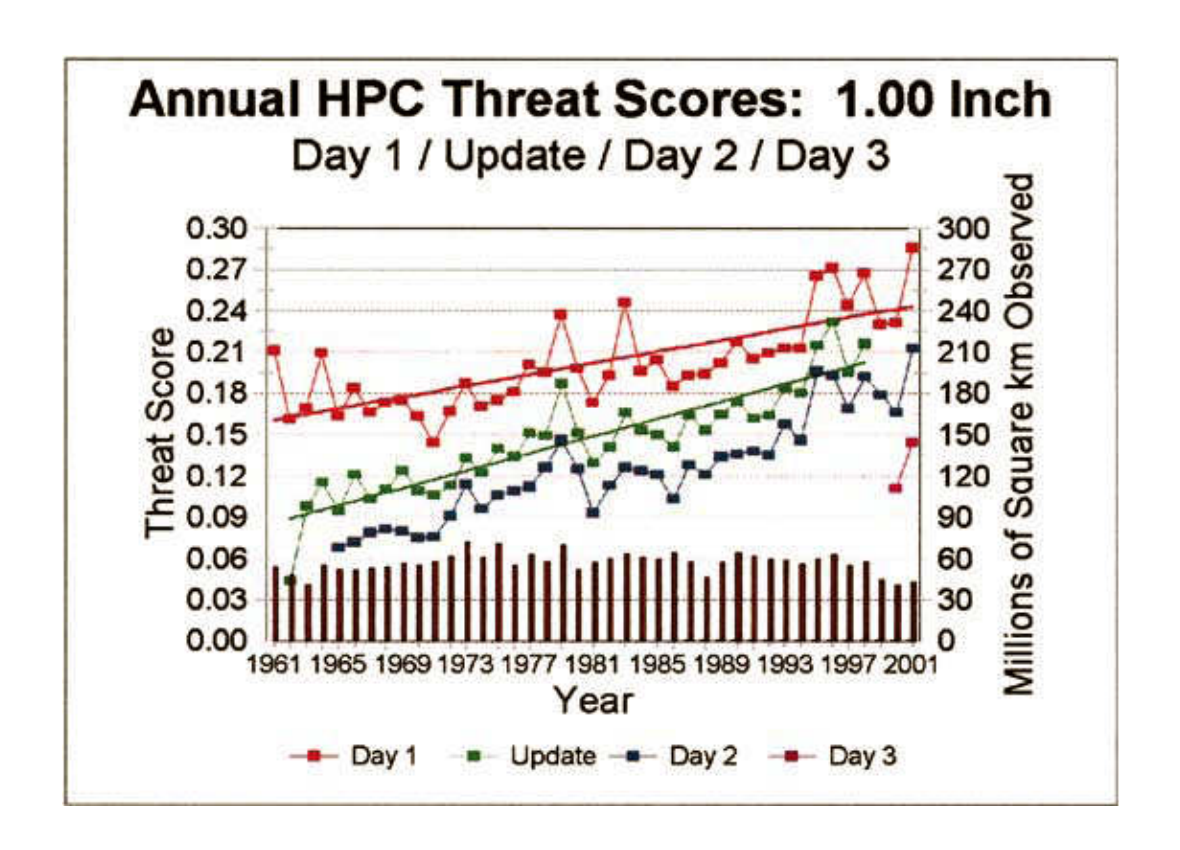


Figure 1.1: From Fritsch and Carbone (2004): Annual threat scores for the National Oceanic Atmospheric Administration (NOAA) Hydrometeorological Prediction Center (HPC) for 24-h forecasts of ≥ 1.00 in. or more of precipitation, showing that QPF improves over the fifty year period of 1961-2001.

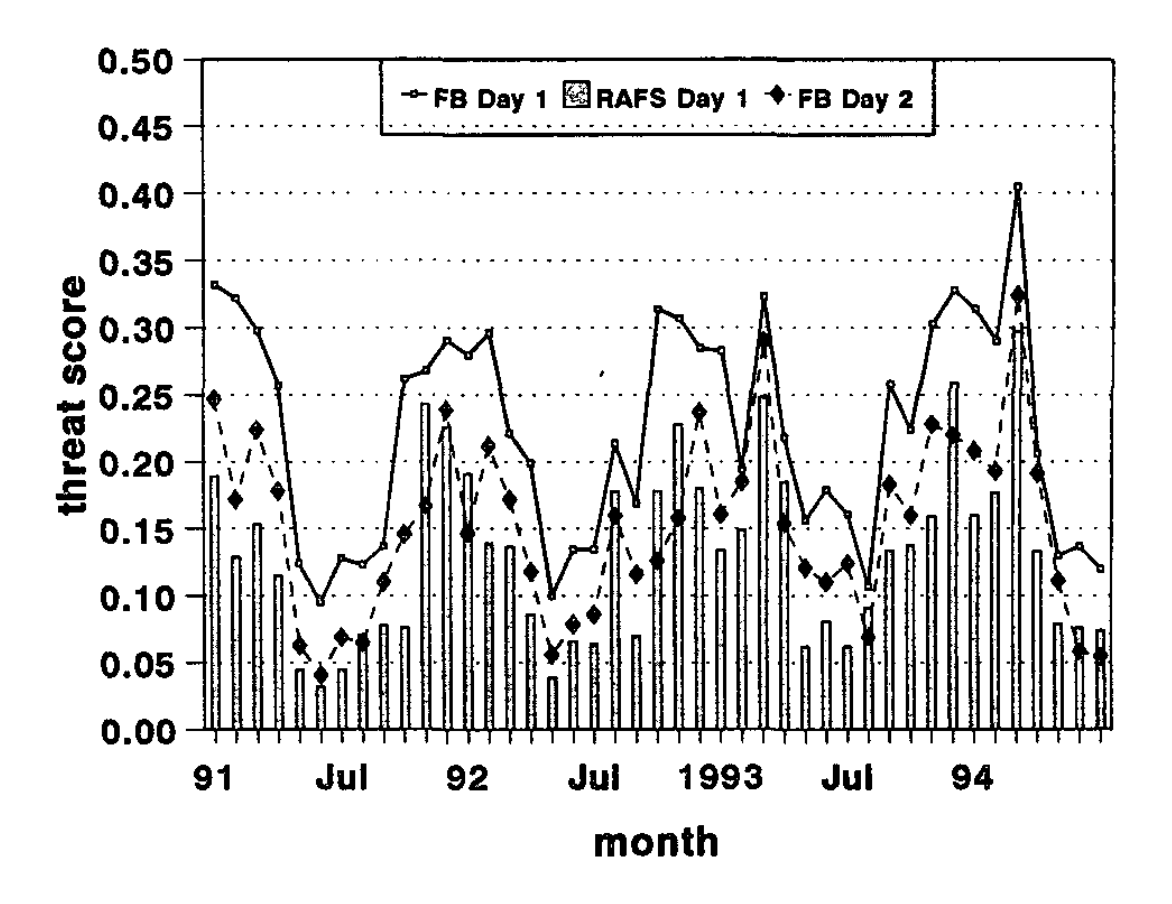


Figure 1.2: From Olson et al. (1995): Monthly threat scores for 24-h forecasts of ≥ 1.00 in. or more of precipitation, for 1991-1994 comparing day one and day two subjective human forecasts issued by the NOAA Forecast Bureau (FB) with the Regional Area Forecast System (RAFS) model used operationally in the U.S. in the early 1990's.

HPC % Improvement vs NCEP Models

1 inch Day 1 QPF Forecast

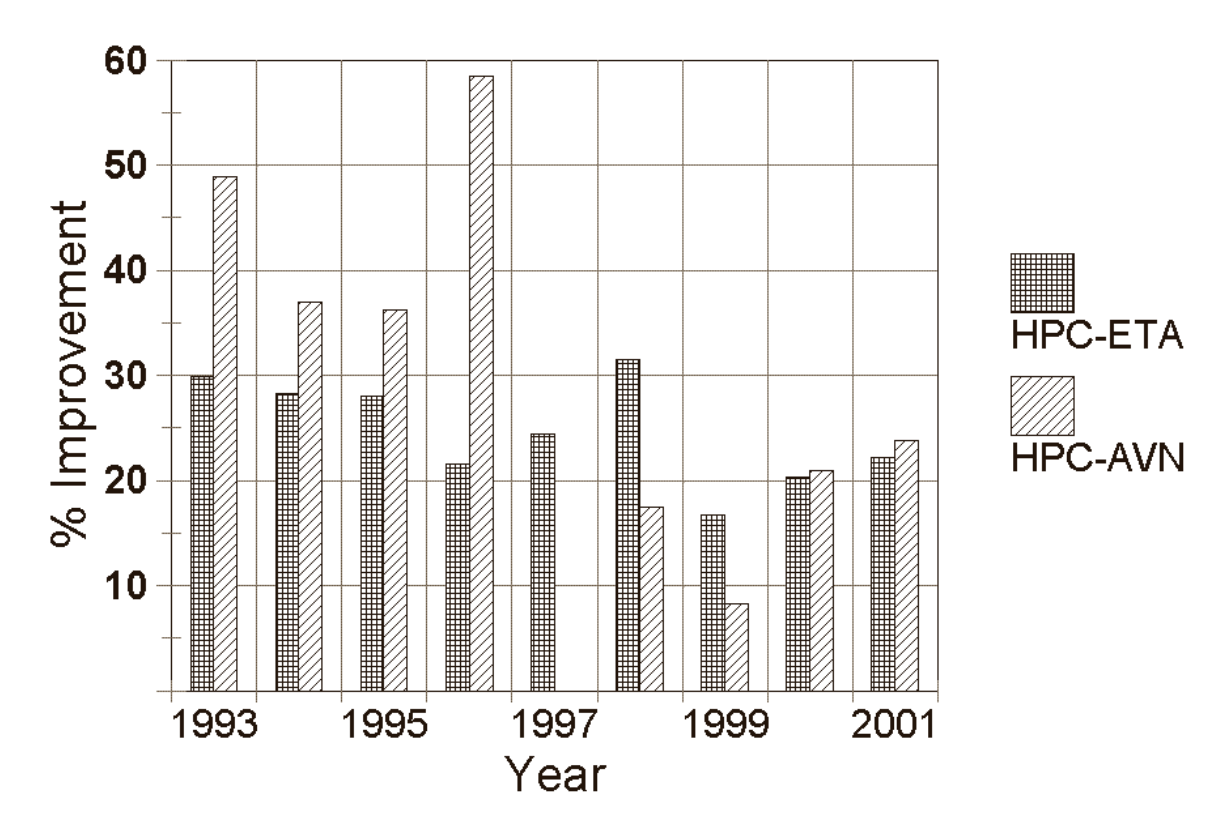


Figure 1.3: From Reynolds (2003): Human forecast improvement in percent versus the main National Centers for Environmental Prediction (NCEP) operational forecast models from 1993-2001.

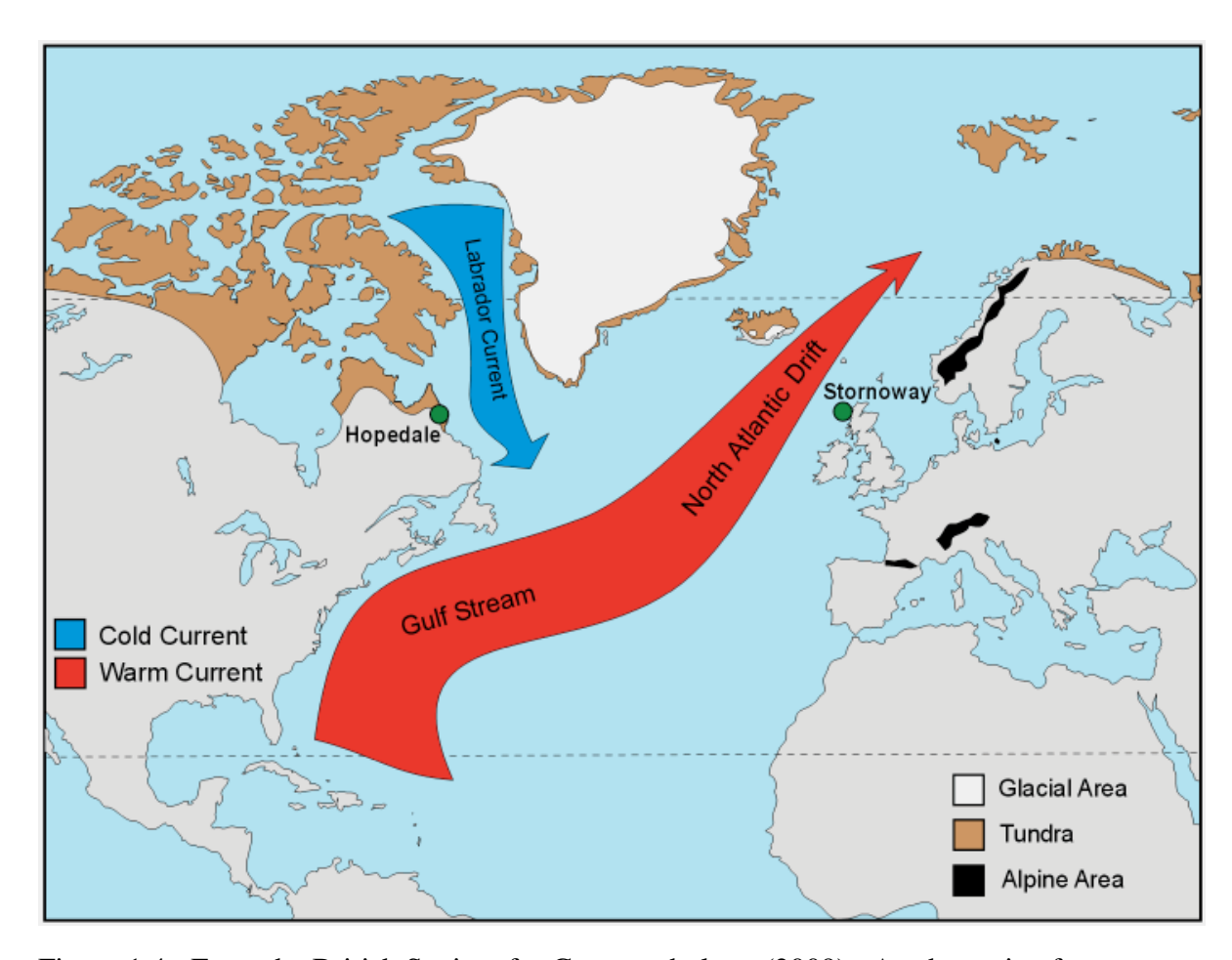


Figure 1.4: From the British Society for Geomorphology (2009): A schematic of ocean currents that impact Atlantic Canada, in particular the confluence of the cold Labrador and warm Gulf Stream current near the coast of Newfoundland and Labrador.

Chapter 2

Climatology and Synoptic-scale Characteristics of Cool-Season Precipitation Events at St. John's, Newfoundland, 1979-2005

In this chapter, the motivations for and data used in this study are discussed in Sections 2.1 and 2.2, respectively. A precipitation event climatology and event separation methodology is developed and detailed in Section 2.3, for 1979-2005. A normal distribution is then used to separate all precipitation events into three intensity bins (extreme, moderate, and light). The median event amount from each bin falls in the 97th, 82nd, and 60th percentile, respectively, creating enough separation between intensity bins to produce reliable synoptic composites. Subsequently, 50 events (25 events above and 25 events below the median amount) in each event category are chosen to produce synoptic composites representative of each event intensity category.

Section 2.4 details the compositing procedure and presents composite plots for sea-level pressure (SLP), 500 hPa height, and precipitable water (PW). There are substantial differences in all three composite fields among the various intensity categories, shown up to 48 hours prior to the onset time of heaviest

precipitation (t=0 h) at St. John's in the SLP and PW fields and up to 72 hours prior in the 500 hPa height fields.

In Section 2.5, a wind climatology (1979-2005) is produced for St. John's. Composite wind roses at t=0 h are also shown for each precipitation intensity category. It is observed that a) certain wind directions are predominant only during extreme events and b) differences in wind directions at St. John's among the three precipitation event intensity categories correspond to variations in storm track. The synoptic-scale ramifications of the composite winds, as well as the aforementioned dynamic composites, are discussed in the final section of the chapter, Section 2.6.

The following is based on: Milrad, Shawn M., E.H. Atallah, and J.R. Gyakum, 2009: Synoptic-scale characteristics and precursors of cool-season precipitation events at St John's, Newfoundland, 1979-2005. *Wea. Forecasting*, **24,** 667–689. (c) American Meteorological Society. Reprinted with permission.

Synoptic-scale characteristics and precursors of cool-season precipitation events at St. John's, Newfoundland, 1979-2005

Shawn M. Milrad, Eyad H. Atallah and John R. Gyakum

Department of Atmospheric and Oceanic Sciences, McGill University

Abstract

The issue of Quantitative Precipitation Forecasting continues to be a significant challenge in operational forecasting, particularly in regions susceptible to frequent and extreme precipitation events. St. John's, Newfoundland is one location affected frequently by such events, particularly in the cool season (October-April). These events can include flooding rains, paralyzing snowfall, and damaging winds.

A precipitation climatology is developed at St. John's for 1979-2005, based on discrete precipitation events occurring over a time period of up to 48 hours. Threshold amounts for three categories of precipitation events (extreme, moderate, light) are statistically derived and utilized to categorize such events. Anomaly plots of sea-level pressure (SLP), 500 hPa height, and precipitable water (PW) are produced for up to three days prior to the event. Results show that extreme events originate along the Gulf Coast of the United States, with the location of anomaly origin being further to the north and west for consecutively

weaker events, culminating in light events which originate from the upper midwest of the United States and south-central Canada. In addition, upper-level precursor features are identified up to three days prior to the events and are mainly located over the west coast of North America.

Finally, results of a wind climatology produced for St. John's depict a gradual shift in predominant wind direction (from easterly to southwesterly) of both the 925 hPa geostrophic wind and 10 m observed wind from extreme to light events, inclusively. In addition, extreme events are characterized by almost exclusively easterly winds.

2.1 Introduction

2.1.1 Motivation

One significant challenge in operational meteorology today is Quantitative Precipitation Forecasting (QPF), particularly in regions of extreme precipitation events (Sisson and Gyakum 2004). As Doswell et al. (1996) point out, "the task is not just to forecast the occurrence of an event, which is difficult enough by itself, but to anticipate the magnitude of the event...It is the amount of the precipitation that transforms an otherwise ordinary rainfall into an extraordinary, lifethreatening situation."

The accuracy of numerical model simulations of extratropical cyclones has progressed at an impressive rate over the past few decades. Both Bosart (1981) and Roebber and Bosart (1998) have concluded that while synoptic-scale

mass-field forecasts (heights, sea level pressure, etc.) have improved dramatically over the past three or four decades, QPF progress has come at a much slower rate. Therefore, it is very important that efforts be made to aid the local forecaster in identifying significant synoptic-scale structures and precursors associated with precipitation events at a particular location. Lackmann and Gyakum (1996), Fischer (1997), Lackmann and Gyakum (1999) and Sisson and Gyakum (2004) accomplish this for the Northwest Territories, Montreal, Quebec, the Pacific Northwest of the United States, and Burlington, Vermont, respectively. Once particular patterns and/or precursors of different thresholds of precipitation events are identified, as was the case at the locations mentioned above, the local forecaster is able to use these benchmarks in addition to whatever forecast model(s) he/she is using.

Extreme precipitation events are prevalent and important in Atlantic Canada, where storms often cause hardship (Stewart et al. 1987), especially in the cool season (defined here as October-April). Atlantic Canada (Fig. 2.1), made up of the provinces of New Brunswick, Prince Edward Island, Nova Scotia and Newfoundland and Labrador, is susceptible to major cool-season storms and resulting heavy precipitation (Stewart et al. 1987). This regional susceptibility is due primarily to the fact that Atlantic Canada is situated at the receiving end of several different storm tracks, in addition to being located at the confluence of the Gulf Stream and Labrador currents. If one assumes that each cyclone responsible for precipitation is associated with a mid-level (500 hPa) trough as is usually the

case, then the predominant climatological North American storm tracks during the months of October-April are depicted to end in Atlantic Canada (Fig. 2.2).

For this study, St. John's, Newfoundland and Labrador is chosen as the location of interest. In addition to being situated in a location commonly affected by several different storm tracks (Fig. 2.2), St. John's has the most precipitation events during our period of study (1979-2005) of all major stations in Atlantic Canada. This information is shown in Table 2.1, where from 1979-2005, St. John's recorded 1983 measurable (greater than or equal to 0.2 mm or 0.01 in), cool season precipitation events, 112 more than any other capital city in Atlantic Canada. In addition, St. John's has the highest average amount of precipitation (Table 2.2) among the four capital cities in Atlantic Canada (Fredericton, New Brunswick; Charlottetown, Prince Edward Island; Halifax, Nova Scotia; and St. John's, Newfoundland and Labrador).

2.1.2 Objectives and Methodology

Given that St. John's has such a preponderance of precipitation, our objective is to identify synoptic-scale characteristics and precursors to coolseason precipitation events, of varying intensities. Furthermore, it will be determined whether there are dynamical precursors that are particularly unique to the more extreme events. As such, the remainder of this paper is organized as follows:

- A cool-season (October-April) precipitation climatology is established at St. John's, Newfoundland and Labrador (CYYT) from 1979-2005 and statistics (e.g. mean, median, standard deviation) associated with this climatology are calculated.
- Using our computed climatological statistics, we establish three categorical thresholds of precipitation events: extreme, moderate, and light.
- 3) Given the aforementioned categorical thresholds of precipitation, we identify synoptic-scale characteristics of these precipitation event groups. This is done primarily by compositing a representative subset of events for each precipitation threshold. It will be shown that differences exist among different precipitation thresholds in terms of large-scale structural anomalies and precursors up to 72 hours prior to the precipitation event. Both dynamical and moisture fields will be examined, including sea-level pressure (SLP), 500 hPa height, and precipitable water (PW).
- 4) An analysis of the observed surface and near-surface (925 hPa) geostrophic wind distributions at St. John's is performed to reinforce conclusions depicted in the dynamical and moisture composite fields.

2.2 Data

This study utilizes 6-hourly precipitation data for St. John's, courtesy of the Environment Canada 6-hour corrected precipitation database (Environment Canada Atlantic Climate Centre, personal communication). The corrected precipitation data is based on work done by Mekis and Hogg (1999), whereby the data has been adjusted to accurately reflect precipitation gauge changes, wind conditions, and changes in station location. It is also of note that all precipitation data in this study is observed in liquid equivalent form (i.e. no data was acquired using ruler methods), thus in theory limiting the errors one might expect at a station such as St. John's, where frozen precipitation is commonplace. The National Centers for Environmental Prediction (NCEP) Global Reanalysis, with a horizontal resolution of 2.5 x 2.5 ° (Kalnay et al. 1996), is used as the dataset of choice for all synoptic-scale composite and anomaly plots. The overwhelming majority of calculations and analyses in this study are performed and displayed using the General Meteorological Package version 5.7.4 (updated from the original package devised by Koch et al. (1983)), a data manipulation and visualization software package commonly used in synoptic analyses. In Section 2.5 (wind climatology and analysis), the wind rose plots are created using WRPLOT view, a program developed by Lakes Environmental, Inc., which is available at http://www.weblakes.com/lakewrpl.html. Actual surface station data is used for the 10 m observed wind values, and the NCEP/NCAR Global reanalysis is used for the 925 hPa geostrophic wind values.

2.3 Precipitation Climatology

As previously detailed and as shown in Table 2.2, the average total amount of liquid equivalent precipitation at St. John's during the cool season is 982.5 mm. The highest monthly average amount is 161.9 mm during October, when a) convection may still be present with strong cold frontal passages and b) a number of tropical or recently transitioned extratropical cyclones have been known to influence the region (Hart and Evans 2001). November, December and January have similar amounts of average precipitation, while there is a stark dropoff in precipitation during February. While not crucial to this particular study, it is speculated here that this drop-off may be due in part to several factors, including more sea ice in the region (and therefore less surface moisture flux for a given storm to work with). This considered, however, St. John's receives more precipitation on average for every month in the defined cool season than any of the other capital cities in Atlantic Canada, with the minimal exceptions of Halifax in November, December, and March.

In order to compile a database of precipitation events for this study, we take the 6-hourly precipitation data provided and locate events that range anywhere from one precipitation recording period (6 hours) to eight recording periods (48 hours). This is done to keep a reasonable synoptic timescale in mind when compiling a list of events. Additionally, to ensure separation of precipitation events, there must be no fewer than two recording periods (12 hours) of zero precipitation. Finally, an event must consist of at least 0.2 mm of

precipitation. Given the parameters above, 1983 measureable precipitation events were recorded in the cool season from 1979-2005 (Table 2.1). As previously discussed, this is a larger number than that of any other capital city in Atlantic Canada during the same time period.

The next step in the process is to statistically analyze and separate the 1983 measureable precipitation events recorded at St. John's from 1979-2005. Here, we utilize a normal distribution, following the methodology of the work done on warm season precipitation events at Burlington, Vermont (Atallah et al. 2005). Accordingly, the mean precipitation amount (9.80 mm) and standard deviation (11.99 mm) are calculated. It is evident from the large value of the standard deviation that precipitation event amounts at St. John's are quite variable and can range anywhere from the minimum of 0.2 mm to a maximum of 82.2 mm. Once the mean and standard deviation have been calculated, the next step is to identify bins, or categorical thresholds, of precipitation amounts. This is done in a fashion similar to Atallah et al. (2005), whereby events with amounts of the mean plus two standard deviations or more (> 33.78 mm) are labeled extreme; the mean plus one-half to one standard deviation (15.81 to 21.79 mm) are moderate events; and the mean plus/minus one-half standard deviation (3.81 to 15.8 mm) are light events. As a result, we find 106 extreme events, 160 moderate events and 681 light events. It is evident (Fig. 2.3) that the number of light events (681) is more than double the value of the other categories combined, reinforcing the conclusion put forth by Sisson and Gyakum (2004) that light events tend to dominate the climatology at a given station. Finally, while the authors

acknowledge the fact that using a normal distribution in this study is unorthodox, it is a primary objective of this study to create categories of precipitation events that are well-separated from each other. The authors believe that this objective has been accomplished with the creation of the extreme, moderate, and light categories, whereby the median amount in each category falls in the 97th, 82nd, and 60th percentile, respectively (Fig. 2.3). It is true that the majority of cases (Fig. 2.3) are events with very small amounts of precipitation (5 mm or less), but these are generally cases that are not of concern in terms of forecasting. Using our methodology, we identify three distinctly separate, but important, classes of precipitation events. This classification can be used to conduct a synoptic analysis.

In order to deal with an equal number of cases in each category, we follow the methodology of Sisson and Gyakum (2004) and select fifty events from each category to be used in composite synoptic analyses. To accomplish this, the median for each category (as computed using the mean and standard deviation methodology described above) of precipitation events is calculated; this value is 41.1 mm for extreme events, 18.4 mm for moderate, and 8.4 mm for light events. Twenty-five events above and below the median for each category are taken as the group of fifty events to be utilized for synoptic compositing. The range of the fifty precipitation events in each category is as follows: 38.2 to 48.6 mm for the extreme events, 17.5 to 19.3 mm for the moderate, and 8 to 8.8 mm for the light.

2.4 Composite Results

2.4.1 Methodology

As Sisson and Gyakum (2004) point out, the reason for completing and displaying composite analyses is to "identify key synoptic-scale circulation features, and their climatological anomalies, associated with each of the intensities of precipitation." Moreover, examining circulation anomalies in addition to the full composite fields allows the depiction of the significance of a particular feature with respect to a monthly weighted 30-year (1971-2000) climatology derived from the NCEP Global Reanalysis dataset. In this study, composite and anomaly plots of selected atmospheric mass fields are displayed every twelve hours (these fields have been examined every six hours, but due to space concerns, are shown every twelve) from t = -48 hours to t = +12 hours (t = -48) 72 to t = +24 hours for the 500 hPa height anomaly plots; this is done specifically because statistically significant 500 hPa height anomalies are observed as early as t=-72 h), where t=0 h is the time of onset of the heaviest precipitation period. First, sea-level pressure anomalies are examined, followed by 500 hPa height and precipitable water. In the case of the 500 hPa height composites, a larger view is chosen for display to emphasize the importance of upstream anomalies. It should be noted that the precursor anomalies depicted in the 500 hPa height composites, while valid, should not be fully used in an operational sense until a check of null events has been completed. This is something that will be explored in future work. Finally, it is unclear exactly how much smearing there is involved with the composite process; however, while some smearing is to be expected in all

composites, frequency maps of 500 hPa vorticity and 850hPa height (similar to Fig. 2.2, but not shown for sake of brevity) depict storm tracks very similar to the composite mean tracks observed for all three precipitation intensity groups (extreme, moderate, light).

2.4.2 Sea-level Pressure (SLP)

2.4.2.1 Extreme Precipitation Cases

In the extreme precipitation cases (Fig. 2.4), the first sign of a statistically significant (at the 99% confidence level) negative SLP anomaly occurs at t=-48 h (Fig. 2.4a) and is centered over the southeastern United States. As the anomaly tracks northeastward over time, it grows in amplitude before it reaches a maximum of -18 hPa at t=0 h (Fig. 2.4e) near St. John's. It is also worth noting that a significant positive SLP anomaly develops downstream of the negative anomaly, beginning at t=-24 h (Fig. 2.4c) and grows in amplitude until it reaches a maximum intensity (highest closed contour) of +8 hPa at t=0 h (Fig. 2.4e).

In terms of the strengthening over time of the downstream positive SLP anomaly, it is important to recognize that two processes are in play here: 1) a stronger negative SLP anomaly would lead to strong warm-air advection decreasing with height, which would act to raise heights in the upper levels of the atmosphere, i.e. build an upper-level ridge just downstream of the surface SLP negative anomaly (Fig. 2.7f-g). This in turn would help to strengthen the surface positive SLP anomaly downstream of the upper-level ridge (Fig. 2.4c-f).

Moreover, 2) as extreme precipitation falls in association with the negative

anomaly, latent heat release in the atmosphere acts to diabatically enhance the upper-level ridge located just downstream of the surface cyclone around t=0 h (Fig. 2.7f-g). Consequently, the suggestion is that the diabatic enhancement of the upper-level ridge could also partially be responsible for the building of a stronger surface high pressure downstream, as is evident in the time evolution of the extreme SLP composite (Fig. 2.4c-f). Nevertheless, it is important to recognize that while the warm air advection and diabatic enhancement processes have the same effect, it is likely that both are at work here.

2.4.2.2 Moderate Precipitation Cases

A statistically significant negative SLP anomaly in the moderate composite is evident as early as t= -48 h (Fig. 2.5a) over the Ohio River valley. The initial location of the negative anomaly is farther north and west than in the extreme (Fig. 2.4a) composite. In addition, the negative anomaly proceeds on a more land-based track compared with the extreme composite. It is also of note that at t= +12 h (Fig. 2.4f), the statistically significant downstream positive SLP anomaly is less intense (by 2 hPa) and less broad than in the extreme composite. This is a suggestion that either or both of the indirect processes described above (warm air advection and the latent heating feedback mechanism) might have less of an impact in the moderate cases than in the extreme cases, as one would expect with both a weaker negative SLP anomaly and lesser amounts of precipitation.

2.4.2.3 Light Precipitation Cases

As in the extreme precipitation composites, a coherent statistically significant negative SLP anomaly is observed at t=-48 h (Fig. 2.6a). However, this negative anomaly is located over the upper Midwest region of the United States, far north and west of the initial anomalies in the extreme (Fig. 2.4a), and moderate (Fig. 2.5a) composites. Also unique to the light composite is the pure zonal track of the negative anomaly toward St. John's (Fig. 2.6a-e). Moreover, the negative anomaly reaches a maximum intensity of only -8 hPa at t=0 h (Fig. 2.6e), which is weaker than the other precipitation intensities. Finally, a weak downstream positive anomaly appears at t=-12 h (Fig. 2.6d), but only reaches a maximum intensity of 4 hPa at t=0 h (Fig. 2.6e) and t=+12 h (Fig. 2.6f), weaker than the positive anomalies in the other precipitation intensity composites. In the light composite, the cyclone responsible for the precipitation at St. John's resembles an Alberta clipper that forms in the lee cyclogenesis region of the Canadian Rockies.

2.4.3 500 hPa Height

2.4.3.1 Extreme Precipitation Cases

In the extreme precipitation composite, a statistically significant (at the 95% confidence level) positive anomaly is located over the Pacific Northwest region of the United States at t=-72 h (Fig. 2.7a). This anomaly grows in both areal extent and intensity by t=-36 h (Fig. 2.7d), at which time the first significant negative anomaly appears just east of the Mississippi River. Twelve hours later, at t=-24 h (Fig. 2.7e), a significant downstream ridge is located right over St. John's. As time proceeds, both the negative anomaly and downstream

positive anomaly grow in amplitude, while the upstream ridge weakens accordingly. The suggestion here is that the precursor ridge over the Pacific Northwest leads to downstream development of the negative anomaly over the Ohio valley, which in turn leads to the downstream ridge over Atlantic Canada. Similar features were noted by Lackmann and Gyakum (1996) in their study of precursor anomalies in the Northwest Territories of Canada. In their study, as well as in this one, the decay of the upstream ridge at the same time at which both the negative anomaly and downstream ridge amplify is consistent with the downstream propagation of Rossby wave energy with the group velocity (Lackmann and Gyakum 1996).

This assertion of downstream development is supported with a time-longitude plot of the meridional (v) component of the wind at 500 hPa (Fig. 2.8). This plot (Fig. 2.8) shows that in the extreme composite, a weak positive anomaly is seen around longitude 130 ° W beginning between t=-72 h and t=-60 h in association with the precursor positive height anomaly (Fig. 2.7a). This weak positive wind anomaly gives way to a stronger downstream (100 ° W) negative anomaly beginning at t=-48 h (and peaking at t=-24 h), in association with the negative height anomaly seen over the southeastern United States (Fig. 2.9). In turn, a downstream positive and second negative anomaly form at t=-24 h (70 ° W) and t=0 h (30 ° W), respectively. It is implied here (Fig. 2.8) that the downstream propagation of Rossby wave energy is evident in the extreme composite, as each 500 hPa meridional wind anomaly maximum lags the previous anomaly maximum in time.

It is also important to note that at t= 0 h (Fig. 2.7g), the negative anomaly associated with the surface cyclone affecting St. John's has reached a maximum of -120 m and the downstream positive anomaly has reached a maximum of +120 m, while the upstream ridge essentially disappears. The increase in amplitude of the negative anomaly associated with the surface cyclone suggests a positive increase in cyclonic vorticity advection at 500 hPa, which in turn would act to strengthen the surface cyclone.

2.4.3.2 Moderate Precipitation Cases

A precursor positive anomaly is depicted at t=-72 h (Fig. 2.9a); unlike in the extreme cases, however, the positive anomaly is located much farther to the north near the Gulf of Alaska. As time progresses, the positive anomaly extends southward into the Pacific Northwest region of the United States, and is of similar strength to the corresponding positive anomaly in the extreme composite at t=-36 h (Fig. 2.9d). Unlike in the extreme cases, however, the upstream positive anomaly does not shrink in areal extent or move eastward as time progresses.

The moderate cases are also different from any other precipitation intensity category because of the large areal extent of the negative anomaly over the eastern third of North America. This suggests that the track variability of the negative anomaly (trough) is largest in the moderate cases. While track variability is not examined explicitly in this paper, this will be a primary focus of future studies. In addition, the weaker downstream positive anomaly (+90 m at t= 0 h (Fig. 2.9g)) suggests four possible conclusions: a) the weaker negative SLP

anomaly (Fig. 2.5) produces less low-level warm air advection, leading to a weaker upper-level ridge (Fig. 2.9), b) the less overall precipitation associated with the surface cyclone produces less latent heat release and thus less downstream ridge intensification, c) the lack of weakening of the upstream positive anomaly is suggestive of the lack of downstream positive anomaly amplification, and d) a combination of (a), (b), and (c).

Finally, in terms of downstream development, a time-longitude plot for the moderate cases (Fig. 2.10) shows that while the initial weak positive 500 hPa meridional wind component anomaly is further to the west at t=-72 h and t=-60 h than in the extreme (Fig. 2.8) composite, Figure 2.10 does display a surprisingly coherent downstream development signal. The first negative meridional wind anomaly forms near 100° W at t=-36 h; although this anomaly is weaker than the negative anomaly seen in the extreme composite (Fig. 2.8), it does seem to excite a downstream positive (70° W) and second negative anomaly (40° W) at t=-24 h and t=0 h, respectively. This structure is very similar to the downstream development seen in the extreme cases (Fig. 2.8), and corresponds with the associated 500 hPa height anomalies observed for the moderate cases (Fig. 2.9).

2.4.3.3 Light Precipitation Cases

As in the sea-level pressure (SLP) composites, the light precipitation cases depict synoptic structures that are entirely different from the other precipitation intensities. In the light precipitation cases, a positive anomaly is apparent over western British Columbia at t = -72 h (Fig. 2.11a). However, unlike in the other

two precipitation intensity composites, this precursor positive anomaly has reached its maximum strength at t = -72 h (Fig 2.11a) and actually proceeds to retrogress northward into Alaska, as is evident by t = -36 h (Fig. 2.11d). At this time, a statistically significant negative height anomaly becomes visible over the upper Midwest region of the United States and Western Ontario. This formation location of the negative anomaly is farther to the north than in any of the other precipitation intensities, supporting the observation from the light SLP composite that light events are primarily driven by quick-moving Alberta Clipper systems that do not appear to have access to Gulf of Mexico moisture. In addition, a downstream positive anomaly is nearly non-existent, until a weak ridge appears at t= 0 h (Fig. 2.11g), east of St. John's. It is likely not coincidental that this occurs just as the negative anomaly reaches the Atlantic Ocean, finally encountering a significant moisture source. While the negative anomaly does reach an intensity, -90 m, at t= +12 h (Fig. 2.11h), similar to that of the negative anomalies moderate composite (Fig. 2.9h), the upstream positive anomaly is almost entirely nonexistent from early in the progression, and the downstream ridge is very weak, suggesting that downstream development plays a significantly reduced role here than it does in the other precipitation intensity composites. A time-longitude plot of the meridional wind component (Fig. 2.12) shows a weaker signal of downstream development than that seen in the extreme (Fig. 2.8) and moderate (Fig. 2.10) composites. In addition, the positive and negative 500 hPa meridional wind anomalies are observed (Fig. 2.12) at later initial times, in association with

the height anomalies previously discussed (Fig. 2.11), starting at t=-12 h, near longitudes 70 ° and 40 ° W, respectively.

2.4.4 Precipitable Water

Precipitable water (PW) composites are examined to explore the differences in terms of moisture among the various precipitation intensities, in addition to the basic synoptic structures examined in the SLP and 500 hPa height fields. The PW field allows us to compare the moisture source location and amount associated with each precipitation intensity category.

2.4.4.1 Extreme Precipitation Cases

It was shown using the sea-level pressure field that the cyclones responsible for the extreme precipitation cases at St. John's appear to originate near the Gulf of Mexico in the southeastern United States. Indeed, a statistically significant positive PW anomaly appears over Northern Florida at t= –48 h (Fig 2.13a). This anomaly proceeds to rapidly intensify as it moves northeastward in the Atlantic Ocean towards St. John's, reaching a maximum intensity of 14 mm at t= 0 h (Fig. 2.13e) near St. John's. In addition, a significant negative PW anomaly forms upstream of the positive anomaly, reaching a maximum intensity of -6 mm at t= 0 h (Fig. 2.13e) and creating a strong anomaly couplet.

2.4.4.2 Moderate Precipitation Cases

In the moderate cases, a statistically significant positive anomaly appears at 72 hours prior to the event (t=-72 h, not shown), in contrast to 48 hours prior

to the event in the extreme cases. In addition, the positive anomaly in the moderate cases originates (t=-48 h, Fig. 2.14a) a bit farther to the north and west, in the eastern Ohio valley. It was suggested earlier that the moderate composite contains the most variability among cyclone tracks; this theory is also supported by the large areal extent of the negative PW anomaly behind the cyclone, which ranges from the gulf coast region of the United States to Southern Quebec at t= 0 h (Fig. 2.14e). Finally, the elongated positive moisture anomaly in the Atlantic Ocean (Fig. 2.14e) is unique to the moderate cases (albeit a hint of such a feature can be seen in the extreme composite, Fig. 2.13). This feature suggests the possibility of a low-level jet or warm conveyor belt in advance of the cold front (i.e. the boundary between positive and negative precipitable water anomalies).

2.4.4.3 Light Precipitation Cases

As was the case in the SLP and 500 hPa height fields, the light PW composite is structurally unique among the three precipitation intensities. First, a significant positive anomaly does not become apparent until twelve hours before the maximum precipitation falls at St. John's (t=-12 h, Fig. 2.15d). It is not a coincidence that the appearance of this anomaly occurs just as the cyclone moves over water for the first time (Fig. 2.6d). This gives even more credence to the claim that the light cases are predominantly moisture-starved Alberta Clipper systems that only become statistically significant when they reach the first moisture source they encounter—the Atlantic Ocean. In terms of precipitable water, the positive anomaly only reaches a maximum (highest closed contour) of

6 mm at t= 0 h (Fig. 2.15e) near St. John's, and the anomaly couplet is much weaker (and has a much later time of onset) than in the other intensity composites. It is therefore clear from the PW field that the moisture source region plays a large role in the eventual amount of precipitation received at St. John's, and that significant differences exist between the precipitation intensities, regardless of the variability within a particular intensity.

2.5 Wind Analysis

2.5.1 Background and Climatology

In order to complete the synoptic analysis of the three precipitation intensities, it is useful to examine the winds at the time of heaviest precipitation, t= 0 h. Wind roses are utilized for this purpose because they show the frequency of occurrence of winds in specified wind direction sectors and wind speed classes, according to the Lakes Environmental website, available online at http://www.lakes-environmental.com. In recent studies, Nadeau (2007) and Knowland (2008) have used wind roses to illustrate both synoptic-scale and terrain-induced flows and effects at locations such as Iqaluit, Nunavut; Norman Wells, Northwest Territories; Montreal, Quebec; and Burlington, Vermont. In this paper, the 925 hPa geostrophic wind and the 10 m observed wind are both displayed using wind roses to illustrate a) the wind climatology at St. John's and b) the particular flows during certain classes (i.e. intensities) of precipitation events at St. John's. All wind roses displayed in this section are divided into

sixteen wind direction sectors and seven wind speed classes, which are (in knots): calm, 1-4, 4-7, 7-11, 11-17, 17-22, and greater than 22.

The wind climatology for the period of 1979-2005 at St. John's is displayed, for both the 925 hPa geostrophic wind (Fig. 2.16a) and 10 m observed wind (Fig. 2.16b). It is evident that the dominant geostrophic wind direction on a climatological basis at 925 hPa ranges anywhere from southwesterly to northwesterly, with pure westerly flow being the primary wind direction sector (Fig. 2.16a). While not a focus of this paper, terrain-induced channeling, friction, or both, seem to skew the climatological distribution towards more southwesterly flow when looking at the 10 m wind, although pure westerly flow remains primary sector (Fig. 2.16b). However, this difference is mitigated upon examination of the wind climatology in the cool season only (Fig. 2.17). From October-April, westerly flow is dominant in both the 925 hPa geostrophic wind (Fig. 2.17a) and the 10 m wind (Fig. 2.17b).

2.5.2 Wind Roses During Precipitation Events

Wind roses are displayed for the fifty extreme precipitation cases described in detail in Section 2.4 (Fig. 2.18). While the climatological wind direction at St. John's is from the west, it is evident that extreme precipitation events are associated winds that are predominantly out of the south-southeast (925 hPa geostrophic) and east (10 m wind) at t=0 h (Fig. 2.18). The geostrophic wind (Fig. 2.18a) is representative of the sea-level pressure pattern observed in the extreme composite (Fig. 2.5g); this pattern involves a strong maritime low-

pressure system located to the south-southwest of St. John's and moving northeasterly over time.

A clockwise rotation of the 925 hPa geostrophic wind distribution at t= 0 h from the extreme (Fig. 2.18a) to the moderate composite (Fig. 2.19a) is evident, with the predominant wind direction sector being south-southwesterly and a secondary maxima of southerly flow. This finding is consistent with a more continental-based storm track originating in the Ohio valley as described in section 4b. It is interesting to note that the 10 m observed wind profile (Fig. 2.19b) for the moderate cases also shows a similar clockwise rotation, with the primary wind direction sector being south-southeasterly. However, a strong secondary sector is found at easterly flow, perhaps suggesting that, as mentioned earlier, the moderate cases contain the largest track variability of any precipitation intensity class.

The clockwise rotation of the 925 hPa geostrophic wind distribution (Fig. 2.20a) described above concludes in the light events composite, where the predominant wind direction sector is south-southwesterly (as in the moderate composite) and secondary maxima are found in the southwesterly and west-southwesterly sectors. This is entirely consistent with the finding in Section 2.4.2.3 that the composite cyclone responsible for the light precipitation events is most likely an Alberta Clipper system that approaches St. John's from the west or west-northwest (Fig. 2.6g). Finally, it is of note that for all precipitation intensity categories, the 10 m observed wind distribution appears to be centered slightly

counter-clockwise of the 925 hPa geostrophic wind distribution. This difference can be explained primarily by friction, but again, it is possible that it is somewhat due to local terrain effects, a point that requires further investigation in the future.

2.6 Concluding Discussion and Future Work

In this study, a precipitation climatology is assembled and statistically analyzed for St. John's, Newfoundland and Labrador (CYYT), for the period of 1979-2005. During this time period, 1983 measurable (.2 mm or greater) precipitation events lasting no more than 48 hours are found to have affected St. John's. Events are then divided into three intensity categories (extreme, moderate, and light) based on the mean and standard deviation, as described in Section 2.3. In order to evaluate the synoptic structures associated with each precipitation intensity category, fifty events are selected from each category. This is done by choosing the twenty-five events above and twenty-five events below the median precipitation amounts in each intensity category.

Once the fifty events from each precipitation category have been chosen, composite and anomaly plots (relative to a 1971-2000 monthly-weighted climatology) from the NCEP Global Reanalysis are completed in order to compare synoptic structures and precursors among the four precipitation intensity categories. In the sea-level pressure (SLP) field for the extreme cases, a statistically significant negative anomaly is depicted over the southeastern United States (Fig. 2.4), two days (t= –48 h) prior to the onset of heaviest precipitation at St. John's. This anomaly then tracks northeastward and reaches St. John's at

t=0 h, with a peak strength of -18 hPa. Precursor negative anomalies are also observed in moderate (Fig. 2.5) and light (Fig. 2.6) composites, but all of these anomalies differ in two respects: a) initial time of observation, and more importantly, b) initial region of observation. While the precursor negative anomaly in the extreme composite is centered near the Gulf Coast region over the southeastern United States, the precursor negative anomalies in the moderate (Ohio valley region) and light cases (upper Midwest region of the United States) are initially observed significantly farther to the north and west of the anomalies in the extreme composite. This observation leads to the conclusion that with decreasing precipitation amount, the track of the SLP anomaly becomes less meridional and more zonal. In other words, there is a clockwise rotation of both the initial observation area and composite storm track as the precipitation intensity category decreases from extreme to light. Additionally, the intensity of the downstream high pressure system is greater in the extreme composite than it is in the moderate and light cases. This suggests that perhaps both the strength of the negative SLP anomaly (through low-level warm-air advection) and the intensity of precipitation (through latent heat release) act to strengthen the upperlevel ridge and thus indirectly impact the intensity of the downstream positive SLP anomaly (as described in Section 2.4.2). Finally, it is of note that the average duration of the events (in 6-hour precipitation periods) is considerably shorter in the light and moderate groups than in the extreme cases. Due to space considerations, these results are not graphically shown in the paper, although it has been concluded that of the fifty extreme events, only six lasted less than

twenty-four hours (or four precipitation periods), while there are nineteen and twenty-nine such events in the moderate and light cases, respectively. This suggests that duration, in addition to anomaly intensity, differ among the three composite groups, although duration and intensity are not necessarily independent of each other.

Composite anomaly plots of 500 hPa height depicted in Section 2.4.3 are used to examine upper-level synoptic structures associated with each precipitation intensity category. The extreme (Fig. 2.7) composite demonstrates that a statistically significant precursor positive height anomaly is observed over the Pacific Northwest region of the United States at t = -72 h, or three days prior to the onset of heaviest precipitation observed at St. John's. This precursor anomaly dissipates over time concurrent with a significant negative anomaly and second positive anomaly building downstream. Additionally, the formation of downstream anomalies (Fig. 2.8) is at least in part due to Rossby wave propagation, as also noted by Lackmann and Gyakum (1996). While the precursor positive anomaly in the moderate composite is located much farther to the north at t = -72 h over British Columbia, downstream Rossby wave propagation does appear to play a role in the formation of the downstream negative and positive anomalies (Fig. 2.10). The light case composite reveals that downstream development due to Rossby wave propagation is weaker and has a later time of onset in our analysis (Fig. 2.12). There is also less southward impingement of the 500 hPa trough (negative anomaly) over the eastern United States, associated with the precipitation-causing cyclone, with decreasing

precipitation amount. Finally, it is of note that a quick calculation (not shown here) of the Rossby wave phase speed both a) agrees with the observed speed of translation of the primary trough in each composite and b) that the primary trough in each composite is faster-moving in the light as compared to the moderate cases and in the moderate cases as compared to the extreme composite. This supports the assertion mentioned above that duration and intensity of the precipitation-causing features are both in play.

Precipitable water (PW) composite anomaly plots are presented in Section 2.4.4, in order to evaluate the amount and origin of the moisture associated with each precipitation intensity category. From these analyses, several conclusions are drawn:

- In the extreme cases, a significant positive PW anomaly can be seen as early as t= -48 h over Northern Florida. The initial location of this positive anomaly travels progressively farther to the north and west with decreasing precipitation amount, signaling a more continental-based moisture source for the lesser intensity categories. This is also consistent with the clockwise rotation of storm tracks seen in the SLP composites.
- The time at which a statistically significant positive PW anomaly becomes visible is different for the various precipitation intensities. For example, in the extreme composite, an anomaly is first seen at t= -48 h; t= -72 h in the moderate; and not until t= -12 h in the light composite. It is suggested here that this is at least partially a result of composite smearing.

- The results in the PW analysis for the light cases are consistent with those shown in the SLP and 500 hPa height analyses. After completing a case-by-case map analysis, it is clear that the overwhelming majority of storm systems responsible for the light cases are Alberta Clippers originating in the lee of the Canadian Rockies. In fact, this system appears to be so moisture-starved that a positive PW anomaly does not appear until t= –12 h, when the cyclone finally reaches its first moisture source, the Atlantic Ocean.
- The moisture anomaly couplet in the extreme cases is noticeably stronger than in the moderate, and especially, the light composite. The fact that very moist air is closely located to very dry air suggests a strong baroclinic zone in the region between the positive and negative moisture anomalies. This, in turn, would be a very conducive environment for low-level cyclogenesis, a reflection of which is seen in the extreme SLP composite (Fig. 2.4).

Lastly, an analysis of the distributions of wind speed and direction at the time of heaviest precipitation at St. John's (t=0 h) is performed in Section 2.5. It is found that there is a preference for low-level (925 hPa) easterly and southeasterly geostrophic winds during extreme precipitation events at St. John's (Fig. 2.18). This direction is not favored at all in the cool-season climatology (Fig. 2.17). In addition, a clockwise rotation of the preferred 925 hPa geostrophic wind direction from east-southeasterly to southwesterly occurs with decreasing

precipitation amount. This observation is consistent with both the SLP and PW fields, where a clockwise rotation of the composite storm track is observed. In other words, a more meridional, ocean-based storm track in the extreme cases is more likely to produce an easterly geostrophic wind at St. John's, whereas a more zonal, continental-based storm track in the light cases is more apt to produce a southwesterly geostophic wind, with the moderate composite somewhere in between. Additionally, the more easterly near-surface winds seen in the extreme composite implies more veering (and thus warm-air advection) throughout the column, compared with the moderate and light cases. This, combined with the finding of the stronger baroclinic zone in the extreme composite described above and the longer average duration of extreme events suggests that the extreme composite shows more forcing for ascent over a generally longer period of time (and thus presumably, more precipitation) than the lesser composites, and should be viewed as a signal that a forecaster would be able to look for during and before extreme events.

There is much work to be done in the analysis of significant precipitation events at St. John's. Future work will include but not be limited to: an investigation of the variability of storm tracks and synoptic structures *within* each precipitation category; an examination of radar images for a subset of precipitation events, to assess the importance of precipitation banding; an evaluation of precipitation events with regard to the North Atlantic Oscillation (NAO). The authors hope that answers to these questions will provide insight and

knowledge to the local forecaster, which will help to improve short-term forecasts at St. John's and similar stations.

Location	# of cool-season measurable precipitation events (1979-2005)
Fredericton, NB (CYFC)	1531
Charlottetown, PEI (CYYG)	1871
Halifax, NS (CYHZ)	1742
St. John's, NF (CYYT)	1983

Table 2.1: The number of cool-season (October-April) measurable precipitation events at four selected station in Atlantic Canada.

	Fredericton (mm)	Charlottetown (mm)	Halifax (mm)	St. John's (mm)
October	97.7	108.6	128.7	161.9
November	103.2	110.8	146	144
December	107.8	123.1	154.8	148.8
January	109.6	106.4	149.2	150
February	79.2	85.5	114.4	125.2
March	102.7	91.8	134.5	130.8
April	87.4	87.8	118.3	121.8
Total	687.6	714	945.9	982.5

Table 2.2: Mean monthly precipitation amounts for the four capital cities in Atlantic Canada during the cool season (October-April).

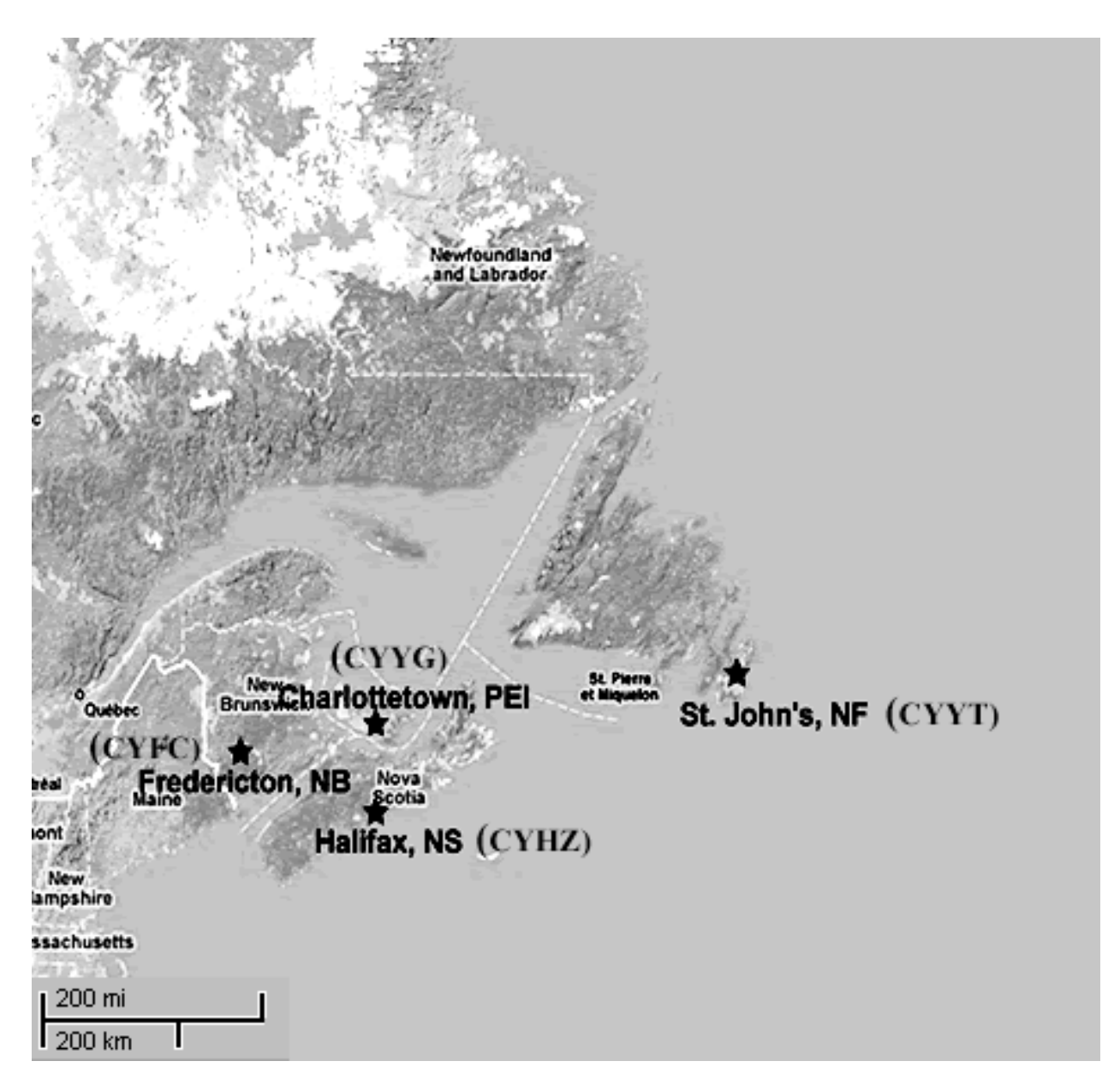


Figure 2.1: The geography of Atlantic Canada, with the capital city of each province identified, and scale as shown.

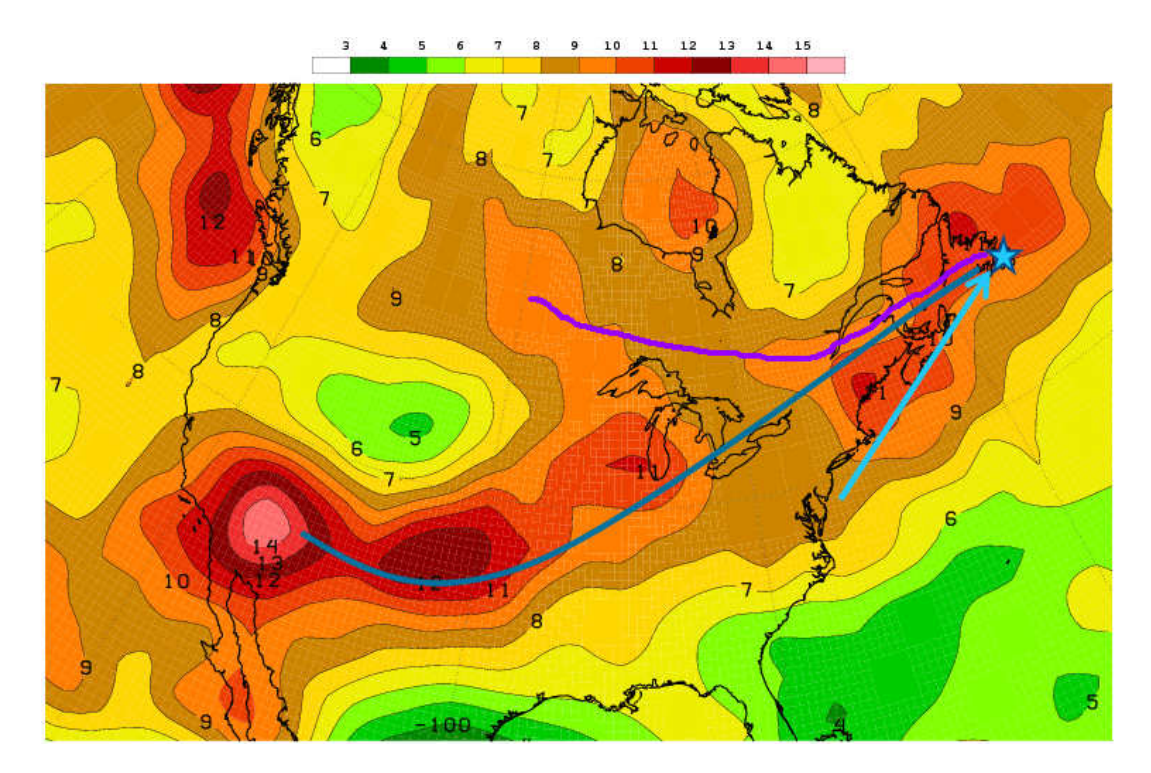


Figure 2.2: October-April 30-year (1971-2000) climatological frequency of 500 hPa absolute vorticity centers, calculated by counting the number of absolute vorticity maxima in the region shown; this roughly depicts the mean North American storm tracks and their importance to Atlantic Canada. The units are number of events per 5 degree by 5 degree area (approximately 500 sq. km) and calculations are completed using the NCEP global reanalysis.

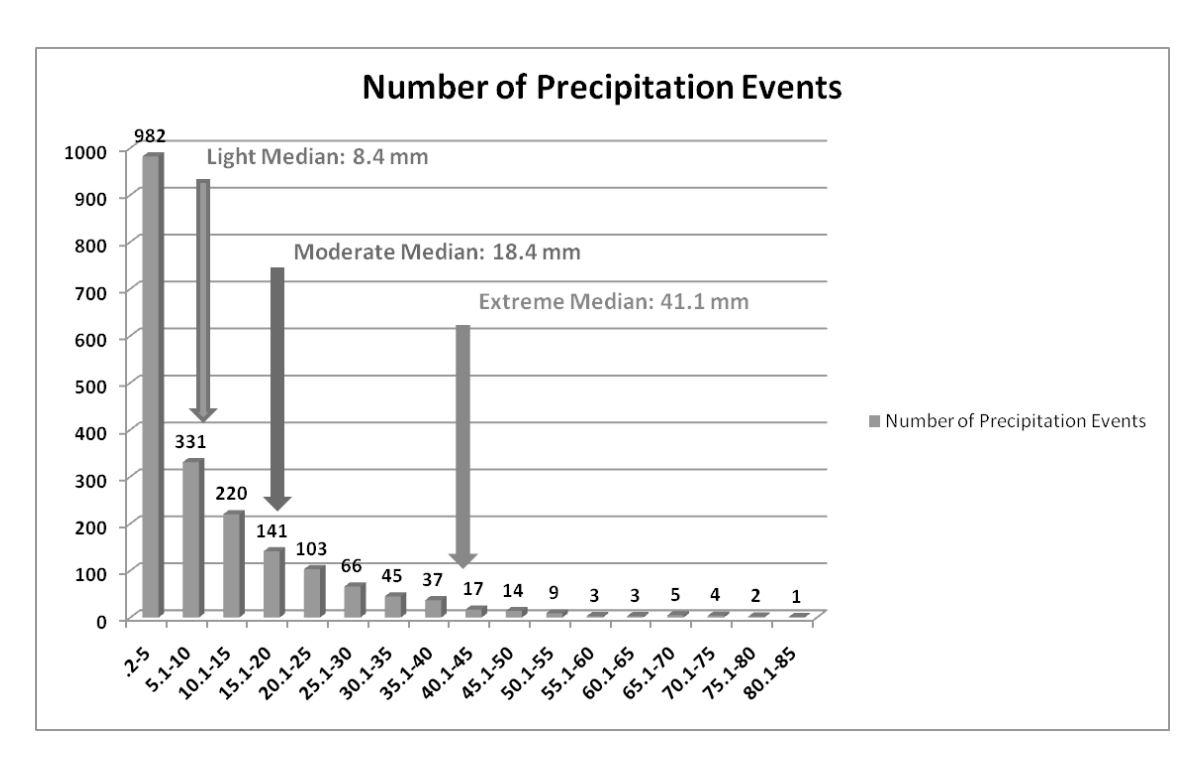


Figure 2.3: The precipitation event distribution histogram, depicting bins every 5 mm, and with the median of each precipitation category indicated.

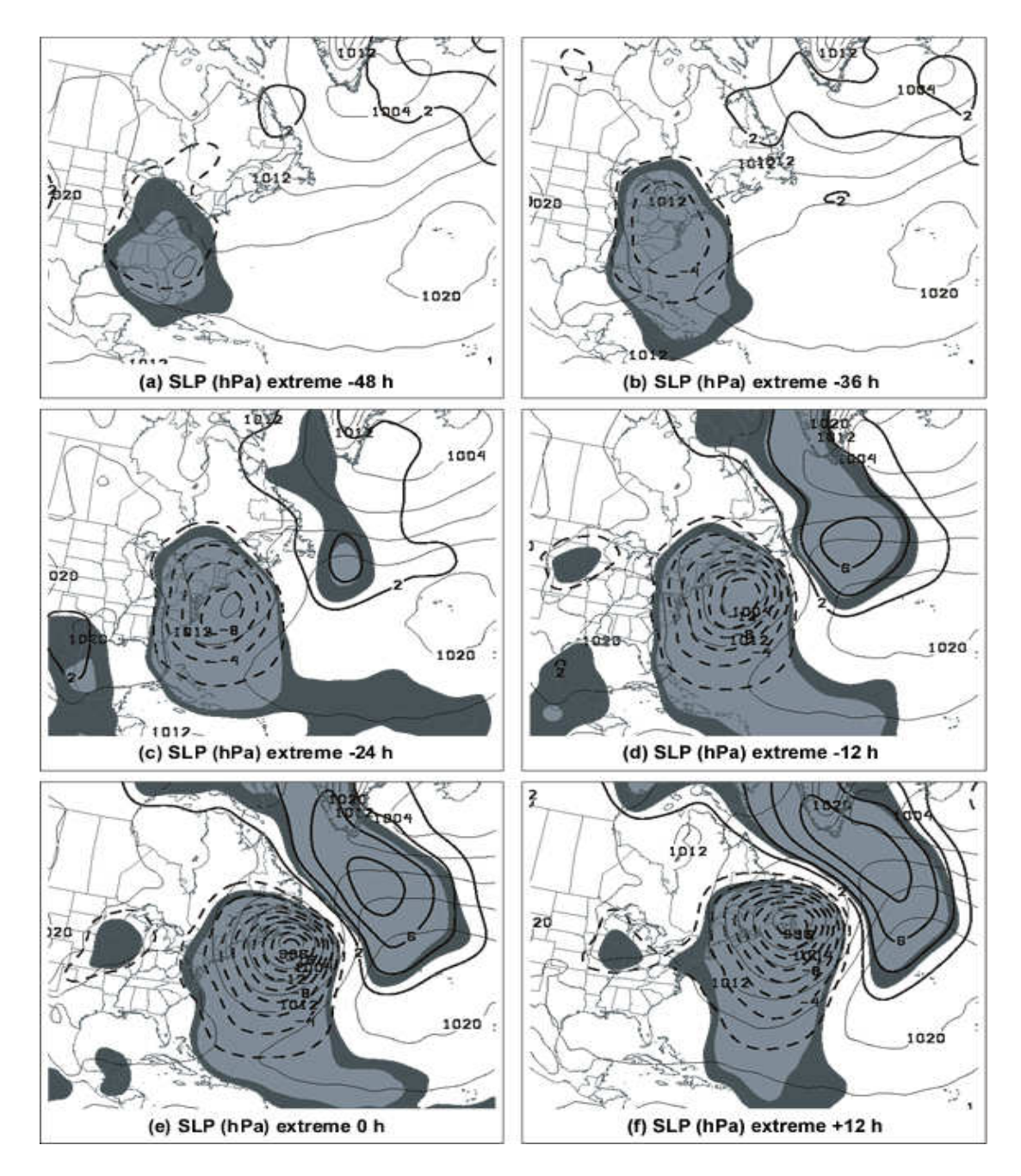


Figure 2.4: Sea-level pressure (SLP) anomalies every 2 hPa, heavy dashed for negative values and heavy solid for positive values, with respect to climatology, for the extreme cases at (a) -48, (b) -36, (c) -24, (d) -12, (e) 0, and (f) +12 h. Light solid contours represent full composite SLP field, every 4 hPa. Shading represents statistical significance of the anomalies at the 95% (darker shading) and 99% (lighter shading) confidence levels, according to the Student's t test. All fields are derived from the NCEP global reanalysis.

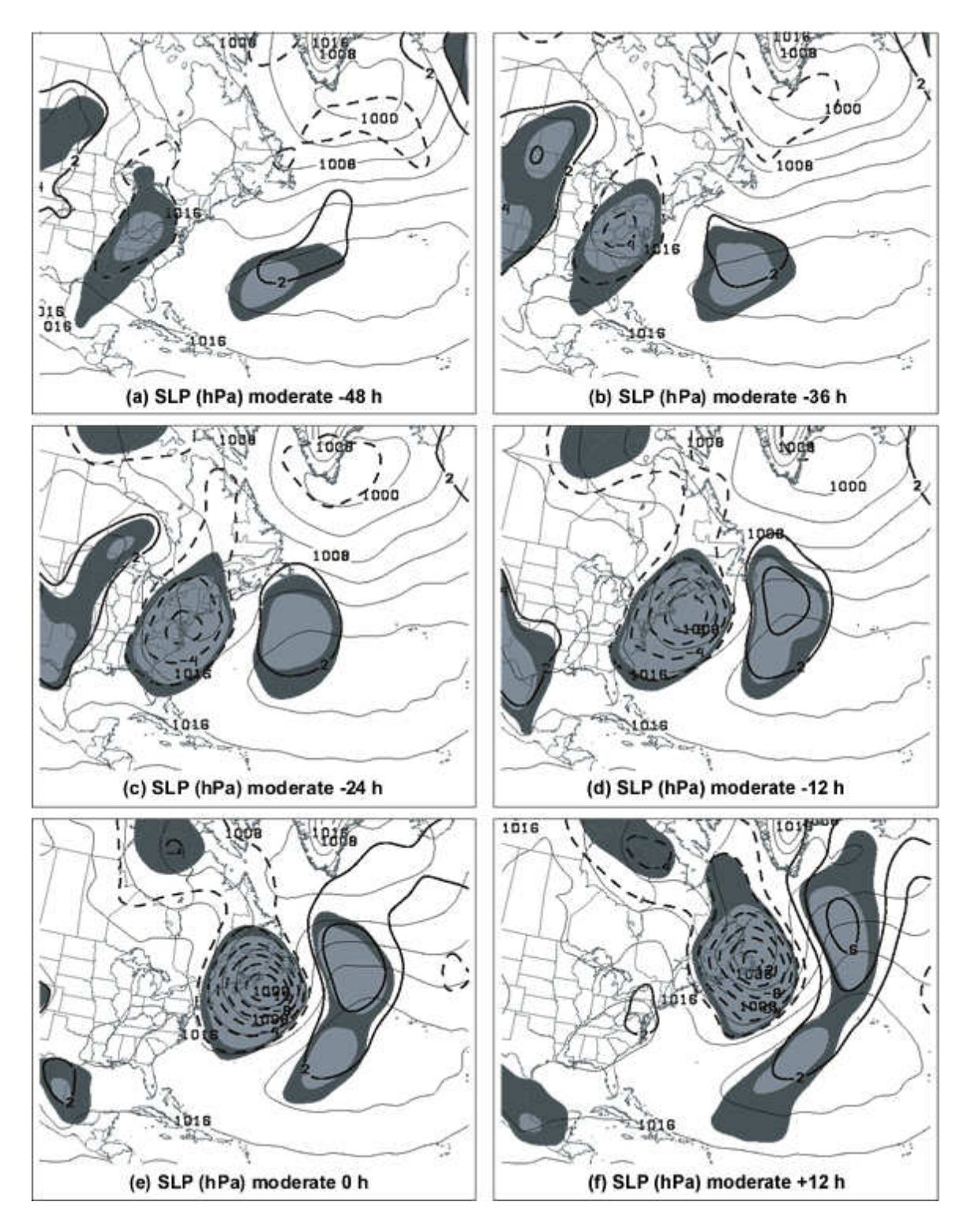


Figure 2.5: As in Fig. 2.4, but for the moderate cases.

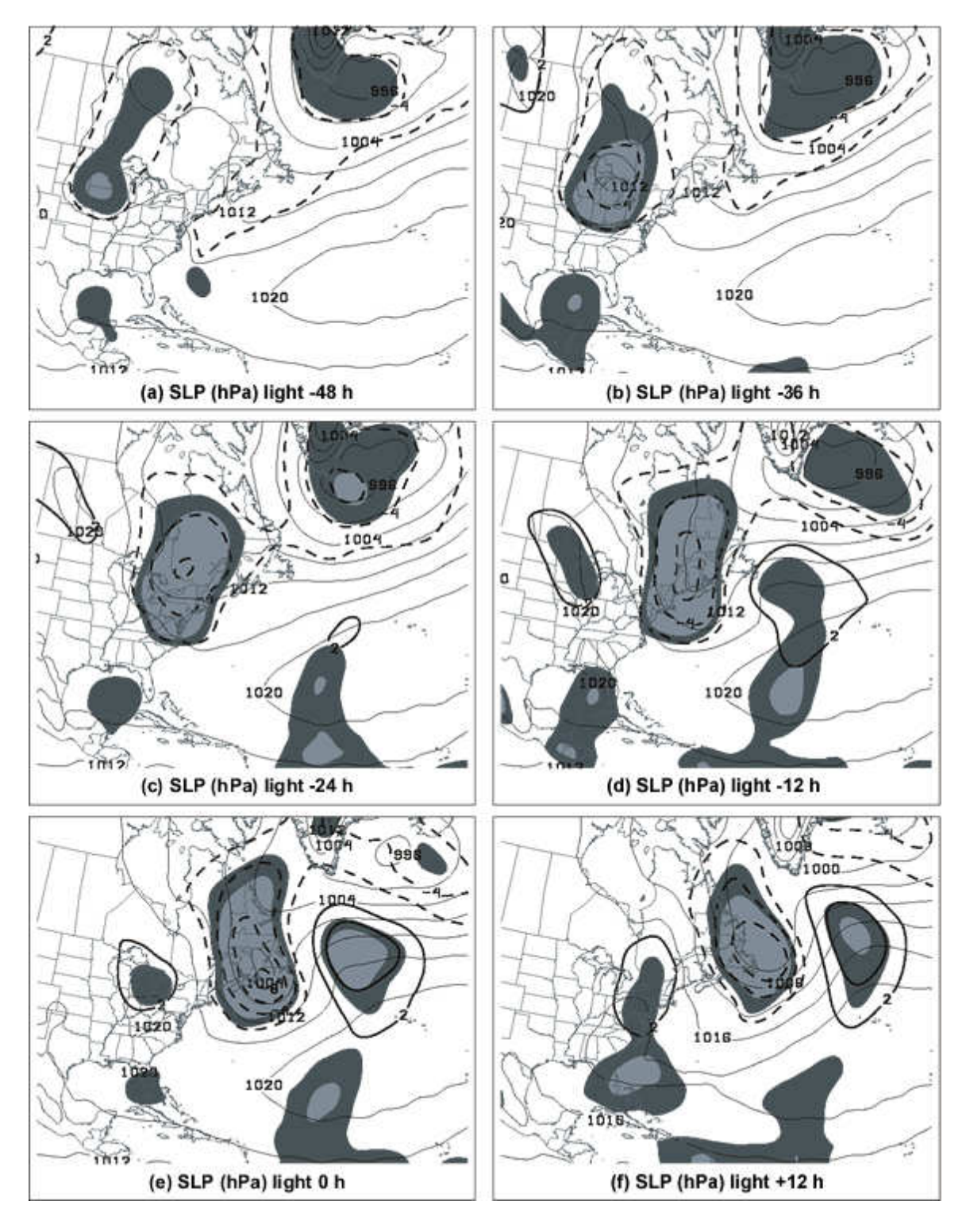


Figure 2.6: As in Fig. 2.4, but for the light cases.

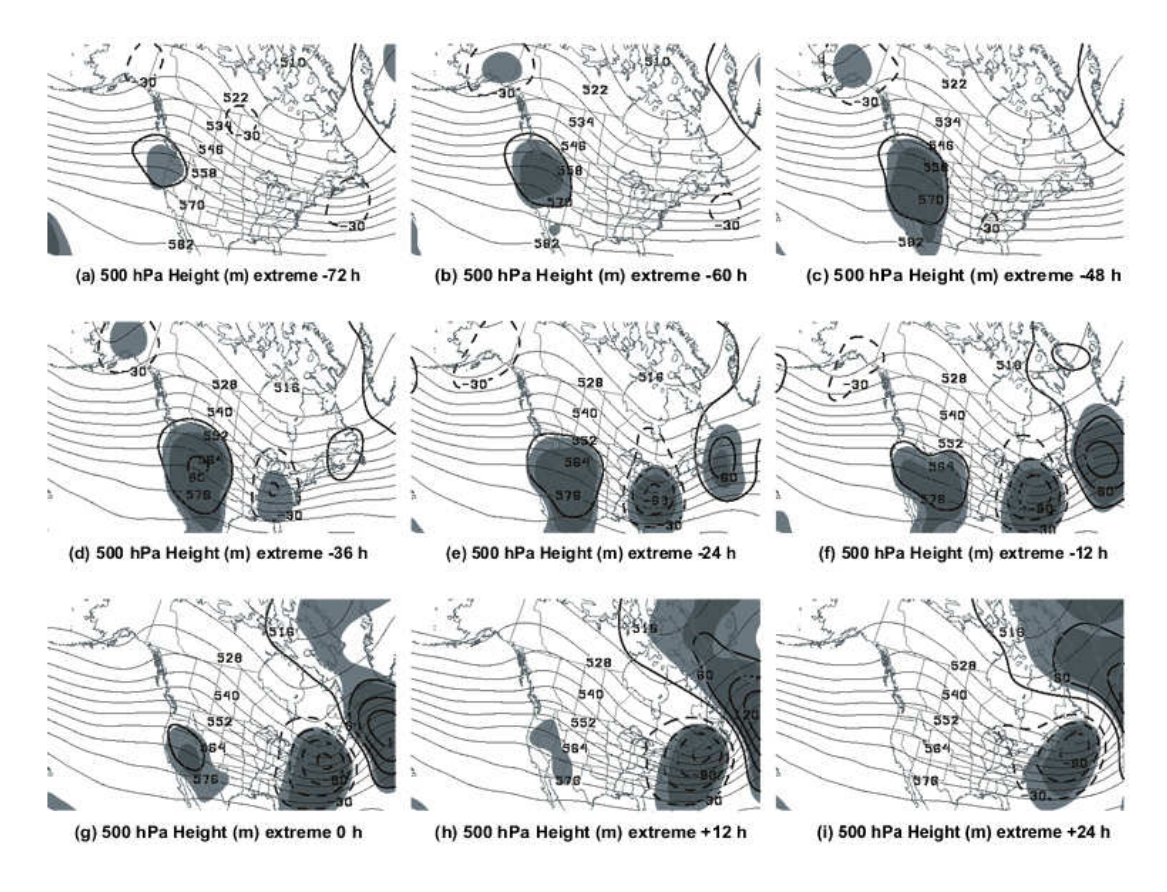


Figure 2.7: 500 hPa height anomalies every 3 dam, heavy dashed for negative values and heavy solid for positive values, with respect to climatology for the composite of the extreme cases at (a) -72, (b) -60, (c) -48, (d) -36, (e) -24, (f) -12, (g) 0, (h) +12, and (i) +24 h. Light solid contours represent full composite 500 hPa field, every 6 dam. Shading represents statistical significance of the anomalies at the 95% (lighter shading) and 99% (darker shading) confidence levels, according to the Student's t test. All fields are derived from the NCEP global reanalysis.

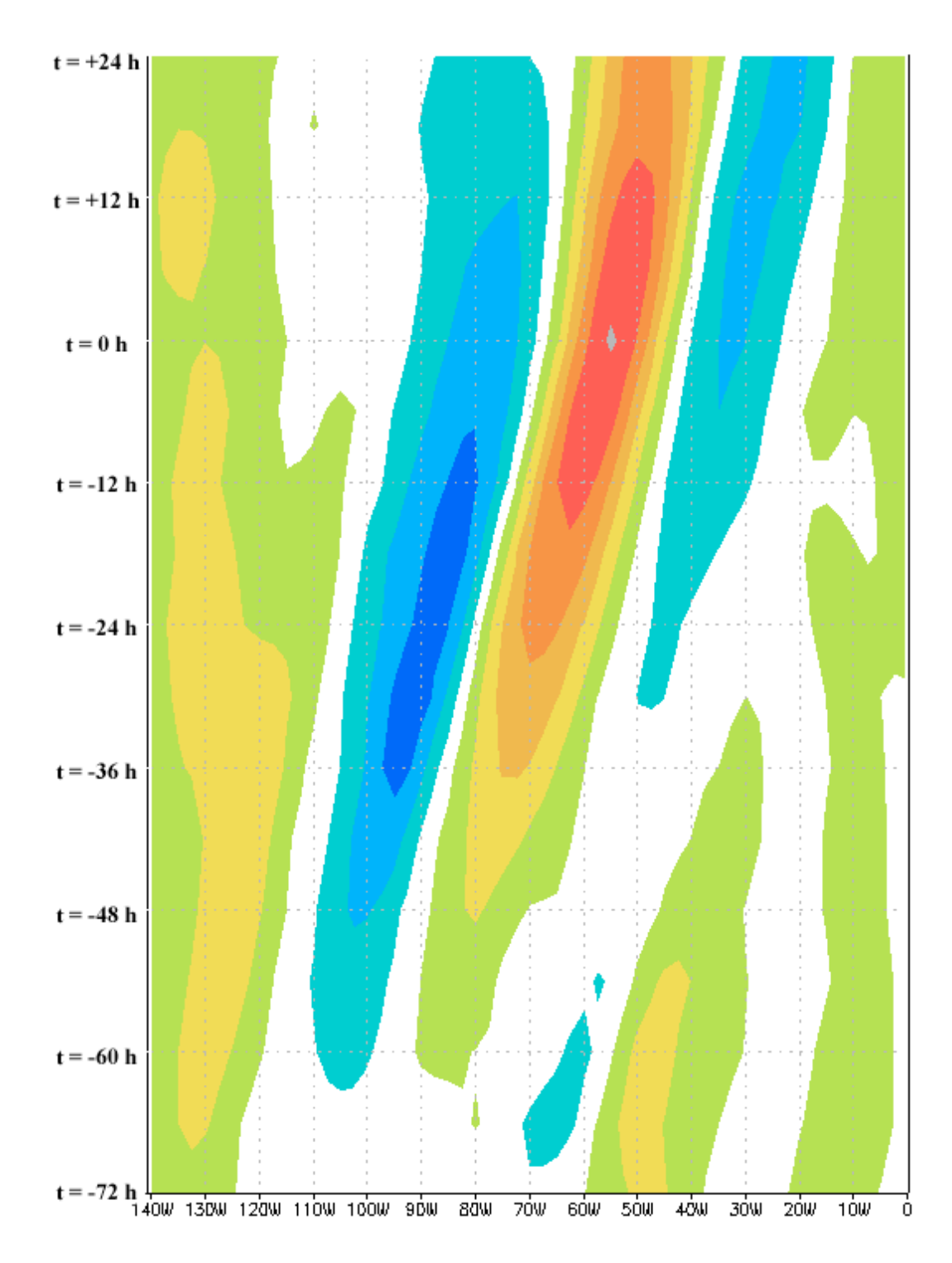


Figure 2.8: Time-longitude plot of the 500 hPa meridional (v) component of the wind anomalies relative to climatology at latitude 40° North (every 3 m s⁻¹, shaded warm colors for positive and cool colors for negative) for the extreme cases from t=-72 h to t=+24 h. All fields are derived from the NCEP global reanalysis.

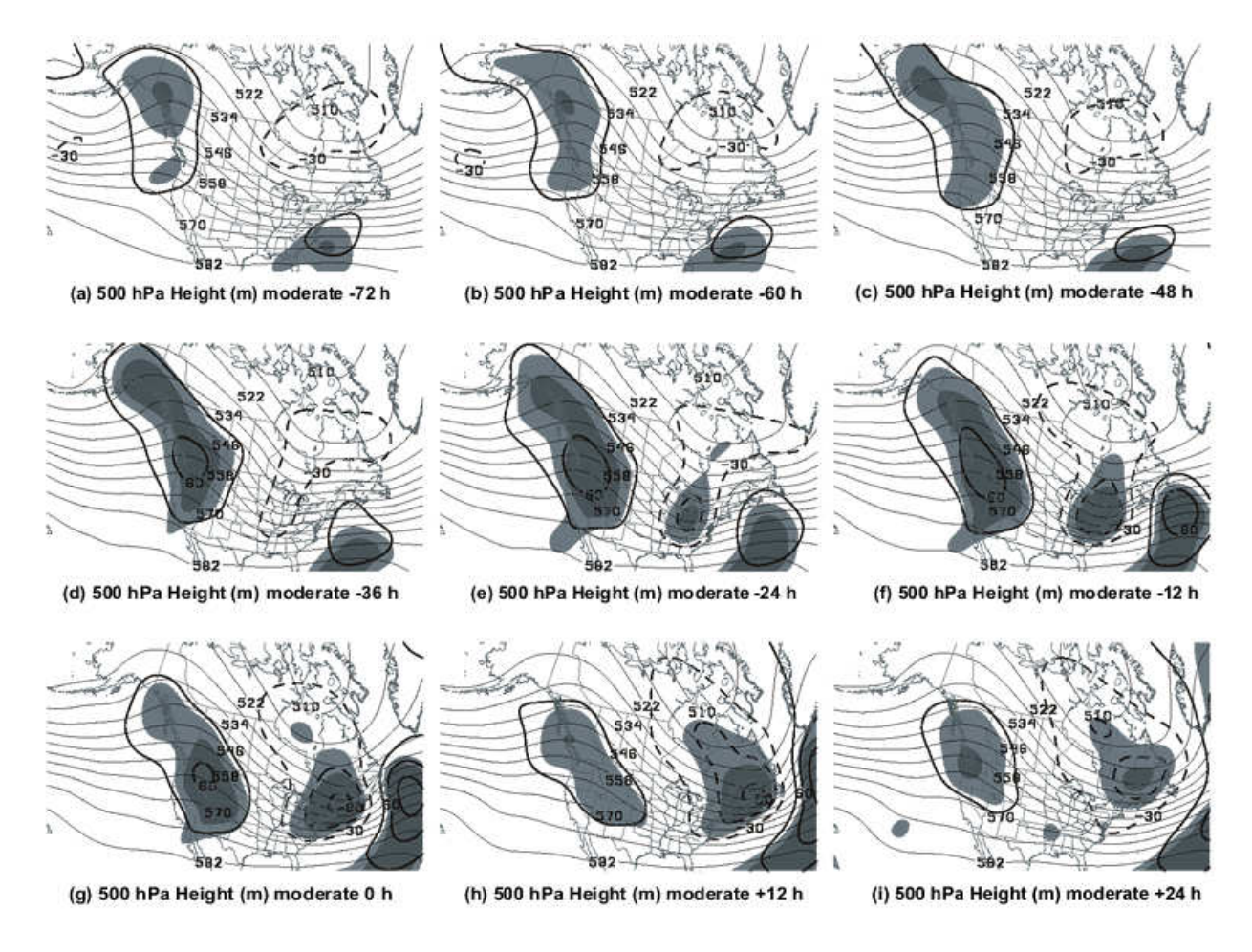


Figure 2.9: As in Fig. 2.7, but for the moderate cases.

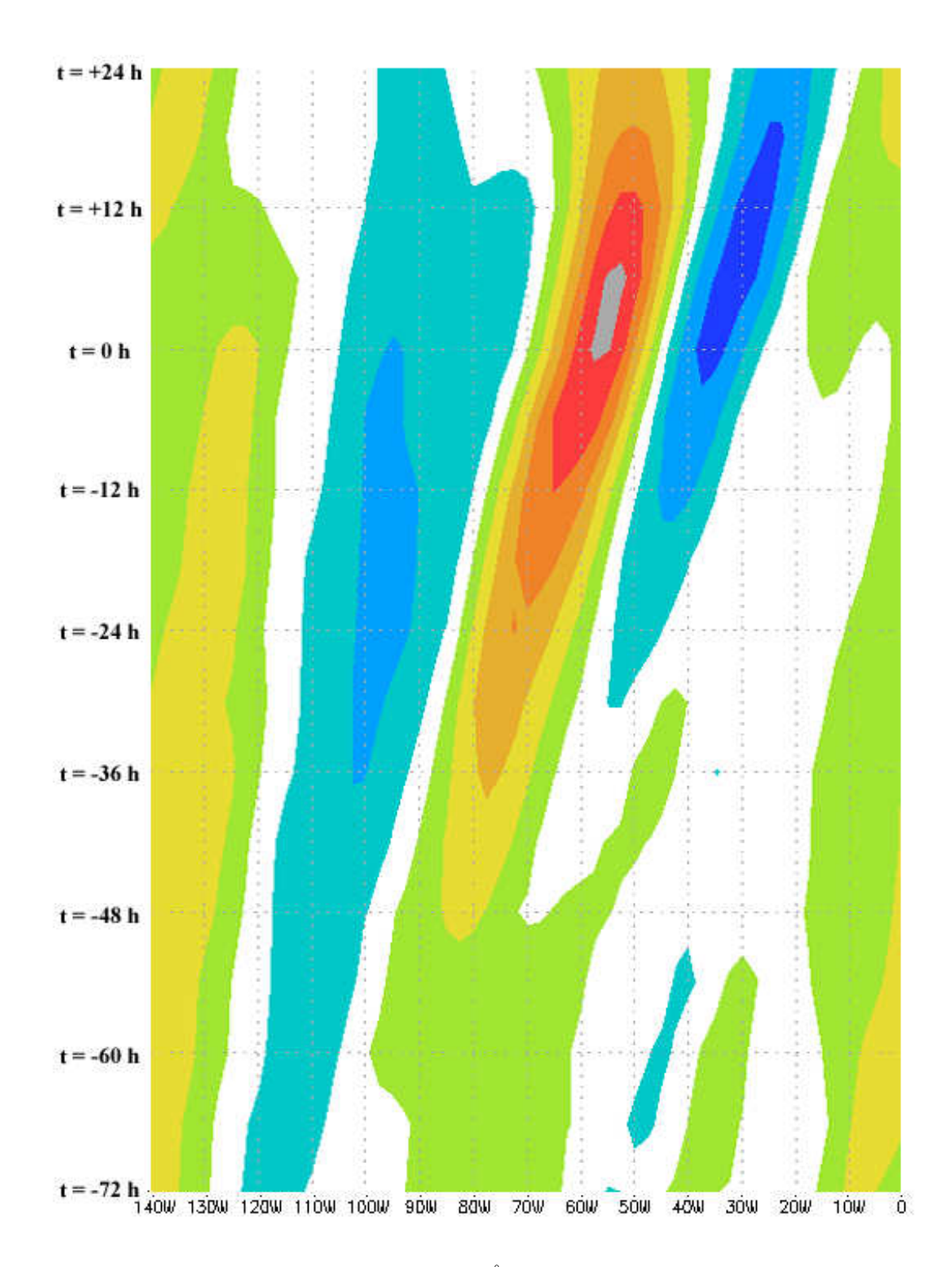


Figure 2.10: As in Fig. 2.8, but at latitiude 45° and for the moderate cases.

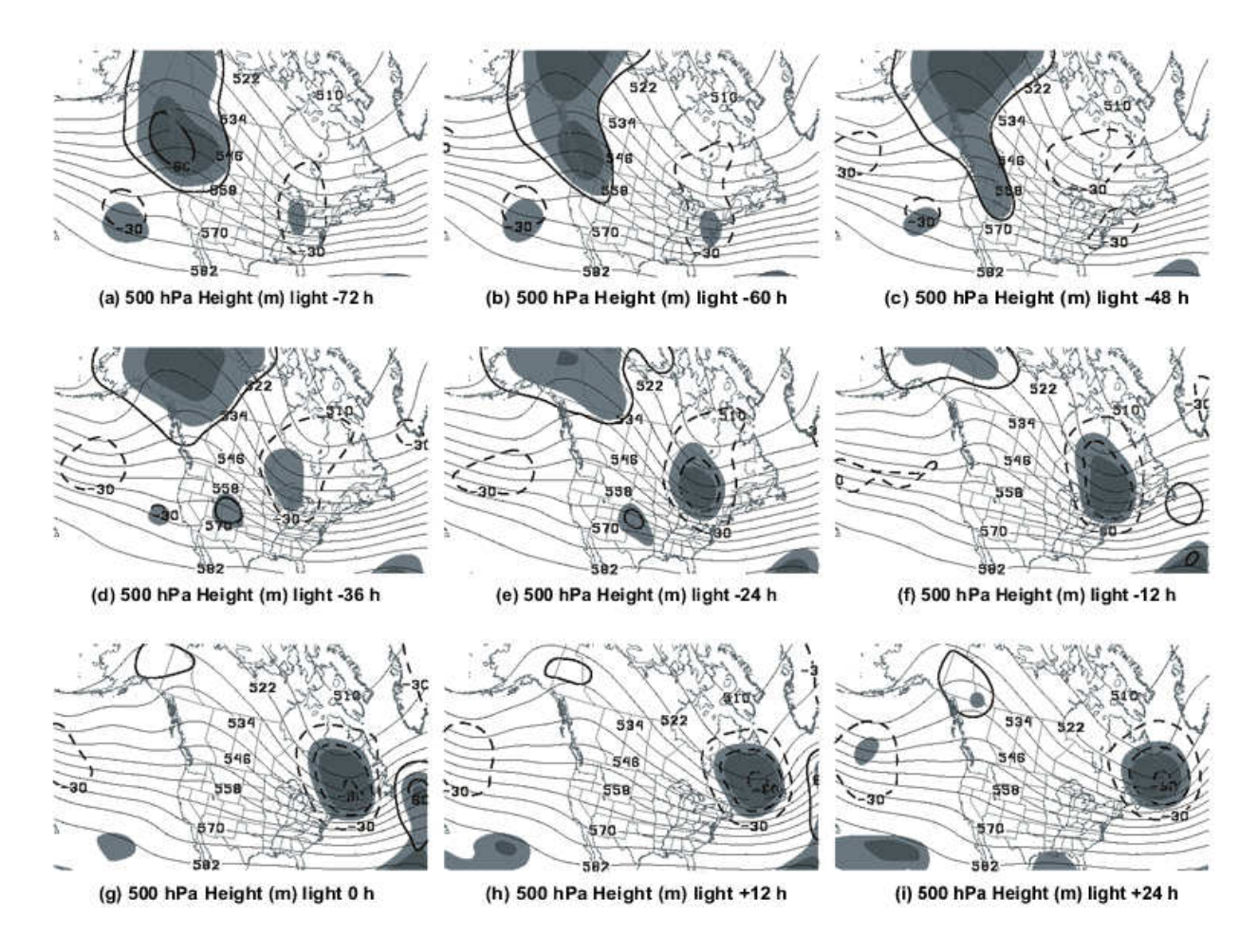


Figure 2.11: As in Fig. 2.7, but for the light cases.

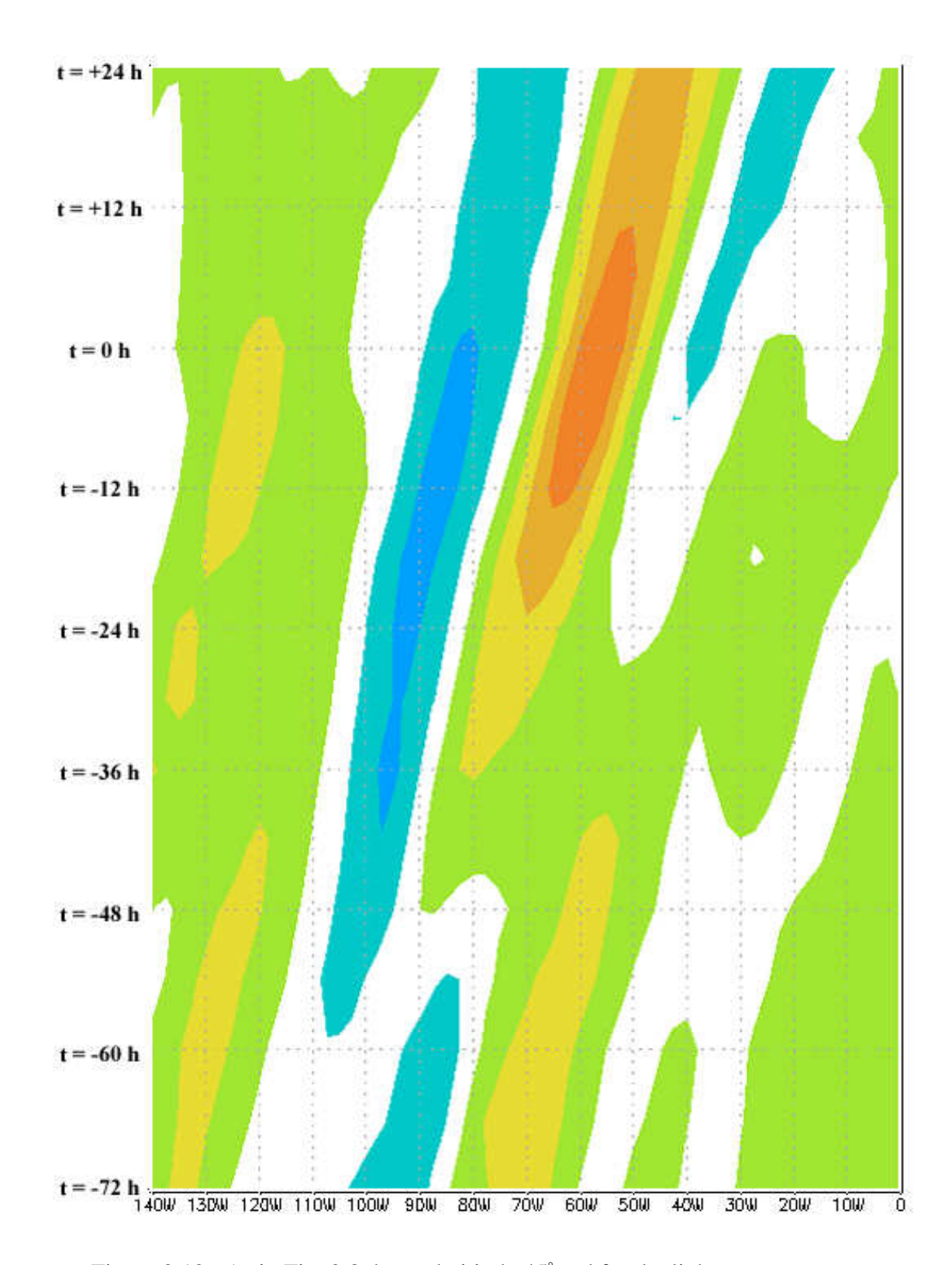


Figure 2.12: As in Fig. 2.8, but at latitude 45° and for the light cases.

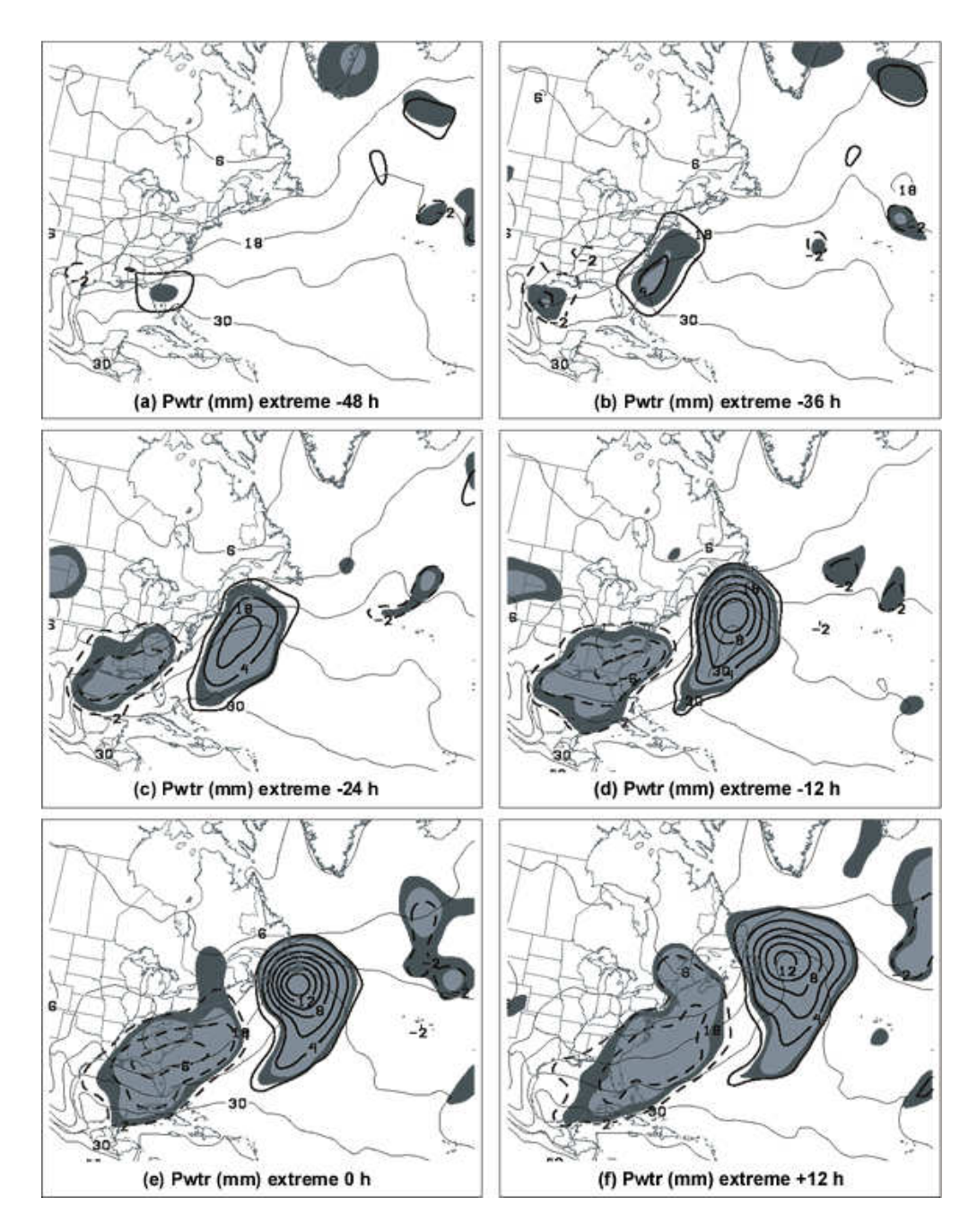


Figure 2.13: Precipitable water anomalies every 2 mm, heavy dashed for negative values and heavy solid for positive values, with respect to climatology, for the extreme cases at (a) -48, (b) -36, (c) -24, (d) -12, (e) 0, and (f) +12 h. Light solid contours represent full composite precipitable water field, every 6 mm. Shading represents statistical significance of the anomalies at the 95% (lighter shading) and 99% (darker shading) confidence levels, according to the Student's t test. All fields are derived from the NCEP global reanalysis.

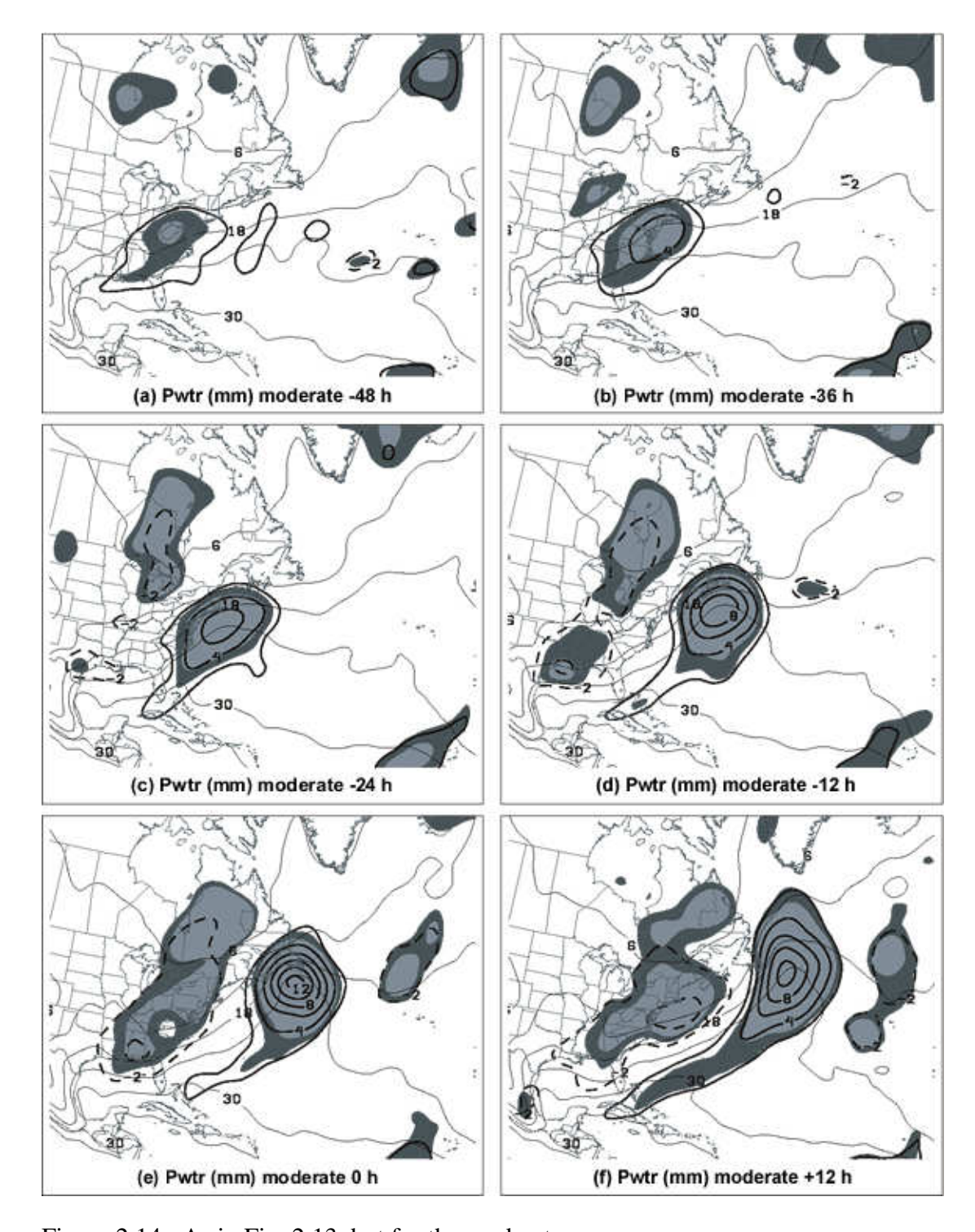


Figure 2.14: As in Fig. 2.13, but for the moderate cases.

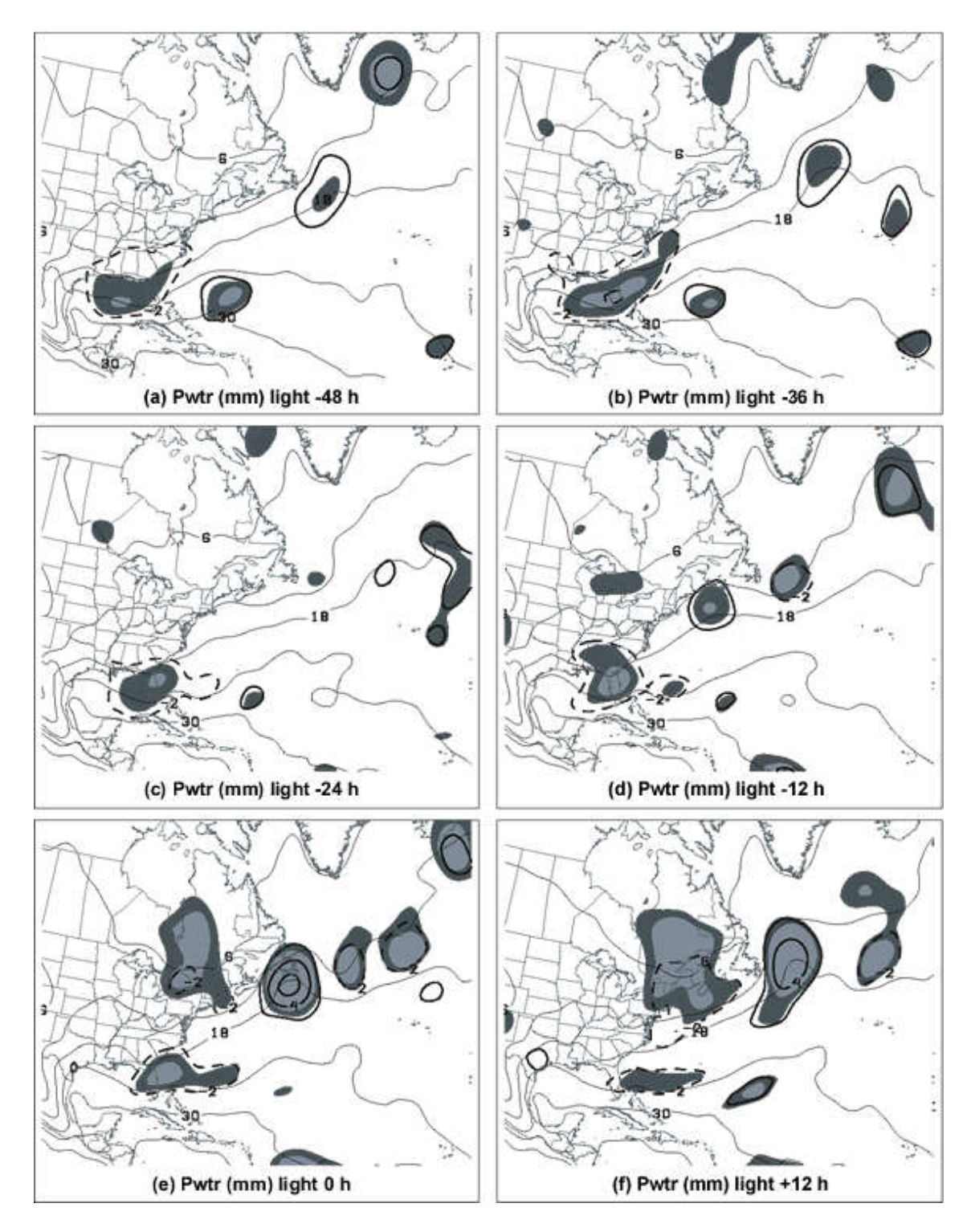


Figure 2.15: As in Fig. 2.13, but for the light cases.

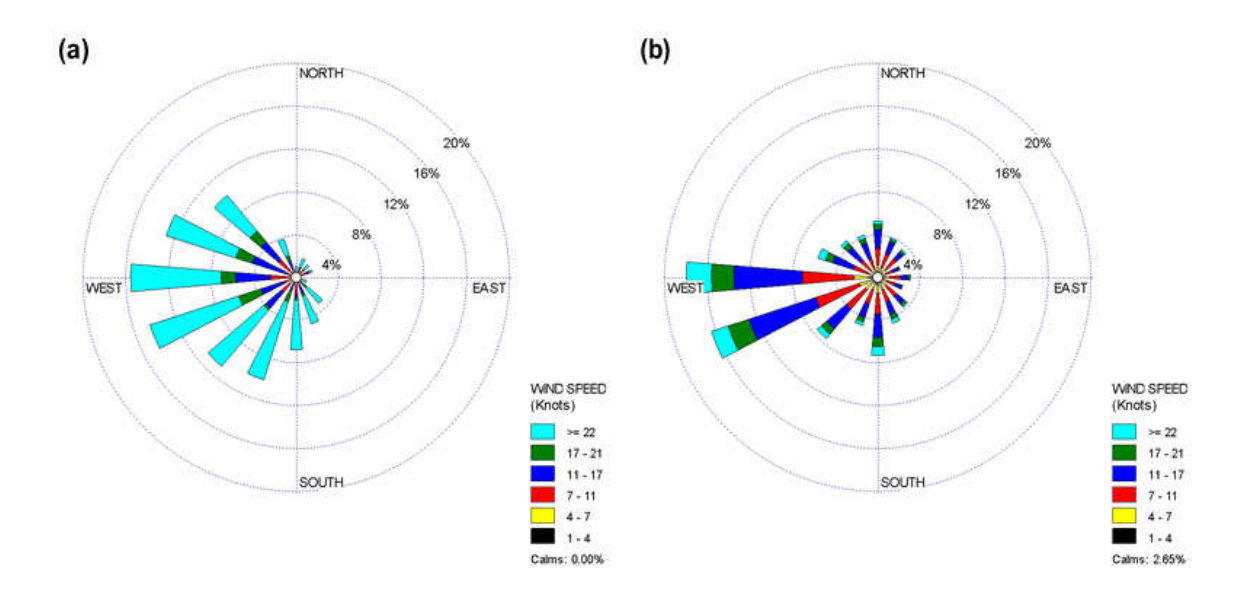


Figure 2.16: Wind rose climatology for the period from 1979-2005, all months inclusive, at St. John's (YYT) (a) 925 hPa geostrophic wind derived from the NCEP global reanalysis and (b) 10 m observed wind, from station data. Wind classes are as follows: 1-4 knots (black), 4-7 knots (yellow), 7-11 knots (red), 11-17 knots (blue), 17-21 knots (green), and greater than 22 knots (turquoise).

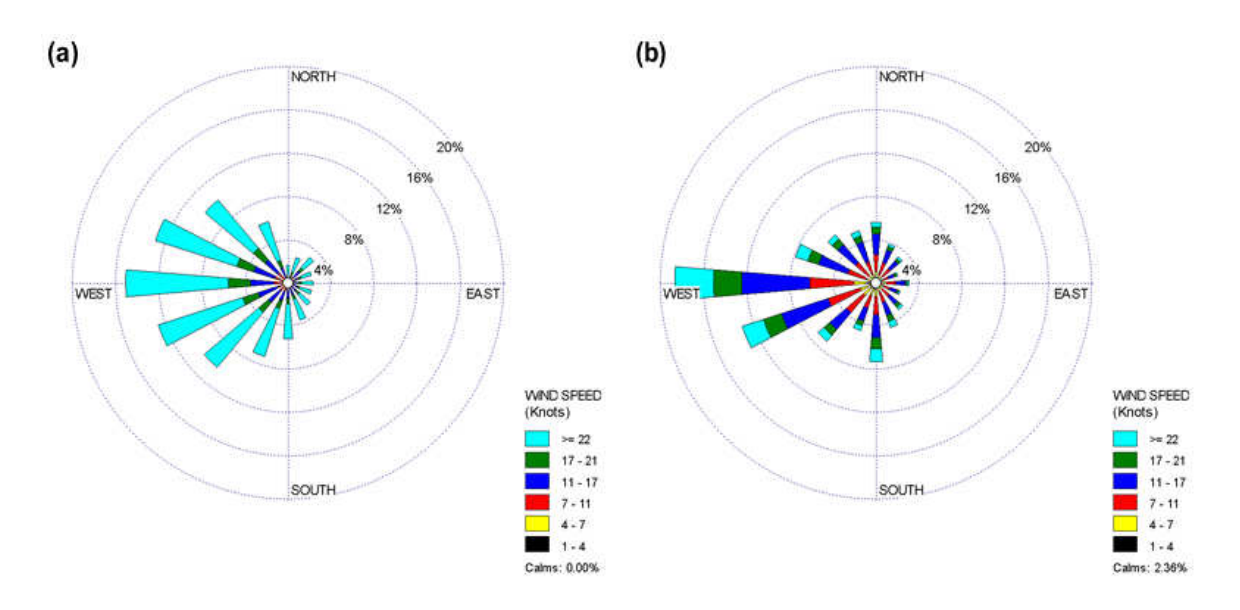


Figure 2.17: As in Fig. 2.16, but for 1979-2005, October-April only.

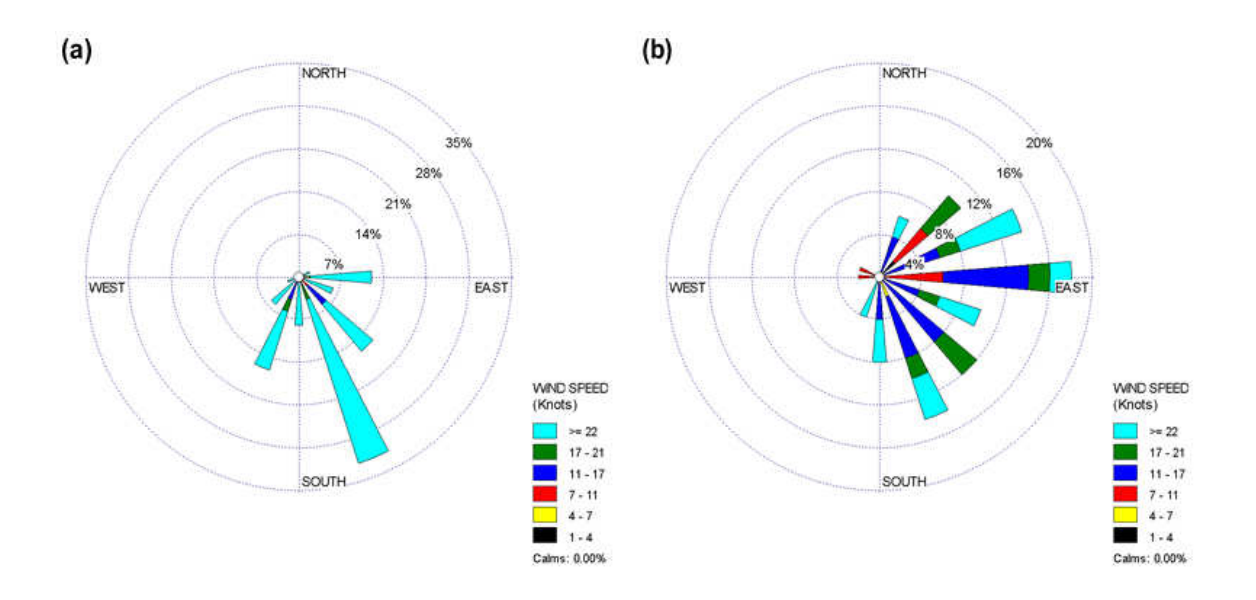


Figure 2.18: As in Fig. 2.16, but for the fifty extreme precipitation cases only, at t=0 h.

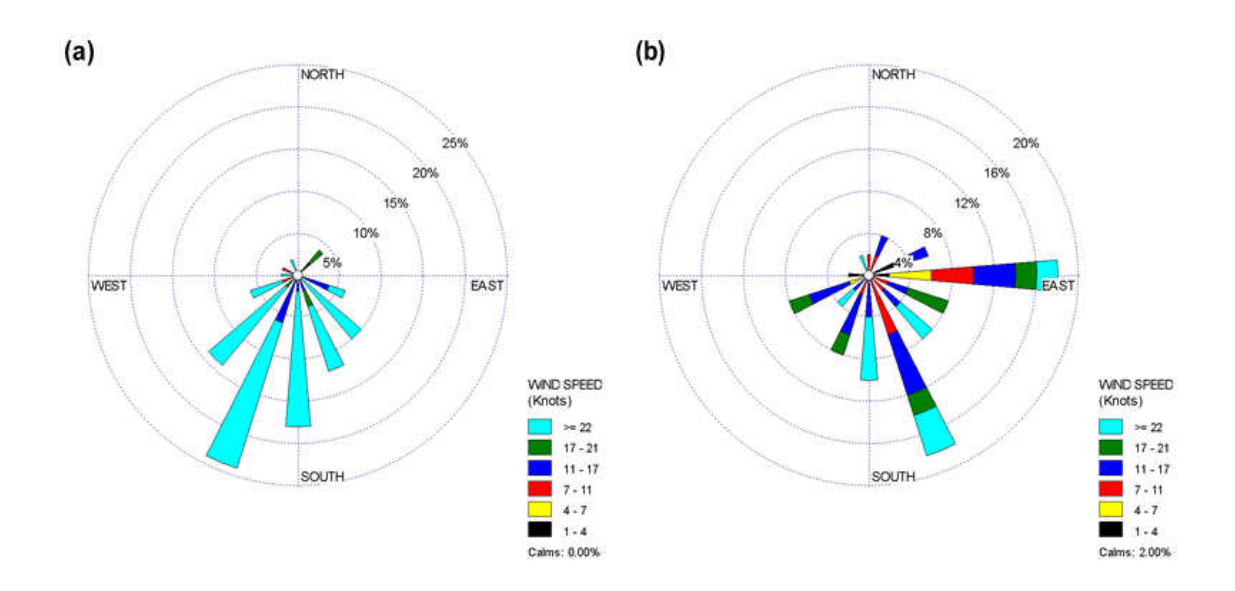


Figure 2.19: As in Fig. 2.16, but for the fifty moderate precipitation cases only, at t=0 h.

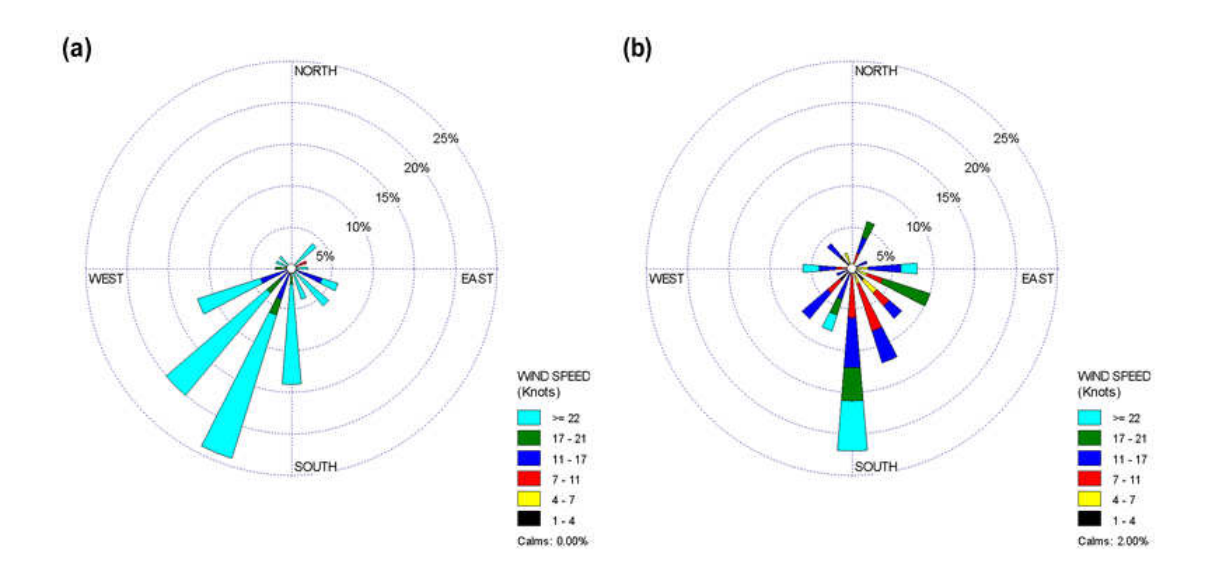


Figure 2.20: As in Fig. 2.16, but for the fifty light precipitation cases only, at t=0 h.

Chapter 3

Synoptic Typing of Extreme Cool-Season Precipitation Events at St. John's, Newfoundland, 1979-2005

The fifty median (25 above and 25 below the median event amount) extreme events used for the extreme composite in Chapter 2 are selected here for further synoptic analysis. First, motivations for this chapter and a review of synoptic typing methodologies are presented in Section 3.1. The two separate methodologies of manual synoptic typing used in this chapter are outlined in Section 3.2.1. The first method utilizes a Lagrangian backward trajectory analysis and the second utilizes time series of three commonly used quasi-geostrophic (QG) ascent-forcing parameters (mid-tropospheric vorticity advection, low-tropospheric temperature advection and low-tropospheric frontogenesis).

In Section 3.3, three synoptic types (south, southwest, and west) are established using the backward trajectory method. A similar process is undertaken for the QG ascent-forcing parameters in Section 3.4, which partitions cases into two synoptic types (cyclone, frontal). Subsequently, composite plots of sea-level pressure (SLP), 500 hPa height, and precipitable water (PW) are presented for each synoptic type.

Finally, Section 3.5 presents a discussion of the main findings of both methodologies of synoptic typing. Moreover, a comparison to corresponding synoptic types from the other threshold amount categories (i.e. moderate, light) of precipitation is presented in tables at the end of the chapter, which illustrates synoptic structures that separate extreme events of a certain synoptic type at St. John's from lesser events of the same type.

The following is based on: Milrad, Shawn M., E.H. Atallah, and J.R. Gyakum, 2010a: Synoptic typing of extreme cool-season precipitation events at St. John's, Newfoundland, 1979-2005. *Wea. Forecasting*, in press. (c) American Meteorological Society. Reprinted with permission.

Synoptic typing of extreme cool-season precipitation events at St. John's, Newfoundland, 1979-2005

Shawn M. Milrad, Eyad H. Atallah and John R. Gyakum

Department of Atmospheric and Oceanic Sciences, McGill University

Abstract

Quantitative precipitation forecasting (QPF) continues to be a significant challenge in operational forecasting, particularly in regions susceptible to extreme precipitation events. St. John's, Newfoundland and Labrador (CYYT) is affected frequently by such events, particularly in the cool season (October-April).

The 50 median events in the extreme (> 33.78 mm during a 48-hour period) precipitation event category are selected for further analysis. A manual synoptic typing is performed on these 50 events, using two separate methodologies to partition events. The first method utilizes a Lagrangian backward air parcel trajectory analysis and the second method utilizes the evolution of dynamically relevant variables, including 1000-700 hPa horizontal temperature advection, 1000-700 hPa (vector) geostrophic frontogenesis, and 700-400 hPa absolute vorticity advection.

Utilizing the first partitioning method, it is found that 'south' cases are characterized by a strong anticyclone downstream of St. John's, southwest events are synoptically similar to the overall extreme composite and are marked by a strong cyclone that develops in the Gulf of Mexico, while 'west' events are characterized by a weak Alberta clipper system that intensifies rapidly upon reaching the Atlantic Ocean. The second partitioning method suggests that while 'cyclone' events are dominated by the presence of a rapidly developing cyclone moving northeastward towards St. John's, 'frontal' events are characterized by the presence of a strong downstream anticyclone and deformation zone at St. John's.

It is our hope that the unique methodology and results of the synoptic typing in this paper will aid forecasters in identifying certain characteristics of future precipitation events at St. John's and similar stations.

3.1 Introduction

Chapter 2 discusses the perils of quantitative precipitation forecasting (QPF) in regions susceptible to extreme precipitation events, even when the mass field forecasts are essentially correct, as also discussed by Roebber and Bosart (1998) and Sisson and Gyakum (2004). Located at the confluence of several North American storm tracks (Fig. 2.2), Atlantic Canada (Fig. 2.1), and specifically, St. John's, Newfoundland, is a place that is particularly susceptible to extreme events during the cool season (Stewart et al. 1987), defined in this study as October-April, which can often produce flooding rains, paralyzing snow, and damaging winds. By selecting a station that has a very small seasonal window for

deep convection, and limiting the events in this study to those that occur from October-April, the role of deep convection is minimized, although the small possibility of convection playing a role in an October or April event exists.

In Chapter 2, three classes of precipitation events (extreme, moderate and light) were identified at St. John's (CYYT) over a 27-year (1979-2005) period. Here, an effort is made to further analyze the 50 extreme events used in the composite detailed in Chapter 2. These fifty events are distributed as follows: 9 events in October, 8 in November, 8 in December, 6 in January, 11 in February, 2 in March, and 6 in April.

The main objective of this paper is to identify important synoptic structures and precursors associated with various synoptic types and subcomposites of the fifty median extreme events defined in Chapter 2. This is achieved by performing a manual synoptic typing, utilizing two separate methodologies.

Manual synoptic typing is not new in atmospheric science, and has been performed for surface and upper-air analyses of weather events in west Texas (Ladd and Driscoll 1980), an environmental baseline and air quality analysis in Louisiana (Muller 1977; Muller and Jackson 1985), and a synoptic climatology for the northeast Gulf of Alaska (Overland and Hiester 1980). Alternatively, automated synoptic typing, typically involving principal component analysis, has been used in countless studies, including Jones et al. (1993), Frakes and Yarnal (1997), and Sheridan (2002). Both Frakes and Yarnal (1997) and Sheridan (2002)

argue that both manual and automated means of synoptic typing can sometimes be used in the same study and are useful for synoptic climatology studies.

3.2 Methodology and Data

3.2.1 Methodology

The methodology used in this paper revolves around two means of manual typing: first, a 3-D Lagrangian backward trajectory analysis categorizes events by air parcel source region, and second, time series of three quasi-geostrophic (hereafter QG) ascent-forcing parameters.

3.2.1.1 Backward Trajectory Analysis

Reap (1972) uses a primitive numerical model to compute 3-D air parcel trajectories from wind forecasts to provide more guidance for severe storm prediction. Uccellini et al. (1985) use trajectories on an isentropic surface in an analysis of the Presidents' Day storm of 1979. In the late 1990's both Wernli and Davies (1997) and Wernli (1997) use a Lagrangian-based method to research the structure and dynamics of extratropical cyclogenesis. Wernli and Davies (1997) state that 3-D trajectories are useful in attaining "i) the identification of the spatial coordinates and physical properties of the air parcels at the reference time (and) ii) the time-trace of the location and physical properties of the same air parcels for prior and/or subsequent time periods."

Bao et al. (2006), Knippertz and Martin (2007) and Roberge et al. (2009) use a backward trajectory analysis in studies of tropical moisture transport.

Roberge et al. (2009) use trajectories as a partitioning tool for cases of tropical moisture transport into northwestern Canada.

In order to partition the fifty extreme events by air parcel source region, five-day (120 hour) three-dimensional backward trajectories are analyzed using the National Centers for Environmental Prediction (NCEP) Global Reanalysis (Kalnay et al. 1996), starting at the beginning of the 6-hour period of maximum recorded precipitation at St. John's (t=0 h). Twenty-seven backward air parcel trajectories are initiated from a 3 ° by 3 ° box centered at 47° 40′ N, 52° 50′ W, roughly the location of St. John's International Airport (CYYT). The trajectories are computed simultaneously and end at either 300 hPa, 500 hPa, or 700 hPa. These levels are chosen based on the fact that these air parcels generally have a history of ascent. As such, these trajectories often originate in the boundary layer in the time frame of the analyses. Three ending levels are displayed to show that trajectories that end at different levels often originate from the same source region up to five days prior to the precipitation event.

All fifty cases and the associated backward trajectories were also evaluated using higher resolution North American Regional Reanalysis (NARR) data (Mesinger et al. 2006). Results indicate that the datasets produce backward trajectories that are very similar, and that the classifications established by the

partitioning methodology in this paper are valid irrespective of which dataset is used.

3.2.1.2 Quasi-Geostrophic Forcing

The second method of manual partitioning is based on time tendencies of three QG ascent forcing parameters at the station during the time of precipitation (mid-level vorticity advection, low-level horizontal temperature advection, and low-level geostrophic frontogenesis). The first two parameters are the first two forcing terms on the right-hand side of the quasi-geostrophic omega equation (Eq. 3.1). The form of the QG omega equation used in this paper (Eq. 3.1) is Equation 5.6.11 in Bluestein (1992a), where (a) is the three-dimensional Laplacian of vertical motion (omega), (b) represents differential vorticity advection, and (c) is the horizontal Laplacian of temperature advection. In Eq. (3.1), f_0 is the Coriolis parameter, σ is the static stability parameter, ω is the vertical velocity in pressure coordinates, $\mathbf{v_g}$ is the geostrophic wind vector, $\nabla_p(\mathbf{\zeta_g} + f)$ is the gradient of geostrophic absolute vorticity on a constant pressure surface and R is the gas constant for dry air.

$$(\nabla^{2}_{p} + \frac{f_{o}^{2}}{\sigma} \frac{\partial^{2}}{\partial p^{2}})\omega = -\frac{f_{o}}{\sigma} \frac{\partial}{\partial p} [-\mathbf{v}_{g} \bullet \nabla_{p} (\zeta_{g} + f)] + \frac{R}{\sigma p} [-\nabla^{2}_{p} (-\mathbf{v}_{g} \bullet \nabla_{p} T)]$$
(a)
(b)
(c)

The third parameter is based on a diagnosis of the frontogenesis, which is defined by the expression found in Eq. 3.2. Eq. 3.2, the vector frontogenetical

function, is Equation 2.5.19 in Bluestein (1992b), where $\mathbf{F_p}$ is the vector frontogenetical function (defined by the Lagrangian time tendency of the potential temperature gradient, $\nabla_p \theta$). The frontogenesis is related to QG forcing for ascent via Eq. 3.3 and Eq. 3.4, where Eq. 3.3 is Equation 2.5.36 in Bluestein (1992b) and Eq. 3.4 is Equation 5.7.58 in Bluestein Volume I (1992a). Eq. 3.3 relates the geostrophic frontogenesis to Q-vectors, where \mathbf{Q} is the Q-vector, σ is the static stability parameter, \mathbf{p} is the pressure, \mathbf{p}_0 is some reference pressure, κ is R divided by \mathbf{C}_p , the specific heat at constant pressure. Eq. 3.4 states the Q-vector form of the inviscid adiabatic QG omega equation in which the sense of vertical motion is related to the divergence of the Q-vector, which is supported by the assertion of Hoskins et al. (1978), which states that "in quasi-geostrophic theory...vertical velocity is forced solely by the divergence of Q."

$$\mathbf{F}_{p} = \frac{D_{p}}{Dt} \nabla_{p} \theta \tag{3.2}$$

$$\mathbf{Q} = \frac{R}{\sigma p} \left(\frac{p}{p_o} \right)^{\mathbf{K}} \mathbf{F}_p \tag{3.3}$$

$$(\nabla^2_p + \frac{f_o^2}{\sigma} \frac{\partial^2}{\partial p^2})\omega = -2\nabla_p \bullet \mathbf{Q}$$
 (3.4)

$$\mathbf{Q}_{s} = \left[\frac{\mathbf{Q} \bullet (k \times \nabla \theta)}{|\nabla \theta|}\right] \frac{k \times \nabla \theta}{|\nabla \theta|}$$
(3.5)

$$\mathbf{Q}_{n} = \left(\frac{\mathbf{Q} \bullet \nabla \theta}{|\nabla \theta|}\right) \frac{\nabla \theta}{|\nabla \theta|} \tag{3.6}$$

Finally, Keyser et al. (1988) suggest that the use of geostrophic frontogenesis as a diagnostic tool for quasi-geostrophic forcing is incomplete without assessing the along-front and normal-to-front components of the frontogenesis. To this end, these components have been evaluated using Equations 6.50 and 6.49 from Martin (2006), which are Eq. 3.5 and 3.6, respectively. These equations allow for the diagnosis of the along-front (\mathbf{Q}_s) and normal-to-front (\mathbf{Q}_n) components of the Q-vector, which are proportional to the corresponding components of frontogenesis (Keyser et al. 1988). Keyser et al. (1988) also point out that the parallel component of frontogenesis is related to forcing associated with temperature advections in association with a synoptic-scale wave and the normal component of frontogenesis relates to mesoscale forcing. Results of these diagnostics are detailed in Section 3.4.1.

3.2.2 Data

This study utilizes 6-hourly precipitation data for St. John's, obtained from the Environment Canada 6-hour corrected precipitation database. The corrected precipitation data are based on work done by Mekis and Hogg (1999), whereby the data have been adjusted to accurately reflect precipitation gauge changes, wind conditions, and changes in station location. In addition, all precipitation data in this study are observed in liquid equivalent form (i.e. no data were acquired using ruler methods), limiting errors associated with frozen precipitation. The NCEP Global Reanalysis is used as the dataset for all synoptic-scale composite and anomaly plots. The backward trajectory analysis is based on a

FORTRAN program originally developed at the State University of New York at Albany (Aiyyer, personal communication 2008). Most calculations and analyses in this study are performed and displayed using the General Meteorological Package version 5.7.4 (updated from the original package devised by Koch et al. (1983)), a data manipulation and visualization software package.

3.3 Synoptic Typing I: Backward Trajectory Analysis

3.3.1 Partitioning Methodology

The area of trajectory origin is used to partition the fifty events into three categories: south, southwest, and west. Of the fifty extreme events, 11 are classified as south cases, 31 as southwest cases, and 8 as west cases.

Figure 3.1 depicts 1 of 11 south trajectory cases, from an event in October 1986 with the onset of heaviest precipitation (t=0 h) being 0600 UTC 18 October 1986 and trajectories extending five days backward. To be considered a south case, the starting points of the majority of the trajectories must be east of 70° W and thus originate completely from the Atlantic Ocean. The relative humidity of the air parcels (Fig. 3.1b) generally increases as the parcels approach t=0 h and St. John's. Fig. 3.1b shows that most of the air parcels are saturated or nearly saturated at the three ending levels in the vicinity of St. John's at t=0 h. Finally, Fig. 3.1c depicts that for trajectories that did not interact with the boundary layer, values of equivalent potential temperature (Θ_e) remain relatively constant over the course of the 5-day evolution of the air parcel trajectories. The use of Θ_e adds a

level of objectivity to the partitioning of cases, as in a few cases the origin of the air parcels was slightly ambiguous and thus the event was classified by the location of the largest Θ_e (Roberge et al. 2009).

Thirty-one cases are classified as southwest, including 0000 UTC 21 April 1988, shown in Fig. 3.2. In order to be classified as a southwest case, the majority of the trajectories must originate from west of 70 ° W and south of 30 ° N. This classification ensures that many of the trajectories in a southwest case originate from the Gulf of Mexico (Fig. 3.2a). Additionally, Fig. 3.2b depicts that most of the trajectories are saturated or nearly saturated by t=0 in the vicinity of St. John's.

Finally, 8 cases are west cases, including Fig. 3.3, where t=0 h is 0000 UTC 8 December 2000. West cases have trajectories that originate west of 70° W, but north of 30° N and thus north of the Gulf of Mexico. Therefore, most of the west cases have primarily continental source regions of air, as far back as 5 days (Fig. 3.3a). Finally, Fig. 3.3c differs from the south and southwest case examples in that the value of Θ_e is significantly lower, which is consistent with the continental origins of the parcels.

3.3.2 Composite Results

Composite anomaly plots of three meteorological fields are displayed in order to understand the synoptic structures and precursors associated with each category of extreme event. Moreover, examining circulation anomalies in addition to the full composite fields allows the depiction of the significance of a

particular feature with respect to a monthly weighted 30-year (1971-2000). This process has been used many times, including by Grumm and Hart (2001). Some care should be taken when examining the statistical significance of the anomalies in the smaller groups, such as the west and south trajectory composites, although an examination of the individual cases within each composite shows high similarity among the synoptic structures shown below. However, since the differences in synoptic structures among composite groups are so stark and make intuitive physical sense, this is not a major concern for the purpose of this paper. Finally, care should also be taken when directly comparing the strength of anomalies in any of the fields displayed in this paper; the monthly weighted climatological means are not always the same and thus may slightly skew the results. In general, a comparison of synoptic structures among different types should be done qualitatively rather than quantitatively.

Composite and anomaly plots of selected atmospheric mass fields are displayed every twelve hours (these fields have been examined every six hours, but due to space concerns are shown every twelve) from t=-48 hours to t=+12 hours (t=-72 to t=+24 hours for the 500 hPa height anomaly plots), where t=0 h is the time of onset of the heaviest precipitation at St. John's.

3.3.2.1 South Trajectory Composites

In the south composite sea-level pressure (SLP) field, a negative anomaly is not evident until t=-24 h (Fig. 3.4c). However, a positive anomaly is centered just downstream at t=-48 h (Fig. 3.4a), and is a precursor to an extreme south

event at St. John's. The positive SLP anomaly east of St. John's amplifies from +8 hPa at t=-48 h (Fig. 3.4a) to +14 hPa at t=-12 h (Fig. 3.4d) just as the negative anomaly to the southwest is also amplifying from -4 hPa at t=-24 h (Fig. 3.4c) to -10 hPa at t= 0 h (Fig. 3.4e). As discussed in Chapter 2, this is a possible indication that as the low pressure strengthens to the southwest of St. John's, both the warm air advection (WAA) and latent heat release (LHR) from precipitation ahead of the low pressure system act to enhance the upper-level ridge (assuming both WAA and LHR increase with height in the lower- to mid-troposphere), which in turn strengthens the surface high via anticyclonic vorticity advection. Although the WAA and LHR can have a competing effect of causing pressure/height falls at the surface near the surface high pressure (assuming colocation), the fact that the positive SLP anomaly strengthens during and shortly following the intensification of the upper-level ridge suggests that the vorticity advection aloft is sufficiently strong.

After t=-12 h (Fig. 3.4d), the mean and anomaly values of the anticyclone remain rather stagnant. The most notable difference between t=-12 h (Fig. 3.4d) and t=0 h (Fig. 3.4e) is the translation of the mean anticyclone to the north, towards Greenland. This, in association with the SLP couplet oriented southwest-to-northeast, induces strong southerly geostrophic flow into St. John's (t=-36 h to t=0 h, Fig. 3.4b-e), suggesting moisture transport from the subtropical Atlantic. Finally, the sea-level cyclone tracks just to the south and east of St. John's; this is

an important point when comparing the south composite to the west and southwest composites.

In the 500 hPa height composite plot for the south cases (Fig. 3.5), an upper-level ridge associated with the surface anticyclone (Fig. 3.4a) is first observed directly south of St. John's at t=-48 h (Fig. 3.5c). At t=-24 h (Fig. 3.5e), the downstream ridge is now centered east-southeast of St. John's, with a magnitude of +150 m, having grown +90 m since t=-48 h (Fig. 3.5c). In addition, a negative anomaly is first observed northeast of the Bahamas (Fig. 3.5e). As time moves forward to t=0 h (Fig. 3.5g), this negative anomaly only strengthens slightly (-60 m), while the positive anomaly strengthens to more than +180 m.

The precipitable water (hereafter PW) composite field supports the assertion of strong moisture transport into St. John's, as a positive anomaly is first evident south of St. John's at t=-36 h (Fig. 3.6b). This anomaly moves eastward and amplifies as time progresses, reaching a maximum amplitude of +20 mm at t=0 h (Fig. 3.6e), located just southeast of St. John's. Anomalously large values of PW are situated over St. John's by time t=0 h.

3.3.2.2 Southwest Trajectory Composites

The southwest composite SLP field is quite different from that of the south cases, and resembles the overall extreme composite depicted in Chapter 2. This is not surprising given that 31 of the 50 extreme cases are in the southwest category. First, there is no evidence of a precursor downstream high pressure east of St. John's. Instead, an anomalously strong cyclone is evident in the southeastern

United States at t=-48 h (Fig. 3.7a). This area of low pressure strengthens and moves northeastward towards St. John's, reaching a minimum of -20 hPa at t=0 h (Fig. 3.7e). An anomalously strong anticyclone starts to form at t=-24 h (Fig. 3.7c) to the east of St. John's and strengthens to an amplitude +10 hPa by t=+12 h (Fig. 3.7f). Overall, the key difference between the south and southwest composites is that the south cases are associated with an anomalously strong anticyclone downstream and the southwest cases are associated with both an anomalously strong cyclone upstream and anomalously strong anticyclone downstream, albeit one that forms at a later time than the anticyclone in the south composite. Geostrophically, the winds at St. John's at t=0 are southeasterly, again bringing moisture from the Atlantic Ocean. The negative SLP anomaly in the southwest cases tracks just to the west of St. John's, suggesting that at least some of the rainfall occurs in association with a warm front ahead of the surface cyclone.

As seen in Chapter 2 for the overall extreme composite, a precursor 500 hPa ridge is observed at t=-72 h in the Pacific Northwest region of the United States (Fig. 3.8a). This anomaly grows in amplitude and slowly slides eastward by t=-48 h (Fig. 3.8c), when a negative anomaly downstream of the initial positive anomaly is first observed. Over the subsequent 24-36 hours, the original upstream positive height anomaly slowly weakens as the negative anomaly grows in strength (-90 m at t=-24 h; Fig. 3.8e). In addition, a new downstream positive anomaly forms at t=-24 h just south of St. John's (Fig. 3.8e). As the negative anomaly maintains its intensity (or slightly weakens) from t=-12 h through t=+24

h, the downstream positive anomaly grows in amplitude (Fig. 3.8f-i). As detailed in Chapter 2, there is evidence here of WAA and LHR enhancing the downstream 500 hPa ridge around the time of maximum precipitation.

The southwest composite depicts a positive PW anomaly at t=-48 h (Fig. 3.9a) located in the northeastern Gulf of Mexico. This anomaly moves northeastward towards St. John's while intensifying from +4 mm at t=-48 h (Fig. 3.9a) to +16 mm at t=0 h (Fig. 3.9e). The spatial scale of the positive anomaly near St. John's at t=0 h (Fig. 3.9e) is very similar to the south composite, with the differences being the formation region and the path traveled to St. John's.

3.3.2.3 West Trajectory Composites

The west composite is notable for the lack of an anomalously strong downstream positive SLP anomaly during the 60-hour evolution shown in Fig. 3.10. An upstream negative anomaly is first visible at t=-36 h (Fig. 3.10b) in the Great Lakes region, much further to the north and west than in the south and southwest cases. The negative anomaly does not intensify until it reaches the warm, lower static stability air over the Gulf Stream by t=-12 h (Fig. 3.10d). The intensification rate of the composite negative anomaly between t=-24 h (Fig. 3.10c) and t=0h (Fig. 3.10e) is 22+ hPa over the course of 12 hours. For a west case to be an extreme event, an Alberta clipper-type system has to rapidly develop once it moves over the western Atlantic. Unlike in the southwest cases, the center of the negative SLP anomaly passes just to the south and east of St. John's.

The 500 hPa height composite field in the west cases (Fig. 3.11) depicts a system that initially has weak upper level support, which increases once the low-level cyclone center starts to intensify over the ocean. A weak negative anomaly is visible at t=-36 h over the Great Lakes region (Fig. 3.11d) and approaches St. John's from the south at t=0 h (Fig. 3.11g). The suggestion here is that baroclinic instability is present, as the near-surface cyclone helps to intensify the upstream upper-level trough by advecting cold air beneath 500 hPa (not shown) into the base of the 500 hPa trough. In examining Fig. 3.11f-h, the 500 hPa negative height anomaly intensifies from -120 m at t=-12 h to -210 m at t=+12 h. The enhancement of the upper-level trough via cold air advection creates a positive feedback loop whereby the differential cyclonic vorticity advection (not shown) associated with the 500 hPa trough indirectly intensifies the surface cyclone, which then acts to intensify the upper-level trough through stronger low-level cold air advection.

Evident in Fig. 3.12a are two precursor anomalies: a negative PW anomaly centered just southeast of St. John's at t=-48 h and a positive anomaly centered over the central United States. While the positive anomaly is not statistically significant, the authors believe this is mostly due to a low number of cases in the west composite (8 cases) and that the structure and location of this anomaly is still important. As time moves forward, the positive PW anomaly over the central plains of the U.S. splits into two anomalies, with one remaining over the area by t=-12 h (Fig. 3.12d) and the other moving eastward off the east coast, where it intensifies by t=-12 h (Fig. 3.12d). The positive anomaly over the

plains is likely in association with the strong Alberta clipper over the Great Lakes, which pulls warm, moist air northward from the Gulf of Mexico. This positive anomaly subsequently continues north-northeastward until it is centered just south of St. John's at t=0 h (Fig. 3.12e).

3.4 Synoptic Typing II: Using Quasi-Geostrophic Forcing Parameters

3.4.1 Partitioning Methodology

The second method of event parsing uses the 1000-700 hPa horizontal temperature advection, 700-400 hPa vorticity advection, and 1000-700 hPa geostrophic frontogenesis. Time series of these three parameters are plotted for a sample case of each category of extreme event in Fig. 3.13a (cyclone) and Fig. 3.13b (frontal). Values are based on an average of the values at the three nearest grid points to the station of interest.

Fig. 3.13a displays the time series of an example of the cyclone group from 30 December 1997. The evolution of the three parameters are typical for the passage of a mid-latitude extratropical cyclone. Values of low-level warm air advection and frontogenesis are relatively high during the first part of the time series, coinciding with the likely passage of the warm front ahead of the main surface cyclone. In subsequent time periods, values of horizontal temperature advection become negative as the main upper-level trough approaches and passes St. John's. Concommitantly, values of mid-tropospheric vorticity advection go

from near zero to positive values as the upstream upper-level trough approaches St. John's. In all of the 35 cyclone cases, the 1000-700 layer-averaged frontogenesis is less than $20 \times 10^{-2} \text{ K}/100 \text{ m/3}$ hr on average during the t=-12 h to t=+12 h time frame. Moreover, the evolution of the three QG forcing parameters described above is evident for the vast majority of cyclone cases (27 of 35). The remainder of the cyclone cases differs in that the values of 700-400 layeraveraged vorticity advection are lower than the other 27 cyclone cases during the time frame discussed, with low-level warm air advection dominating. These eight events are characterized by an intense sea-level cyclone that tracks well west of St. John's, placing the station in a broad area of warm air advection, and by an upper-level trough that moved sufficiently west of St. John's such that values of mid-level vorticity advection at the station are significantly weaker than the other 27 cyclone cases. While it is arguable that the cyclone group could be broken down into two subgroups, a main goal of this paper is to isolate the synoptic structures associated with extreme precipitation events in which a strong sea-level cyclone is not present (i.e. the frontal group) and compare them with structures during events in which a strong sea-level cyclone is present (cyclone group).

Fig. 3.13b displays an example of the frontal group from 5 February 1984. Both horizontal temperature advection and mid-level vorticity advection values are near zero during the event. However, the value of the 1000-700 hPa geostrophic frontogenesis is consistently large throughout the event. The evolution of the three QG forcing parameters is examined during the period from

twelve hours prior (t=-12 h) to twelve hours after (t=+12 h) the onset of the heaviest precipitation at St. John's. The criteria for frontal events are as follows:

- 1000-700 hPa layer-averaged geostrophic frontogenesis: >= 30 x 10^{-2} K/100 m/3 hr;
- 1000-700 hPa layer-averaged temperature advection: $\leq 20 \times 10^{-5}$ ${\rm Ks}^{-1}$
- 400-700 hPa layer-averaged vorticity advection: $\leq 10 \times 10^{-10} \text{ s}^{-2}$.

While these values may appear arbitrary, all 11 frontal cases fit these criteria extremely well, while no other cases come close to doing so.

The 1000-700 hPa frontogenesis is chosen for use in this paper primarily because it is a commonly examined variable operationally and is useful in pinpointing the location of developing low-level temperature gradients, which serve as the primary mechanism for quasi-geostrophic ascent.

Finally, results for the cases in this study show that in the frontal cases, the magnitude of the normal component of frontogenesis (for which \mathbf{Q}_n is used as a proxy, as defined in Section 3.2.1.2) is greater than that of the parallel component (for which \mathbf{Q}_s is used as a proxy, as defined in Section 3.2.1.2), while the opposite is true in most of the cyclone cases (not shown). In the remaining cyclone cases, the magnitudes of both components are near-zero. The observed evolution of the two components of frontogenesis further supports the partitioning methodology outlined in this section. The frontogenesis components in the frontal cases

suggest that as time passes, the focus of the frontogenesis moves from the synoptic scale to the mesoscale, as found by Gyakum and Barker (1988). A caveat to this point is that real wind frontogenesis, not geostrophic frontogenesis, more accurately represents what is happening in mesoscale frontal circulations,. While this is beyond the scope of this paper, the time evolutions of the 1000-700 hPa layer-averaged geostrophic frontogenesis and 1000-700 hPa layer-averaged frontogenesis derived from the real wind are similar for all of the cases in this paper (not shown).

In total, there are thirty-five cases classified in the cyclone group and eleven cases classified in the frontal group.

3.4.2 Composite Results

3.4.2.1 Cyclone Composites

In the SLP field, an anomalously strong cyclone is visible at t=-48 h (Fig. 3.14a) over northern Florida. This anomaly moves northeastward and rapidly strengthens, reaching an amplitude of -10 hPa at t=-24 h (Fig. 3.14c) and -20 hPa at t=0 h, when the cyclone center is located just southwest of St. John's. Although there is a positive anomaly downstream starting at t=-48 h (Fig. 3.14a), the amplitude of this feature over time (Fig. 3.14a-f) remains relatively weak until t=0 h and t=+12 h.

A precursor positive 500 hPa height anomaly is evident on the west coast of the United States at three days (t=-72 h) prior (Fig. 3.15a) to the onset of the heaviest precipitation at St. John's. The positive anomaly grows in size until

around t=-36 h (Fig. 3.15d), after which it slowly begins to weaken. Additionally, a negative height anomaly downstream of the initial positive anomaly is first evident at t=-36 h (Fig. 3.15d) and grows in size and amplitude to a maximum intensity of -150 m at t=0 h (Fig. 3.15g) and t=+12 h (Fig. 3.15h). The fact that the negative anomaly steadily strengthens as the upstream positive anomaly weakens is supportive of the downstream Rossby wave development discussed in Chapter 2. This is also supported by the development of a second positive anomaly downstream of the negative anomaly, first evident at t=-12 h (Fig. 3.15f) just east of St. John's. This downstream negative anomaly grows in amplitude through t=0 h (Fig. 3.15g) and beyond.

A positive PW anomaly is evident just off the southeastern coast of the United States at t=-36 h (Fig. 3.16b). This anomaly strengthens and moves northeastward towards St. John's, reaching a maximum intensity of +14 mm at t=0 h (Fig. 3.16e).

3.4.2.2 Frontal Composites

In the SLP field, a strong downstream high pressure system (positive anomaly) is located east of St. John's at t=-48 h (Fig. 3.17a). This positive anomaly grows in amplitude and reaches a maximum of +14 hPa at t=-24 h (Fig. 3.17c). It helps to initiate moist southerly flow off the Atlantic Ocean and into St. John's. Concomitantly, a weak negative SLP anomaly moves eastward from the Great Lakes region at t=-48 h (Fig. 3.17a) and re-develops to the southeast once it reaches the Atlantic Ocean at t=-12 h (Fig. 3.17d). This weak negative anomaly

then moves northeastward until it is located just southwest of St. John's at t=0 h (Fig. 3.17e) by which time it has an amplitude of -8 hPa, compared with -20 hPa in the cyclone composite. The emergence of a new anomaly to the southeast between t=-24 h (Fig. 3.17c) and t=-12 h (Fig. 3.17d) suggests that as the original cyclone moves eastward from the Great Lakes, a second wave of low pressure develops along a quasi-stationary baroclinic zone that is established to the west of the downstream high pressure system and along the eastern seaboard.

In the 500 hPa height composite, a downstream 500 hPa ridge is evident (Fig. 3.18) and remains quasi-stationary during the period of precipitation at St. John's, supporting the presence of a downstream surface anticyclone.

Meanwhile, a weak upstream trough is present from t=-72 h (Fig. 3.18a) to t=+24 h (Fig. 3.18i).

A positive PW anomaly is first evident at t=-36 h (Fig. 3.19b), centered just southwest of St. John's. This anomaly proceeds to strengthen and slowly move eastward through t=0 h (Fig. 3.19e), when it reaches a maximum intensity of +16 mm centered just southeast of St. John's. In contrast to the cyclone group, the positive PW anomaly in the frontal group is relatively stationary, in accordance with the suggestion that a quasi-stationary deformation zone is situated upstream of the sea-level anticyclone, right over St. John's. The PW anomaly finally starts to move eastward as the weak wave of low pressure moves northeastward along the stationary front, bringing the heaviest of the precipitation into St. John's by t=0 h (Fig. 3.19e).

3.5 Concluding Discussion and Future Work

This study takes a closer look at the fifty median extreme precipitation events identified in Chapter 2. Two manual classification schemes are utilized to explore associated synoptic structures. The first methodology involves a five-day backward trajectory analysis, out of which three groups of extreme events are defined based on the origin of the majority of air parcels. These groups are defined as south (11 events), southwest (31 events), and west (8 events). The second methodology revolves around a time-series analysis of three QG ascent-forcing parameters. Forty-six of the fifty events are subsequently classified into cyclone (35 events) and frontal (11 events) groups.

In the south cases, the pattern is dominated by a downstream surface anticyclone and corresponding mid-tropospheric ridge (Figs. 3.4 and 3.5). This southerly flow helps to transport moisture and create a positive precipitable water (PW) anomaly just south of St. John's at t=-24 h (Fig.3.6c). Subsequently, the PW anomaly amplifies and moves towards St. John's. In theory, the downstream ridge is then amplified by both warm air advection ahead of the low-level cyclone and latent heat release from heavy precipitation, as discussed in Chapter 2; once the downstream ridge has amplified, the surface anticyclone amplifies in response to enhanced anti-cyclonic vorticity advection above the surface anticyclone center.

The southwest trajectory cases are pointedly similar to that of the overall extreme composite presented in Chapter 2. In the southwest composite, an

anomalous sea-level cyclone forms near the northeastern Gulf of Mexico at around t=-72 h (not shown) and slowly amplifies as it progresses northeastward. By time t=-12 h (Fig. 3.7d), a downstream anticyclone begins to form just east of St. John's. It is suggested that two processes are at play: 1) downstream development associated with Rossby wave energy transfer and 2) enhancement of the downstream ridge due to warm air advection and latent heat release ahead of the surface cyclone, which in turn strengthens the surface anticyclone via differential anti-cyclonic vorticity advection.

Corresponding to the first point, a precursor 500 hPa height ridge is evident over the western United States at three days (t=-72 h) prior to the onset of heaviest precipitation at St. John's. This positive anomaly first amplifies, then subsequently weakens around t=-36 h (Fig. 3.8a-i) as the downstream negative anomaly starts to amplify. The trough initially amplifies, then approximately maintains its intensity while a downstream ridge amplifies east of St. John's. This downstream development is not evident in the south or west cases. Finally, the positive PW anomaly is more transient in the southwest cases than in the south cases, forming over Northern Florida (Fig. 3.9a) at t=-48 h and moving northeastward towards St. John's while intensifying.

The west trajectory cases feature synoptic structures that are markedly different from both the south and southwest cases. In the SLP composite field, a weak cyclone emerges from the Great Lakes region around t=-24 h (Fig. 3.10c) and rapidly intensifies upon reaching the Atlantic Ocean. In the 500 hPa height

field, the negative anomaly (trough) associated with the surface cyclone also rapidly intensifies upon reaching the Atlantic Ocean. The amplitude of the 500 hPa trough suggests that the overall dynamics of the west cases are relatively strong, but there is a lack of low-level baroclinicity and relatively high static stability while the system is over the continent. Upon reaching the Atlantic Ocean (i.e. a moisture source with overlying lower static stability air), the near-surface cyclone rapidly intensifies, which further intensifies the upper-level trough. As time progresses, these systems continue to rapidly intensify each other via baroclinic instability.

While the Atlantic Ocean clearly plays an important role in providing enough moisture for a west case to be an extreme event, the PW composite for the west cases suggests a potential precursor signal to these events is located in the Great Plains of the United States. A positive PW anomaly is present over the Great Plains of the United States at t=-48 h (Fig. 3.12a), two days before the onset of heaviest precipitation at St. John's. While a piece of this anomaly remains relatively stationary over time, another piece moves eastward, reaching the Atlantic Ocean at the same time (t=-24, Fig. 3.12c) that the sea-level cyclone begins to rapidly intensify off the east coast of the United States. This positive PW anomaly subsequently moves northeastward towards St. John's in conjunction with the surface cyclone. It is of note that both the strength of the 500 hPa trough and the track of the sea-level cyclone in the west trajectory composite in this paper are similar to that seen in the light precipitation event

composite shown in Chapter 2. Thus, the light cases in Chapter 2 may serve as null cases to the extreme west cases described in this paper.

The second manual classification methodology produces two groups of cases, deemed cyclone (35 cases) and frontal (11 cases). The synoptic signals in the frontal group are masked by the cyclone group in the overall extreme composite discussed in Chapter 2.

In the cyclone composite, negative SLP and positive PW anomalies form concurrently over northern Florida at t=-48 h (Fig. 3.14a and 3.16a). These anomalies proceed to strengthen and move northeastward towards St. John's, reaching a maximum amplitude by t=0 h (Figs. 3.14e and 3.16e). Meanwhile, the downstream SLP anomaly is relatively weak compared with the frontal composite. The same processes involved in strengthening the downstream anomalies in the southwest and overall extreme composite are at work in the cyclone composite. To that end, a positive 500 hPa precursor height anomaly is visible over the west coast of the United States at t=-72 h (Fig. 3.15a). Finally, soundings produced for t=-12 h to t=+12 h at St. John's (not shown) depict a strong 1000-700 hPa veering wind signal, which supports the assertion of strong low-level warm air advection as the cyclone passes St. John's. The soundings also exhibit a relatively low tropopause, consistent with the passage of a cool-season cold-core low.

In the frontal SLP composite, a negative anomaly upstream of St. John's and positive anomaly downstream of St. John's are evident at t=-48 h (Fig. 3.17a).

The origin of the negative anomaly appears to be the Great Lakes region, much further north than the location of the surface cyclone in the cyclone composite. Moreover, while the anomalous cyclone only slightly strengthens as it moves slowly eastward towards St. John's, the downstream positive anomaly rapidly intensifies, reaching its maximum amplitude at t=-24 h (Fig. 3.17c). The intensification of the anomalous anticyclone downstream helps to set up a baroclinic zone near St. John's, facilitating secondary cyclogenesis by t=-12 h (Fig. 3.17d). This is evident in the SLP composite, as the position of the new cyclone at t=-12 h (Fig. 3.17d) is significantly to the southeast of the position of the original cyclone at t=-24 h (Fig. 3.17c). The relatively weak secondary sealevel cyclone then proceeds to move along the east coast of North America bringing relatively small associated values of QG forcing for ascent. This will be more explicitly detailed in future work.

The 500 hPa height composites also indicate that the upstream trough/cyclone is relatively weak. The positive height anomaly downstream of St. John's is evident as early as t=-48 h. This positive height anomaly proceeds to strengthen over the subsequent 48-60 hours (Fig. 3.18), likely partially in response to latent heat release from heavy precipitation at St. John's. The PW composite in the frontal group (Fig. 3.19) depicts a positive anomaly near Nova Scotia at t=-36 h (Fig. 3.19b). The positive PW anomaly subsequently intensifies as it moves slowly northeastward, coincidental with the stronger southerly geostrophic flow into St. John's caused by the intensification of the anticyclone downstream and the secondary cyclogenesis upstream. In sum, the frontal

composite is representative of a group of events which are characterized by relatively weak mid-level vorticity advection and low-level horizontal temperature advection in a low static stability environment. The forcing for ascent provided by the low-level frontogenesis seems to be sufficient in the frontal cases provided the air mass at St. John's is characterized by particularly low static stability.

Finally, soundings at St. John's examined for the t=-12 h to t=+12 h time period depict three main differences from the cyclone composite soundings: a) a strong boundary layer inversion and b) a much higher tropopause, suggesting different air masses, one associated with a typical cold-core low (cyclone composite) and the other a subtropical anticyclone (frontal composite).

One issue that immediately arises out of the use of two different manual typing methodologies is the extent of overlap between the two methodologies. While sub-composites have not yet been produced, the authors do hope to address this issue in future research. For now, a statistical representation of the overlap between the two methodologies is visible in Table 3.1. As is suggested by the identification of synoptic structures (particularly the presence of the downstream anticyclone), a significant portion of the south cases are also considered to be frontal cases. While there are minor differences between the south and frontal composites, the induced southerly geostrophic flow into St. John's is consistent in both cases. Finally, all eight of the west cases and three-quarters of the southwest cases are also part of the cyclone composite, which supports the assertion that

both the southwest and west cases involve a rapidly developing upstream sealevel cyclone.

The authors hope that the structures identified in this paper will be of use to the local forecaster at St. John's and similar stations. To that end, a quick reference guide to important conclusions highlighted in this paper is available in Tables 3.2 and 3.3 for the trajectory and QG forcing types, respectively.

A final issue that arises out of the analysis in this paper is the comparison of the synoptic structures associated with a particular composite group (e.g. west trajectory events) among the different precipitation amount categories (e.g. extreme, moderate, light). Such an analysis could be quite useful to the forecaster. However, due to space concerns, the figures for the moderate and light events are not shown and the focus in this paper remains on the extreme events, since they have the greatest potential impact on St. John's. That said, Tables 3.4 and 3.5 display statistics for the different precipitation amount categories defined in Chapter 2, broken down by composite group. In addition, Tables 3.6 and 3.7 serve as a summary of important structural differences for each composite group in this paper, among the different precipitation threshold categories. The findings include:

• The track of the cyclone in the southwest cases and position of the precursor (t=-72 h) west coast ridge is further to the north and west in the moderate and light cases than in the extreme composite

- The precursor positive PW anomaly seen over the midwestern U.S.
 in the extreme west trajectory composites is not present in either
 the moderate or light west trajectory cases.
- In the cyclone group, both upper-level and sea-level synoptic structures are located further to the north and west in the moderate and light cases than in the extreme composite.
- The downstream ridging and corresponding surface high that is seen in the extreme frontal cases is much stronger than in the moderate and light frontal cases.

Synoptic composite plots for the various synoptic types (both partitioning methodologies) are available online at http://www.meteo.mcgill.ca/~milrad/Milrad2009b.htm.

In the future, detailed case studies of recent extreme precipitation events at St. John's will be produced, synoptically typing the events into the categories defined in this paper, while also explicitly detailing the associated dynamics.

	Cyclone (n=35)	Frontal (n=11)	Neither (n=4)
South (n=11)	4	6	1
Southwest (n=31)	23	5	3
West (n=8)	8	0	0

Table 3.1: The fifty extreme cases broken down by methodology and synoptic typing.

	Sea-Level Pressure	500 hPa Height	Precipitable Water
South (n=11) Avg. Event (mm): 42.93	 Strong downstream anticyclone Cyclone passes south and east of St. John's 	 Intense downstream ridging Lack of upstream trough 	 Strong southerly flow just south of St. John's Pooling of moisture
Southwest (n=31) Avg. Event (mm): 42.17	 Strong upstream cyclone passes west of St. John's Weak downstream anticyclone to start, slowly strengthens 	 Intense upstream trough Slowly building downstream ridge, possibly due to WAA and LHR 	• Transient significant positive anomaly in Gulf of Mexico 2 days prior to event rapidly strengthens, moving northeastward towards St. John's
West (n=8) Avg. Event (mm): 42.49	 Strongest cyclone of any type, passing just south and east of St. John's Alberta Clipper- like track that rapidly intensifies over Atlantic complete lack of downstream anticyclone 	 No upstream trough until t=0, probably associated with baroclinic instability following rapid surface development lack of downstream ridge 	• Positive anomaly becomes statistically significant over Atlantic, just south and east of St. John's

Table 3.2: Average event precipitation and synoptic characteristics associated with each trajectory type, for the fifty extreme precipitation cases.

	Sea-Level Pressure	500 hPa Height	Precipitable Water
Cyclone (n=35) Avg. Event (mm): 42.39	 Strong cyclone develops on U.S. mid-atlantic coast and moves northeastward while strengthing rapidly Cyclone center passes directly over station Downstream anticyclone builds slowly 	 Anomalous ridge over U.S west coast 3 days prior to event Possible downstream Rossby wave development leads to strong trough upstream of St. John's and slowly strengthening downstream ridge 	Significant positive anomaly develops off U.S. mid-atlantic coast at t=-36 h; Rapidly intensifies and center passes just south and east of St. John's
Frontal (n=11) Avg. Event (mm): 42.69	 Strong downstream anticyclone at t=-48 h Weak Alberta-clipper-type cyclone from Great Lakes region, redevelops to the southeast as weak frontal wave along the coast 	 Lack of upstream trough Strong ridge downstream of St. John's at t=-48 h 	 Positive anomaly intensifies upon reaching the Atlantic at t=-36 h Propagates eastward towards St. John's, with center passing just south and east

Table 3.3: Average event precipitation and synoptic characteristics associated with each quasi-geostrophic forcing type.

	Extreme (n=50)	Moderate (n=50)	Light (n=50)
South	11	2	4
Southwest	31	38	22
West	8	10	24

Table 3.4: The fifty cases from each precipitation amount group defined in Chapter 2, listed by trajectory classification.

	Extreme (n=50)	Moderate (n=50)	Light (n=50)
Cyclone	35	30	28
Frontal	11	15	10
Neither	4	5	12

Table 3.5: The fifty cases from each precipitation amount group defined in Chapter 2, listed by Quasi-Geostrophic forcing classification.

	Extreme	Moderate	Light
South	Table 3.2	Not enough cases	Not enough cases
Southwest	Table 3.2	Anomalous cyclone and positive PW anomaly of similar strength to extreme cases, but originate further north and west	Anomalous cyclone substantially weaker than in extreme and moderate cases, as well as originating further to the north and west
		 Precursor 500 hPa ridge at t=-72 h further north on west coast than in extreme cases and downstream trough/ridge less amplified 	500 hPa precursor ridge on west coast substantially further to the north than in extreme or moderate cases, while downstream trough/ridge much less amplified
			• Lack of coherent PW anomaly until t=-12 h (when disturbance reaches the ocean)
West	Table 3.2	Precursor negative SLP anomaly near St. John's at t=-48 h, precipitation-causing anomalous cyclone not visible until t=-12 h, upon reaching the ocean,	• Precursor negative SLP anomaly northeast of St. John's at t=-48 h; anomalous cyclone over Minnesota at t=-48 h, which becomes precipitation-causing system at St. John's;
		• 500 hPa trough less amplified and further to the north than in extreme composite	• 500 hPa flow less amplified than extreme and moderate cases
		No precursor positive PW anomaly over central U.S.	 No substantial PW anomaly in Central U.S. before event or at St. John's during event

Table 3.6: Important synoptic-scale structures and precursors associated with each trajectory composite group, among the three precipitation amount categories defined in Chapter 2.

	Extreme	Moderate	Light
Cyclone	Table 3.3	 Negative SLP anomaly at t=-48 h substantially further to the north than in extreme cases 500 hPa precursor ridge over west coast of North America at t=-72 h slightly further to north, while downstream development is less amplified than in 	 Cyclone intensifies upon reaching Atlantic at t=0 h 500 hPa precursor ridge at t=-72 h over Pacific northwest similar to moderate cases; east-coast trough weaker and further north than in moderate
		 extreme cases; Positive PW anomaly forms further to the north than extreme cases at t=-36 h; more intense upon reaching St. John's (t=0 h) 	 weaker PW anomaly not seen until t=-12 h, later than moderate cases
Frontal	Table 3.3	 Much weaker downstream sea-level anticyclone than in extreme cases → weaker southerly geostrophic flow Downstream 500 hPa ridge weaker and further south than in extreme cases → flow much less amplified; 	 Anomalous sea-level anticyclone/mid-level ridge east of St. John's further north than moderate cases; similar structures to extreme cases but appears later and is slightly weaker Upstream anomalous cyclone weaker than moderate cases
		Positive PW anomaly, further south of St. John's than in extreme cases, likely due to slightly different position of anticyclone	Positive PW anomaly much weaker than in extreme and moderate composites

Table 3.7: Important synoptic-scale structures and precursors associated with each Quasi-Geostrophic (QG) forcing composite group, among the three precipitation amount categories defined in Chapter 2.

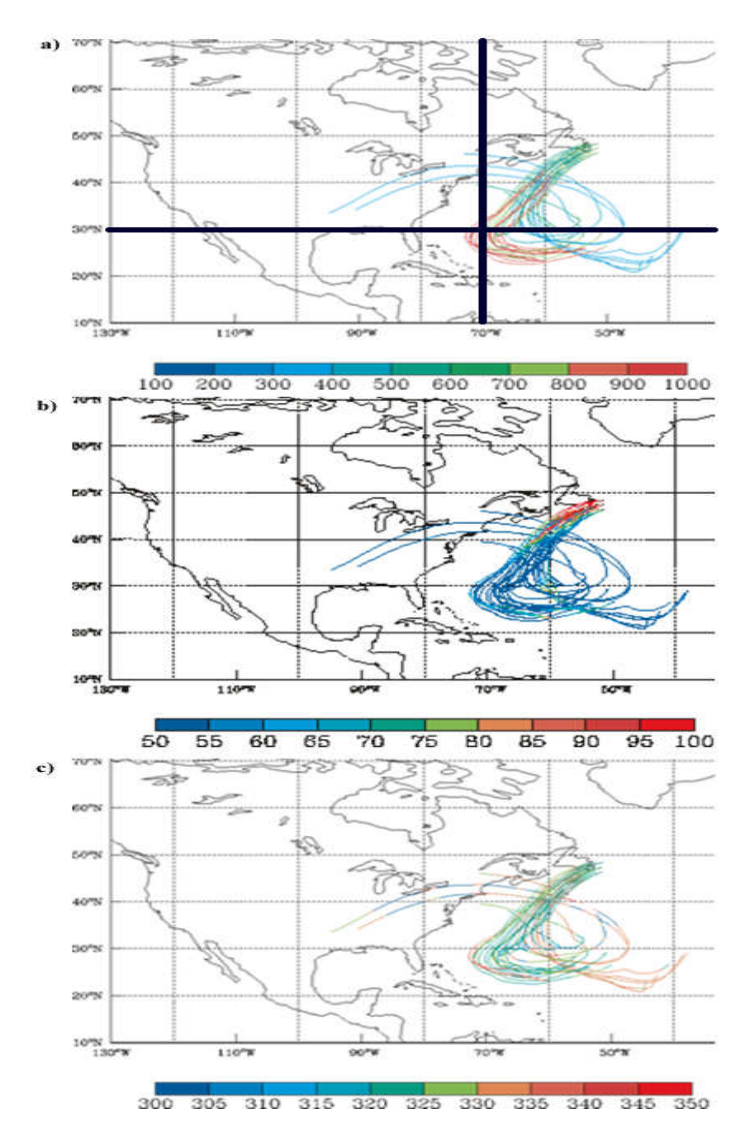


Figure 3.1: Twenty-seven backward trajectories with the origin being five days earlier and the ending points at 300, 500, and 700 hPa at 0600 UTC October 18th, 1986. Ending points are distributed within a box whose corners are 48.4°N 53.5°W and 46.4°N 51.5°W. This is an example of a 'south' event. Latitude 30°N and Longitude 70°W are critical to the partitioning and are in bold in panel (a).

- a) The tracer used is pressure (hPa) where warm colors indicate closer to the surface.
- b) Tracer used is relative humidity (%) where warm colors indicate values closer to 100%.
- c) Tracer used is $\theta_e(k)$ where warm colors indicate greater values of θ_e .

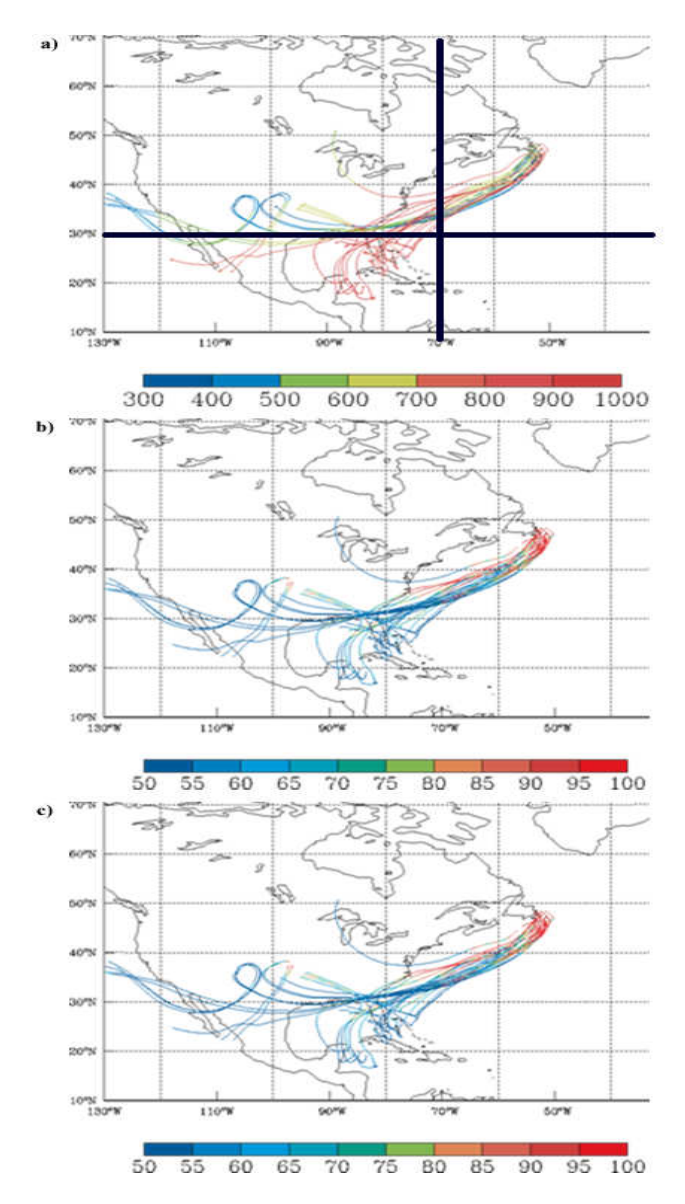


Figure 3.2: Twenty-seven backward trajectories with the origin being five days earlier and the ending points at 300, 500, and 700 hPa at 0000 UTC April 21st, 1988. Ending points are distributed within a box whose corners are 48.4°N 53.5°W and 46.4°N 51.5°W. This is an example of a 'southwest' event. Latitude 30°N and Longitude 70°W are critical to the partitioning and are in bold in panel (a).

- a) The tracer used is pressure (hPa) where warm colors indicate closer to the surface.
- b) Tracer used is relative humidity (%) where warm colors indicate values closer to 100%.
- c) Tracer used is $\theta_e(k)$ where warm colors indicate greater values of θ_e .

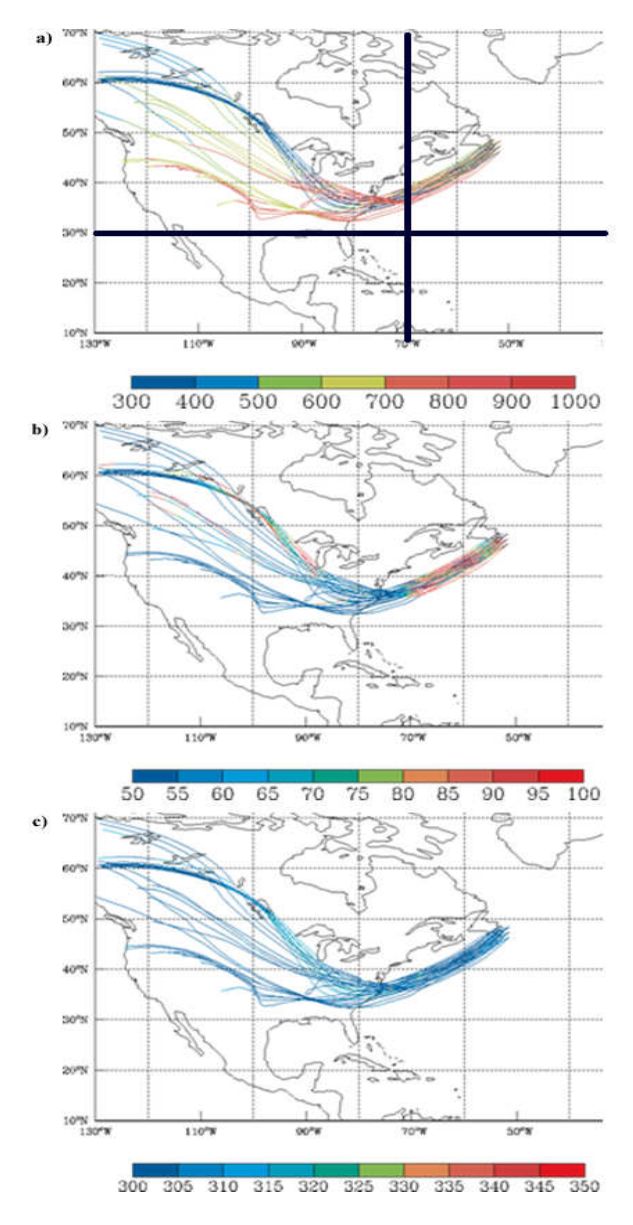


Figure 3.3: Twenty-seven backward trajectories with the origin being five days earlier and the ending points at 300, 500, and 700 hPa at 0000 UTC December 8th, 2000. Ending points are distributed within a box whose corners are 48.4°N 53.5°W and 46.4°N 51.5°W. This is an example of a 'west' event. Latitude 30°N and Longitude 70°W are critical to the partitioning and are in bold in panel (a).

- a) The tracer used is pressure (hPa) where warm colors indicate closer to the surface.
- b) Tracer used is relative humidity (%) where warm colors indicate values closer to 100%.
- c) Tracer used is θ_e (k) where warm colors indicate greater values of θ_e .

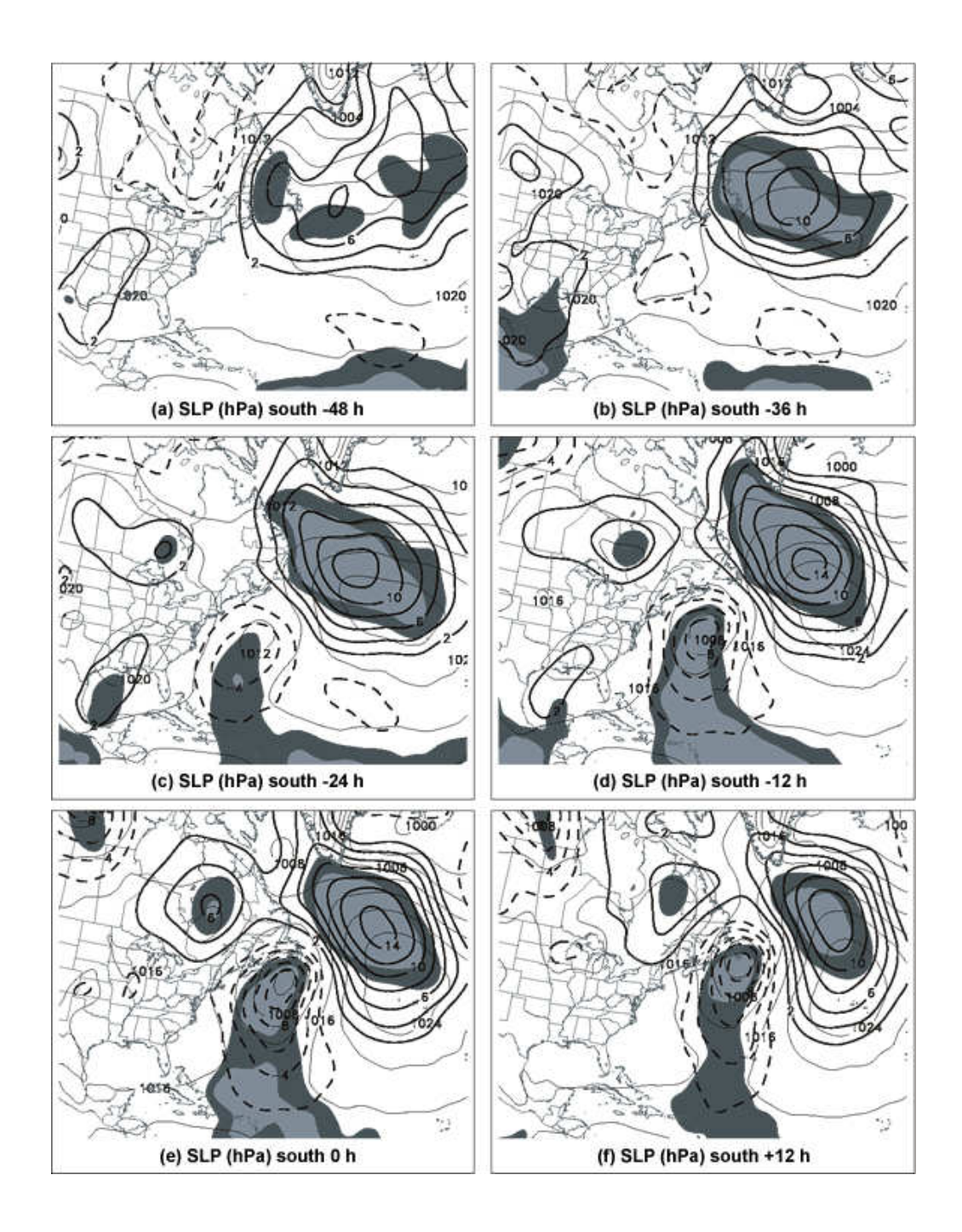


Figure 3.4: Sea-level pressure (SLP) anomalies every 2 hPa, heavy dashed for negative values and heavy solid for positive values, with respect to climatology, for the south cases at (a) -48, (b) -36, (c) -24, (d) -12, (e) 0, and (f) +12 h. Light solid contours represent full composite SLP field, every 4 hPa. Shading represents statistical significance of the anomalies at the 95% (darker shading) and 99% (lighter shading) confidence levels, according to the Student's t test.

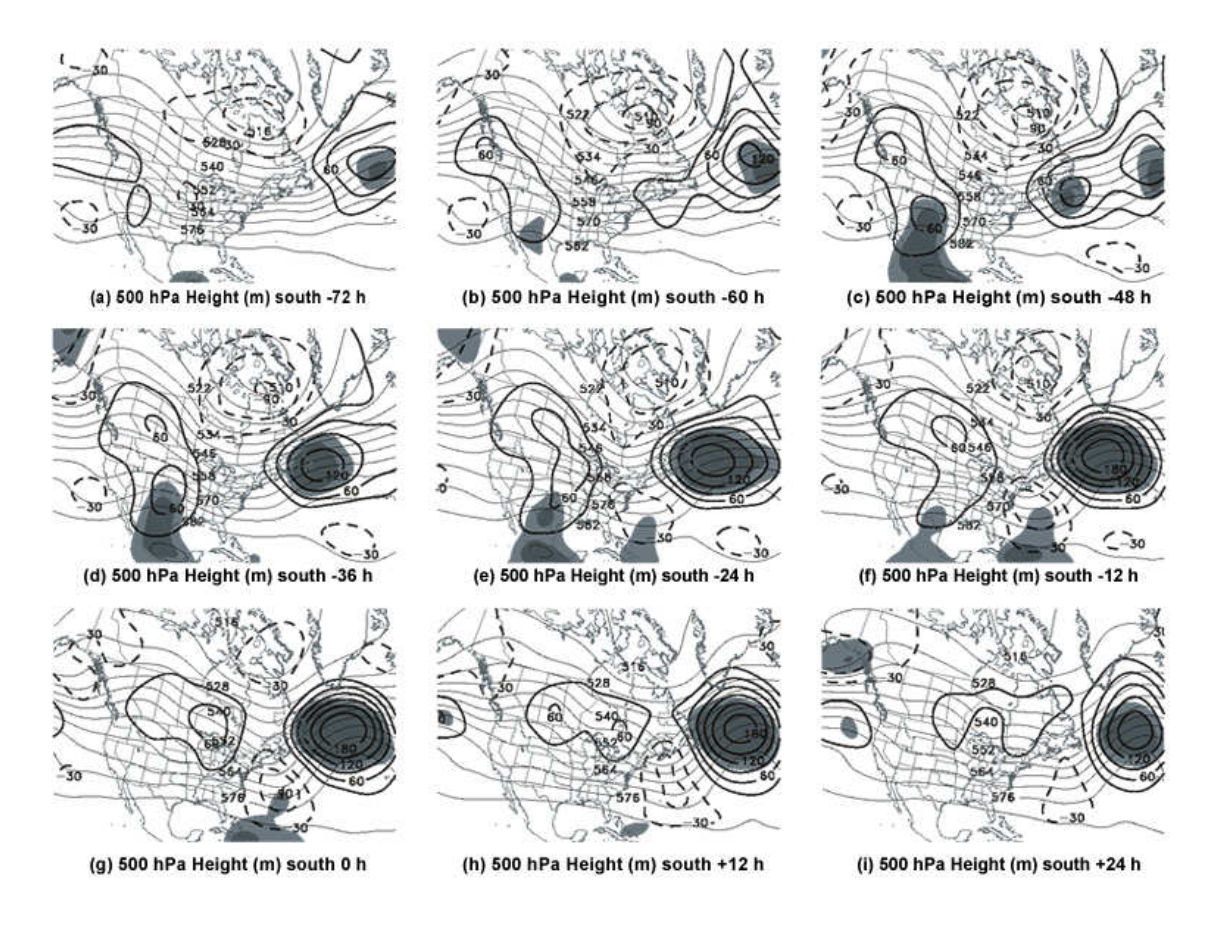


Figure 3.5: 500 hPa height anomalies every 3 dam, heavy dashed for negative values and heavy solid for positive values, with respect to climatology for the composite of the south cases at (a) -72, (b) -60, (c) -48, (d) -36, (e) -24, (f) -12, (g) 0, (h) +12, and (i) +24 h. Light solid contours represent full composite 500 hPa field, every 6 dam. Shading represents statistical significance of the anomalies at the 95% (lighter shading) and 99% (darker shading) confidence levels, according to the Student's t test.



Figure 3.6: PW anomalies every 2 mm, heavy dashed for negative values and heavy solid for positive values, with respect to climatology, for the south cases at (a) -48, (b) -36, (c) -24, (d) -12, (e) 0, and (f) +12 h. Light solid contours represent full composite PW field, every 6 mm. Shading represents statistical significance of the anomalies at the 95% (lighter shading) and 99% (darker shading) confidence levels, according to the Student's t test.

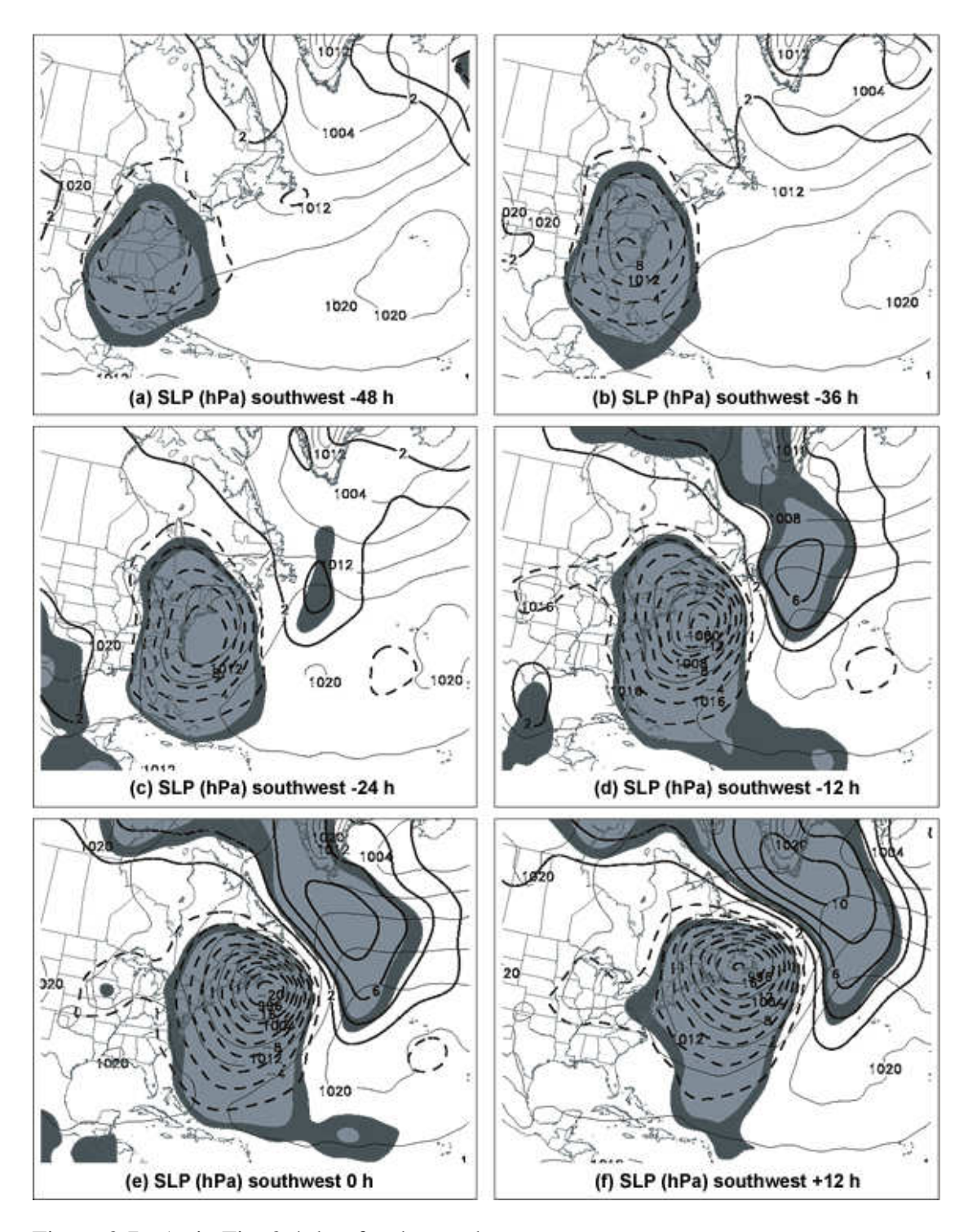


Figure 3.7: As in Fig. 3.4, but for the southwest cases.

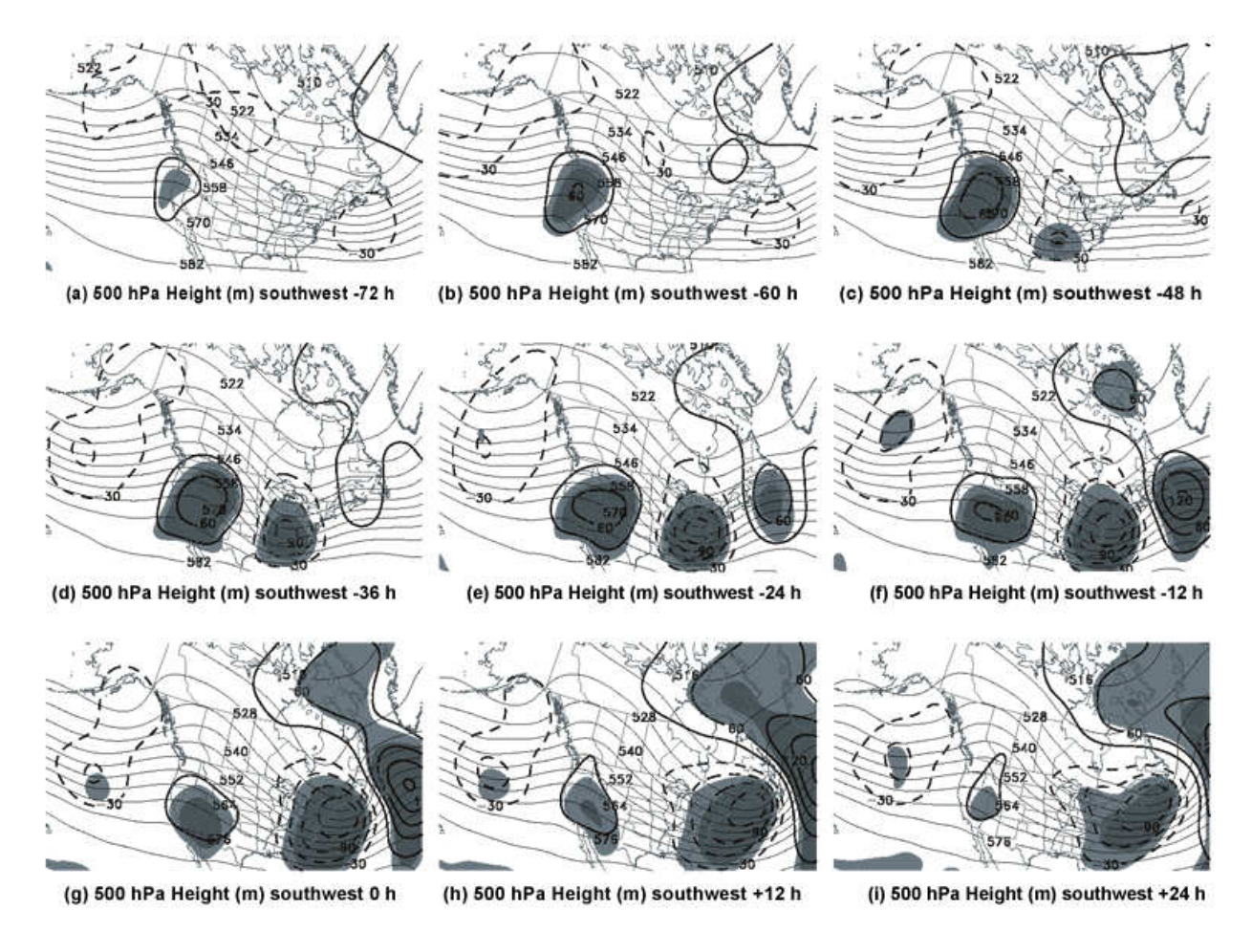


Figure 3.8: As in Fig. 3.5, but for the southwest cases.

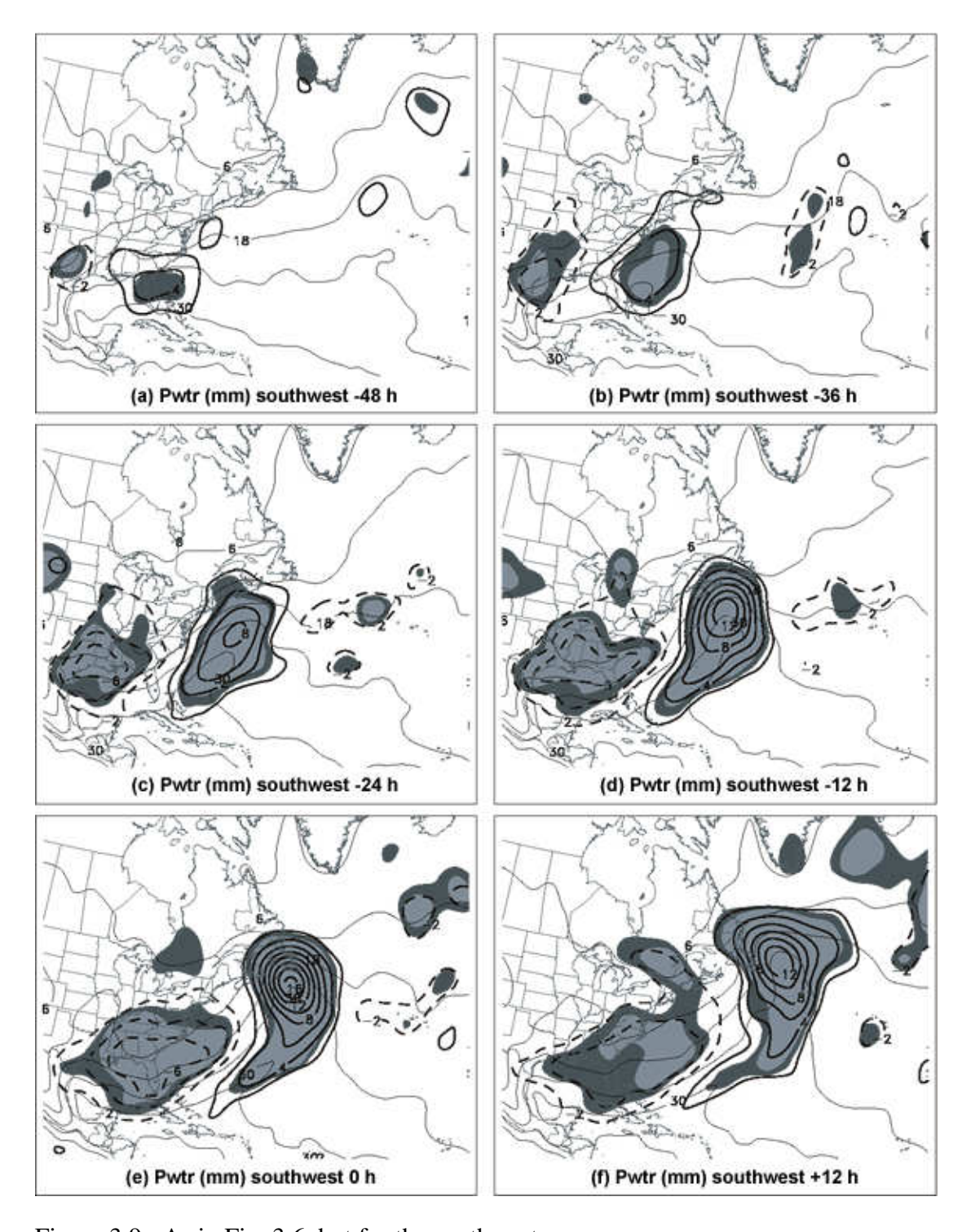


Figure 3.9: As in Fig. 3.6, but for the southwest cases.

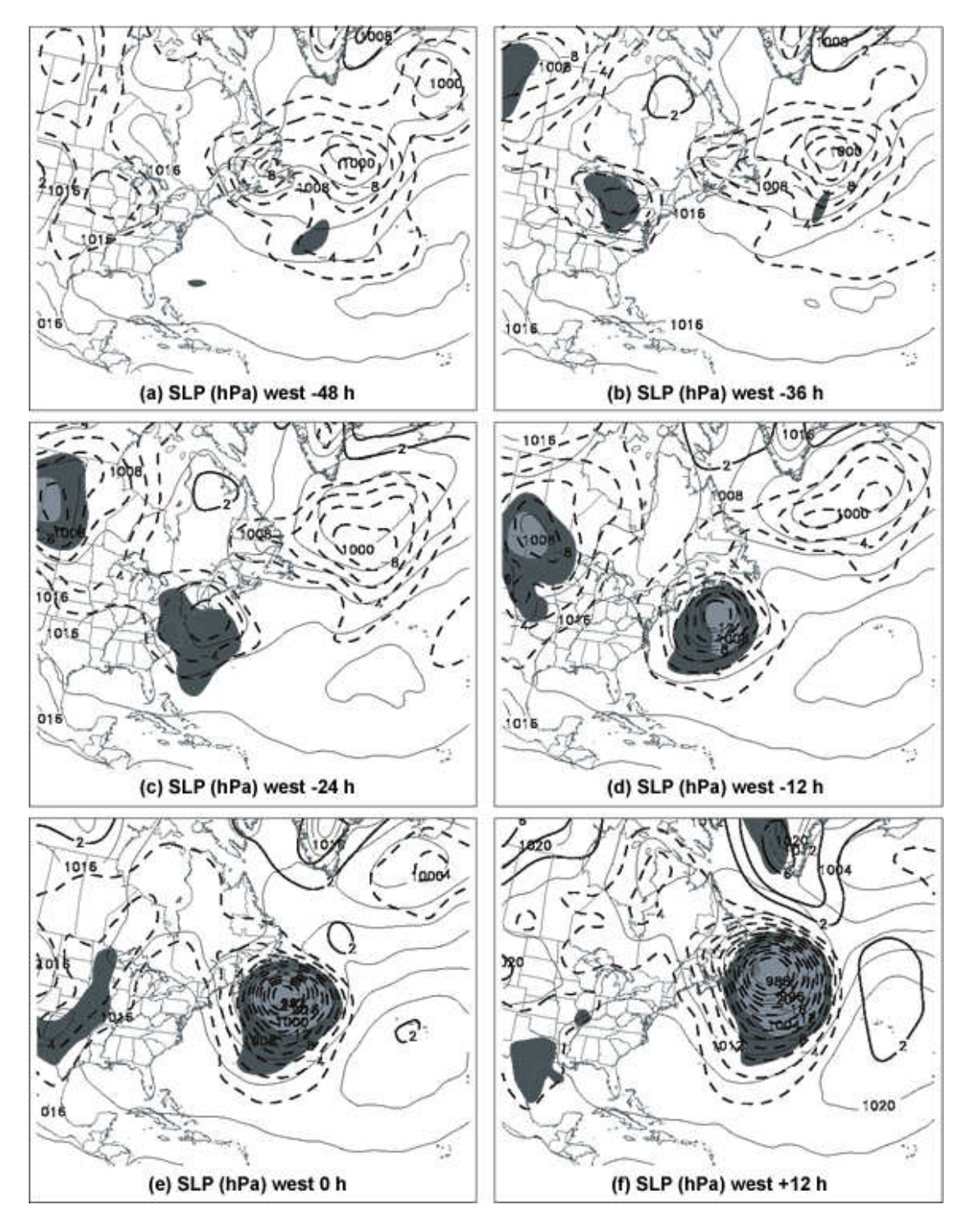


Figure 3.10: As in Fig. 3.4, but for the west cases.

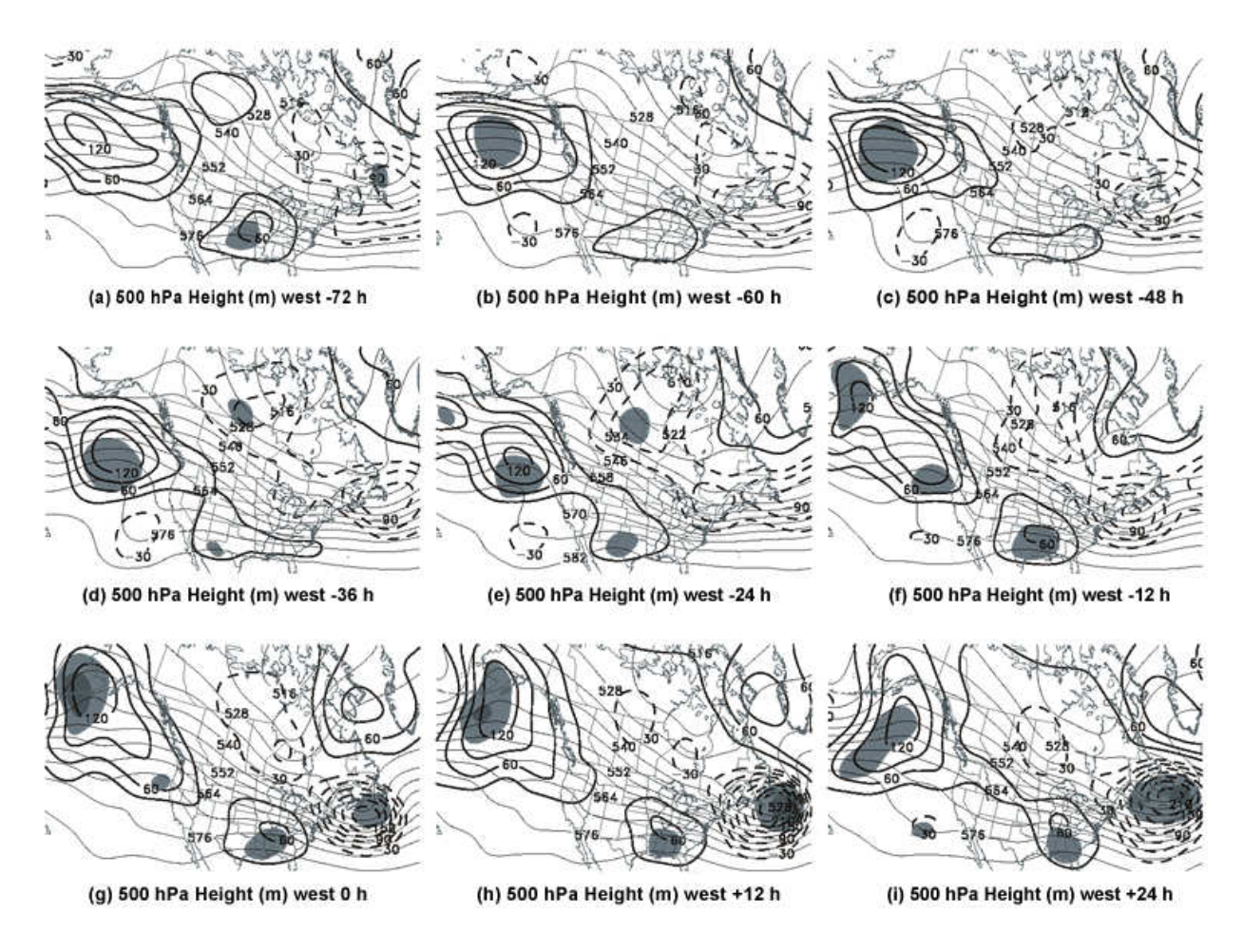


Figure 3.11: As in Fig. 3.5, but for the west cases.

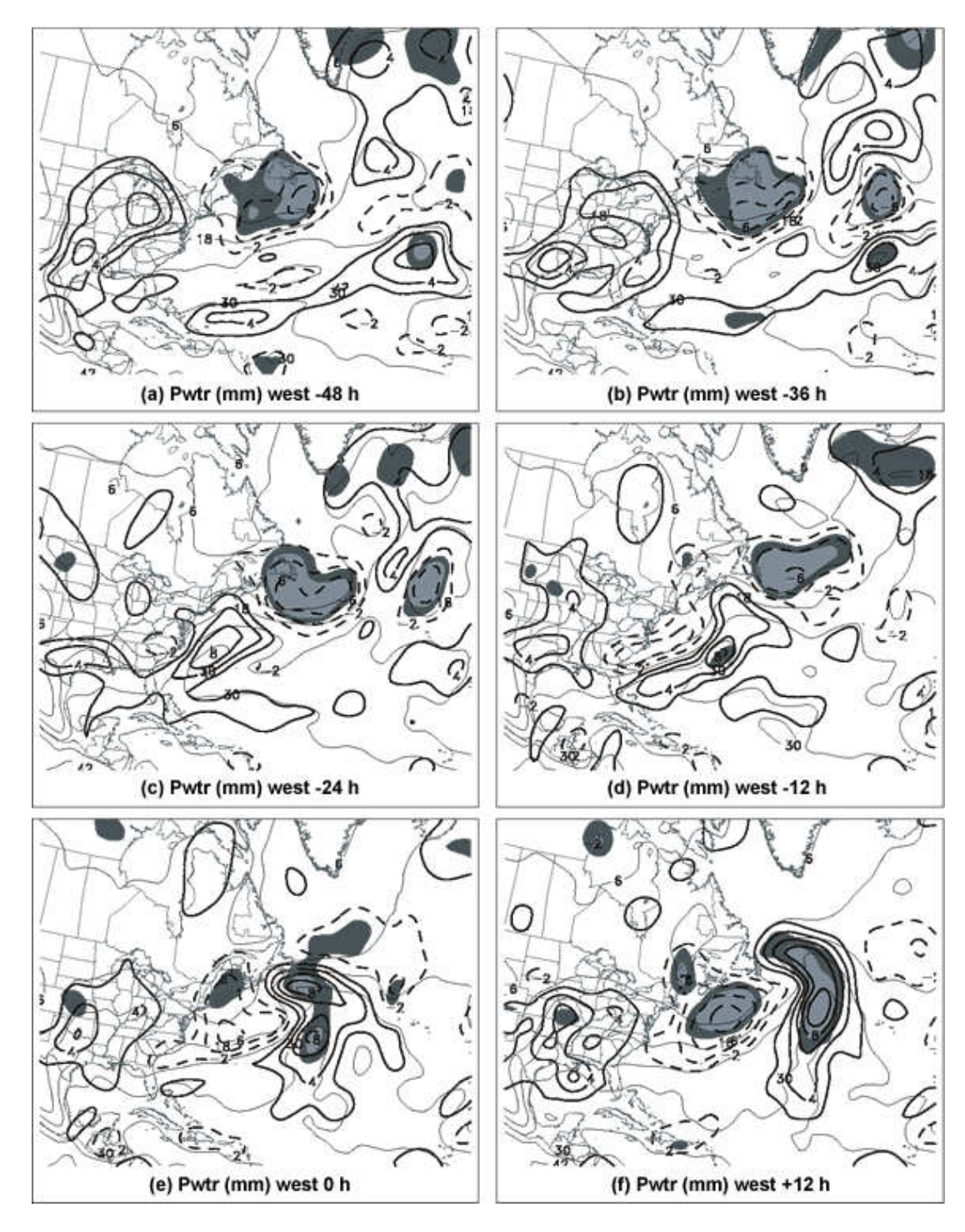


Figure 3.12: As in Fig. 3.6, but for the west cases.

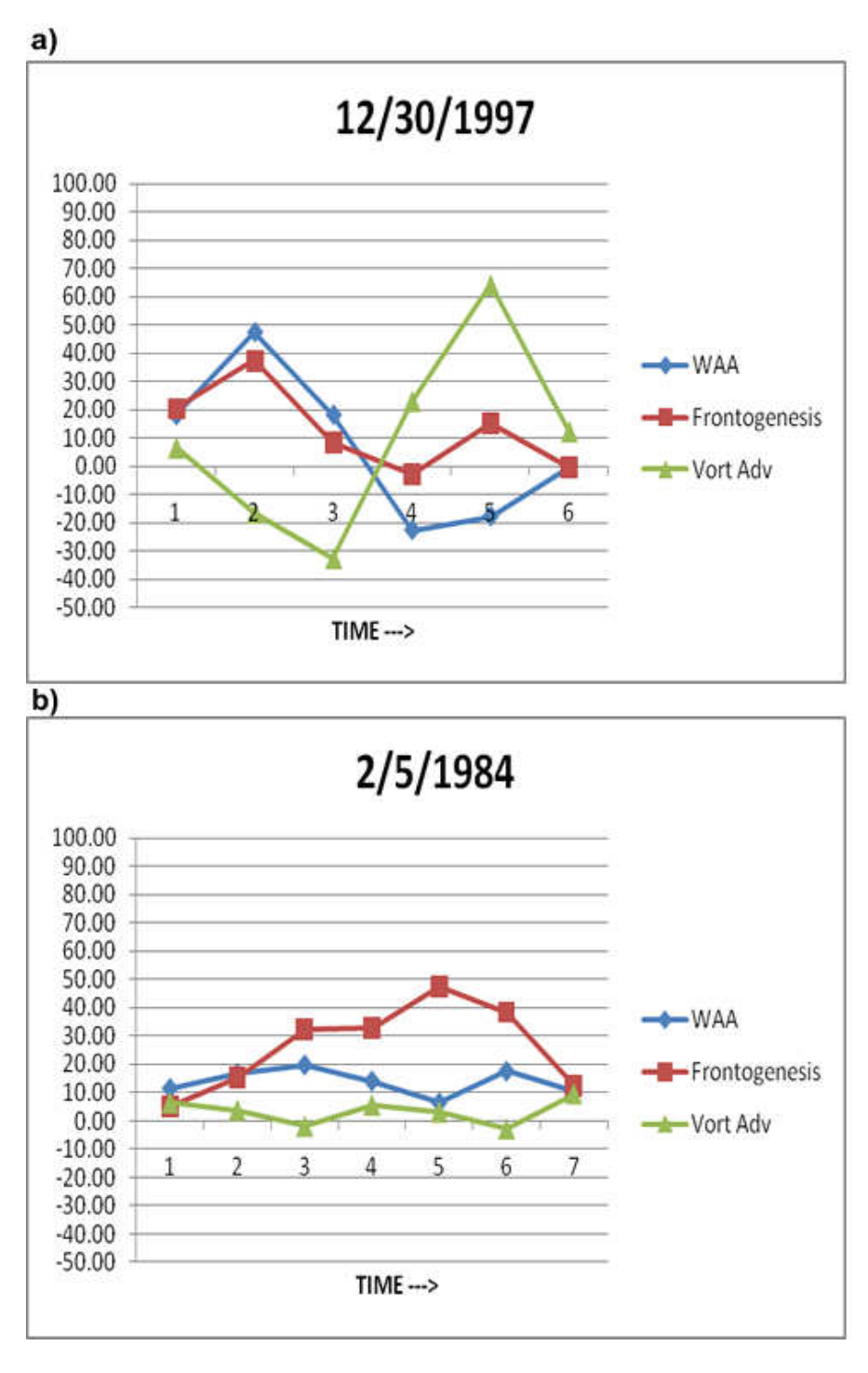


Figure 3.13: Time series during which precipitation was recorded at St. John's of NCEP Global Reanalysis 700-400 hPa layer-averaged relative vorticity advection $\times 10^{-10}$ s⁻² (green), 1000-700 hPa layer-averaged horizontal temperature advection $\times 10^{-5}$ Ks⁻¹ (blue), and 1000-700 hPa layer-averaged frontogenesis $\times 10^{-2}$ K/100 m/3 hr (red) for (a) a cyclone case and (b) a frontal case. Time on the horizontal axis is every six hours, with time "4" being t=0 h.

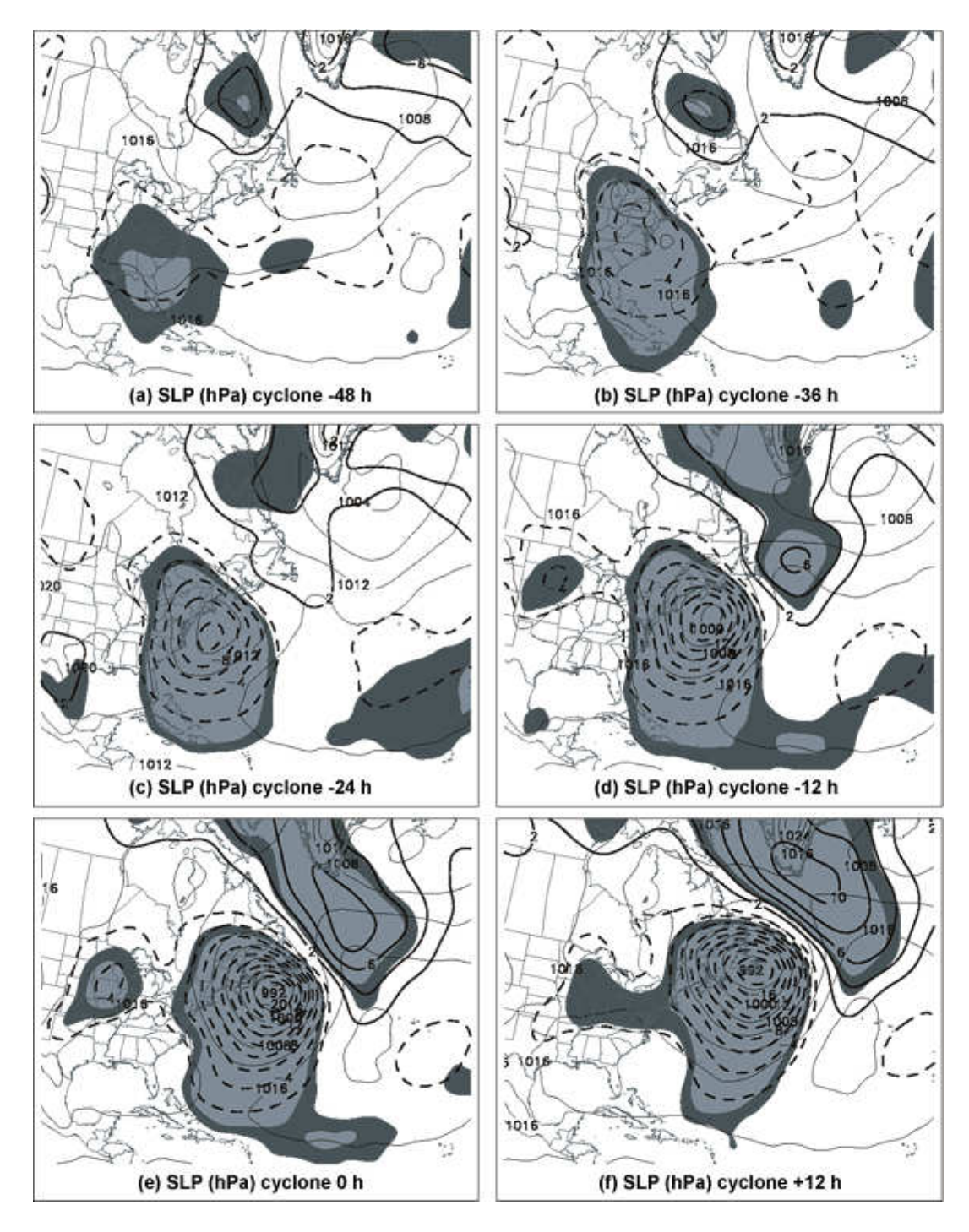


Figure 3.14: Sea-level pressure (SLP) anomalies every 2 hPa, heavy dashed for negative values and heavy solid for positive values, with respect to climatology, for the cyclone cases at (a) -48, (b) -36, (c) -24, (d) -12, (e) 0, and (f) +12 h. Light solid contours represent full composite SLP field, every 4 hPa. Shading represents statistical significance of the anomalies at the 95% (darker shading) and 99% (lighter shading) confidence levels, according to the Student's t test.

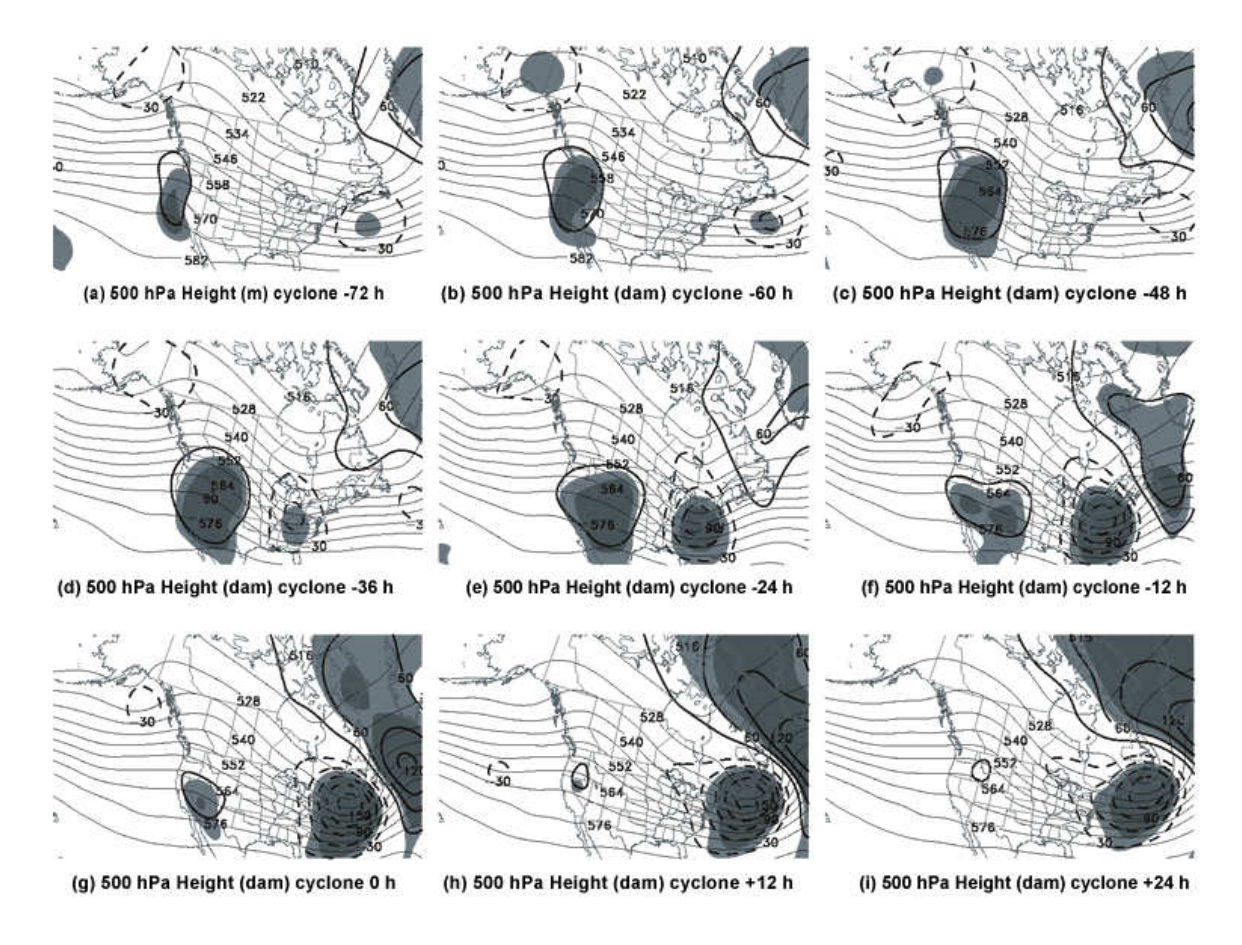


Figure 3.15: 500 hPa height anomalies every 3 dam, heavy dashed for negative values and heavy solid for positive values, with respect to climatology for the composite of the cyclone cases at (a) -72, (b) -60, (c) -48, (d) -36, (e) -24, (f) -12, (g) 0, (h) +12, and (i) +24 h. Light solid contours represent full composite 500 hPa field, every 6 dam. Shading represents statistical significance of the anomalies at the 95% (lighter shading) and 99% (darker shading) confidence levels, according to the Student's t test.

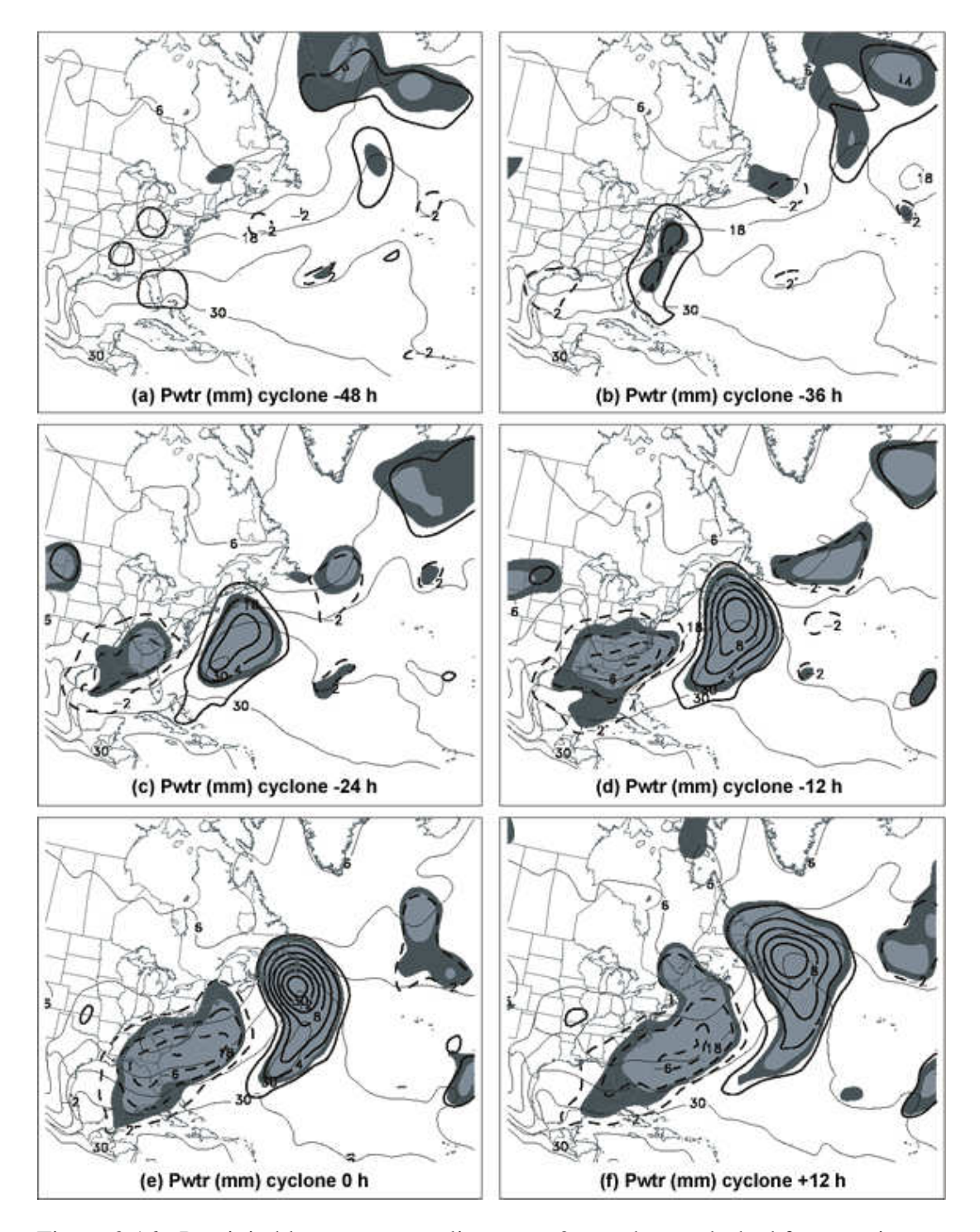


Figure 3.16: Precipitable water anomalies every 2 mm, heavy dashed for negative values and heavy solid for positive values, with respect to climatology, for the cyclone cases at (a) -48, (b) -36, (c) -24, (d) -12, (e) 0, and (f) +12 h. Light solid contours represent full composite PW field, every 6 mm. Shading represents statistical significance of the anomalies at the 95% (lighter shading) and 99% (darker shading) confidence levels, according to the Student's t test.

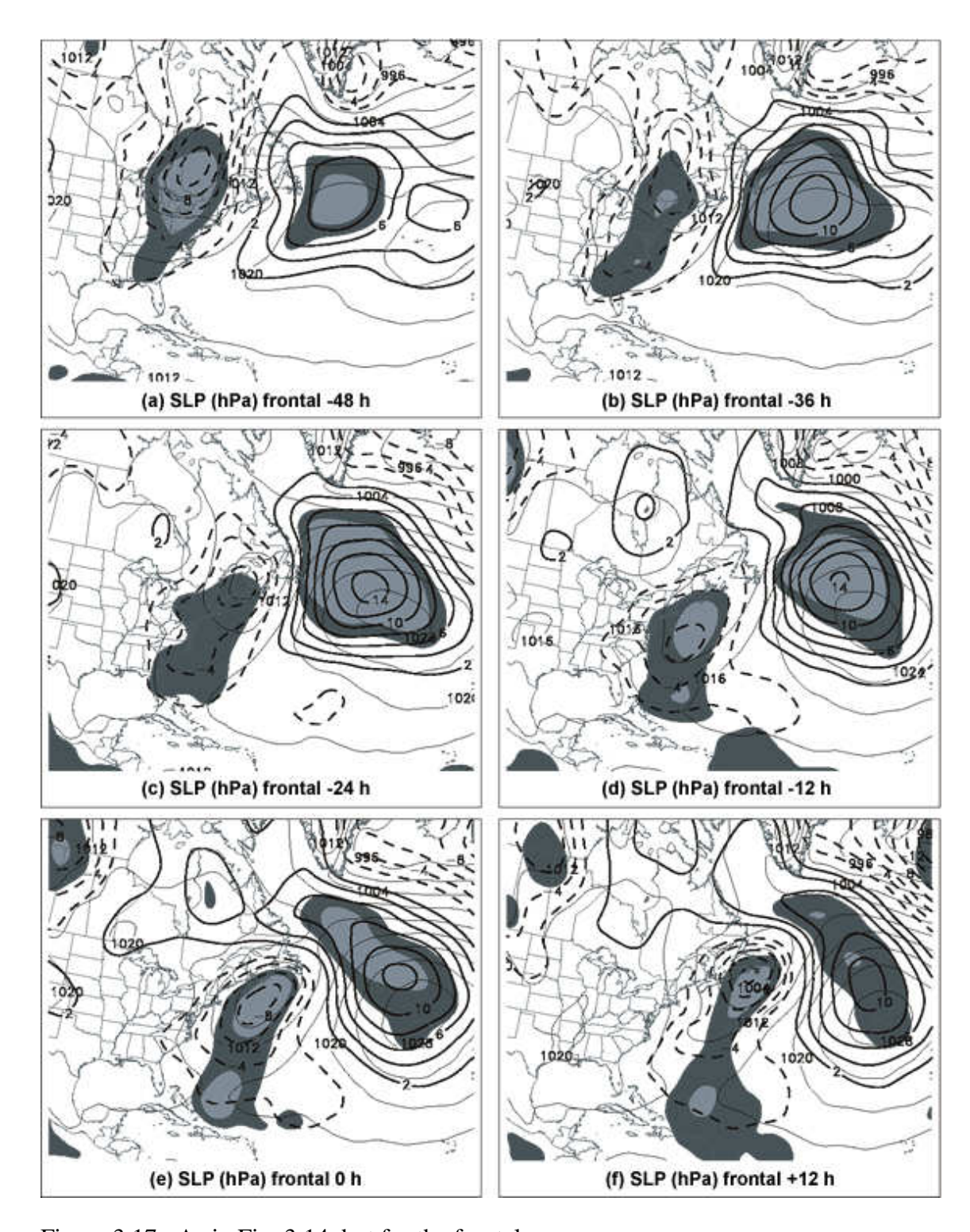


Figure 3.17: As in Fig. 3.14, but for the frontal cases.

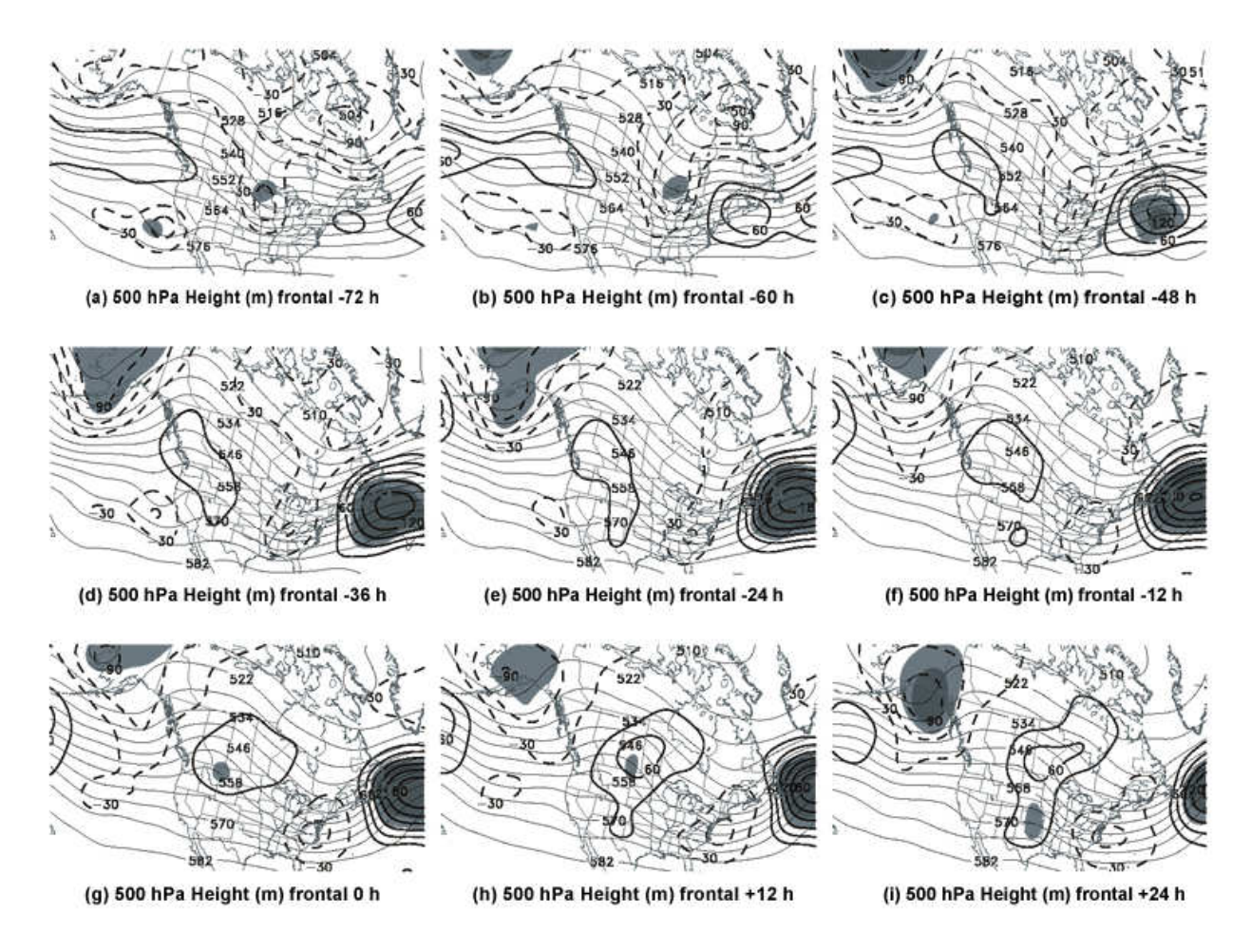


Figure 3.18: As in Fig. 3.15, but for the frontal cases.

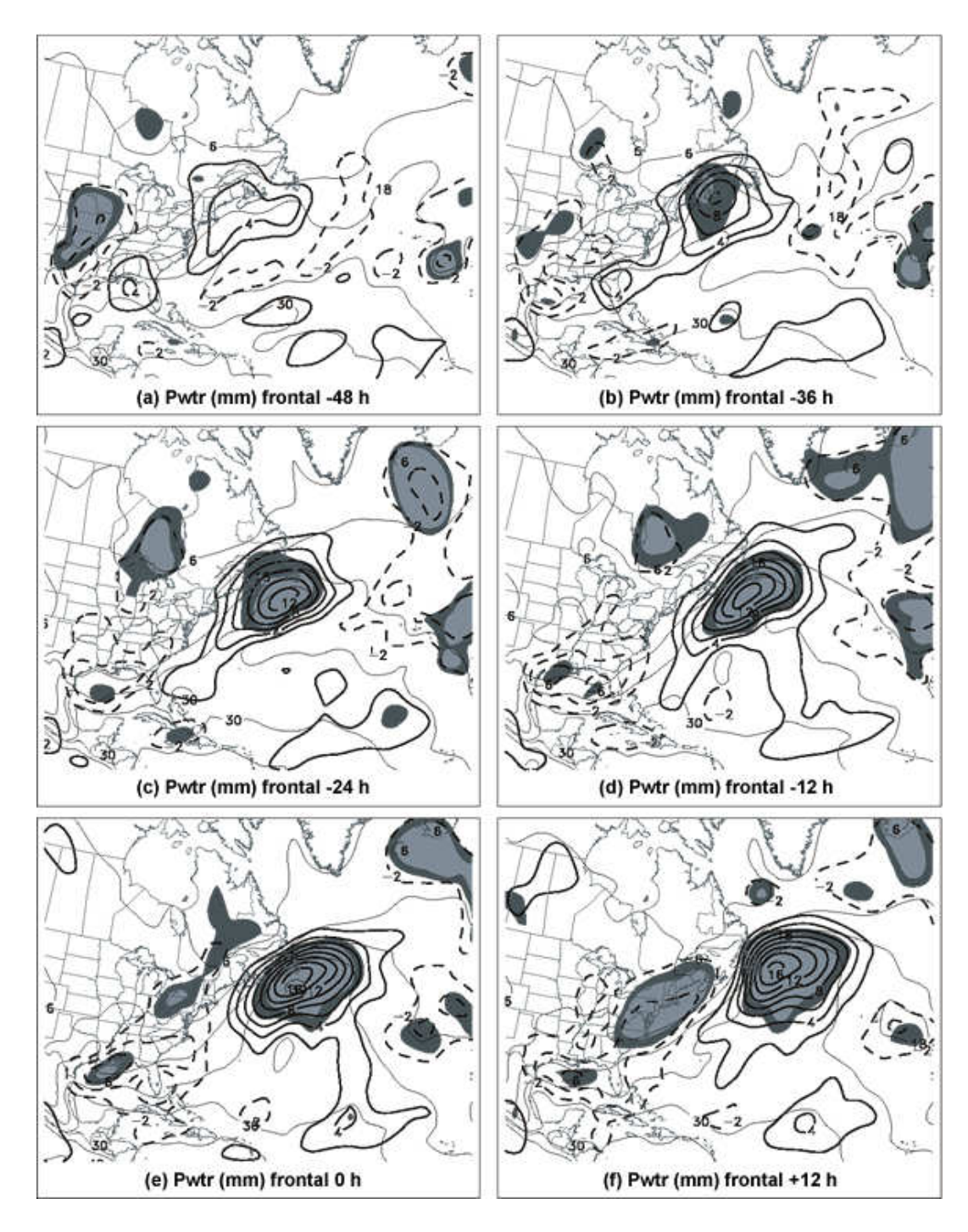


Figure 3.19: As in Fig. 3.16, but for the frontal cases.

Chapter 4

A Diagnostic Examination of Consecutive Extreme Cool-Season Precipitation Events at St. John's, Newfoundland in December 2008

Chapter 3 focuses primarily on a sub-compositing (manual synoptic typing) of the fifty extreme events defined in Chapter 2. The synoptic typing is accomplished by utilizing two separate partitioning methodologies. The first methodology is a 5-day backward trajectory analysis, which separates extreme precipitation events by air parcel source region. Three types of events are established: south, southwest, and west. South events are associated with relatively weak sea-level cyclones that originate in the Atlantic Ocean south of St. John's and with a strong sea-level anticyclone downstream of St. John's. Southwest events are those with air parcels originating in the Gulf of Mexico and are typically caused by an intense sea-level cyclone that forms in the Gulf of Mexico and rapidly intensifies as it moves northeastward towards St. John's. Finally, west events are associated with sea-level cyclones that take an Alberta Clipper track and contain strong upper-tropospheric dynamics that do not produce a strong sea-level cyclone until reaching lower static stability air over the Atlantic Ocean.

The second partitioning methodology utilized in Chapter 3 revolves around three commonly used quasi-geostrophic ascent-forcing variables: low-tropospheric horizontal temperature advection, mid-tropospheric vorticity advection, and low-tropospheric frontogenesis. Two event types are established, cyclone and frontal. The composite features in the cyclone group exhibit a stark resemblance to the features in the overall extreme composite presented in Chapter 2, primarily a strong sea-level cyclone originating in the Gulf of Mexico. In contrast, the frontal group composite displays a relatively benign synoptic pattern dominated by an anticyclone downstream, strong southerly flow and moisture transport into St. John's, and a northeast-southwest oriented baroclinic zone that is quasi-stationary near St. John's.

The goal of this chapter is to apply the lessons learned and synoptic types of Chapter 3 to an investigation of consecutive extreme precipitation events at St. John's in December 2008. First, Section 4.1 mentions past infamous precipitation events in eastern North America over the last few decades and highlights some of the important analyses performed with regard to those cases. In Section 4.2, the data used for this analysis is described, along with the primary objectives of this chapter.

Section 4.3 discusses the evolution of the first case, which produces 73.6 mm of precipitation at St. John's in 48 hours, exceeding the median extreme amount defined in Chapter 2 by over 30 mm. Specifically, Section 4.3.1 presents meteograms and time series of infared satellite imagery, in addition to applying the synoptic typing methodologies outlined in Chapter 3. It is found that the first

case in this chapter is a southwest trajectory and cyclone case. Finally, Section 4.3.2 presents a detailed synoptic-dynamic analysis of the first case, including but not limited to the following analyses: Dynamic tropopause (DT), sea-level pressure, coupling index (CI), observed soundings, and cross sections (to investigate the possibility of convective and slantwise instability).

Section 4.4 discusses the second case, which produces 54 mm of precipitation in a 48-hour period at St. John's and exceeds the median extreme event by ~10 mm. Section 4.4.1 details the finding that the second case is a southwest trajectory and frontal case and Section 4.4.2 presents a synoptic-dynamic analysis. Finally, Section 4.5 presents a concluding discussion of the two events, including the assertion that these two cases are unusual not only in their extremity, but also in the fact that they occur within two days of each other, yet are caused by rather disparate synoptic-dynamic means.

The following is based on: Milrad, Shawn M., E.H. Atallah, and J.R. Gyakum, 2010b: A diagnostic examination of consecutive extreme cool-season precipitation events at St. John's, Newfoundland in December 2008. *Wea. Forecasting*, submitted. (c)American Meteorological Society. Reprinted with permission.

A diagnostic examination of consecutive extreme cool-season precipitation events at St. John's, Newfoundland in December 2008

Shawn M. Milrad, Eyad H. Atallah and John R. Gyakum

Department of Atmospheric and Oceanic Sciences, McGill University

Abstract

St. John's, Newfoundland (CYYT) is frequently affected by extreme precipitation events, particularly in the cool season (October-April). Previous work classifies precipitation events at St. John's into categories by precipitation amount and a manual synoptic typing is performed on the fifty median extreme precipitation events, using two separate methods.

Here, consecutive extreme precipitation events in December 2008 are analyzed. These events occur over a 6-day period and produce over 125 mm of precipitation at St. John's. Using a backward trajectory analysis, each event is classified as southwest, although with parcel evolutions that are more complicated than seen in median extreme events. The second methodology of manual synoptic typing finds that the first event is classified as a cyclone, while the second is a frontal event.

A synoptic analysis of both events is conducted, highlighting important dynamic and thermodynamic structures. The first event is characterized by strong quasi-geostrophic ascent in a weakly stable atmosphere in association with a rapidly intensifying extratropical cyclone off the east coast of North America and transient high values of tropical moisture. The second event is characterized by moderate ascent in a more stable atmosphere in the presence of high values of low-level frontogenesis and quasi-stationary high values of subtropical moisture, in association with a northeast-southwest oriented baroclinic zone situated near St. John's. The synoptic structures responsible for the two events highlight rather disparate means to affect an extreme precipitation event at St. John's.

4.1 Introduction

Atlantic Canada (Fig. 2.1), and more specifically, St. John's,

Newfoundland (CYYT), is a location susceptible to extreme precipitation events,
particularly in the cool season (Stewart et al. 1987), and defined in Chapter 2 as

October-April. Located at the confluence of several North American storm tracks
(Fig. 2.2) and near the convergence zone of the cold southward-flowing Labrador
current and the warm northward-flowing Gulf Stream current (Aguado and Burt
2007), St. John's is prone to extreme precipitation events, often (but not always)
associated with intense cyclogenesis.

The motivation for this paper centers around utilizing the analyzed synoptic structures and manual typing methodologies in Chapters 2 and 3 as the basis for a dynamic and thermodynamic analysis of consecutive extreme precipitation events that occur from 7 to 12 December 2008. During this time,

over 125 mm of precipitation is recorded at St. John's. The precipitation totals for each event would rank in the top 20 cool-season precipitation events at St. John's (Chapter 2) since 1979. The first event (hereafter MAG 1), from 1200 UTC 7 December-1200 UTC 9 December, results in 73.6 mm of precipitation (Fig. 4.1), while the second event (hereafter MAG 2), from 0000 UTC 11 December-0000 UTC 13 December, results in 54 mm of precipitation (Fig. 4.12).

Case studies of extreme precipitation events (often involving intense cyclogenesis) are not new in atmospheric science. The Presidents' Day snowstorm of 18-19 February 1979 is outlined by Bosart (1981), Bosart and Lin (1984), Uccellini et al. (1984, 1985), and Whitaker et al. (1988). Bosart (1981) finds that the rapid deepening of the sea-level cyclone is not in accordance with quasi-geostrophic theory and instead is related to convection near the storm center where Bosart (1981) states that "cold polar air is rapidly being warmed, moistened, and destabilized by oceanic sensible and latent heat fluxes." In Bosart and Lin (1984), the authors argue that a tropopause fold is present west of the cyclone, in addition to the presence of *in-situ* low-level vorticity near the center of the evolving sea-level cyclone. Uccellini et al. (1984) isolate three separate jet streaks which they believe play a crucial role in the evolution of the storm, especially during the period of rapid cyclogenesis, while Uccellini et al. (1985) closely examine the tropopause fold and extrusion of stratospheric air associated with an intensifying upper-level trough located to the west of the sea-level cyclone. Finally, Whitaker et al. (1988) utilize a backward trajectory analysis to identify different airstreams that converge into the region of cyclogenesis.

Kocin et al. (1995) discuss the storm track, precipitation amounts, and damage caused by the Superstorm of 12-14 March 1993. Time series of satellite imagery are provided and show the classic comma-cloud structure expected from a rapidly intensifying cool-season cyclone. Bosart et al. (1996) examine precursor structures to the Superstorm of 1993 on a global scale, including elements of downstream Rossby wave development that is also found to have an impact in the extreme event composite presented in Chapter 2. Moreover, Bosart et al. (1996) and Dickinson et al. (1997) present an analysis of the uppertropospheric dynamics of the Superstorm using potential vorticity (PV) analyses on the dynamic tropopause (DT), the latter of which includes a discussion of the enhancement of the downstream upper-level ridge due to latent heat release from extreme precipitation. Dickinson et al. (1997) also comment on the fact that the Gulf of Mexico is a well-known source region for cyclogenesis, albeit one in which rapid intensification (as was the case with the Superstorm) is rarely seen during the cool season. Finally, Huo et al. (1995) perform a diagnostic analysis of the Superstorm of 1993, focusing on the static stability of the environment prior to and during rapid cyclogenesis, and the interaction of positive PV anomalies on the DT.

Other important events in the past thirty years include but are not limited to: the "surprise" snowstorm over the mid-Atlantic region in January 2000 (Brennan and Lackmann 2006), the QE II cyclone of September 1978 (Uccellini 1986; Gyakum 1991), an explosive cyclogenesis event detailed by Wash et al. (1990) that was observed during the Genesis of Atlantic Lows Experiment

(GALE), and the crippling ice storm of January 1998, which impacted much of southern Quebec and Ontario, as well the interior northeast U.S. (Gyakum and Roebber 2001; Roebber and Gyakum 2003).

The analyses of historical cases of extreme precipitation are important to this paper because they serve as a basis for the synoptic analysis presented. Many of the processes examined in these previous studies are highlighted in MAG 1, which is associated with a rapidly intensifying sea-level cyclone off the coast of North America. While MAG 2 does not involve a rapidly intensifying cyclone, similarities to previous case studies of extreme precipitation include: moisture transport to higher latitudes observed by Huo et al. (1995) in the Superstorm, and tropical moisture source regions, as observed in the 1998 Ice Storm by Gyakum and Roebber (2001).

Another motivation for this paper is the relative lack of literature regarding extreme precipitation events in Atlantic Canada. Much of the work on extreme precipitation events in Atlantic Canada is associated with occurrences of intense cyclogenesis during the field project known as the Canadian Atlantic Storms Program (CASP), Phase I of which was conducted from January to March 1986 (Stewart et al. 1987), coinciding with GALE (Dirks et al. 1988) and Phase II of which took place during the same period in 1992 (Stewart et al. 1991). While much of the work associated with CASP I and II focuses on mesoscale structures within east coast cyclones (e.g. Stewart et al. 1990; Reuter and Yau 1990), a few published works detail cases of intense cyclogenesis (e.g. Yau and Jean 1989; Stewart and Donaldson 1989; Gyakum et al 1996; Gyakum and Stewart 1996;

Huo et al. 1996). Gyakum et al. (1996) address the climatological characteristics of storm tracks and areas of cyclogenesis in the Atlantic Canada region and state that while explosive intensification typically takes place off the east coast of the United States and Canada, the "formative stages of these dangerous storms do occur in regions far upstream," and that proper analysis of these upstream features is crucial to producing an accurate forecast for Atlantic Canada.

The main objective of this paper is to analyze and contrast the dynamic and thermodynamic structures associated with, and responsible for, MAG 1 and MAG 2, two extreme events at St. John's that are caused by substantially disparate means. The composite structures and manual synoptic typing methodologies outlined in Chapters 2 and 3, respectively, serve as a basis for the analysis presented in this study.

4.2 Data and Methodology

4.2.1 Data

This study utilizes 6-hourly precipitation data for St. John's, obtained from the Environment Canada 6-hour corrected precipitation database. The corrected precipitation data are based on work done by Mekis and Hogg (1999), whereby the data have been adjusted to accurately reflect precipitation gauge changes, wind conditions, and changes in station location. All precipitation data in this study are observed in liquid equivalent form (i.e. no data are acquired using ruler methods), limiting errors associated with frozen precipitation. The National Centers for Environmental Prediction (NCEP) Global Forecast System (GFS)

final analysis, with a horizontal resolution of 0.5 degrees, is used as the dataset for all synoptic analyses, which differs from the choice of analyses in Chapters 2 and 3, where the NCEP/NCAR Global Reanalysis, with a horizontal resolution of 2.5 degrees (Kalnay et al. 1996), and NCEP North American Regional Reanalysis (NARR) (Mesinger et al. 2006), with a horizontal resolution of 32 km, are used. The authors believe that while the dataset does not extend far enough back historically to be used for the composites in Chapters 2 and 3, the GFS 0.5 degree analysis is a superior tool for MAG 1 and 2, primarily in terms of resolution with respect to the NCEP Global Reanalysis, and accuracy with respect to the NARR, the details of the latter which are presented in Section 4.2.2. The backward trajectory analysis is performed using the National Oceanic and Atmospheric Administration's (NOAA) Air Resources Laboratory HYSPLIT model, available for download at http://www.arl.noaa.gov/HYSPLIT.php. In Chapter 3, the HYSPLIT model was found to produce nearly identical results to the program developed by Aiyyer (personal communication 2008) that is used in Chapter 3. The radar data are provided by Environment Canada's Atlantic Climate Centre and the satellite imagery is obtained from NOAA's Comprehensive Large Arraydata Stewardship System (CLASS), available online at http://www.class.ncdc.noaa.gov/saa/products/welcome. The vast majority of calculations and analyses in this study are displayed using the General Meteorological Package version 5.11.1 (updated from the original package devised by Koch et al. (1983)), a data manipulation and visualization software package.

4.2.2 Methodology

The methodology of this paper revolves around two main points:

- The application of both methods of manual synoptic typing outlined in Chapter 3 to MAG 1 and MAG 2, as well as a validation of the composite synoptic structures observed for the median extreme cases (Chapter 2) and the various synoptic types (Chapter 3).
- When discussing heavy precipitation, Eq. 4.1 should be considered, where precipitation (P) is assumed equal to condensation, g is the acceleration of gravity, ω is the vertical motion in pressure coordinates, and (dr_s/dp)_{ma} is the saturation mixing ratio lapse rate along the moist adiabat (i.e. a measure of air mass). Eq. 4.1 relates the precipitation rate to the integrated ascent (assumed for the purpose of this paper to be primarily quasigeostrophic) and incipient air mass. These quantities should be considered to be integrated from the surface to the tropopause. The dynamic and thermodynamic analyses in Sections 4.3.2 and 4.4.2 for MAG 1 and MAG 2, respectively, strive to illustrate the relative contributions of dynamic forcing and thermodynamic properties of the air mass involved.

$$\mathbf{P} = -\frac{1}{g} \int \omega \left(\frac{dr_s}{dp} \right)_{ma} dp \tag{4.1}$$

The definition of time t=0 h is consistent with that established in Chapters 2-3, and refers to the onset of the 6-hour period of maximum recorded precipitation at St. John's. Comparisons of backward trajectories and synoptic structures among the GFS analysis, the NCEP/NCAR Global Reanalysis and NARR have been made (not shown) and are confirmed to be similar. While the precipitation output from the GFS analysis is not perfect for either case, it is superior to the NCEP/NCAR Global Reanalysis and especially to the NARR. The superiority of the GFS analysis to the NARR over Canada is largely due to substantial observed errors in the NARR precipitation and moisture flux convergence fields over Canada. These problems include, but are not limited to precipitation 'stopping' at the Canadian border prior to a change in assimilation scheme in 2002 and substantial positive errors in the precipitation and moisture convergence fields since the switch to the model-based assimilation scheme in 2002 (Carrera and Hryciw, personal communication 2009). While the NARR problems are not a focus of this paper, the authors hope to address them in-depth in the future.

4.3 MAG 1: December 8th, 2008

4.3.1 Overview and Synoptic Typing

MAG 1 affects St. John's from 1200 UTC 7 December 2008 until 1200 UTC 9 December 2008, where t=0 is 0600 UTC 8 December 2008. Overall, 73.6 mm of precipitation fell at St. John's during MAG 1 (Fig. 4.1), which would rank as the fifth most extreme precipitation event compiled in Chapter 2. To put this in context, MAG 1 exceeds the median extreme event defined in Chapter 2 by approximately 30 mm. As shown in Fig. 4.1, most of the precipitation (63 mm) falls in a 24-hour period from 1200 UTC 7 December to 1200 UTC 8 December, in association with the approach of a rapidly intensifying cyclone. During this time period, the atmosphere at St. John's is almost completely saturated (Fig. 4.1a, b) and the temperature slowly rises from around 0° C at 1200 UTC 7 December to just above 10° C shortly after 0600 UTC 8 December. Subsequently, the surface proceeds to slowly cool, reaching a temperature of around -3° C by 1200 UTC 9 December, at the end of the event.

Observed surface winds during MAG 1 shift from easterly at 1200 UTC 7

December to southerly during the period of heaviest precipitation, from 0000

UTC 8 December to 1400 UTC 8 December, and finally, westerly from 1400

UTC 8 December until the end of the event (Fig. 4.1). Light to moderate snow falls for the first few hours of the event (Fig. 4.1a), but quickly changes to light to moderate rain by 1700 UTC 7 December (Fig. 4.1a) in association with rising temperatures, and tapers to rain showers by 0000 UTC 9 December, and finally, light snow by 1000 UTC 9 December (Fig. 4.1c). The observations of temperature trends, wind shifts and precipitation types are consistent with the passage of a typical mid-latitude cyclone at St. John's. Moreover, the wind shift

to the south just before 0000 UTC 8 December (Fig. 4.1a) is consistent with the rising surface temperature associated with a warm front moving through St.

John's in advance of the rapidly intensifying sea-level cyclone. The subsequent wind shift to the west after 1800 UTC 8 December (Fig. 4.1b) and accompanying surface cooling is associated with the passage of a trailing cold front. The heaviest precipitation at St. John's during MAG 1 occurs when the station is located in the warm sector of the cyclone, while the surface winds are onshore (southerly), bringing in moist air from the Atlantic Ocean. Finally, the observation of easterly surface winds during part of MAG 1 is consistent with the extreme composite in Chapter 2.

The evolution of MAG 1 is displayed in infared satellite imagery in Fig. 4.2. A coastal cyclone is not evident until t=-24 h (0600 UTC 7 December), when an area of clouds is present off the coast of Virginia and North Carolina (Fig. 4.2d). By t=-12 h, the cyclone has acquired the typical comma cloud structure often seen in rapidly intensifying extratropical cyclones, located just south of the Nova Scotia coast (Fig. 4.2e). At t=0 h and t=+6 h, the trailing cold front remains just west of St. John's as the sea-level cyclone moves northward into Labrador (Figs. 4.2f-h). Between t=+6 h and t=+12 h, the trailing cold front (Figs. 4.2h-i) moves through St. John's, coinciding with the surface wind shift to the west and surface temperature drop.

In Fig. 4.3, a time series of radar imagery from the Holyrood,

Newfoundland (St. John's) radar is presented, with images every six hours from

t=-18 h to t=+12 h. Fig. 4.3 shows that light precipitation is present at St. John's at t=-18 h (Fig. 4.3a) and bands of heavy precipitation are located just west of St. John's at t=-12 h (Fig. 4.3b) and t=-6 h (Fig. 4.3c). At t=0 h (Fig. 4.3d), heavy precipitation is located directly over the station and by t=+6 h (Fig. 4.3e), the precipitation has moved east of the station, following the passage of the trailing cold front. Fig. 4.3c-e suggest a rapid evolution of the mesoscale structure of the precipitation wherein the structure of precipitation is primarily banded at t=-6 h (Fig. 4.3c), cellular at t=0 h (Fig. 4.3d), and again banded at t=6 h (Fig. 4.3e). Similar results were found by Sanders and Bosart (1985a, b) in the case of the 1983 Megalopolitan snowstorm of 1983 and were suggested to be manifestations of symmetric instability. A further discussion on instabilities in the case of MAG 1 is presented in Section 4.3.2.

A five-day backward trajectory analysis is performed for MAG 1 at t=0 h (see Chapter 3 for methodology details). Trajectories end at approximately 300 hPa, 500 hPa, and 700 hPa. In Chapter 3, most of the extreme cases fit into one of three types based on parcel origin (west, southwest, and south). This is not true in the case of MAG 1, where the lower-level parcels primarily originate from the Atlantic Ocean (south), the mid-level parcels from the Gulf of Mexico (southwest) and the upper-level parcels from both the west and southwest (Fig. 4.4). In following Chapter 3, since the majority of the trajectories originate in the Gulf of Mexico, MAG 1 is classified as a southwest event. However, the bulk of the upper-level trajectories originate in the North Pacific, when the parcels curve

anticyclonically around an upper-level ridge over the west coast of North America at about t=-72 h, consistent with the extreme case composite of Chapter 2.

A time series of three dynamically relevant QG ascent-forcing parameters is displayed in Fig. 4.5a. The evolution of MAG 1 in Fig. 4.5a is in general agreement with the 'cyclone' cases in Chapter 3, such that the values of the 1000-700 hPa horizontal temperature advection and 1000-700 hPa frontogenesis are relatively high at St. John's at the start of the event, but rapidly become less positive around t=0 h, whereas the mid-level vorticity advection becomes substantially positive after t=0 h (Fig. 4.5). These values are consistent with the assertion in Chapter 3 of a typical mid-latitude cyclone passage just west of St. John's, such that a warm front moves through St. John's ahead of the sea-level cyclone and is followed 12-36 hours later by the passage of a trailing cold front and the approach of the associated upper-level trough. Additionally, it suggests a system that is tilted westward with height.

4.3.2 Synoptic-Dynamic Analysis

The accuracy of the GFS precipitation forecasts is not a major focus of this paper. However, the 6-hour precipitation forecasts are included as part of Fig. 4.6, where the precipitation forecasts are for the 6-hour period following the analyzed time. The GFS is fairly accurate in the timing of the precipitation associated with MAG 1, as the heaviest forecast precipitation falls between t=-6 h (Fig. 4.6f) and t=+6 h (Fig. 4.6g), during which 41 mm of precipitation actually falls (Fig. 4.1). The GFS precipitation amounts are under-forecasted by about 10

mm during the twelve hours of heaviest precipitation (Fig. 4.6f-g) and somewhat under-forecasted by about 5 mm during the surrounding times (t=-18 h to t=-6 h and t=+6 h to t=+12 h, Figs. 4.6e-f and 4.6h-i). In sum, the GFS manages to predict about 75% of the actual observed precipitation. However, the accuracy of the QPF does vary substantially with lead time and that will be the primary focus of future work.

Figure 4.7a indicates high values of potential temperature (θ) on the dynamic tropopause (DT), defined as the 2 PVU surface, over the west coast of North America at t=-72 h, consistent with the precursor composite ridge seen in the fifty median extreme cases in Chapter 2 and the thirty-five cyclone cases in Chapter 3. Additionally, a downstream upper-level trough (low values of θ on the DT) is present over the central portion of North America (Fig. 4.7a). In association with the upper-level trough, a weak sea-level cyclone is located over the northern Great Lakes at t=-48 h (Figs. 4.6b, 4.7b), which moves eastward and is situated near Lake Ontario at t=-24 h (Fig. 4.7d). By t=-24 h (Fig. 4.7d), the trough on the DT is approaching the eastern seaboard of the U.S. Concurrently, a secondary area of low pressure develops off the North Carolina coast (Fig. 4.7d). At t=-12 h (Fig. 4.7e), the initial sea-level cyclone over the Great Lakes disappears and is replaced by a 992 hPa sea-level cyclone off the eastern seaboard. The base of the trough on the DT is now located southwest of the developing sea-level cyclone, as the system establishes a westward tilt with height. From the initial sea-level cyclone development at t=-24 h (1008 hPa, Fig. 4.7d) to its position just west of St. John's at t=0 h (980 hPa, Fig. 4.7g), the

cyclone intensifies by 28 hPa, surpassing the "bomb" criterion established by Sanders and Gyakum (1980). By t=+12 h, after the trailing cold front has passed through St. John's, the cyclone center is located northeast of Labrador, with a minimum sea-level pressure of 968 hPa, completing a 50 hPa intensification in 36 hours.

At t=0 h, as the sea-level cyclone passes just west of the station (Fig. 4.6g), high values of θ on the DT are located over St. John's (Fig. 4.7g). In fact, the values of θ near St. John's steadily increase from t=-36 h (Fig. 4.7c) until the passage of the trailing cold front between t=+6 h and t=+12 h (Fig. 4.7h-i), and are quantitatively similar to values observed over the southern U.S. and Gulf of Mexico. The extremely warm DT at St. John's while the station is in the warm sector of the cyclone suggests the presence of a moist subtropical air mass. In addition, it is hypothesized that the downstream ridge on the DT intensifies from t=-24 h (Fig. 4.7d) to t=+6 h (Fig. 4.7h) due to a) strong low-level warm air advection ahead of the sea-level cyclone (Fig. 4.5a), and b) latent heat release as a result of the heavy precipitation seen in Fig. 4.3b-d. This is consistent with the hypotheses of Chapters 2 and 3, for the extreme and cyclone group composites, respectively. The presence of large values of low-level warm air advection ahead of the surface cyclone (in a region and time period marked by near-zero values of mid-level vorticity advection, Fig. 4.5a) suggests that there is unequivocal quasigeostrophic forcing for ascent during the time of heaviest precipiation. Accordingly, Fig. 4.5b shows that values of ω are most negative at t=-12 h and t=0 h, concurrent with the highest observed precipitation values (Fig. 4.1).

MAG 1 is a classic case of rapid east coast cyclogenesis; however, the climatology of Chapter 2 shows that 70+ mm of precipitation at St. John's during one precipitation event has occurred only five times in the past thirty years, strongly implying that only a small percentage of rapid cyclongenesis events near St. John's result in such a large amount of precipitation. Therefore, it is likely that the extreme precipitation as a result of MAG 1 is due to a potent combination of a myriad of factors. While it is established that large amounts of QG forcing for ascent (low-level warm air advection and low-level frontogenesis) are present at St. John's from t=-18 h to t=+6 h (Fig. 4.5a), both moisture availability and the thermodynamic properties of the air mass at St. John's during this time period are also crucial in explaining the amount of precipitation.

Figure 4.9 displays the 1000-700 hPa moisture transport vectors and associated moisture flux divergence, the latter of which is defined by Banacos and Schultz (2005). Even before the development of the sea-level cyclone off the North Carolina coast at t=-24 h (Fig. 4.9d), substantial moisture transport from the Atlantic Ocean and Gulf of Mexico is present on the western side of the downstream anticyclone. As the sea-level cyclone develops and rapidly intensifies, the moisture transport on the eastern flank of the cyclone increases, resulting in a broad area of moisture convergence at St. John's from t=-12 h to t=0 h (Figs. 4.9e-g). In addition, Fig. 4.5b shows that remarkably large values of precipitable water are present at St. John's from t=-12 h to t=+6 h; at t=0 h, in the middle of December at 47° N, the precipitable water value at St. John's is over 32 mm, concomitant with the strongest values of QG ascent (Fig. 4.5b). This value

of precipitable water is over 20 mm greater than the climatological (1971-2000) average at St. John's for the month of December (9.47 mm).

Supporting the assertion of warm moist air at St. John's on the east side (warm sector) of the rapidly intensifying cyclone, is the presence of large values of equivalent potential temperature (θ_e) at 850 hPa (Fig. 4.8). These θ_e values are greater than those present in the Gulf of Mexico, as a plume of moist subtropical air extends from near Bermuda northward to Atlantic Canada from t=-12 h to t=+6 h (Fig. 4.8e-h), before finally moving east of Newfoundland after t=+6 h (Fig. 4.8i), as the sea-level cyclone moves away.

The coupling index (CI), a measure of the bulk atmospheric stability, is used by Bosart and Lackmann (1995), Roebber and Gyakum (2003), and Galarneau and Bosart (2006) as θ on the DT minus the low-level θ_e . Here, the DT is the 2 PVU surface and the low-level θ_e is taken at 850 hPa (Galarneau and Bosart 2006). Figure 4.8e-h shows that an area of relatively low CI (< 8 K) approaches St. John's from the southwest, at the time of heaviest precipitation, suggesting that the atmospheric stability is relatively weak at the time of heaviest precipitation. As such, this implies a large response for a given QG forcing for ascent (Fig. 4.5). After t=+6 h, the area of low CI moves well east of St. John's as the trailing cold front ushers in more stable air from the west, concomittant with lesser amounts of precipitation at the end of the event.

Figure 4.10 displays a time series of observed soundings taken every twelve hours at CYYT (St. John's). At 0000 UTC 7 December (t=-30 h, Fig.

4.10a), the upper troposphere is quasi-saturated with respect to ice, while the lower troposphere remains dry. As the rapidly intensifying cyclone moves towards St. John's and subtropical moisture is advected northward, the atmosphere quickly saturates by t=-18 h (Fig. 4.10b). From t=-18 h (Fig. 4.10b) to t=+6 h (Fig. 4.10d), the tropopause remains extremely elevated (near 200 hPa), and saturated with respect to ice, supporting the observation in Fig. 4.7 that a warm moist air mass exists at St. John's ahead of the sea-level cyclone. Following the passage of the trailing cold front and the approach of the main upper-level disturbance between t=+6 h and t=+12 h, the thermodynamic structure of the atmosphere shifts extremely quickly to one associated with a cold-core low, with a depressed tropopause of around 400 hPa at t=+18 h (Fig. 4.10e) and 500 hPa at t=+30 h, much cooler temperature values (~10° C), and lower saturation mixing ratio throughout the column. This illustrates the stark difference in air mass ahead on either side of the trailing cold front and suggests that the bulk of precipitation during MAG 1 falls during a period marked by strong QG forcing for ascent, weak stability, and a saturated warm moist air mass (large values of dr_s/dp , from Eq. 4.1).

Emanuel (1983) states that conditional symmetric (slantwise) instability can be largely responsible for some mesoscale precipitation bands within larger-scale storms, and that "the most straightforward method of assessing moist symmetric instability from soundings involves constructing vertical cross sections from two or more soundings which are aligned across the vertical shear," A caveat is that regions of vertical convective instability ($d\theta_e/dz < 0$, Bluestein

1992a) should be considered before performing a diagnosis of slantwise instability, as the convective instability mode dominates a situation where both types of instability are present (Emanuel 1983). In addition, later work by Novak et al. (2004) and Novak et al. (2006) quantifies and enhances the ability of the forecaster to predict these events in northeast U.S. cyclones. To assess convective and slantwise instability for MAG 1, west-east cross-sections of θ_e and momentum (M) surfaces along the latitude of St. John's are presented in Fig. 4.11.

In Fig. 4.11c, it is evident that at t=-6 h, a region of convective instability develops near St. John's (located in the center of the cross section) in a layer extending from approximately 900 hPa upwards to about 800 hPa. By t=0 h (Fig. 4.11d), this region of convective instability has grown, and is now in a layer from the center of a θ_e maximum at about 875 hPa upwards to about 600 hPa. This convective instability is concurrent with the time of heaviest precipitation at St. John's during MAG 1 and is reflected in the radar imagery by a large area of heavy precipitation (Fig. 4.3d). By t=+6 h and t=+12 h, the area of convective instability has moved to the east of St. John's (Fig. 4.11e-f), concurrent with the passage of the trailing cold front and the associated heavy precipitation (Fig. 4.3ef). The observations of convective instability in the cross sections around t=0 h substantiate the low values of the coupling index observed in Fig. 4.8. It is clear from this diagnosis that slantwise convection did not play a major role, in accordance with the statement of Emanuel (1983) near St. John's. However, the previously discussed radar imagery presented in Fig. 4.3c-e suggests than

slantwise convection might have been present west or east of St. John's, although further investigation is required. Finally, an examination of the 2 PVU surface in the cross-sectional analysis (Fig. 4.11d-f) shows that unlike the Presidents' Day cyclone of 1979, a tropopause fold does not appear to be present during MAG 1.

4.4 MAG 2: December 11th, 2008

4.4.1 Overview and Synoptic Typing

MAG 2 affects St. John's from 0000 UTC 11 December to 0000 UTC 13 December, with t=0 h at 0600 UTC 11 December. The total amount of precipitation observed at St. John's is 54 mm (Fig. 4.12), which is approximately 10 mm above the median extreme event defined in Chapter 2. MAG 2 occurs in three stages: an initial warm stage, a subsequent cold stage following a coldfrontal passage, and a second warm stage, as a quasi-stationary northeastsouthwest oriented baroclinic zone retreats back to the north of St. John's ahead of an approaching cyclone. Over half of the total event precipitation falls during the initial warm stage and subsequent cold frontal passage (Fig. 4.12), between 0000 and 1200 UTC 11 December. During this time period, unseasonably warm surface temperatures close to 15 ° C are replaced by a much cooler yet still saturated atmosphere (Fig. 4.12). Accompanying the temperature drop between 0600 and 1200 UTC (t=0 h and t=+6 h) 7 December is a wind shift from 20 knot westerly surface flow to 10 knot northerly flow (Fig. 4.12a). While moderate rain is reported at several time periods during the initial warm period and subsequent

frontal passage, the precipitation slowly transitions to light frozen precipitation by t=+12 h and remains frozen until around t=+27 h when slowly rising surface temperatures cause a changeover to light rain. Towards the end of the event (Fig. 4.12b), cold boundary-layer air remains in place until around 2100 UTC (t=+39 h) 8 December when the aforementioned boundary returns as a northward-moving warm front, initiating the second warm stage, ahead of a developing cyclone off the southeastern U.S. coast.

Figure 4.13 shows clouds associated with the aforementioned frontal zone, stretching from northeastern Quebec to Louisiana at t=-36 h (Fig. 4.13c). The baroclinic zone slowly propagates eastward towards St. John's and by t=-6 h (Fig. 4.13f), stretches from an area northeastward of Newfoundland southwestward into the Gulf of Mexico. Slightly upstream of the frontal zone is a closed upper-level low over the western Gulf of Mexico (Figs. 4.13f-h, 4.18f-h) that impacts the later stages of MAG 2, as well as the subsequent few days along the Atlantic seaboard.

Unfortunately, the Holyrood radar was not operating from t=-10 h to t=+12 h, including the time of maximum precipitation at St. John's. However, Fig. 4.14b-d confirms light precipitation oriented along the baroclinic zone, from t=+12 h to t=+18 h, when precipitation is still being recorded at St. John's (Fig. 4.12).

As in MAG 1, the evolution of the backward trajectories is more complicated than most of the cases in Chapter 3. Figure 4.15 shows that almost all of the upper-level trajectories (300 hPa) originate southwest of St. John's to the

Gulf of Mexico. However, while some of the mid-level (500 hPa) trajectories also trace backward to the Gulf of Mexico, most of the mid- and low-level parcels spend a large amount of time over the Gulf Stream. In summary, MAG 2 is classified as a southwest event, with the caveat that the low-level trajectories originate in the upper troposphere early in the time evolution, over the American and Canadian prairies. Subsequently, the majority of these trajectories sink to the boundary layer while making an anticyclonic loop over the western Atlantic, likely helping to transport large amounts of subtropical moisture northward towards St. John's. Finally, in MAG 1 (Fig. 4.4), the upper-level trajectories originate from an area much further north than is observed in MAG 2 (Fig. 4.15). This implies that the air aloft is warmer in MAG 2 than MAG 1 (due to radiative cooling) and that the atmosphere near St. John's is thusly more stable than in

Figure 4.16 displays time series of the QG ascent-forcing parameters utilized in Chapter 3. As stated earlier with regard to all eleven frontal cases in Chapter 3, low-level frontogenesis dominates the other two variables in the time series (Fig. 4.16). Mid-level vorticity advection values near zero for the entire period of precipitation suggest that a strong upper-level trough does not come into play during the evolution of MAG 2; MAG 2 is categorized as a frontal case.

4.4.2 Synoptic-Dynamic Analysis

Figure 4.18 displays a downstream ridge on the DT, similar to structures in the frontal composite of Chapter 3. Prior to MAG 2, as the intense sea-level

cyclone responsible for MAG 1 moves away from Newfoundland, the associated upper-level trough moves over Newfoundland at t=-72 h and t=-48 h (Fig. 4.18a-b). By t=-24 h, the sea-level anticyclone is established downstream of St. John's and potentially cold air aloft is replaced by high θ on the DT, advected by strong southerly flow in association with the downstream anticyclone and a closed upper-level low in the western Gulf of Mexico, as indicated in the 1000-500 hPa thickness field (Fig. 4.17d-i).

By t=-24 h, a quasi-stationary baroclinic zone, oriented northeast-southwest, is present near St. John's (Fig. 4.17d). This feature persists for 36-48 hours. Figure 4.16b shows that during the entire period of precipitation at St. John's, absolute values of 700 hPa omega are relatively small, while the precipitable water remains at 20 mm or above, minimized following the passage of the cold front just before t=+6 h. The maximum precipitable water value (~28 mm) is at t=0 h ('2' on the horizontal axis), coincident with the heaviest precipitation (21 mm). Unlike in MAG 1, however, the precipitable water remains over 20 mm for the duration of the event; the smaller negative magnitudes of ω help to explain the lesser amounts of precipitation at t=+6 h and beyond.

The assertion that MAG 2 is a three stage event is supported by Fig. 4.18d-i, which show warm θ on the DT prior to t=+6 h, replaced by cooler θ at t=+6 h. By t=+12 h, however, the high θ air returns as the surface baroclinic zone retreats northward in association with the developing cyclone in the Gulf of

Mexico. By t=+24 h (not shown), the baroclinic zone is fully to the north of St. John's and the station remains in the subtropical air mass until the passage of the Gulf of Mexico cyclone on 13 December.

Figure 4.19 highlights a plume of warm low-level θ_e extending parallel to the baroclinic zone from the Gulf of Mexico to northeastward of Newfoundland. Figure 4.20d shows that strong moisture transport on the western flank of the downstream high is already established by t=-24 h. This northward moisture transport continues unabated for more than 48 hours, with the largest vectors and a persistent area of moisture convergence located over St. John's (Fig. 4.20d-i).

Figure 4.19 also confirms that the bulk atmospheric stability in MAG 2 is substantially higher than in MAG 1. While there are low (<8 K) values of the CI observed off the U.S. coast on the southern edge of the baroclinic zone, the lowest values do not make it into the St. John's area, even at t=0 h (Fig. 4.19g). However, the lowest plotted threshold (16 K) of the CI comes closest to St. John's between t=0 h and t=+6 h (Fig. 4.19g-h). While these values (greater than 16 K) are still substantially higher than those observed in MAG 1 at t=0 h (8 K), it still suggests that the weakest atmospheric stability is concurrent with the heaviest precipitation.

Figure 4.21 shows that the tropopause remains very high, hovering between 150 and 200 hPa during the t=-6 h to t=+42 h time period. Figures 4.21c-e show that the cold-air is extremely shallow following the initial cold frontal passage, and remains local to the boundary layer with a 200-300 hPa

inversion layer situated above it. While the air mass aloft remains warm throughout MAG 2, the near-surface temperatures remain cool from the time of the cold frontal passage (just before t=+6 h, Fig. 4.21d), until after t=+30 h (Fig. 4.21e-f), near the end of MAG 2.

The 6-hour GFS precipitation forecasts (Fig. 4.17) are fairly accurate, although precipitation is overestimated in the early part of the event (t=-12 h), and underestimated during both the heaviest precipitation (t=0 h) and later in the event (t=+12 h and beyond). The underestimation of precipitation during the later time periods leads to an overall underestimation of the total event precipitation.

However, it is the GFS precipitation forecasts at longer lead times that are extremely inaccurate in the case of MAG 2. A preliminary examination indicates that the poor performance of the GFS at earlier lead times is mostly due to an inaccurate handling of the upstream closed low pressure system in the Gulf of Mexico; this will be detailed more substantially in future work.

Figure 4.22 is a cross section oriented northwest-southeast (see Fig. 4.14), perpendicular to the quasi-stationary baroclinic zone. At t=-6 h (Fig. 4.22c), an area of slight convective instability is located southeast of St. John's, below 850 hPa. By t=0 h (Fig. 4.22d), this area expands and is now located in the vicinity of St. John's, just above 850 hPa. Concurrently, there is a second area of convective instability in the same layer, but in the warm sector, southeast of St. John's and the frontal boundary. Subsequently, the second (and larger) area of convective instability remains in the warm sector, well southeast of St. John's at t=+6 and

t=+12 h (Fig. 4.22e-f), below 700 hPa. The initial smaller area of instability is still present above 700 hPa at t=+6 h and just below 700 hPa at t=+12 h. Both these areas are persistent throughout the remaining portion of MAG 2 (not shown) and by the end of MAG 2 (around t=+36 h), a large area of convective instability exists in the 850-600 hPa layer in the vicinity of St. John's and to the southeast (not shown). This is consistent with a) the relatively low values of the coupling index at St. John's observed in Fig. 4.19 at t=0 h and b) the assertion that the frontal boundary moves back to the northwest of St. John's late in the event, placing the station back in the warm sector, until the passage of the Gulf of Mexico cyclone on 13 December. Finally, Fig. 4.22 shows that there is no area of possible slantwise instability. The suggestion here is that frontogenesis is the primary ascent-forcing mechanism for this case.

4.5 Concluding Discussion and Future Work

Case studies are presented for consecutive extreme precipitation events that produce over 125 mm of precipitation at St. John's from 7 to 12 December 2008 (Fig. 4.1). The first case, MAG 1, is associated with a rapidly intensifying extratropical cyclone that tilts westward with height (Fig. 4.7). The synoptic typing methodologies of Chapter 3 are utilized, and MAG 1 is classified as a southwest and cyclone event. The remarkable amount of precipitation as a result of MAG 1 is associated with large values of QG forcing for ascent (Fig. 4.5a) in the presence of weak atmospheric stability (Fig. 4.8) and an extremely moist subtropical air mass (Figs. 4.7 and 4.10). In addition, a cross-sectional analysis

shows an area of convective instability located near St. John's at t=0 h (Fig. 4.11d). As soon as the cyclone passes St. John's, there is a drastic shift in air mass (Fig. 4.10) from maritime tropical to continental polar (associated with a cold-core low), as the tropopause descends from near 200 hPa at t=+6 h to around 400 hPa at t=+12 h. While St. John's is located in a region prone to rapidly intensifying cyclones, MAG 1 presents an infrequently seen combination of conditions that are ripe to produce an extreme precipitation event.

MAG 2, which produced 54 mm of precipitation, is primarily associated with a quasi-stationary northeast-southwest baroclinic zone near St. John's (Fig. 4.17). MAG 2 is classified as a southwest and frontal event. Unlike MAG 1, there is no evidence of a strong extratropical cyclone near St. John's during the period of precipitation. The bulk of precipitation during MAG 2 is associated with large values of low-level frontogenesis (Fig. 4.16a) in the presence of relatively large, persistent values of precipitable water, within a moderately stable atmosphere. MAG 2 occurs during three stages: an initial warm stage, a cold frontal passage leading to a cool stage, and a second warm stage (Fig. 4.12). The second warm stage concludes when a large closed upper-level low from the Gulf of Mexico approaches and passes St. John's (not shown).

Consistent with the composite analysis of frontal events in Chapter 3, the synoptic environment during MAG 2 is dominated by a downstream upper-level ridge and corresponding sea-level anticyclone (Figs. 4.17-4.18), which helps to sustain the baroclinic zone by initiating strong southerly flow on the warm side of

the temperature gradient. Although about 40 percent of the precipitation in MAG 2 falls during the cold frontal passage, the longevity and quasi-stationary nature of the baroclinic zone is important in producing the remaining 30+ mm of precipitation over a 36-48 hour time period. Additionally, observed soundings at St. John's during MAG 2 show that the tropopause remains exceedingly high for December for the duration of the event (Fig. 4.21). Finally, although a large area of low-level convective instability does develop in the warm sector east of St. John's toward the end of the event, it is reasonable to conclude that the greatest forcing for QG ascent (as defined by Eqns. 3.1-3.4) and greatest convective instability are not concomitant at St. John's.

While both MAG 1 and MAG 2 are characterized by the presence of a warm and moist subtropical air mass at St. John's, the large negative values of ω and small static stability in MAG 1 are substantially more conducive to a more extreme precipitation event and could at least in part explain the 20 mm difference in observed precipitation between the two events. Nevertheless, considering the relatively benign dynamic structures present for MAG 2 (no cyclone, warm air advection, or cyclonic vorticity advection), the fact that MAG 2 exceeds the median extreme event at St. John's by 10 mm suggests that the primary factor in the event is strong low-level frontogenesis over a long period of time (48 hours) in the presence of extremely moist subtropical air mass. While this is not a common occurrence (11 cases from 1979-2005, as seen in Chapter 3), it shows that these conditions can occasionally produce an extreme cool-season precipitation event at St. John's.

In sum, the examinations of MAG 1 and MAG 2 show that two extreme precipitation events at St. John's can be produced by disparate synoptic-scale structures. In the near future, the authors hope to use the detailed synoptic analyses of MAG 1 and MAG 2 in this paper as a basis for an examination of the performance of the operational forecasts (both numerical and human) during these events.

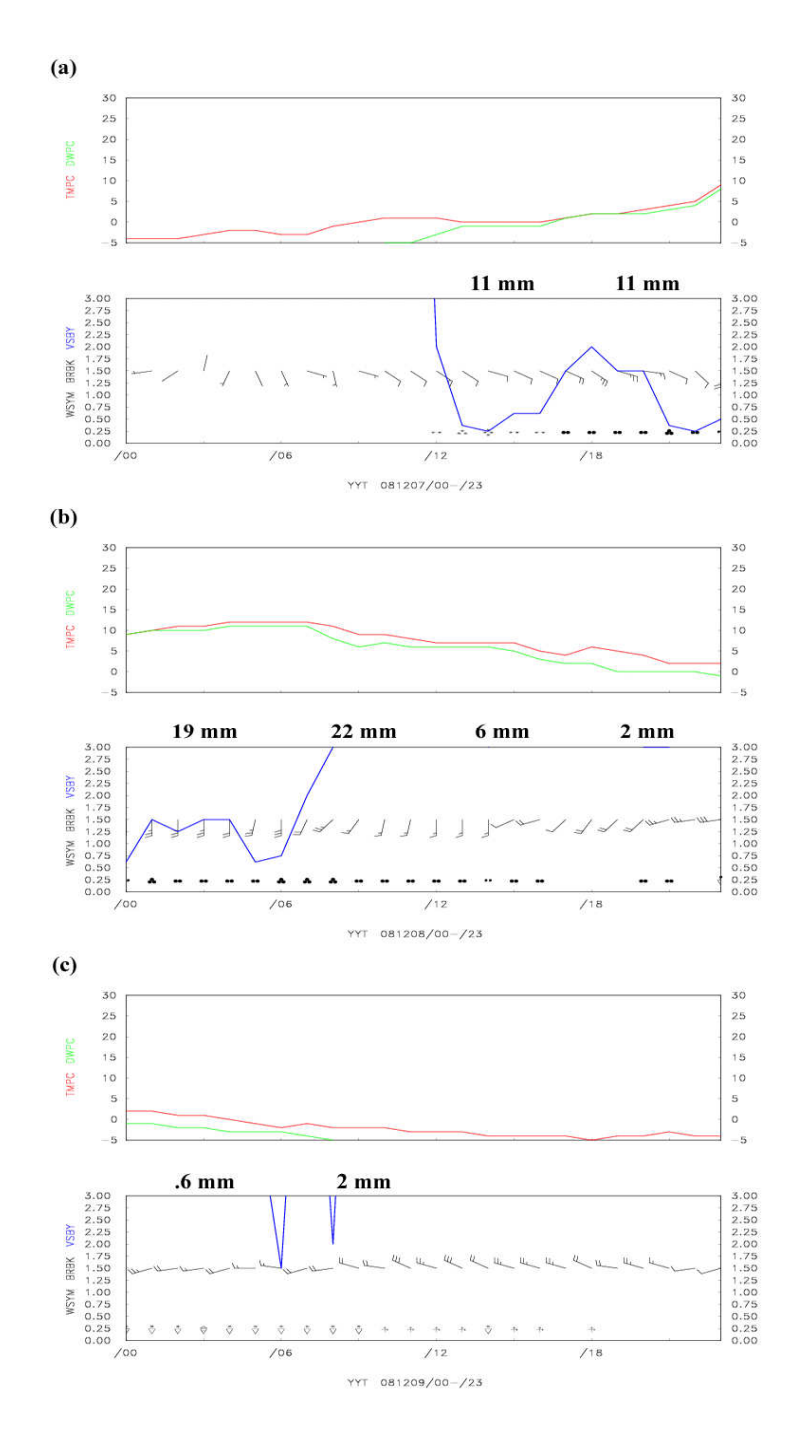


Figure 4.1: Meteograms for the entire period of precipitation at St. John's (CYYT) for the first case in the study. In the top panel of (a) 7 December 2008, (b) 8 December 2008, and (c) 9 December 2008, temperature (dewpoint) is plotted in red (green). In the bottom panel of (a), (b), and (c), time on the horizontal axis is in UTC, visibility (statute miles) on the vertical axis is plotted in blue (not shown for values greater than 3 statute miles), wind (in knots) is represented by barbs, and 6-hour precipitation amounts are bold.

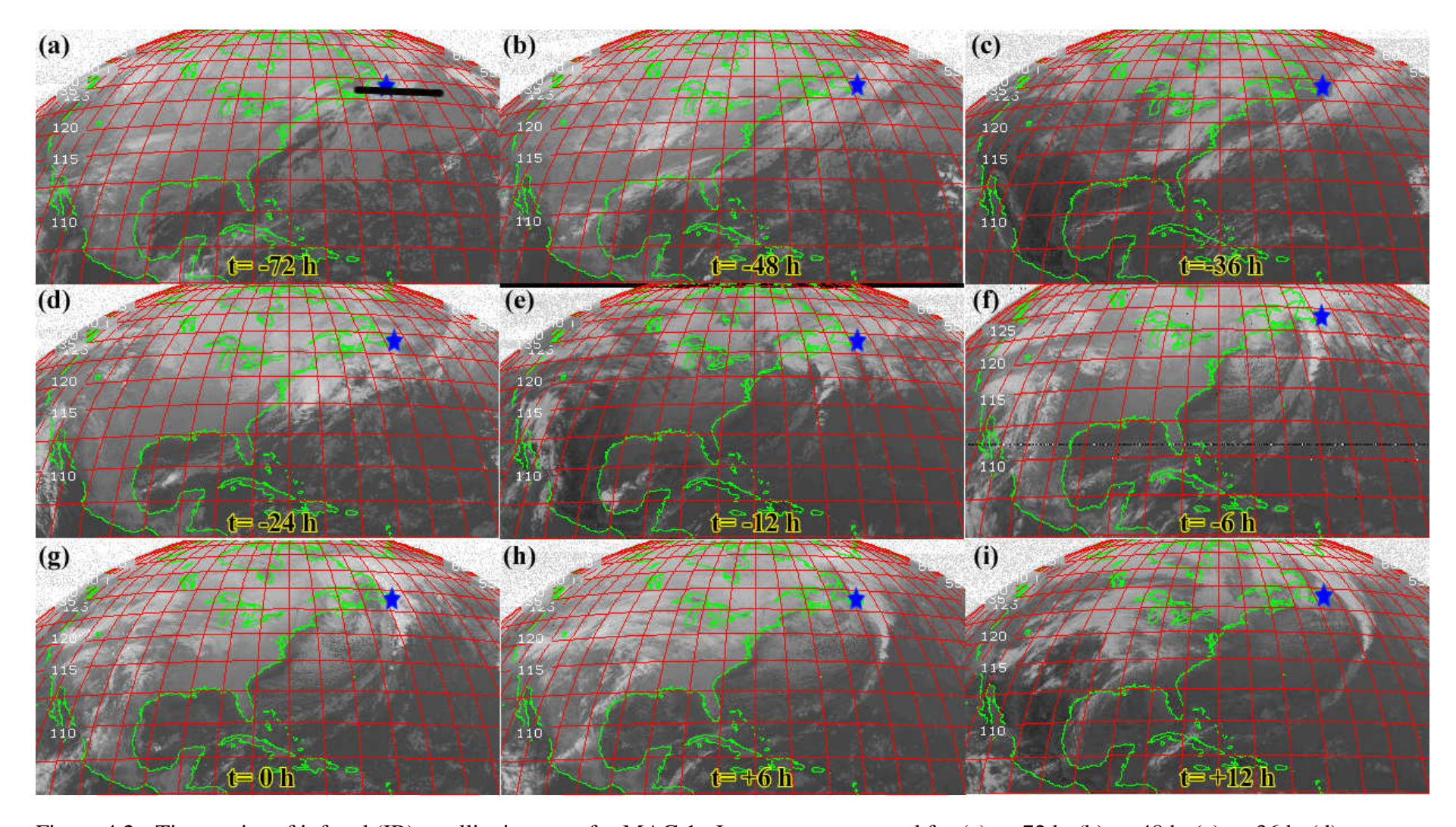


Figure 4.2: Time series of infared (IR) satellite imagery for MAG 1. Images are presented for (a) t=-72 h, (b) t=-48 h, (c) t=-36 h, (d) t=-24 h, (e) t=-12 h, (f) t=-6 h, (g) t=0 h, (h) t=+6 h, and (i) t=+12 h, where t=0 h is 0600 UTC 8 December 2008. A blue star is placed in each panel at the approximate location of St. John's and the area of interest explored in Fig. 4.11 (cross section) is outlined with a black line in panel (a).

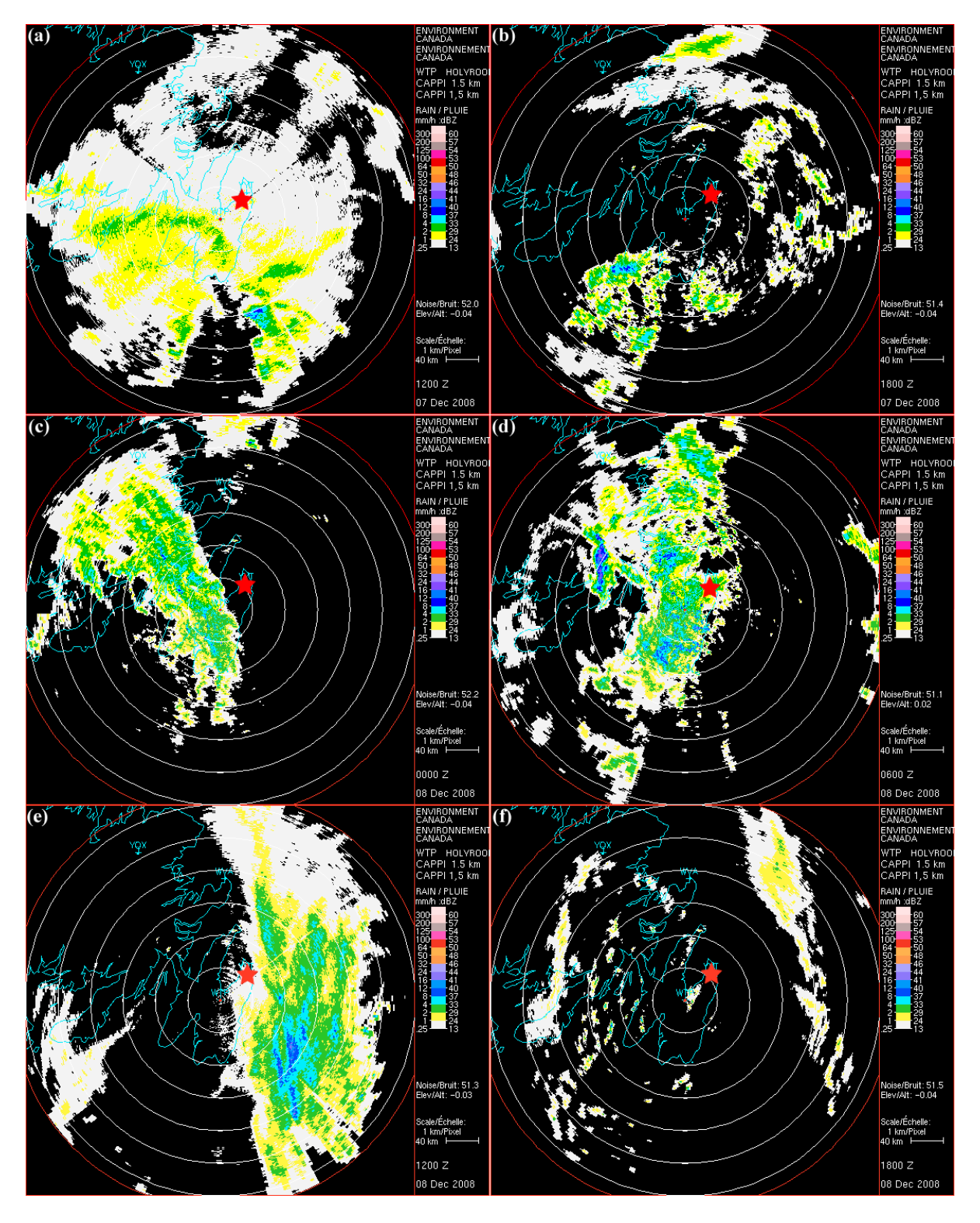


Figure 4.3: Time series of radar imagery for MAG 1, from the Environment Canada radar located in Holyrood, Newfoundland. Radar imagery is shown for (a) t=-18 h, (b) t=-12 h, (c) t=-6 h, (d) t=0 h, (e) t=+6 h, and (f) t=+12 h, where t=0 h is 0600 UTC 8 December 2008. A red star is placed at the approximate location of the St. John's international airport (CYYT).

NOAA HYSPLIT MODEL Backward trajectories ending at 0600 UTC 08 Dec 08 GDASMeteorological Data

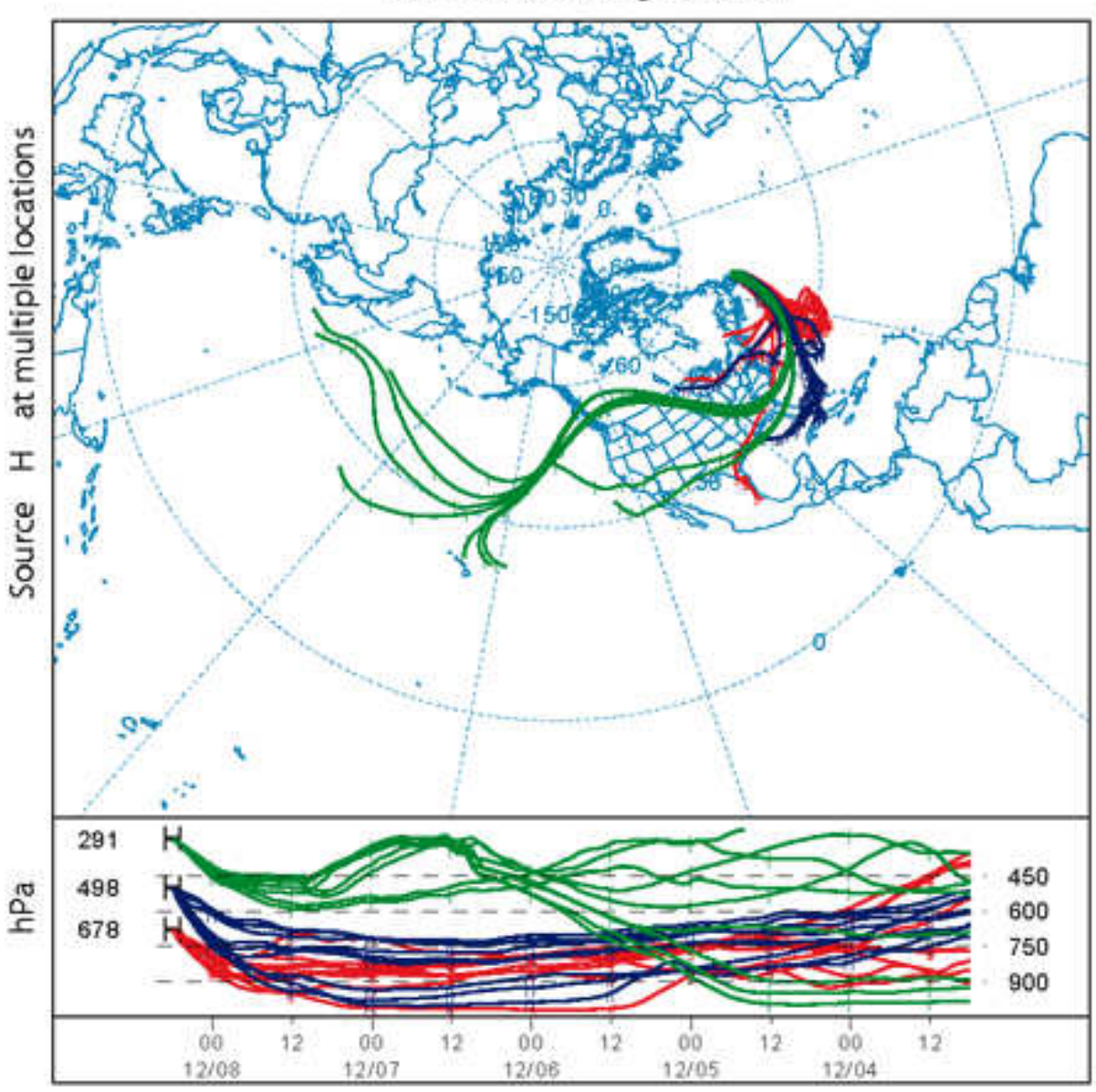


Figure 4.4: Twenty-seven backward trajectories derived from the NCEP GFS 0.5 degree analysis, with the origin being five days earlier and the ending points at 300, 500, and 700 hPa at 0600 UTC 8 December 2008. Ending points are distributed within a box whose corners are 48.4°N 53.5°W and 46.4°N 51.5°W. This is for MAG 1.

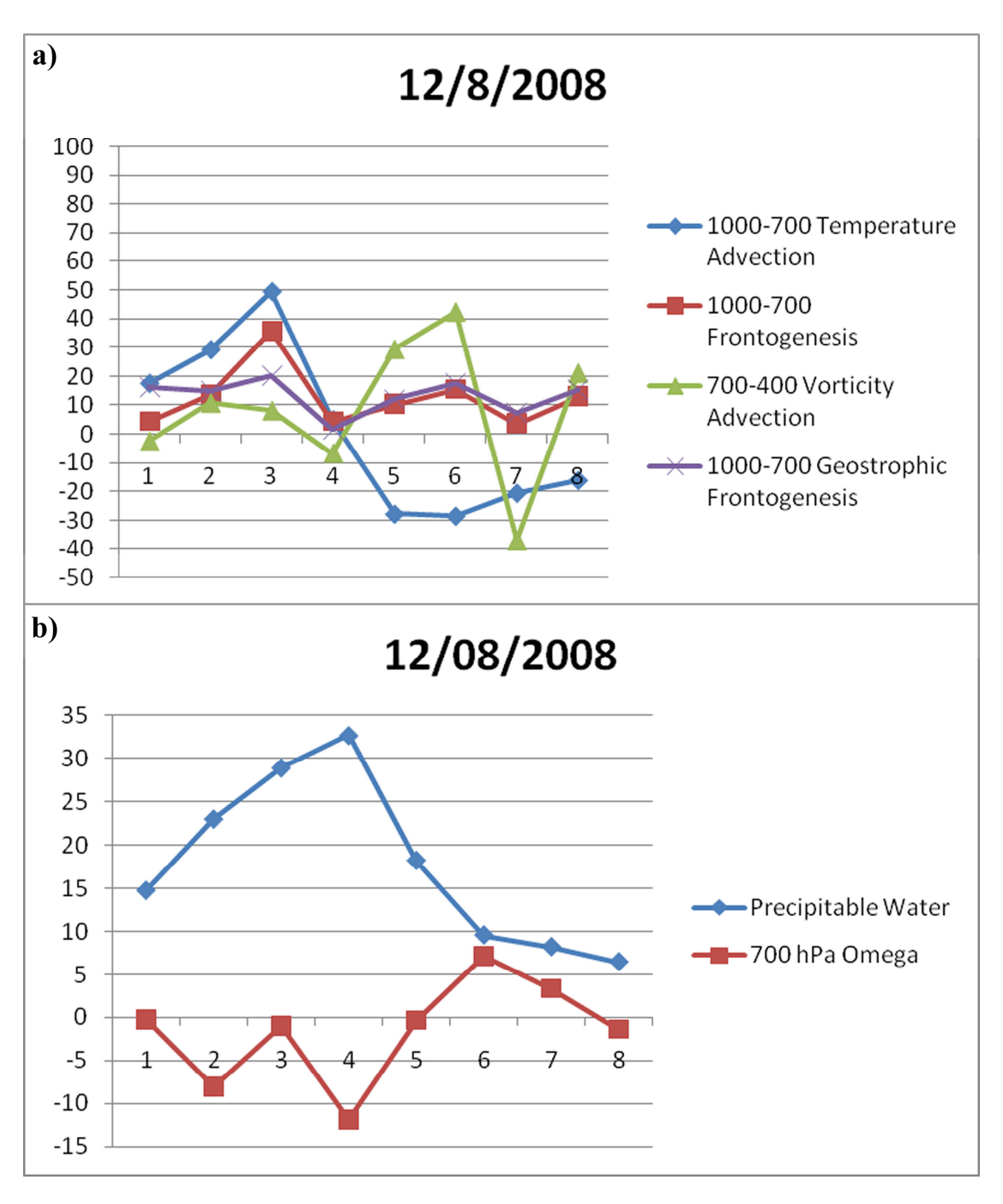


Figure 4.5: Time series for MAG 1 during the period of precipitation at St. John's (t=-18 h, 1200 UTC 7 December to t=+24 h, 0600 UTC 9 December), of GFS half-degree analysis for (a) 700-400 hPa layer-averaged relative vorticity advection $\times 10^{-10} \, \mathrm{s}^{-1}$ (green), 1000-700 hPa layer-averaged horizontal temperature advection $\times 10^{-5} \, \mathrm{K s}^{-1}$ (blue), and 1000-700 hPa layer-averaged frontogenesis $\times 10^{-2} \, \mathrm{K (100 \, km)}^{-1} \, (3 \, \mathrm{hr})^{-1}$ (red), and 1000-700 hPa layer-averaged geostrophic frontogenesis $\times 10^{-2} \, \mathrm{K (100 \, km)}^{-1} \, (3 \, \mathrm{hr})^{-1}$ (purple) and (b) column precipitable water (mm, blue) and 700 hPa omega (cm s⁻¹, red).

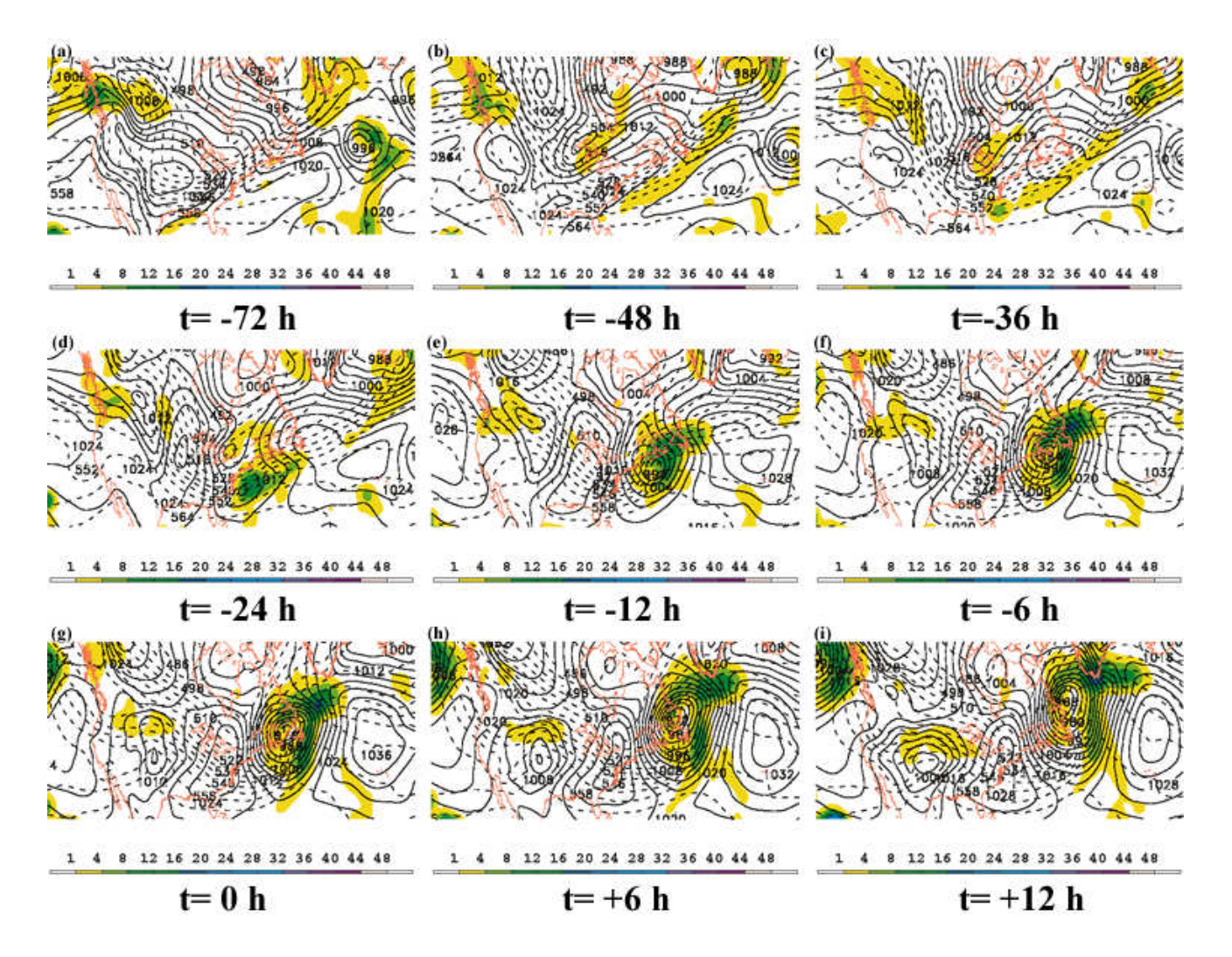


Figure 4.6: Time series of GFS half-degree analyses sea-level pressure (SLP, solid) contoured every 4 hPa, 1000-500 hPa thickness (dashed) contoured every 6 dam, and 6-hourly precipitation totals (shaded) in mm, for MAG 1 Results are shown for (a) t=-72 h, (b) t=-48 h, (c) t=-36 h, (d) t=-24 h, (e) t=-12 h, (f) t=-6 h, (g) t=0 h, (h) t=+6 h, and (i) t=+12 h, where t=0 h is 0600 UTC 8 December 2008.

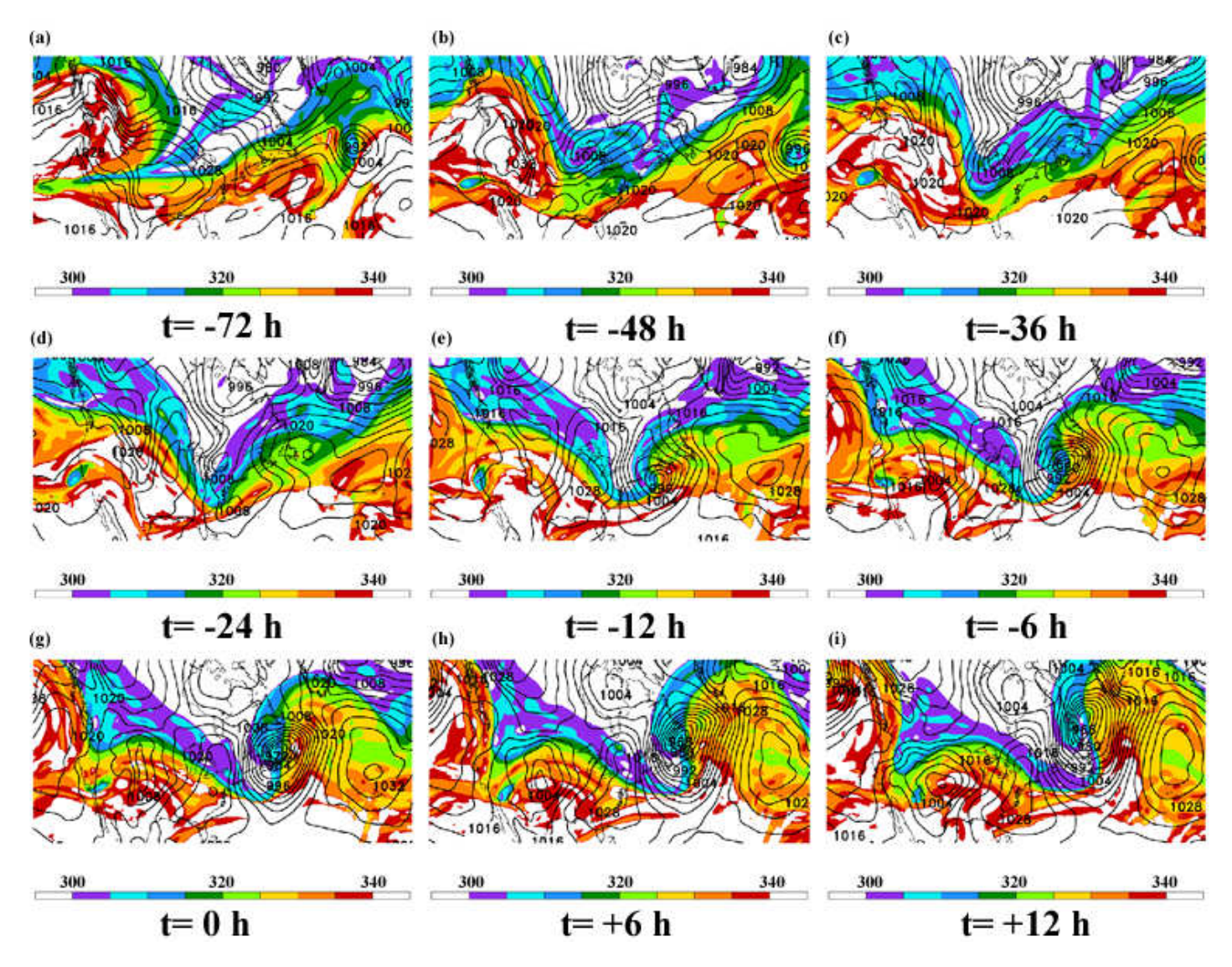


Figure 4.7: As in Fig. 4.6, but for SLP (solid, every 4 hPa) and potential temperature (K) on the Dynamic Tropopause (shaded). 166

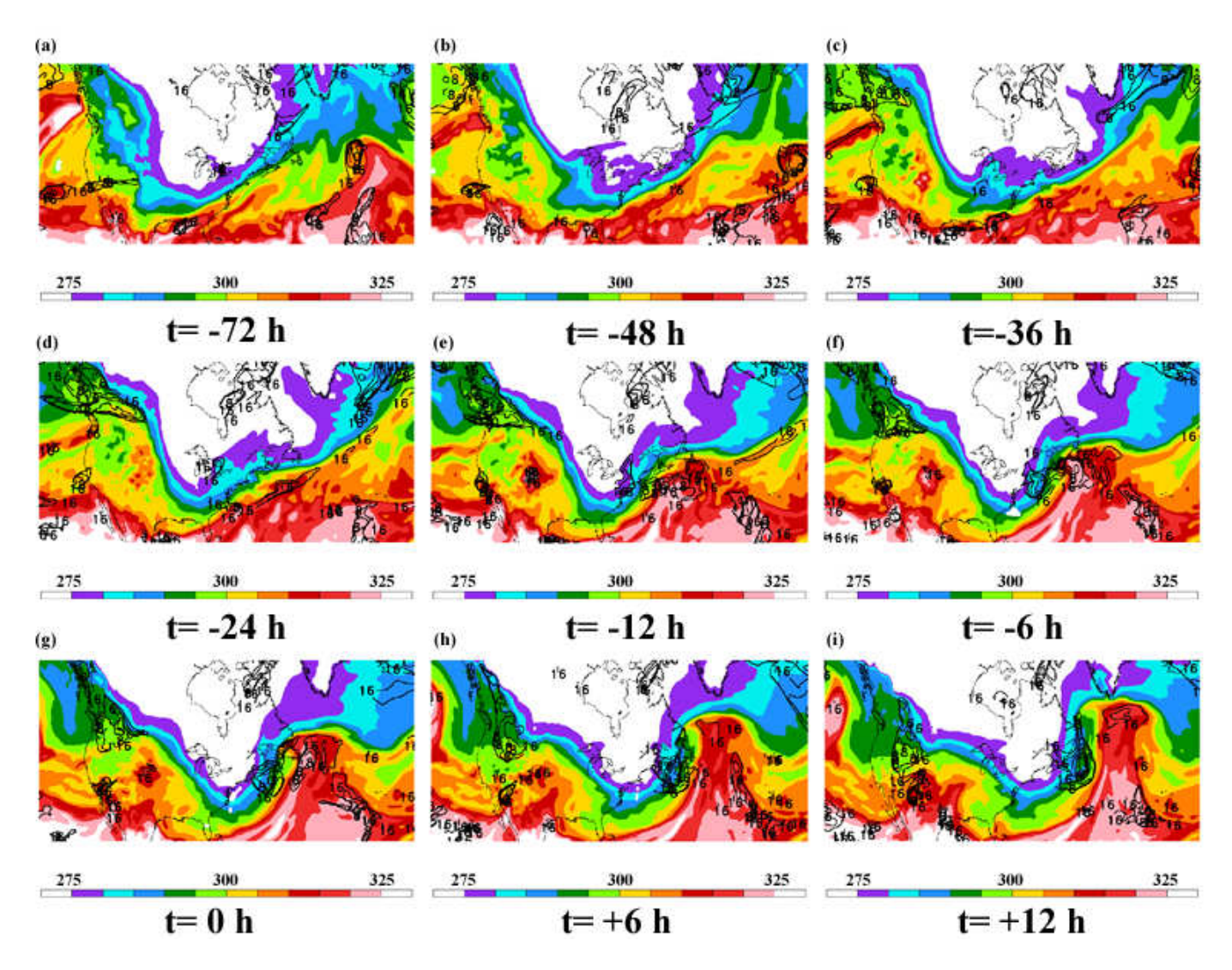


Figure 4.8: As in Fig. 4.6, but for 850 hPa equivalent potential temperature (K, shaded), and Coupling Index (K, solid, every 4 K from 0 to \pm 16).

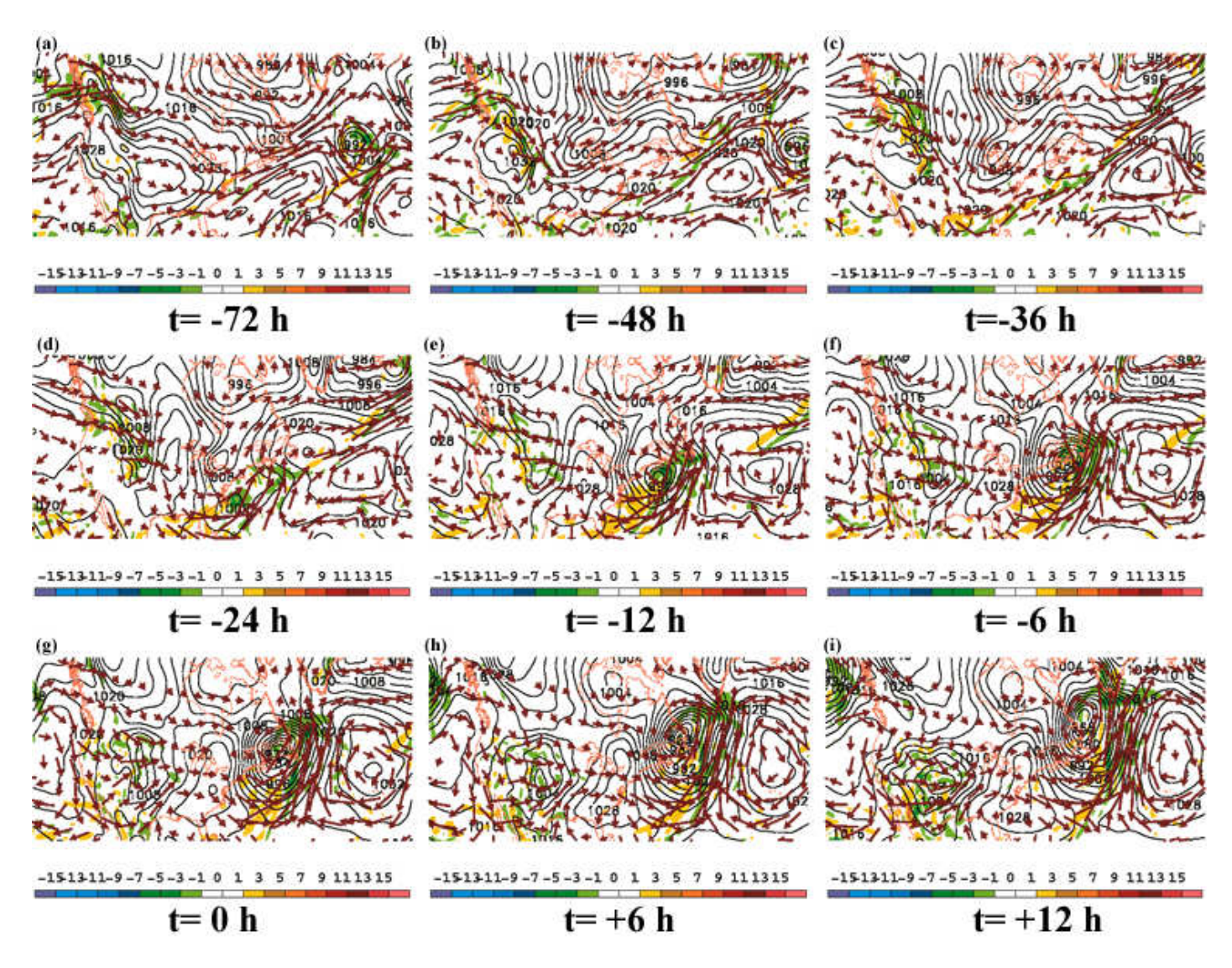


Figure 4.9: As in Fig. 4.6, but for SLP (solid, every 4 hPa), 1000-700 hPa moisture flux convergence (kg m⁻² s⁻¹, shaded), and 1000-700 hPa moisture transport vectors (red).

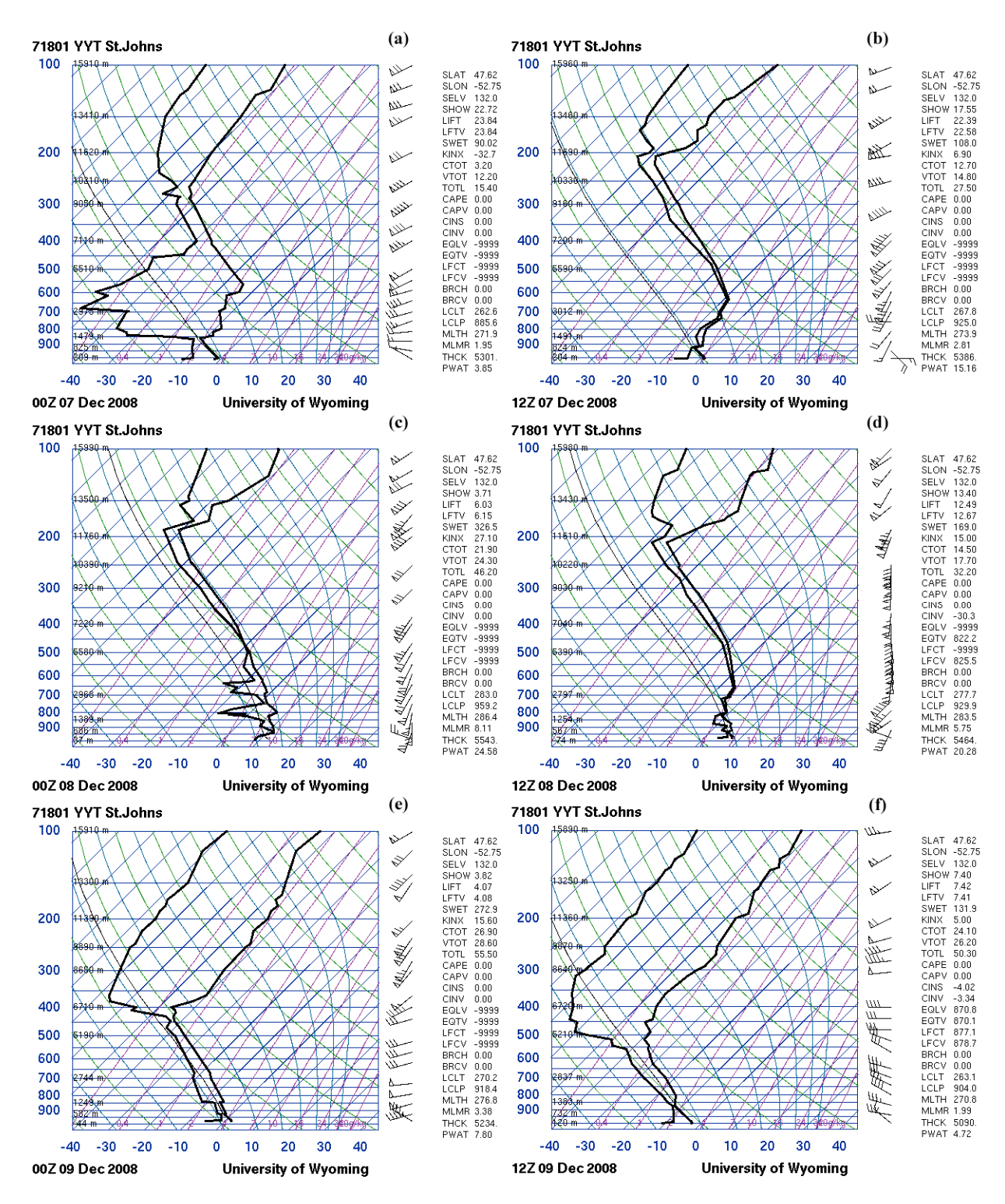


Figure 4.10: Time series of observed soundings at St. John's (CYYT) for MAG 1. Soundings are shown for (a) t = -30 h, (b) t = -18 h, (c) t = -6 h, (d) t = +6 h, (e) t = +18 h, and (f) t = +30 h, where t = 0 h is 0600 UTC 8 December 2008.

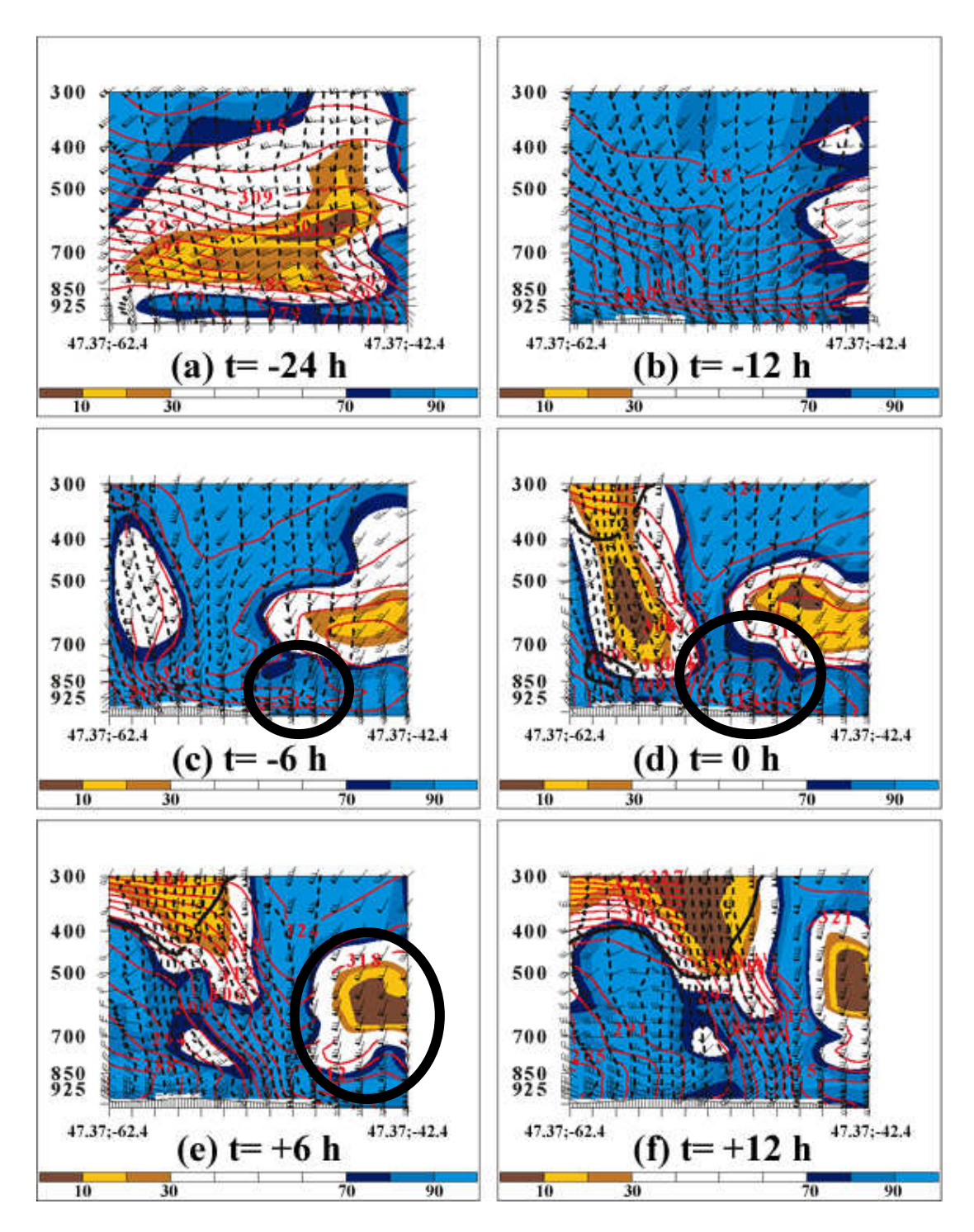


Figure 4.11: Time series of cross-section plots along latitude 47.37 N, from -62.4 W to -42.4 W, for MAG 1. Relative humidity (%, shaded), equivalent potential temperature (K, red solid lines), momentum (M) surfaces (m s⁻¹, black dashed) and winds (barbs) shown for (a) t =-24 h, (b) t=-12 h, (c) t=-6 h, (d) t=0 h, (e) t=+6 h, and (f) t=+12 h, where t=0 h is 0600 UTC 8 December 2008. Regions of convective instability are outlined by the black ovals. The 2 PVU surface is also contoured (bold black), when present.

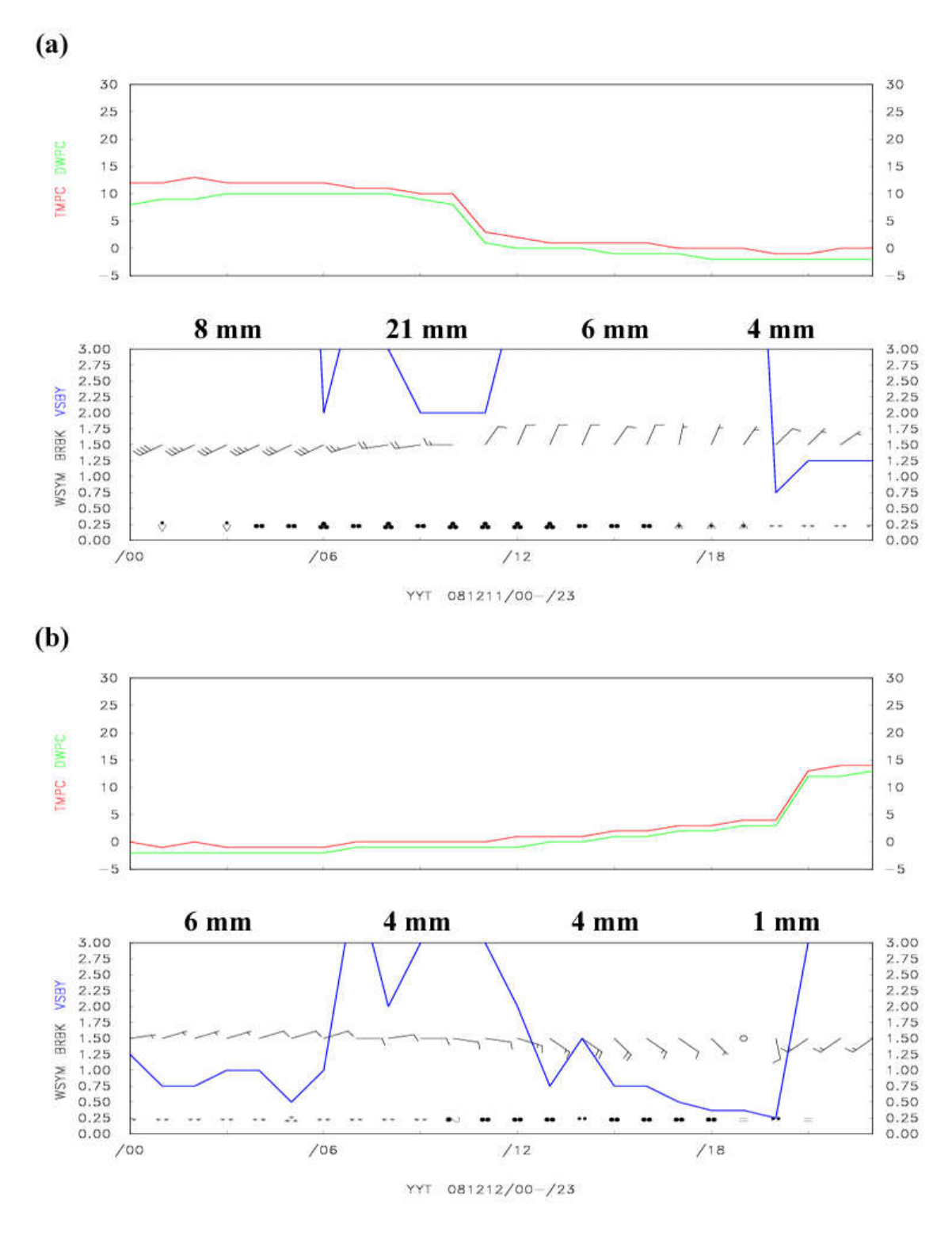


Figure 4.12: Meteograms for the entire period of precipitation at St. John's (CYYT) for MAG 2. As in Fig. 4.1, but for (a) 11 December 2008, and (b) 12 December 2008.

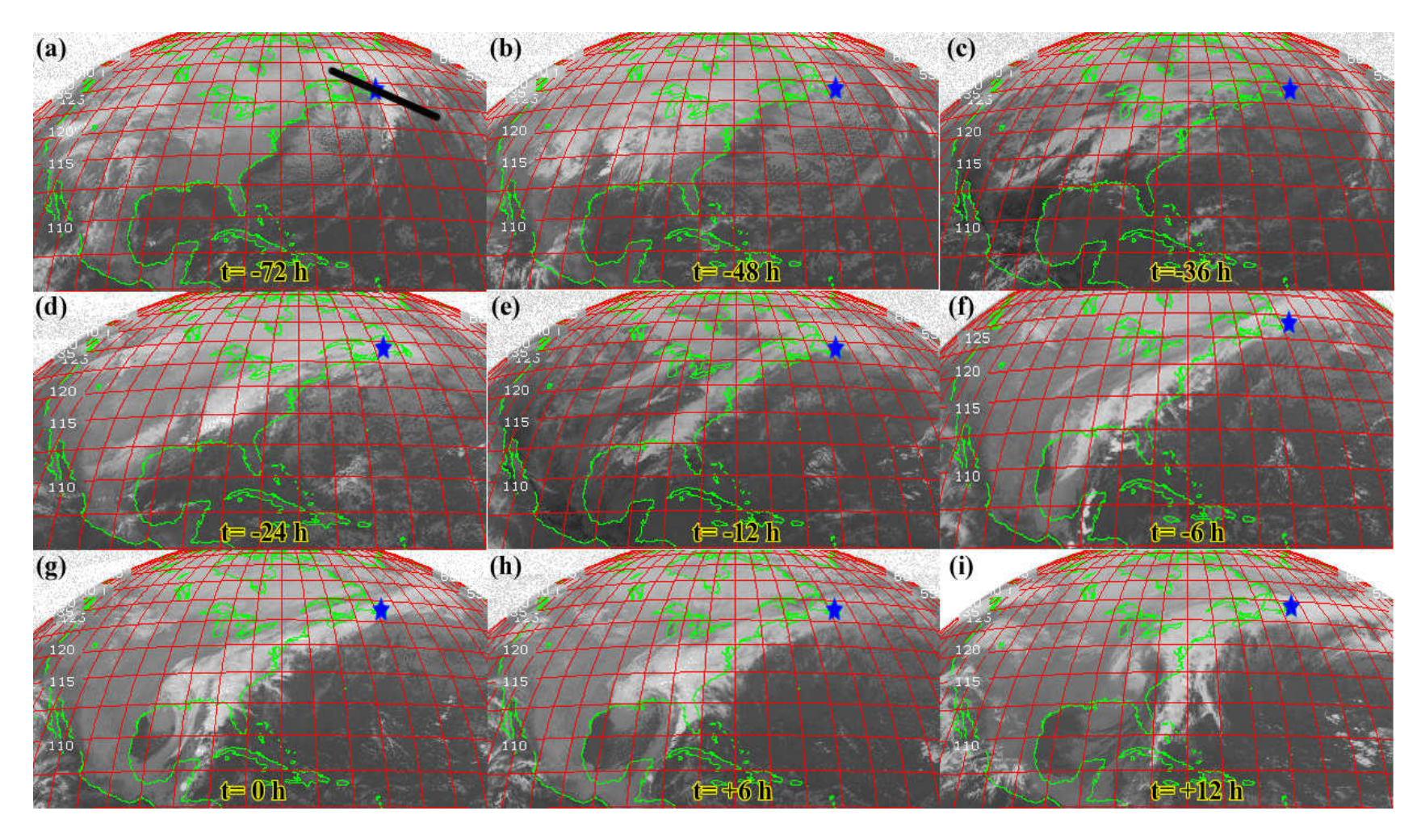


Figure 4.13: Time series of infared (IR) satellite imagery for MAG 2. Images are presented for (a) $t=-72 \, h$, (b) $t=-48 \, h$, (c) $t=-36 \, h$, (d) $t=-24 \, h$, (e) $t=-12 \, h$, (f) $t=-6 \, h$, (g) $t=0 \, h$, (h) $t=+6 \, h$, and (i) $t=+12 \, h$, where $t=0 \, h$ is 0600 UTC 11 December 2008. A blue star is placed in each panel at the approximate location of St. John's and the area of interest explored in Fig. 4.22 (cross section) is outlined with a black line in panel (a).

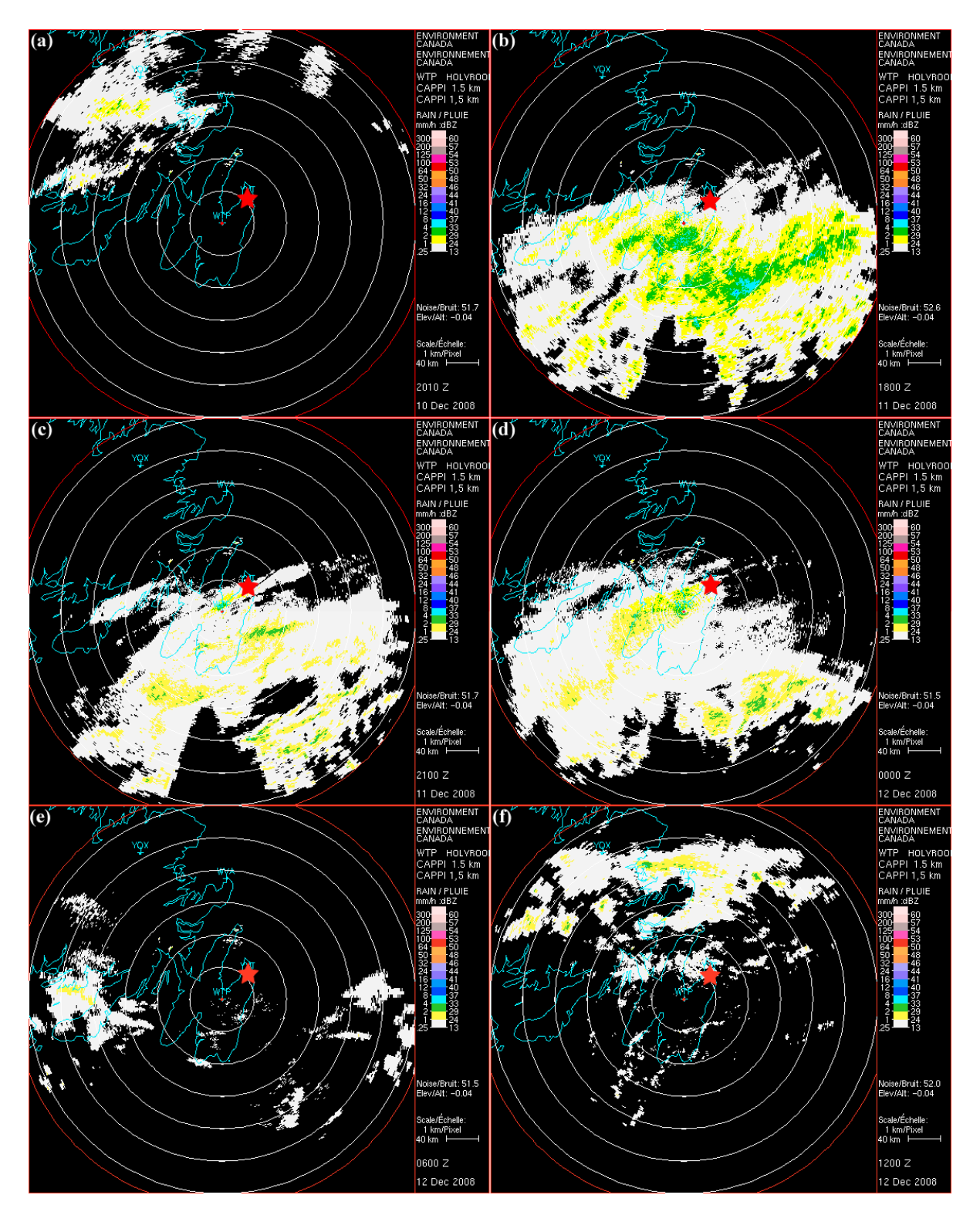


Figure 4.14: Time series of radar imagery for MAG 2, from the Environment Canada radar located in Holyrood, Newfoundland. Radar imagery is shown for (a) $t=-10 \, h$, (b) $t=+12 \, h$, (c) $t=+15 \, h$, (d) $t=+18 \, h$, (e) $t=+24 \, h$, and (f) $t=+30 \, h$, where $t=0 \, h$ is 0600 UTC 11 December 2008. A red star is placed at the approximate location of the St. John's international airport (CYYT).

NOAA HYSPLIT MODEL Backward trajectories ending at 0600 UTC 11 Dec 08 GDASMeteorological Data

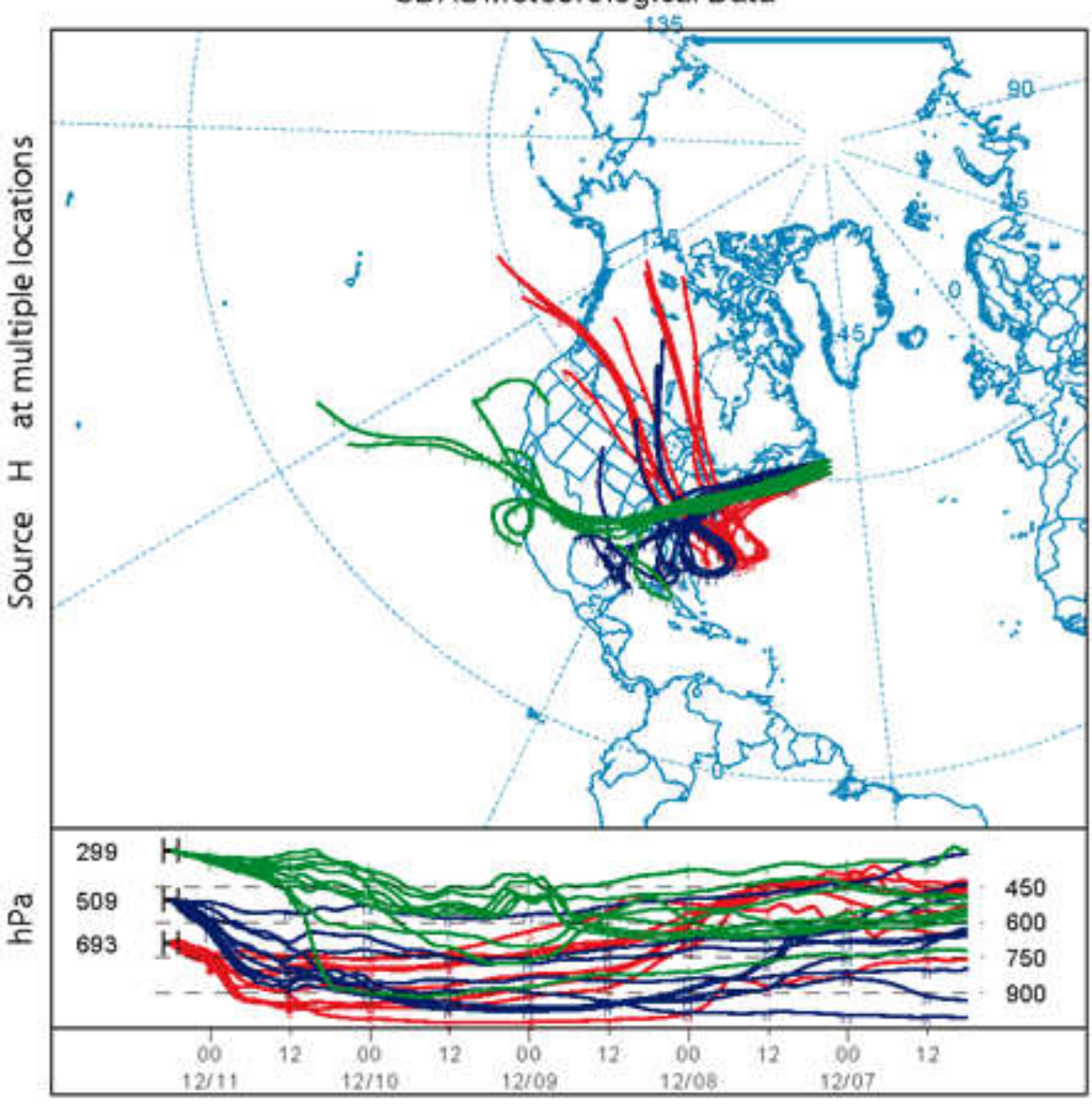


Figure 4.15: Twenty-seven backward trajectories derived from the NCEP GFS 0.5 degree analysis, with the origin being five days earlier and the ending points at 300, 500, and 700 hPa at 0600 UTC December 11th, 2008. Ending points are distributed within a box whose corners are 48.4°N 53.5°W and 46.4°N 51.5°W. This is for MAG 2.

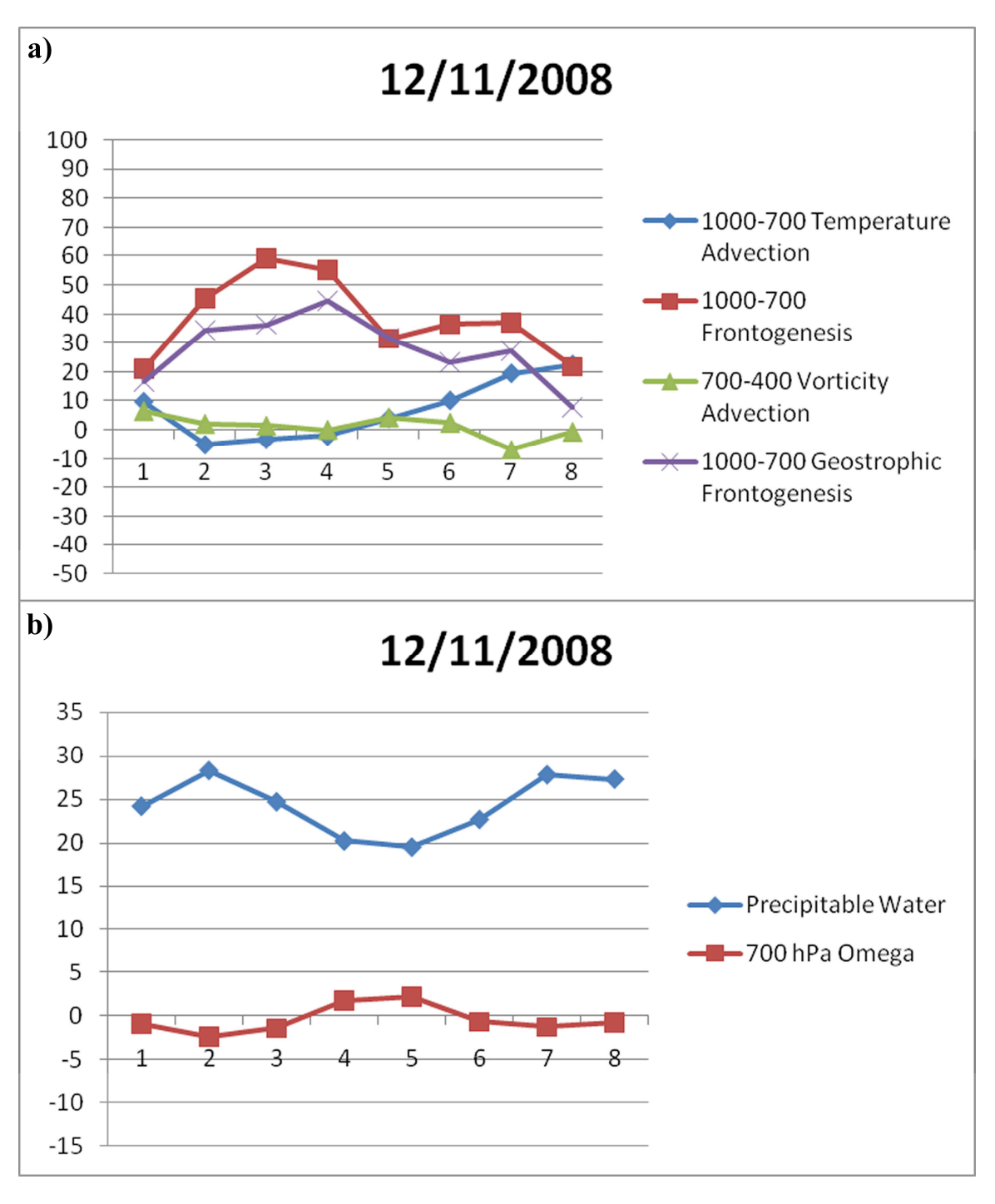


Figure 4.16: Time series for MAG 2 during the period of precipitation at St. John's (t=-6 h, 0000 UTC 11 December to t=+36 h, 1800 UTC 12 December), of GFS half-degree analysis for (a) 700-400 hPa layer-averaged relative vorticity advection $\times 10^{-10}$ s⁻¹ (green), 1000-700 hPa layer-averaged horizontal temperature advection $\times 10^{-5}$ K s⁻¹ (blue), and 1000-700 hPa layer-averaged frontogenesis $\times 10^{-2}$ K (100 km)⁻¹ (3 hr)⁻¹ (red), and 1000-700 hPa layer-averaged geostrophic frontogenesis $\times 10^{-2}$ K (100 km)⁻¹ (3 hr)⁻¹ (purple) and (b) column precipitable water (mm, blue) and 700 hPa omega (cm s⁻¹, red).

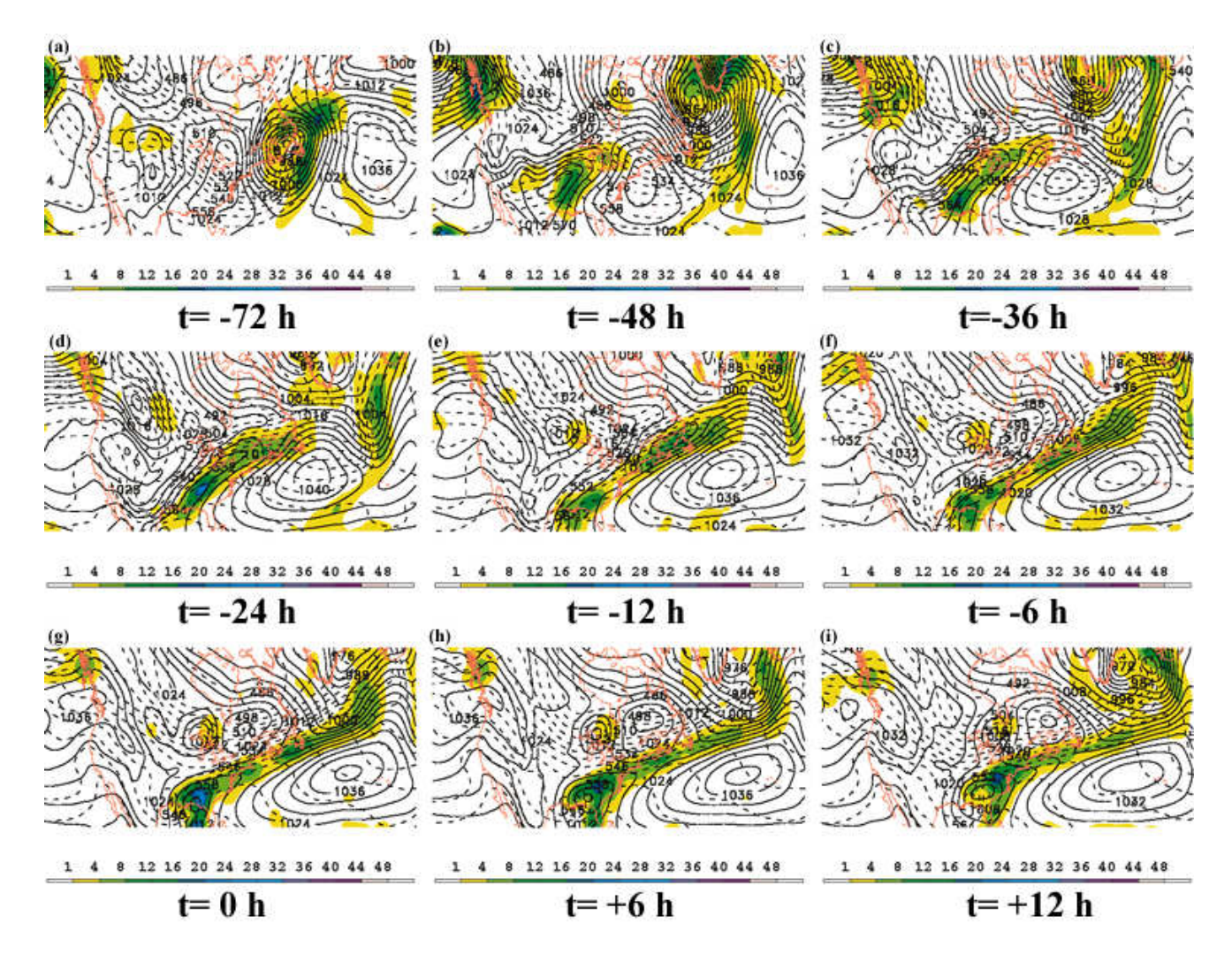


Figure 4.17: Time series of GFS half-degree analyses sea-level pressure (SLP, solid) contoured every 4 hPa, 1000-500 hPa thickness (dashed) contoured every 6 dam, and 6-hourly precipitation totals (shaded) in mm, for MAG 2. Results are shown for (a) t=-72 h, (b) t=-48 h, (c) t=-36 h, (d) t=-24 h, (e) t=-12 h, (f) t=-6 h, (g) t=0 h, (h) t=+6 h, and (i) t=+12 h, where t=0 h is 0600 UTC 11 December 2008.

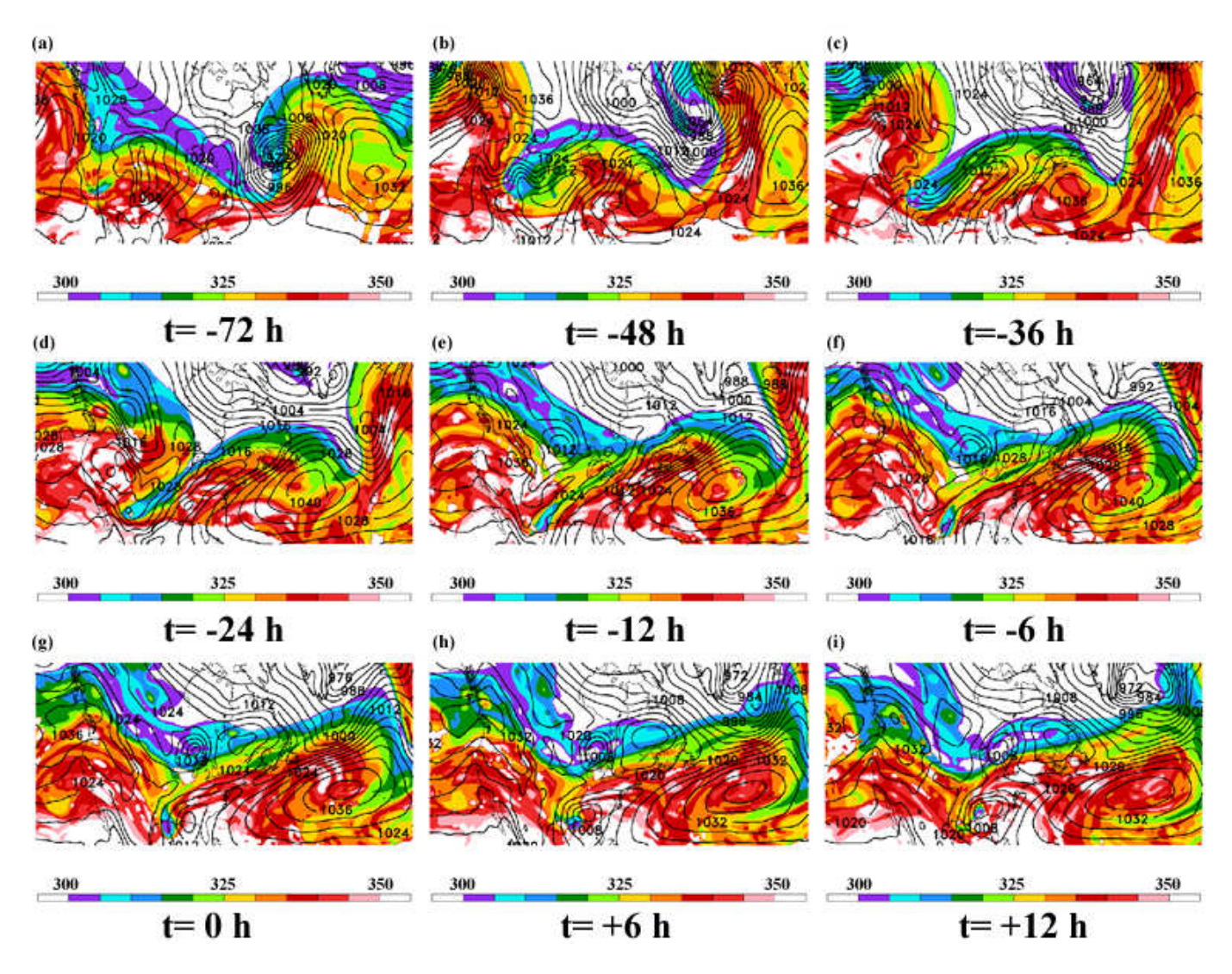


Figure 4.18: As in Fig. 4.17, but for SLP (solid, every 4 hPa) and potential temperature (K) on the Dynamic Tropopause (shaded).

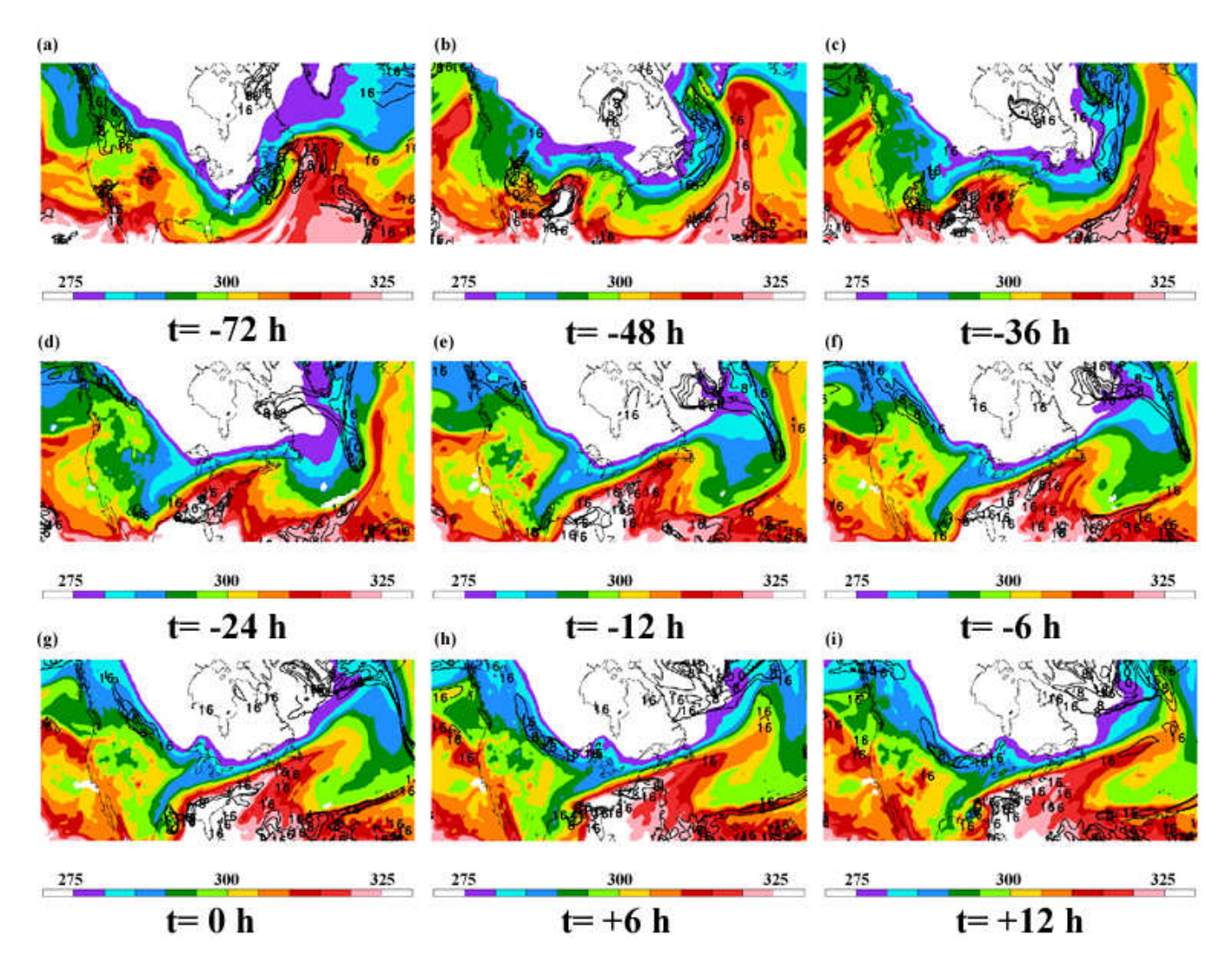


Figure 4.19: As in Fig. 4.17, but for 850 hPa equivalent potential temperature (K, shaded), and Coupling Index (K, solid, every 4 K from 0 to +16).

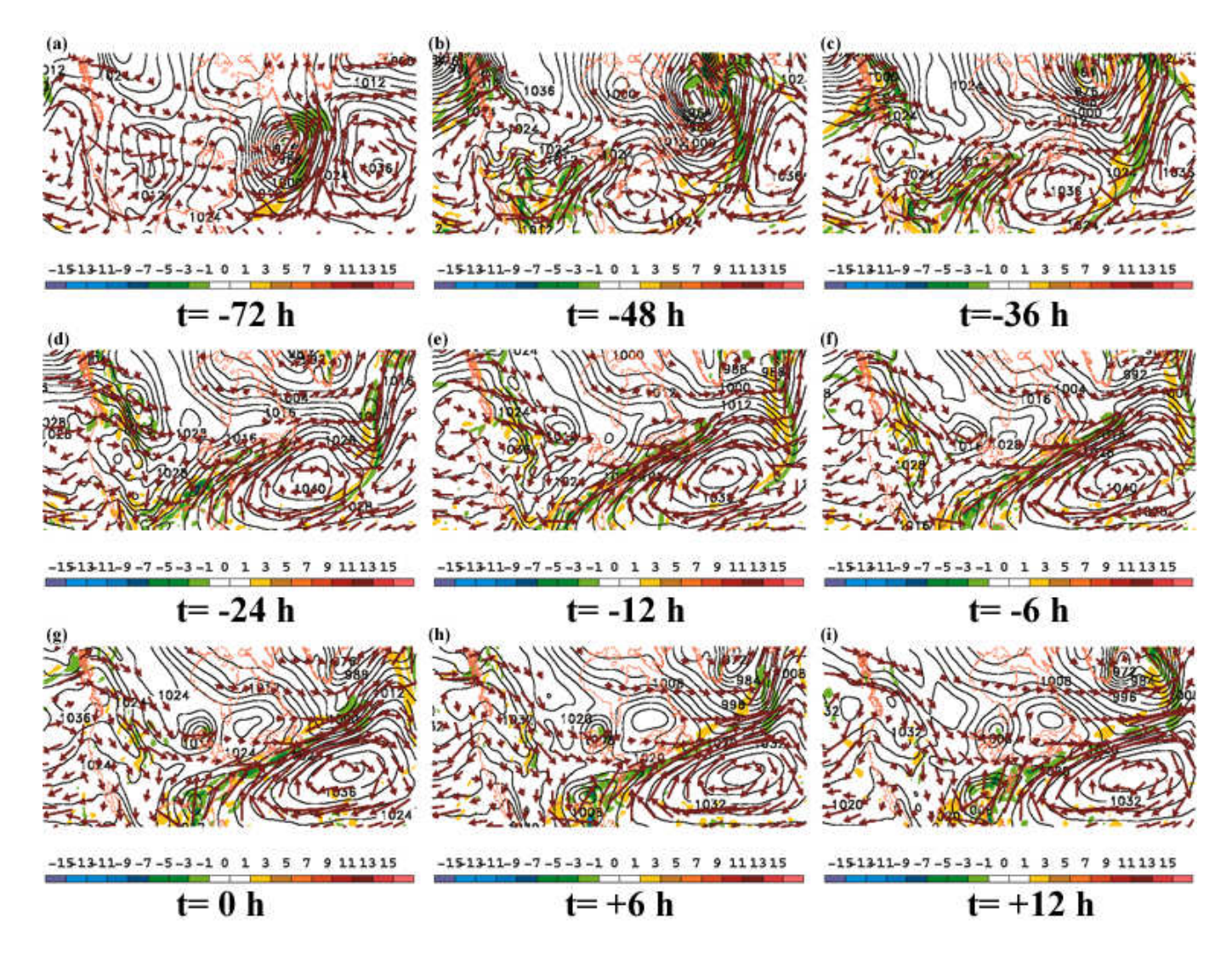


Figure 4.20: As in Fig. 4.17, but for SLP (solid, every 4 hPa), 1000-700 hPa moisture flux convergence (kg m⁻² s⁻¹, shaded), and 1000-700 hPa moisture transport vectors (red).

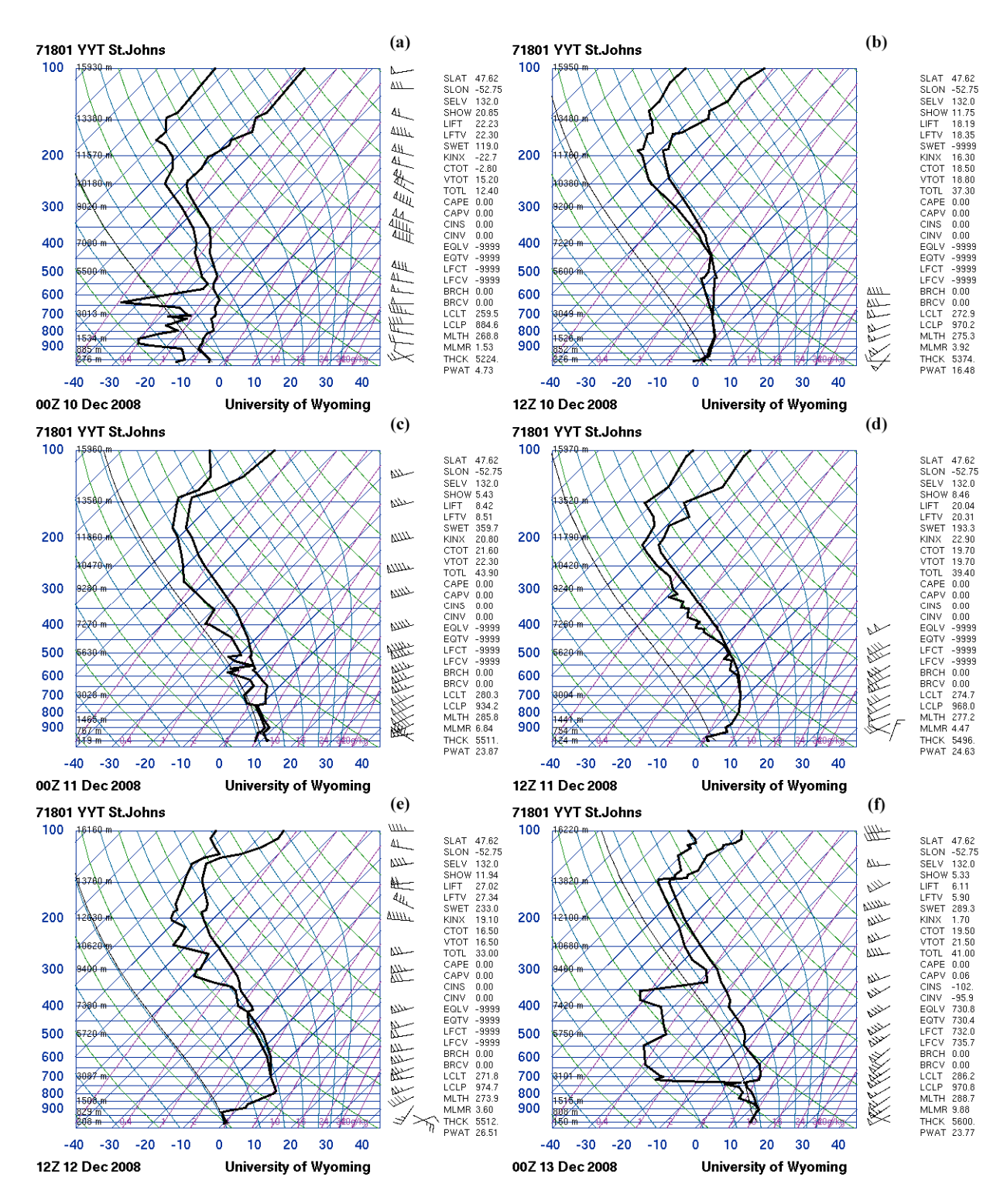


Figure 4.21: Time series of observed soundings at St. John's (CYYT) for MAG 2. Soundings are shown for (a) t =-30 h, (b) t=-18 h, (c) t=-6 h, (d) t=+6 h, (e) t=+30 h, and (f) t=+42 h, where t=0 h is 0600 UTC 11 December 2008. The sounding from t=+18 h is missing in the dataset.

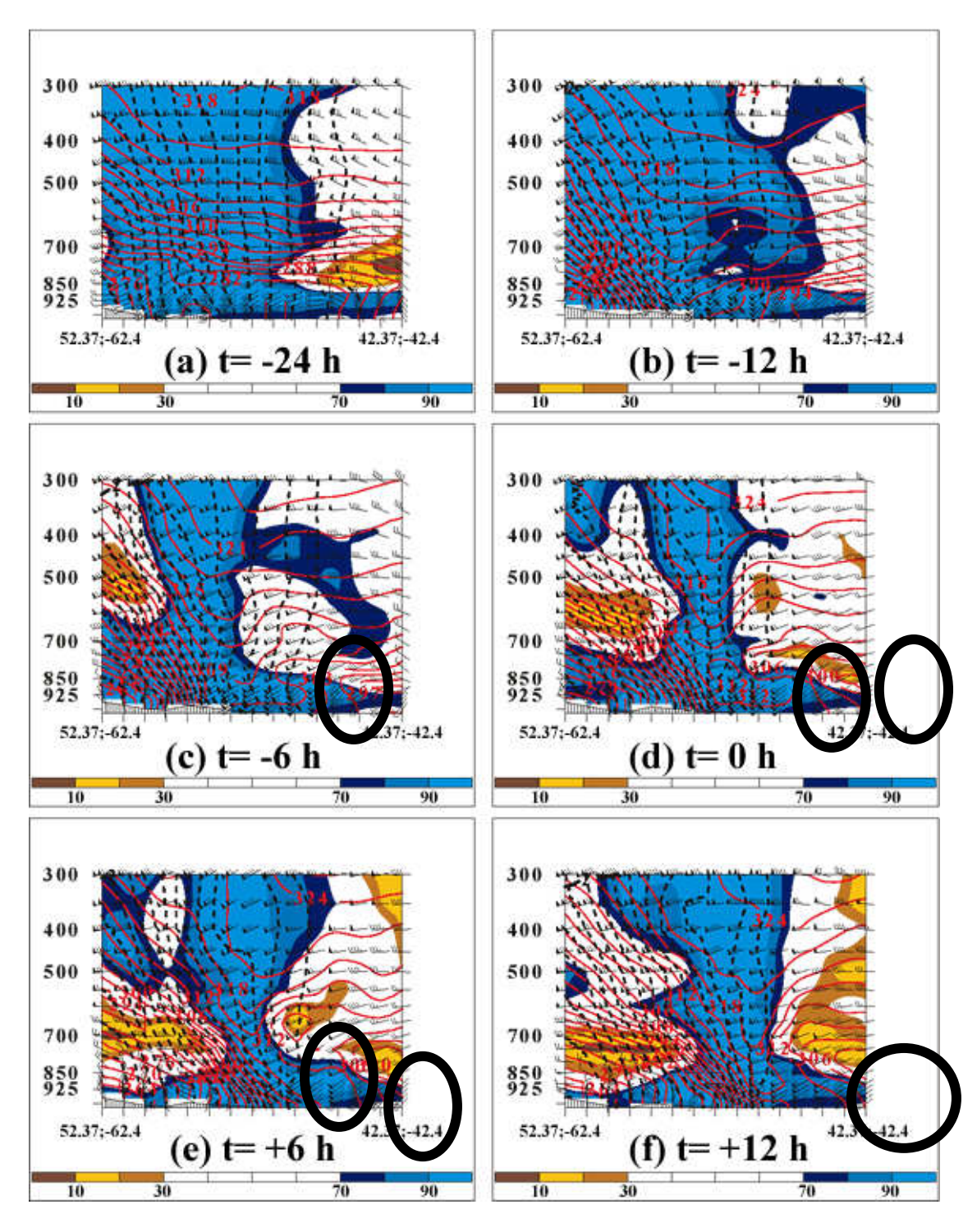


Figure 4.22: Time series of northwest-southeast cross-section plots from 52.37 N, -62.4 W to 42.37 N, -42.4 W, for MAG 2. Relative humidity (%, shaded), equivalent potential temperature (K, red solid lines), momentum (M) surfaces (m s⁻¹, black dashed) and winds (barbs) shown for (a) t =-24 h, (b) t=-12 h, (c) t=-6 h, (d) t=0 h, (e) t=+6 h, and (f) t=+12 h, where t=0 h is 0600 UTC 11 December 2008. Regions of convective instability are outlined by the black ovals.

Chapter 5

Evaluation of Two Independent Operational Forecasts during Consecutive Extreme Cool-Season Precipitation Events at St. John's, Newfoundland in December 2008

5.1 Introduction

Chapter 4 presents an overview and synoptic-dynamic analysis of consecutive extreme precipitation events that affect St. John's in December 2008. The first case, MAG 1, produced 73.6 mm of precipitation from 1200 UTC 7 December to 1200 UTC 9 December, while the second case, MAG 2, produced 54 mm, from 0000 UTC 11 December to 0000 UTC 13 December. Using the National Centers for Environmental Prediction (NCEP) Global Forecast System (GFS) half-degree analysis, and following the synoptic typing methodologies outlined in Chapter 3, it is found that MAG 1 is a southwest and cyclone case, while MAG 2 is a southwest and frontal case. The difference in synoptic type between the two cases (cyclone vs. frontal) that results from the second typing methodology in Chapter 3 (quasi-geostrophic forcing) highlights the disparate means by which MAG 1 and MAG 2 produce an extreme precipitation event at St. John's.

In this chapter, the main objective is to perform an evaluation of two separate operational forecast systems, the GFS half-degree model and the Environment Canada Global Environment Multiscale (GEM) model, the latter of which is represented by proxy using the Environment Canada operational forecasts. Such evaluations of model performance are not new in atmospheric science; as examples, Sanders (1986) analyzes the performance of the Limited Fine Mesh (LFM) model with regard to explosive cyclogenesis events in the western North Atlantic, while Caplan (1995) reports on the performance of the National Centers for Environmental Prediction (NCEP, formerly NMC) global medium-range forecast model (MRF) during the March 1993 Superstorm. In his analysis, Caplan (1995) presents plots of sea-level pressure (SLP), 500 hPa height, and low-level wind forecasts at different initialization and verification times.

The first part of each section in this chapter follows a similar verification scheme as in the study of Caplan (1995), focusing on GFS half-degree SLP forecasts, upper-tropospheric forecasts (dynamic tropopause, DT), as well as the thermodynamic environment at and around St. John's. Since operational model performance is not a major theme in this thesis, and for the sake of brevity, the synoptic plots in the GFS portions of this chapter are limited to forecasts that verify at t=0 h, or the time of onset of the heaviest precipitation at St. John's during each event, as previously defined in Chapters 2 and 3.

The second part of each section in this chapter utilizes the operational forecasts issued by Environment Canada before and during MAG 1 and MAG 2. The intention of this analysis is not to criticize the operational forecasts issued during these events, but instead use them as a proxy to evaluate the performance of the Environment Canada Global Environment Multiscale (GEM) model, which is used as the basis for all operational forecasts in Canada (Environment Canada, personal communication 2009). The analysis of the operational forecasts is limited to the 0-36 hour lead time range; this is due to the fact that Environment Canada only issues precipitation amount forecasts for day one and day two, as documented in the Environment Canada PUBPRO (2003) document, available online at http://www.msc.ec.gc.ca/msb/manuals/pubpro/index_e.cfm. In December, when MAG 1 and MAG 2 occur, operational forecasts from the Newfoundland Weather Office in Gander, Newfoundland are generally issued three times per day, at 530 am Newfoundland Standard Time (NST, 0900 UTC), 11 am NST (1430 UTC), and 4 pm NST (1930 UTC), with intermittent updates if necessary. Finally, two types of weather warnings are issued during MAG 1 and MAG 2, which will be further discussed in Sections 5.2.2 and 5.3.2, respectively: a rainfall warning, issued when amounts are predicted to exceed 25 mm in twelve hours or less, and a wind warning, issued for Newfoundland and Labrador if winds are expected to attain a steady speed of 75 km hr⁻¹ (40 knots), or to reach a speed of 100 km hr⁻¹ (54 knots) in gusts (PUBPRO 2003).

It is not the objective of this chapter to compare and contrast the performance of each forecast system (GFS and GEM), but instead to evaluate

each independently. Ideally, the author would like to perform an analysis of the model performance of several different forecast systems, including utilizing the actual GEM grids (instead of using the operational forecasts as a proxy). However, due to data availability and time constraints, this cannot be accomplished for the purpose of this thesis. With that said, the author feels that an analysis of the model performance using the data that is available is still a valuable contribution to this study.

5.2 Forecasts for MAG 1

5.2.1 GFS Half-Degree Model Forecasts

In Chapter 4, time series of precipitable water and 700 hPa vertical motion (ω) are presented to illustrate moisture availability (associated with subtropical moisture transport from the Atlantic and Gulf of Mexico) and forcing for ascent, respectively. Figure 4.5b displays the precipitable water and 700 hPa ω during MAG 1 from the GFS half-degree analysis; these parameters are evaluated at St. John's using the gdpoint function in GEMPAK (Koch 1983), which interpolates values to a 3 x 3 point grid, and subsequently takes the value of the center point.

It is found in Fig. 4.5b that precipitable water values are very high during the time period in which the heaviest precipitation falls at St. John's. From t=-12 h to t=0 h, the precipitable water ranges from ~24 to ~32 mm, peaking at t=0 h (approximately 32 mm). Concommitantly, ω is most negative at t=-12 h and t=0 h, supporting the assertion in Chapter 4 that the largest amounts of precipitation are associated with strong ascent in the presence of extreme amounts of moisture.

Fig. 5.1 contains time series of GFS forecasts for precipitable water and for eight different model initialization times, every twelve hours from t=-96 h (0600 UTC 4 December 2008) to t=-12 h (1800 UTC 7 December 2008), where t=0 is 0600 UTC 8 December 2008, as defined in Chapter 4. Time series of 700 hPa ω are not included because it was determined that evaluating point forecasts of an inherently noisy field would produce potentially arbitrary results (Casati et al. 2008; McTaggart-Cowan, personal communication). Although it is beyond the scope of this thesis, the author is planning to address this issue in future work (see Chapter 6 for details).

In Fig. 5.1, it is evident that the precipitable water values at all included initialization times follow similar evolutions. However, the t=-12 h forecasts (pink) and GFS analysis (black) values are slightly higher, particularly around the verification time of t=0 h (labeled '4' on the horizontal axis in Fig. 5.1). This suggests that while the GFS forecasts are accurate in terms of the timing and evolution of the moisture, the model slightly underforecasts (approximately 2-5 mm, varying by initialization time) the moisture at St. John's that verifies at t=0 h.

Figure 5.2 shows time series of GFS precipitation forecasts, for the initialization times highlighted in Fig. 5.1 and discussed above for precipitable water. It is evident in Fig. 5.2 that during the time of the heaviest precipitation (t=-6 h to t=+6 h), the precipitation is greatly underforecasted as compared to the observed values at St. John's. In the t=-6 h to t=0 h time period, most of the initialization times forecast precipitation values that are approximately 10-15 mm

below the observed value. This error is even larger (approximately 15-20 mm) in the t=0 h to t=+6 h time range. To further investigate the issue of inaccurate QPF (especially in the t=-12 h to t=+6 h verification time range), the following synoptic-dynamic analysis concentrates on the differences among initialization times at the verification time of t=0 h.

Figure 5.3 shows that at earlier initialization times, the rapidly deepening cyclone associated with MAG 1 is forecast to be substantially farther to the north and east at t=0 h than in the GFS analysis. Additionally, the central sea-level pressure of the aforementioned cyclone is 15-20 hPa weaker in the 72-96 hour initialization time range (Fig. 5.3a-c) than in the analysis (Fig. 5.3i). For initialization times of t=-60 h to t=-24 h (Fig. 5.3d-g), the differences in central SLP and cyclone location are minimal. However, small differences such as these in the SLP (mass) field can often make a large difference in QPF (e.g. Sisson and Gyakum 2004). A generally accurate representation of a mass field such as SLP can result in a precipitation forecast that is inaccurate in terms of amount, timing, or both. In this case, this result is perhaps attributable to mesoscale ascent (such as localized frontogenesis) in the GFS analysis that is not suggested by the synoptic-scale mass fields alone, although this hypothesis requires further investigation.

In Chapter 4, it is revealed that between t=-12 h and t=+6 h (the period of heaviest precipitation at St. John's), potential temperatures (θ) on the DT are extremely high and represent a warm moist subtropical air mass that is advected

from the central north Atlantic and the Gulf of Mexico ahead of the sea-level cyclone. Figure 5.4 confirms that at earlier initialization times (t=-96 h to t=-72 h, Fig. 5.4a-c), the intensity of potentially warm air downstream of the sea-level cyclone is underforecast. However, the most important finding in Fig. 5.4 comes from a comparison of the medium-range initialization times (t=-60 h to t-24 h, Fig. 5.4d-g) with the t=-12 h initialization time and the analysis (Fig. 5.4h-i); that is, while the large-scale structures such as a negatively titled trough on the DT to the southwest of the sea-level cyclone and a strongly amplified ridge on the DT downstream of St. John's are accurately represented, the θ values on the DT are substantially underforecast at St. John's until the t=-12 h initialization time. Specifically, the GFS analysis shows DT θ values 15-20 K warmer than is forecasted in the medium-range model initialization times. Since the overall structure on the DT is similar between the analysis and earlier initialization times, it is reasonable to conclude that the markedly higher θ values on the DT in the analysis are a result of the model (belatedly) properly analyzing diabatic consequences of heavy precipitation at St. John's that occurs before t=0 h (~40 mm in 18 hours from t=-18 h to t=0 h). The failure of the model to properly analyze the diabatic impacts of the earlier precipitation at medium-range lead times (Fig. 5.3d-g) may help to account for the 10-20 mm underforecast of precipitation in the t=-6 h to t=+6 h verification time period (Fig. 5.2).

In Chapter 4, it is found that relatively low values of the coupling index (CI), a measure of bulk atmospheric stability (Galarneau and Bosart 2006), are associated with MAG 1 in the warm sector of the sea-level cyclone, of which St.

John's is located in from t=-18 h to t=+6 h, until the passage of the trailing cold front. To that end, Fig. 5.5 shows 850 hPa equivalent potential temperature (θ_e), along with contours of low values of the CI. It is evident in Fig. 5.5a-c that at earlier initialization times, the GFS keeps the lowest stability air to the east of St. John's, which corresponds with the incorrect position forecasts of the sea-level cyclone evident in Fig. 5.3a-c. The medium-range forecasts from t=-60 h to t=-24 h (Fig. 5.5d-g) resolve the low values of CI relatively well, although the lowest values of CI (< 8 K) that are observed in the analysis (Fig. 5.5i) are not co-located with St. John's until the t=-12 h initialization time. Moreover, the t=-12 h initialization time and the analysis (Fig. 5.5h-i) both suggest that the 850 hPa θ_e values are underforecast at earlier initialization times by ~5 K. Although further research needs to be done, this suggests that the GFS does not accurately capture the full extent of the subtropical air mass at St. John's until twelve hours before the heaviest precipitation, after some precipitation has already fallen at the station. It is likely that this also helps to explain the gross underforecast of precipitation in the t=-6 to t=+6 time period (Fig. 5.2).

Figure 5.6 displays GFS forecast soundings at St. John's, all verifying at t=0 h; minor, but physically significant differences are evident among the soundings. First, at earlier initialization times (t=-96 h to t=-72 h, Fig. 5.6a-c), the low-level temperature and dewpoint are approximately 3-5° C too cool compared with the analysis (Fig. 5.6i). Secondly, the mixing ratio values in the lower 300 hPa are substantially lower than in the analysis, particularly at the t=-96 h and t=-84 h initialization times (Fig. 5.6a-b). Finally, the level of the tropopause in all

the forecasts is approximately 50 hPa lower than in the analysis, the latter of which matches up with the observed soundings at St. John's discussed in Chapter 4 (Fig. 4.10).

5.2.2 Environment Canada Operational Forecasts

Since operational forecasts issued by Environment Canada are solely based on the GEM model (Environment Canada, personal communication), they are used as a proxy for GEM model forecasts. Table 5.1 and 5.2 detail the Newfoundland Weather Office forecasts for St. John's at various forecast times before and during MAG 1. Owing to the fact that precipitation amounts are only forecasted for Day 1 and Day 2, only the forecasts for those times are displayed in Tables 5.1 and 5.2. As documented by Environment Canada (PUBPRO 2003), 'today' refers to the forecast time through 6 pm NST (2130 UTC), 'tonight' (or e.g. 'Sunday night') refers to the 6 pm to 6 am NST (2130 to 0930 UTC) time period and 'tomorrow' refers to the 6am to 6 pm NST (0930 to 2130 UTC) time period on the subsequent day.

In general, forecasts in the 24-36 hour initialization time range underforecast the total MAG 1 precipitation by approximately 20-30 mm. That is, while the Environment Canada forecasts do predict an extreme event (as defined in Chapter 2) at St. John's, they fail to anticipate the magnitude of an event that ranks among the top 5 most extreme cool-season events of the past three decades. Specifically, the forecast issued at 0900 UTC 7 December (t=-21 h) calls for 10 mm of rain prior to 2130 UTC, 15 to 25 mm of rain between 2130 UTC 7

December and 0930 UTC 8 December (t=+3.5 h), and 10 to 15 mm of additional rain from 0930 to 2130 UTC 8 December, corresponding to a maximum total of 50 mm. In reality, 73.6 mm of precipitation is recorded at St. John's during this time period. This potentially suggests that the GEM model forecasts contain errors relating to the intensity of the warm-sector air mass, as well as the diabatic issues mentioned in Section 5.2.1 with respect to the GFS, although this point would require investigation of the actual GEM forecast grids. A rainfall warning is not issued for St. John's until a special updated forecast at 0443 8 December, or roughly one hour prior to t=0 h, which calls for 30 to 40 mm of precipitation for the remainder of the night, a value that generally verifies.

In summary, the Environment Canada operational forecast errors appear to occur not in the structure or location of the system (e.g. temperatures are correctly forecasted in the medium-range initialization times), but in the underforecast of the extreme values of precipitation. Therefore, it is reasonable to assume that the GEM fails to accurately represent the fine details of the air mass and the diabatic impacts of the early precipitation.

5.3 Forecasts for MAG 2

5.3.1 GFS Half-Degree Model Forecasts

In Chapter 4, it is found that MAG 2 is associated with a quasi-stationary baroclinic zone situated near St. John's, and is marked by relatively small values of ascent forced by strong low-level frontogenesis, in the presence of relatively low-stability air and large amounts of subtropical moisture, particularly at

t=0 h. Fig. 5.7 displays time series of eight different GFS model initialization times and the GFS analysis for the period of precipitation at St. John's, which runs from t=-6 h to t=+36 h. Thus, t=0 is labeled '2' on the horizontal axis. In the precipitable water field (Fig. 5.7), there are mixed results in the evolution of the moisture at St. John's, with the exception being the very accurate forecasts of the t=-12 h initialization time. Specifically, the earliest initialization times (t=-96 h and t=-84 h) underestimate the precipitable water by almost 10 mm at the verification times of t=-6 h and t=0 h. Later initialization times (t=-72 h to t=-24 h) do correctly analyze a precipitable water maximum, but one that verifies 6-12 hours too late. This is important because over half of the MAG 2 total precipitation (29 of 54 mm) falls during the t=-6 h to t=+6 h time period (Fig. 4.12), including 21 mm between t=0 h and t=+6 h. While the t=-48 h to t=-24 h initialization times do capture the three-stage evolution of MAG 2 described in Chapter 4 (warm to cool stage and then back to warm), the forecasts at initialization times of t=-72 h and t=-60 h completely fail to predict the second warm stage. As will be discussed later in this section, this is primarily due to large GFS model errors in the prediction of a closed cyclone over the Gulf of Mexico.

Figure 5.8 confirms the observations of Fig. 5.7, in that the GFS does not predict any precipitation at St. John's in the t=-96 h and t=-84 h initialization time forecasts. Moreover, the later model runs (t=-72 h to t=-36 h) do predict fairly accurate values of precipitation, but show the maximum precipitation amounts verifying 6-12 hours too late, as seen with the precipitable water forecasts in Fig.

5.7. By the t=-24 h and t=-12 h initialization times, the precipitation forecasts, although slightly underdone, are generally accurate compared to the observed values (Fig. 5.8), and certainly closer to reality than the forecasts for MAG 1 at similar lead times.

As is evident in Fig. 5.9a-b, the earlier model initialization times (t=-96 h and t=-84 h) incorrectly predict a strong sea-level cyclone in northeastern Quebec. This incorrect forecast causes the baroclinic zone to be oriented north-south instead of the northeast-southwest orientation that verifies in the analysis. At later initialization times, the aforementioned strong sea-level cyclone in Quebec is no longer present, and the GFS generally captures the orientation of the baroclinic and the structure of the precipitation at St. John's, which is associated with the improved precipitation forecasts (Fig. 5.8)

However, it is the closed cyclone in the Gulf of Mexico which hampers the model at verification times later than t=0 h (not shown). At early initialization times (t=-96 and t=-84 h), the model is too progressive with this feature, while in the medium range forecasts (e.g. t=-60 h and t=-48 h), the model is too slow. This is evidenced in Figs. 5.9d-e, where the GFS analyzes the closed low over the western Gulf of Mexico while in the analysis it is actually located in the Florida Panhandle (Fig. 5.9i). In addition, the earlier initialization times predict a much weaker circulation, which is consistent with the assertion in Fig. 5.7 that a second warm stage is not predicted by the t=-72 h and t=-60 h model runs in the precipitable water field. In fact, the model is so slow with the

progression of the Gulf of Mexico cyclone that the warm moist air ahead of the circulation on the south side of the baroclinic never makes it far enough northward towards St. John's at the end of MAG 2, at verification times later than t=0 h (not shown). By the t=-48 h and t=-36 h initialization times, the GFS forecasts are more accurate than previous initialization times, which is exhibited by the better precipitable water (Fig. 5.7a) and precipitation forecasts (Fig. 5.8).

The model forecast errors discussed in the previous paragraph are also evident in Fig. 5.10, wherein the high θ values on the DT seen in the GFS analysis are not fully realized until the t=-12 h initialization time. This suggests that as in MAG 1, the extent of the tropical air mass at St. John's is somewhat, but not entirely accurately forecast until just before the time of maximum precipitation at St. John's. However, the θ errors on the DT in the medium-range initialization times are substantially smaller than those observed for MAG 1.

The forecast errors with the Gulf of Mexico closed low are evident in Fig. 5.10; in short, the GFS appears to phase the northern and southern jet too quickly in earlier model initialization times (t=-96 h and t=-84 h) and too late at medium range initialization times (t=-72 h and t=-60 h). As stated earlier, by the t=-48 h initialization time, the model appears to place the Gulf of Mexico circulation in the correct location.

As discussed in Chapter 4, the lowest values of coupling index (CI) remain well to the southwest of St. John's at the peak of MAG 2, which may help to account for some of the approximately 20 mm precipitation difference between

MAG 1 and MAG 2. Figure 5.11 shows that with the exception of the earliest initialization times when the erroneous Quebec sea-level cyclone is forecasted (Fig. 5.11a-b, t=-96 h and t=-84 h), the GFS forecasts are generally accurate with the structure of the low-level θ_e and CI fields. In association with the assertion that the precipitable water forecasts verifying at t=0 h are generally accurate after the t=-84 h initialization time (Fig. 5.7), it appears the main errors in the QPF at t=0 h likely result from slight differences in the position of the baroclinic zone and timing of the frontogenetical forcing for ascent.

Figure 5.12 displays GFS forecast soundings for St. John's. It is clear that with the exception of the t=-96 h and t=-84 h initialization times (Fig. 5.12a-b), the GFS accurately predicts the thermodynamic structure of the atmosphere at St. John's, up to three days prior to t=0 h, including the elevated tropopause seen in the observed soundings in Fig. 4.21. This supports the earlier claim that the main errors in the precipitation forecasts at t=0 are due to the improper prediction of forcing for ascent, not the thermodynamic environment. The inaccurate representation of the thermodynamic environment at later verification times, particularly in the t=-72 h and t=-60 h initialization time forecasts, is mostly due to the aforementioned issues with the Gulf of Mexico cyclone (not shown).

5.3.2 Environment Canada Operational Forecasts

Environment Canada operational forecasts for MAG 2 are presented in Tables 5.3 and 5.4, and show that while there is a slight underforecast of the event, over 80% of the precipitation amount recorded at St. John's is forecasted. The main

forecast issue deals with the timing of the heaviest precipitation, which is forecast to occur about six hours later than it actually does. For example, Table 5.3 shows the forecast issued at 0900 UTC 10 December, 21 hours prior to t=0 h. For the 2130 UTC 10 December to 0930 UTC 11 December period, 20 mm of precipitation is forecasted, but 30 mm falls by 1200 UTC 11 December (Chapter 4). Moreover, 10 to 20 mm is forecast for the 0930 UTC to 2130 UTC 11 December time period, and only 10 mm is actually recorded from 1200 UTC 11 December to 0000 UTC 12 December.

Total precipitation amounts and duration for MAG 2 are generally accurate in the 1-2 day lead times. However, it is suspected that errors are likely to be discovered in a closer examination of the 3-5 day lead time forecasts, but to do so, one would have to analyze the GEM model fields themselves, and we are unable to do that at this time. The operational forecasts, however, do confirm that the GEM model is mostly accurate in terms predicting MAG 2 at shorter lead times, and contains a much smaller QPF error than that seen for MAG 1.

5.4 Summary and Discussion

For MAG 1, it is found in Section 5.2 that the precipitable water forecasts at all initialization times in the GFS are slightly less than the GFS analysis values. However, the timing and evolution of precipitable water is fairly consistent for all forecast initialization times, and matches up well with the GFS analysis. Errors at the earlier initialization times (t=-96 h to t=-72 h) are in part related to the model being too fast and too weak with the precipitation-causing sea-level cyclone (Fig.

5.3). Later initialization times produce a relatively accurate representation (both in position and intensity) of the sea-level cyclone. A caveat should be mentioned in that previous work (e.g. Roebber and Bosart 1998) has noted that the subtle details of a mass-field forecast can often be important in the prediction or evaluation of QPF. Nevertheless, it appears the main GFS forecast errors for MAG 1 stem from the under-prediction of the warm moist subtropical air mass located over St. John's, in the warm sector of the sea-level cyclone. Fig. 4.4 and 4.5 both show evidence that the intensity of the subtropical air mass (on the DT and at 850 hPa, respectively) at St. John's is underestimated by the model at all initialization times, with the possible exception of the t=-12 h initialization time. The suggestion here is that this is at least in part related to the model not capturing the diabatic heating as a result of latent heat release due to heavy precipitation during the early part of MAG 1.

An analysis of the Environment Canada operational forecasts shows a similar underforecast of precipitation until just before the onset of heavy precipitation. While it is possible that the model underforecast is due to the failure to predict diabatic heating as seen in the GFS, further work that quantifies the output of the actual GEM model grids should be undertaken. This is also discussed in Chapter 6.

In sum, the GFS does a fairly good job of predicting the thermodynamic environment verifying at t=0 h at St. John's during MAG 2, especially at initialization times later than t=-84 h, when the model stops predicting the false

intense surface cyclone over northeastern Quebec. The slight differences in forecasts from the t=-72 h initialization time forward are in the position and orientation of the baroclinic zone. However, these slight variations among model runs can contribute to large errors in QPF, both in terms of amount and timing (Fig. 5.9). This is especially true since the ascent in MAG 2 is almost entirely forced by low-level frontogenesis (Chapter 4), which is often located in a narrow band close to the strongest portion of the baroclinic zone. The larger errors that occur at verification times well after t=0 h are due to the inaccurate prediction of the Gulf of Mexico cyclone and, while interesting, are less crucial to human interest at St. John's, since the majority of precipitation falls prior to t=+6 h (Fig. 5.8).

Environment Canada operational forecasts in the 1-2 lead time range are fairly accurate for MAG 2. However, since most of the GFS errors associated with this event occurred at longer lead times, a full analysis of the GEM model grids should be completed in order to compare GEM forecasts with those from the GFS. This is also discussed in the future work section of Chapter 6.

Forecast Issue Time	Forecast for St. John's
0900 UTC 6 December	Sunday (7 December): Cloudy. Flurries beginning near noon (1530 UTC) changing to periods of rain in the afternoon. Snowfall amount 2 cm. Rainfall amount 5 to 10 mm. High 7° C.
1930 UTC 6 December	Sunday: Cloudy. Flurries beginning in the morning changing to periods of rain near noon. Snowfall amount 2 cm. Rainfall amount 5 mm. High 7° C. Sunday Night: Periods of rain. Amount 15 to 25 mm. Low 5° C.
0900 UTC 7 December	Today: Cloudy. Flurries beginning this morning changing to rain later this morning. Risk of freezing rain this morning. Rainfall amount 10 mm. High 9° C. Tonight: Rain. Amount 15 to 25 mm. Temperature
	steady near 10° C. Monday: Periods of rain ending in the afternoon then cloudy with 40% chance of showers. Amount 10 to 15 mm. Temperature falling to 3° C in the afternoon.
1430 UTC 7 December	Today: Snow changing to rain near noon. Risk of freezing rain near noon. High 9° C.
	Tonight: Rain. Amount 15 to 25 mm. Temperature Steady near 10° C.
	Monday: Periods of rain ending in the afternoon then cloudy with 40% chance of showers. Temperature falling to 3° C in the afternoon.
1930 UTC 7 December	Tonight: Rain. Amount 15-25 mm. Temperature rising to 11° C this evening then falling.
	Monday: Showers. Amount 10 mm. Temperature falling to 2° C in the afternoon.
	Monday Night: Cloudy. 40 percent chance of rain showers in the evening and of flurries overnight. Low -4° C

Table 5.1: Environment Canada operational forecasts issued by the Newfoundland Weather Office, for St. John's, before and during the first part of MAG 1 (Saturday 6 December 2008 and Sunday 7 December 2008).

Forecast Issue Time	Forecast for St. John's
0443 UTC 8 December	***Rainfall warning in effect***
	Tonight: Rain. Amount 30 to 40 mm. Temperature steady near 12° C.
	Monday: Showers. Amount 5 to 10 mm. Temperature falling to 2 ° C in the afternoon.
	Monday Night: Cloudy. 40% chance of rain showers in the evening and of clurries overnight. Low -4° C.
0900 UTC 8 December	***Rainfall warning in effect***
	Today: Periods of rain. Amount 5 to 10 mm. Temperature falling to 3° C this afternoon.
	Tonight: Showers ending this evening then cloudy. Low -4° C.
	Tuesday: Clearing in the morning. High -1° C.
1430 UTC 8 December	Today: Showers or drizzle. Temperature falling to 3° C this afternoon.
	Tonight: A few showers or drizzle ending this evening then cloudy. Low -4° C.
	Tuesday: Clearing in the morning. High -1° C.
1930 UTC 8 December	Tonight: Increasing cloudiness. A few flurries or rain showers this evening. Low-3° C.
	Tuesday: Sunny with cloudy periods. Temperature steady near -3° C.

Table 5.2: Environment Canada operational forecasts issued by the Newfoundland Weather Office, for St. John's, during the latter part of MAG 1 (Monday 8 December 2008 and Tuesday 9 December 2008).

Forecast Issue Time	Forecast for St. John's
1930 UTC 9 December	Wednesday: Cloudy. Periods of rain beginning in the morning. Amount 5 mm. High 10° C.
	Wednesday Night: Rain. Amount 15 mm. Temperature steady near 9° C.
0900 UTC 10 December	***Wind warning in effect***
	Today: Flurries changing to periods of rain this morning. Rainfall amount 5 mm. High 10° C.
	Tonight: Rain. Amount 15 mm. Temperature steady near 9° C.
	Thursday: Rain. Amount 10 to 20 mm. Temperature falling to 1° C in the afternoon.
1430 UTC 10 December	***Wind warning in effect***
	Today: P eriods of rain. Amount 5 to 10 mm. High 10° C.
	Tonight: Rain. Amount 15 mm. Temperature steady near 9° C.
	Thursday: Rain. Amount 10 to 20 mm. Temperature falling to 1° C in the afternoon.
1930 UTC 10 December	***Wind warning in effect***
	Tonight: Periods of rain. Amount 10 mm. Temperature steady near 9° C.
	Thursday: Rain changing to snow late in the day. Rainfall amount 10 to 20 mm. Temperature falling to 1° C in the afternoon.
	Thursday Night: Snow changing to rain near midnight. Rainfall amount 5 mm. Temperature steady near 1° C.

Table 5.3: Environment Canada operational forecasts issued by the Newfoundland Weather Office, for St. John's, before the first part of MAG 2 (Tuesday 9 December 2008 and Wednesday 10 December 2008).

Forecast Issue Time	Forecast for St. John's
0900 UTC 11 December	Today: Rain changing to flurries this afternoon. Risk of freezing rain this afternoon. Rainfall amount 10 to 20 mm. Temperature falling to 0° C this afternoon.
	Tonight: Flurries changing to ice pellets overnight. Risk of freezing rain overnight. Snow and ice pellet amount 2 cm. Low -1° C.
	Friday: Ice pellets changing to periods of rain early in the morning. Risk of freezing rain early in the emorning. Rainfall amount 5 to 10 mm. High 13° C.
1430 UTC 11 December	Today: Rain changing to flurries near noon. Risk of freezing rain this afternoon. Temperature falling to 0° C this afternoon.
	Tonight: Flurries changing to ice pellets overnight. Risk of freezing rain overnight. Snow and ice pellet amount 2 cm. Low -1° C.
	Friday: Ice pellets changing to periods of rain early in the morning. Risk of freezing rain early in the emorning. Rainfall amount 5 to 10 mm. High 13° C.
1930 UTC 11 December	Tonight: Rain changing to periods of snow mixed with ice pellets early this evening. Risk of freezing rain. Snow and ice pellet amount 2 cm. Low -1° C.
	Friday: Ice pellets changing to rain early in the morning and ending in the afternoon then cloudy. Rainfall amount 5 to 10 mm. High 12° C.

Table 5.4: Environment Canada operational forecasts issued by the Newfoundland Weather Office, for St. John's, during MAG 2 (Thursday 11 December 2008).

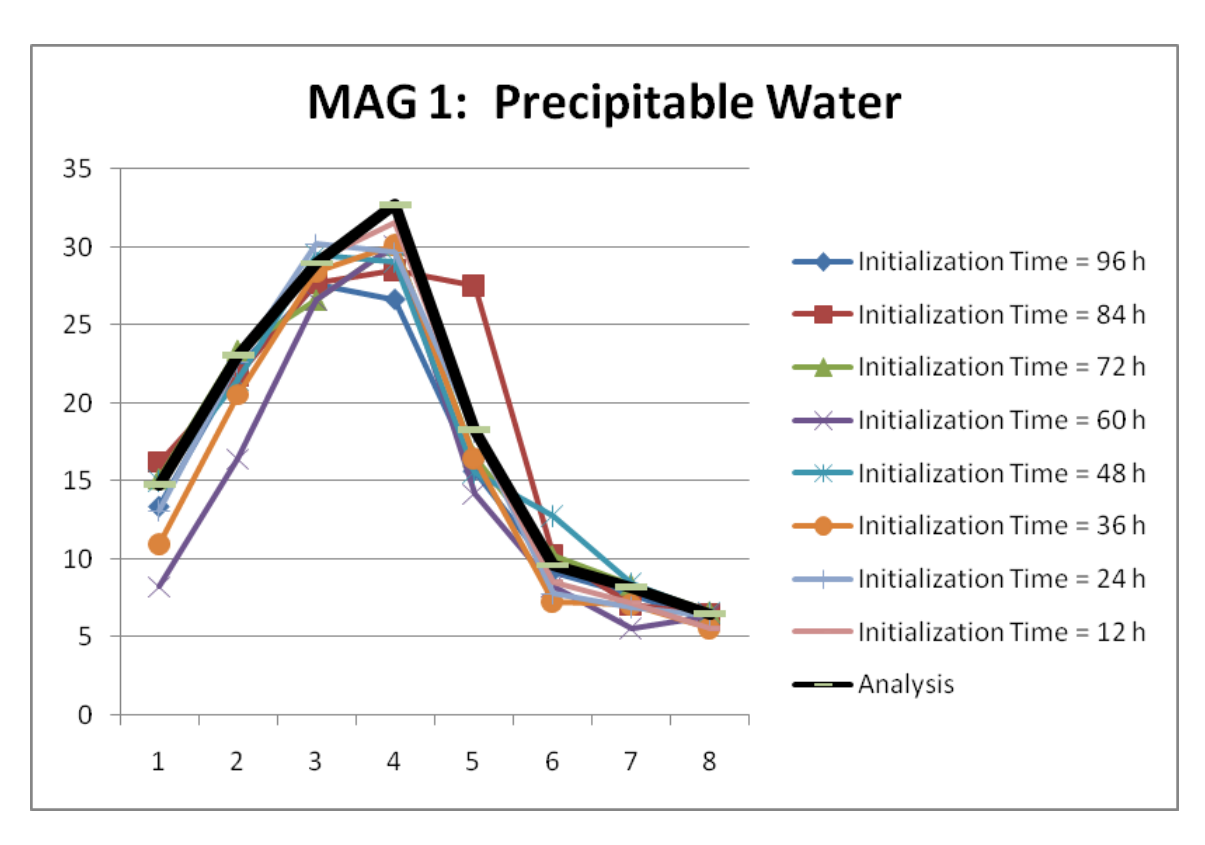


Figure 5.1: Time series for MAG 1 of GFS half-degree forecasts for precipitable water (mm). Each line is a different initialization time, with forecasts for every six hours (horizontal axis) during the period of precipitation at St. John's, which is t=-18 h (1200 UTC 7 December 2008) to t=+24 h (0600 UTC 9 December 2008). The GFS half-degree analysis is represented by a bold black line.

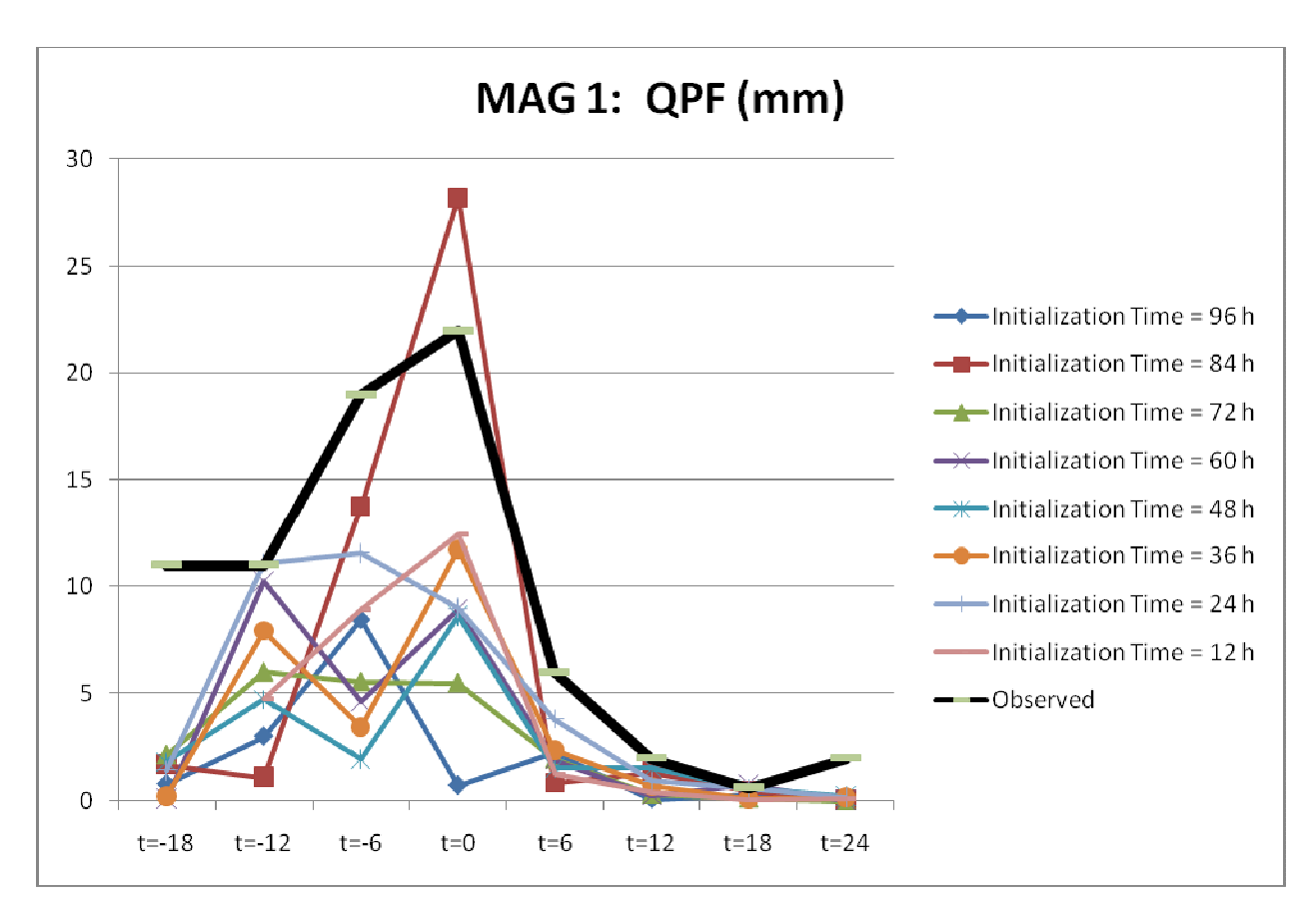


Figure 5.2: Time series for MAG 1 of GFS half-degree forecasts for precipitation (mm) for six hour periods beginning at each verification time (horizontal axis). Each line is a different initialization time, with forecasts for every six hours (horizontal axis) during the period of precipitation at St. John's, which is t=-18 h (1200 UTC 7 December 2008) to t=+24 h (0600 UTC 9 December 2008). The GFS half-degree analysis is represented by a bold black line.

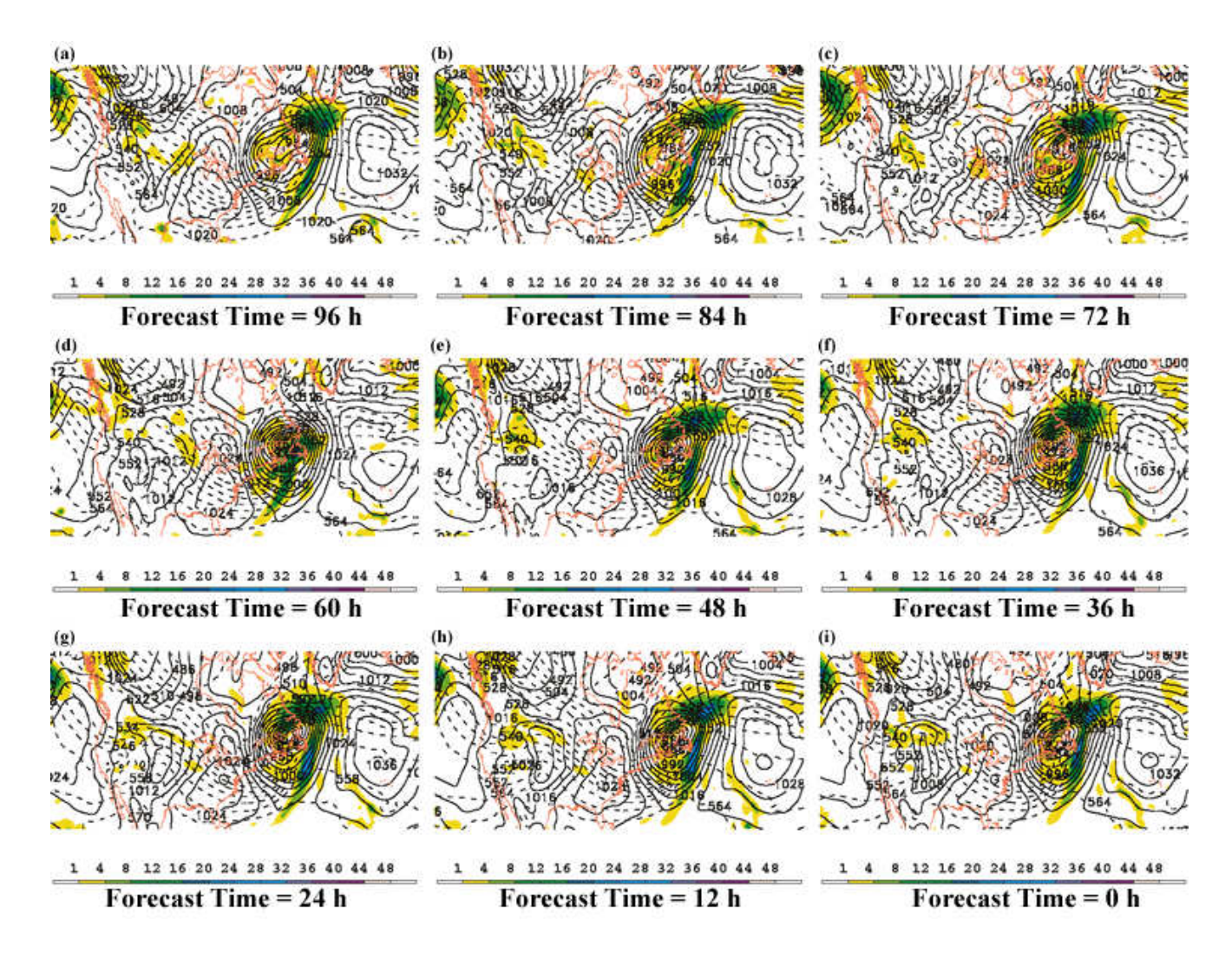


Figure 5.3: Time series of GFS half-degree analyses sea-level pressure (SLP, solid) contoured every 4 hPa, 1000-500 hPa thickness (dashed) contoured every 6 dam, and 6-hourly precipitation totals (shaded) in mm, for MAG 1, all validating at t=0 h, 0600 UTC 8 December 2008. Results are displayed for forecast lead times of (a) t=96 h, (b) t=84 h, (c) t=72 h, (d) t=60h, (e) t=48 h, (f) t=36 h, (g) t=24 h, (h) t=12 h, and (i) t=0 h.

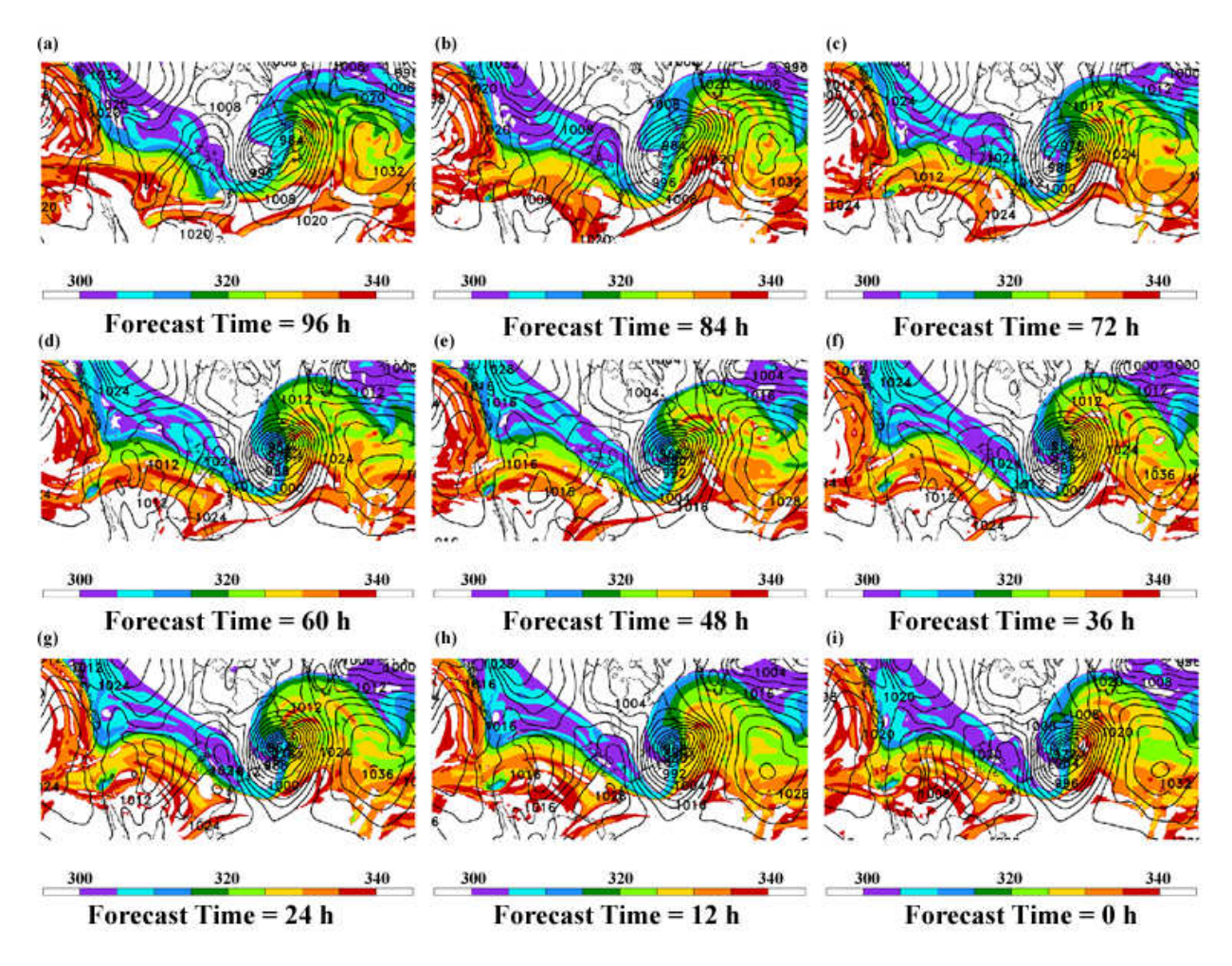


Figure 5.4: As in Fig. 5.3, but for SLP (solid, every 4 hPa) and potential temperature (K) on the Dynamic Tropopause (shaded).

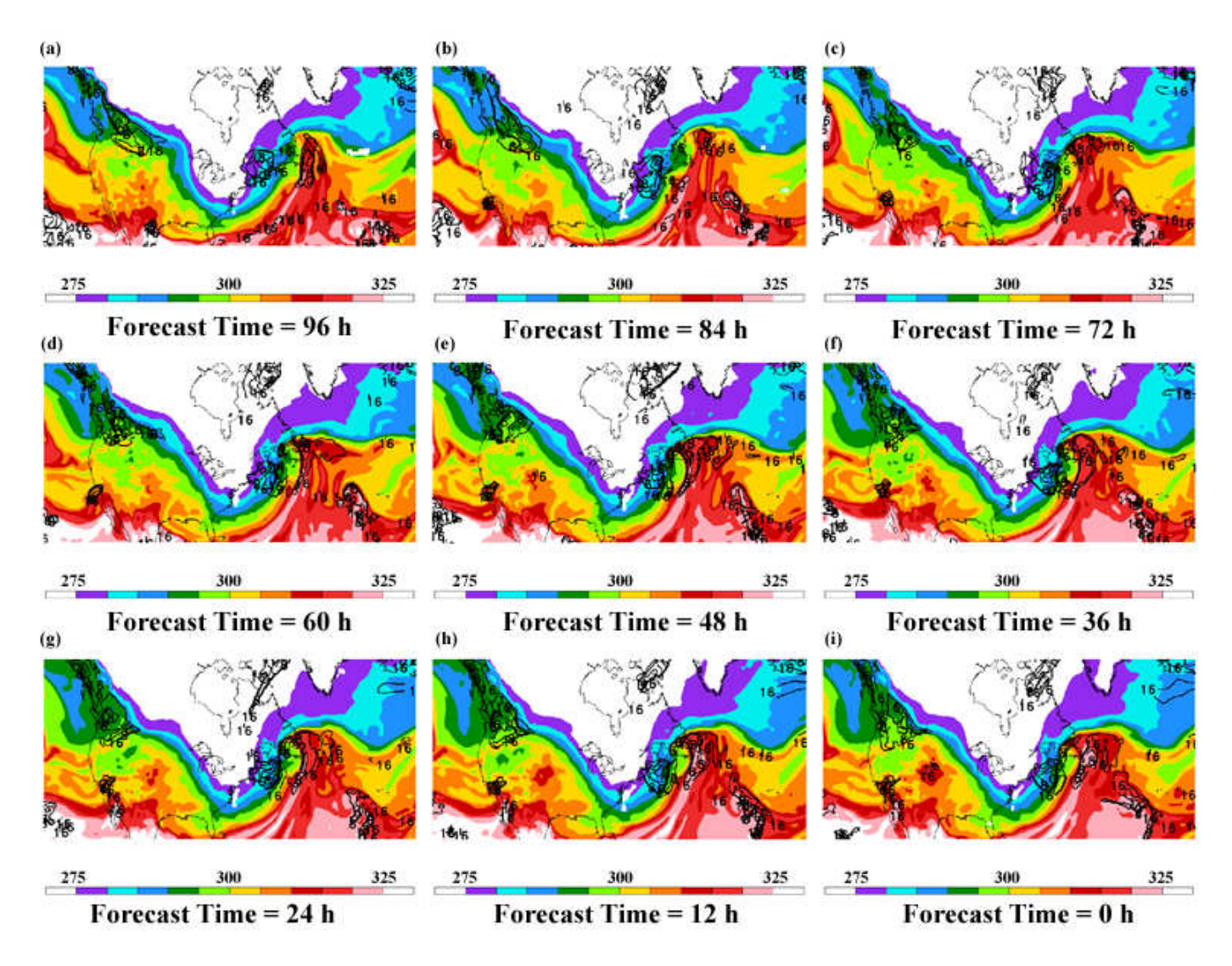


Figure 5.5: As in Fig. 5.3, but for 850 hPa equivalent potential temperature (K, shaded), and Coupling Index (K, solid, every 4 K from 0 to +16).

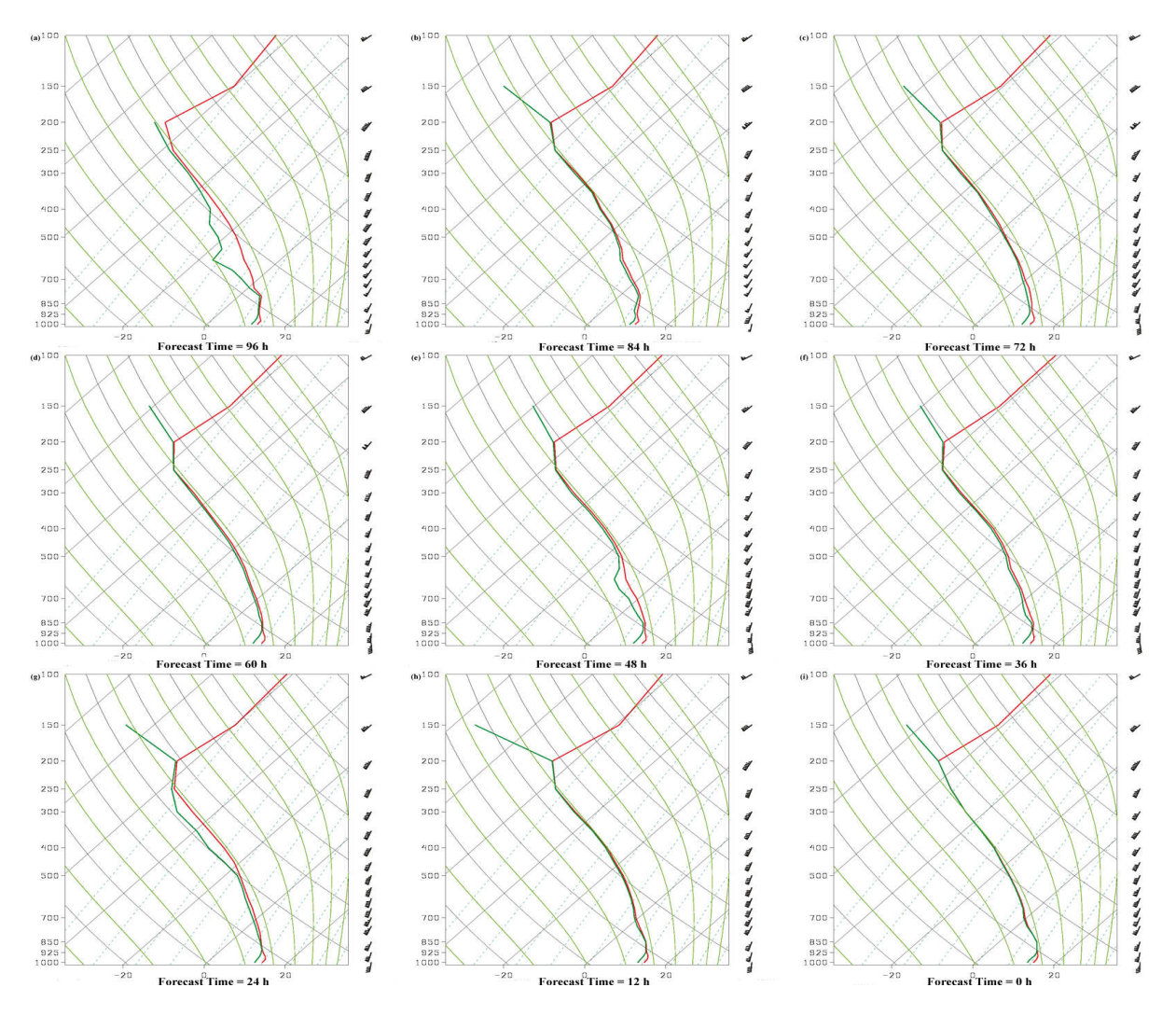


Figure 5.6: As in Fig. 5.3, but for GFS forecast soundings at St. John's (CYYT) with temperature (°C, red) and dewpoint (°C, green).

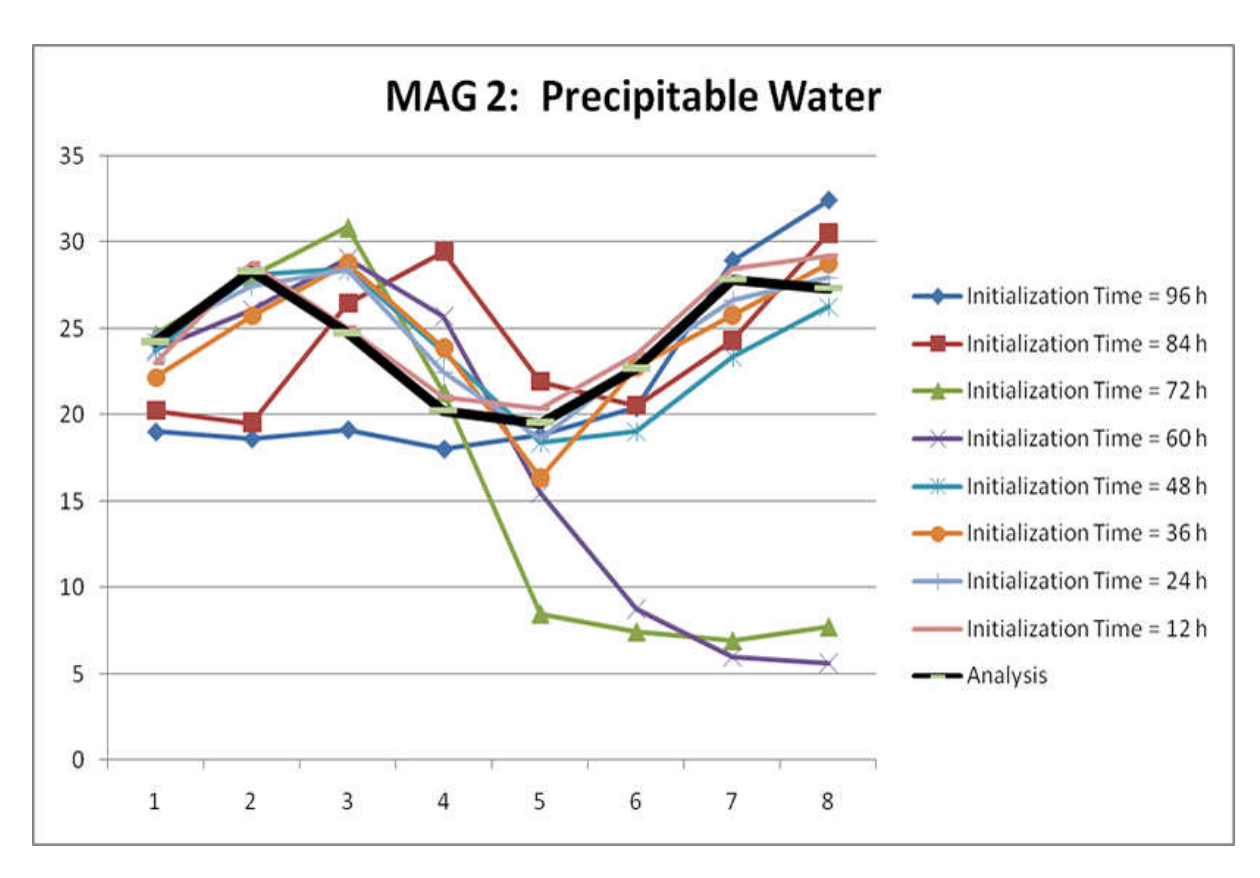


Figure 5.7: Time series for MAG 2 of GFS half-degree forecasts for precipitable water (mm). Each line is a different initialization time, with forecasts for every six hours (horizontal axis) during the period of precipitation at St. John's, which is t=-6 h (0000 UTC 11 December 2008) to t=+36 h (1800 UTC 12 December 2008). The GFS half-degree analysis is represented by a bold black line.

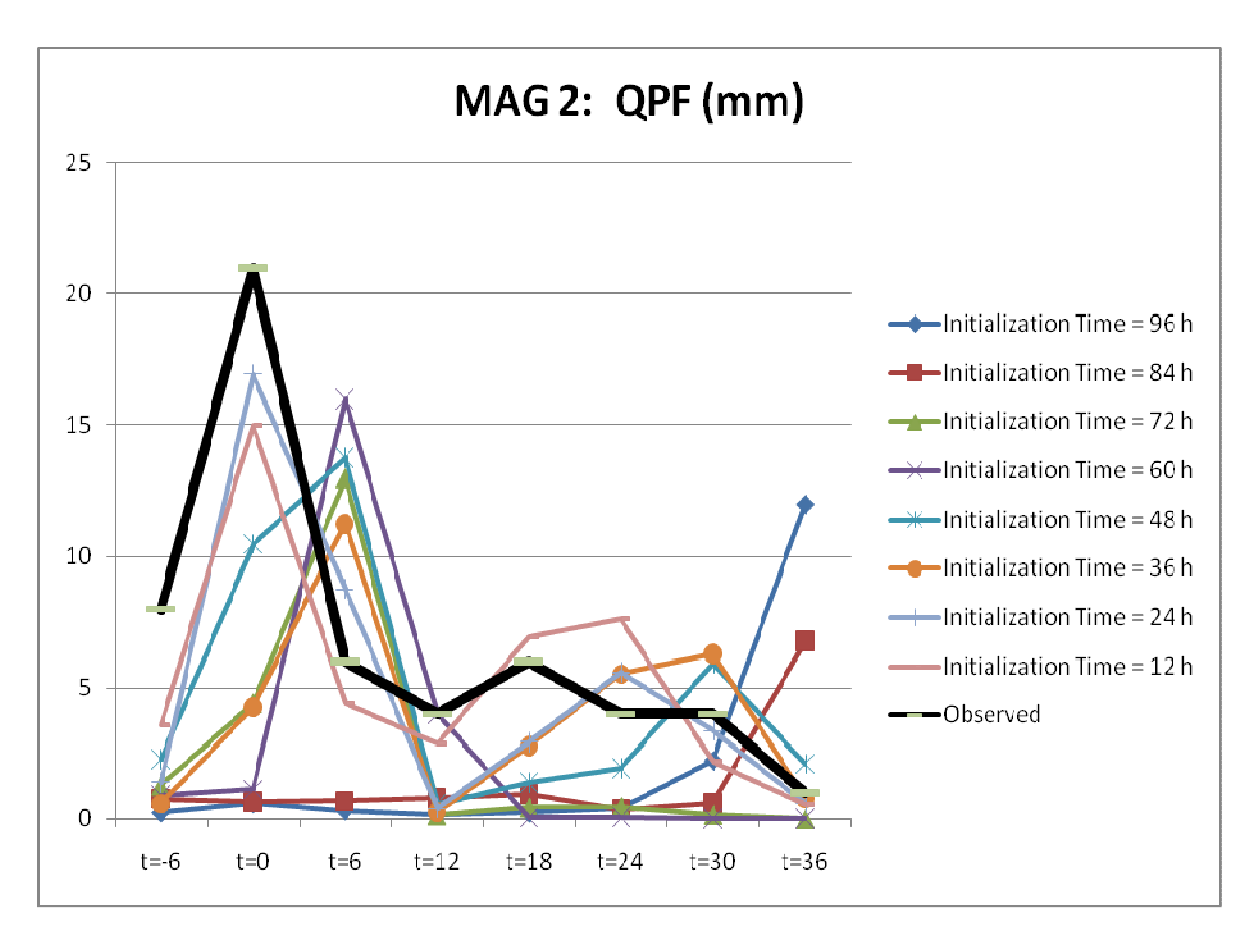


Figure 5.8: Time series for MAG 2 of GFS half-degree forecasts for precipitation (mm) for six hour periods beginning at each verification time (horizontal axis). Each line is a different initialization time, with forecasts for every six hours (horizontal axis) during the period of precipitation at St. John's, which is t=-6 h (0000 UTC 11 December 2008) to t=+36 h (1800 UTC 12 December 2008). The GFS half-degree analysis is represented by a bold black line.

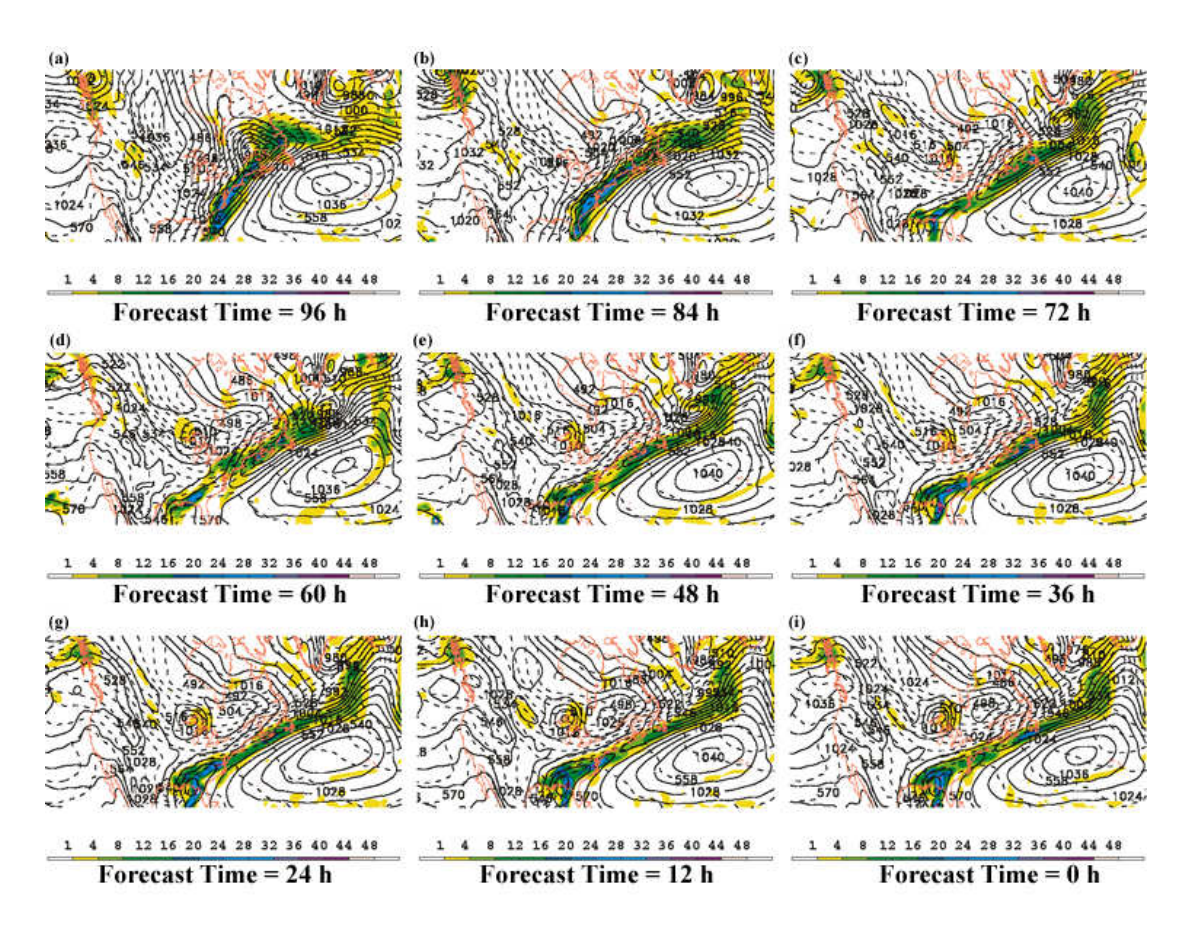


Figure 5.9: Time series of GFS half-degree analyses sea-level pressure (SLP, solid) contoured every 4 hPa, 1000-500 hPa thickness (dashed) contoured every 6 dam, and 6-hourly precipitation totals (shaded) in mm, for MAG 2, all validating at t=0 h, 0600 UTC 11 December 2008. Results are displayed for forecast lead times of (a) t=96 h, (b) t=84 h, (c) t=72 h, (d) t=60h, (e) t=48 h, (f) t=36 h, (g) t=24 h, (h) t=12 h, and (i) t=0 h.

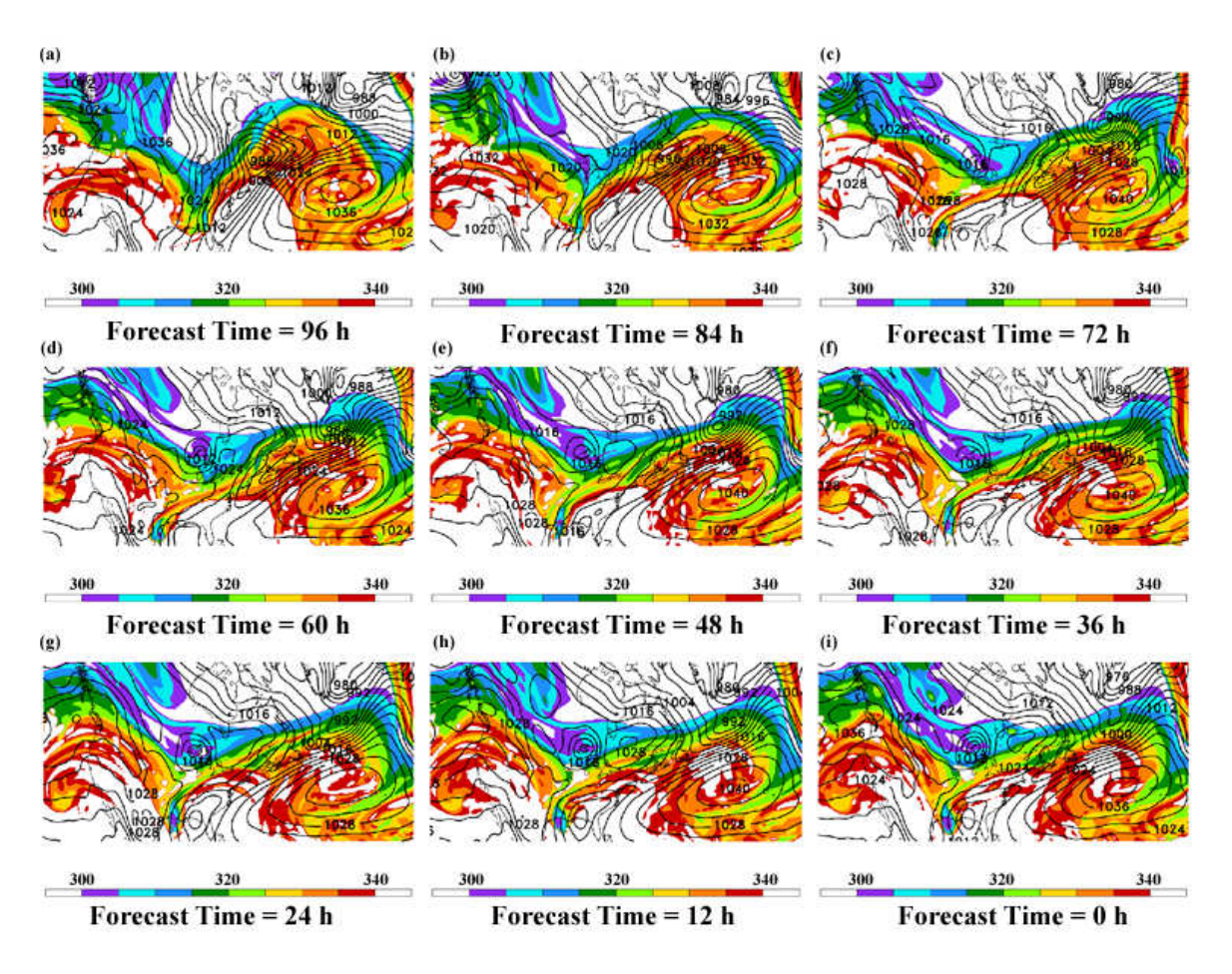


Figure 5.10: As in Fig. 5.9, but for SLP (solid, every 4 hPa) and potential temperature (K) on the Dynamic Tropopause (shaded).

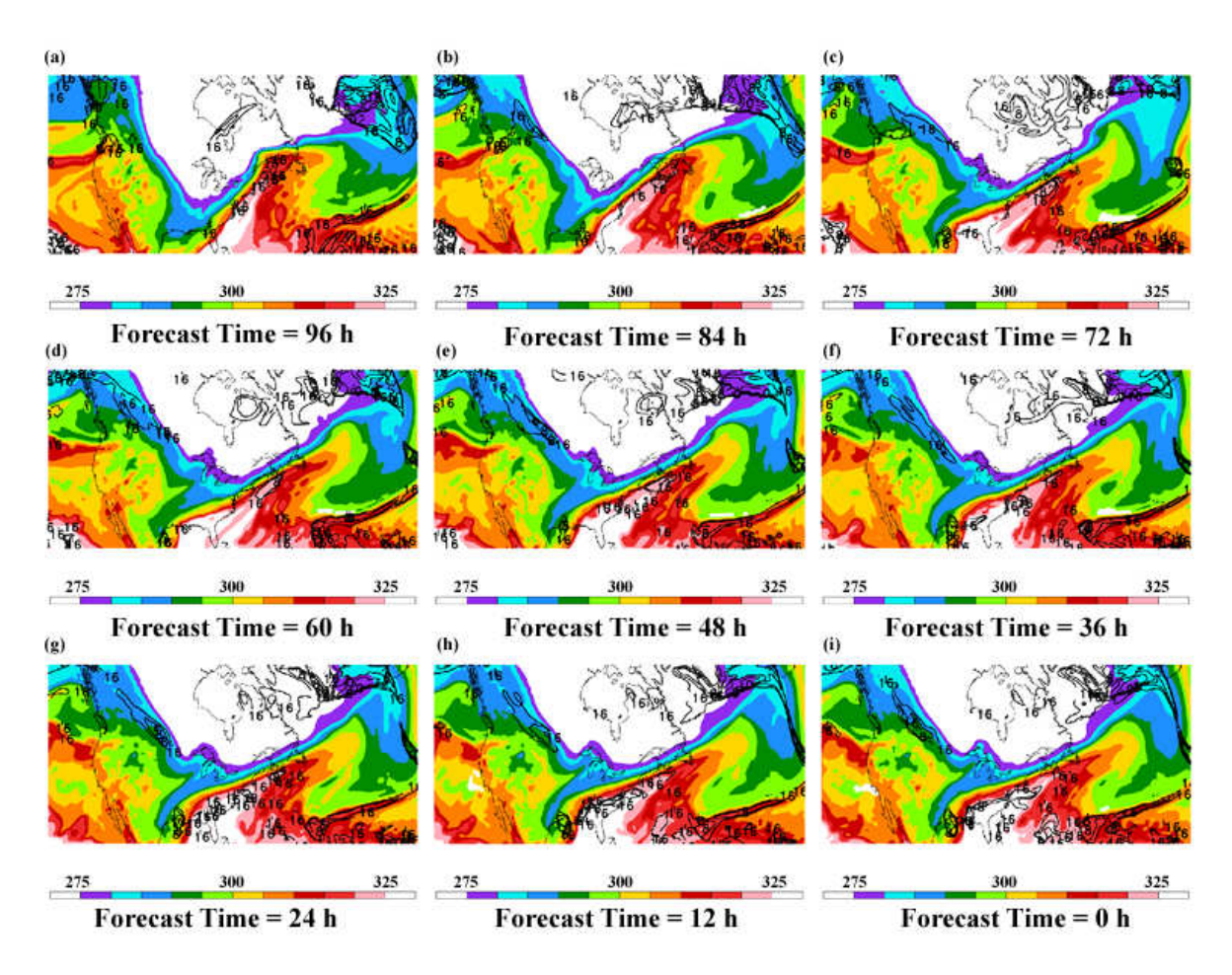


Figure 5.11: As in Fig. 5.9, but for 850 hPa equivalent potential temperature (K, shaded), and Coupling Index (K, solid, every 4 K from 0 to +16).

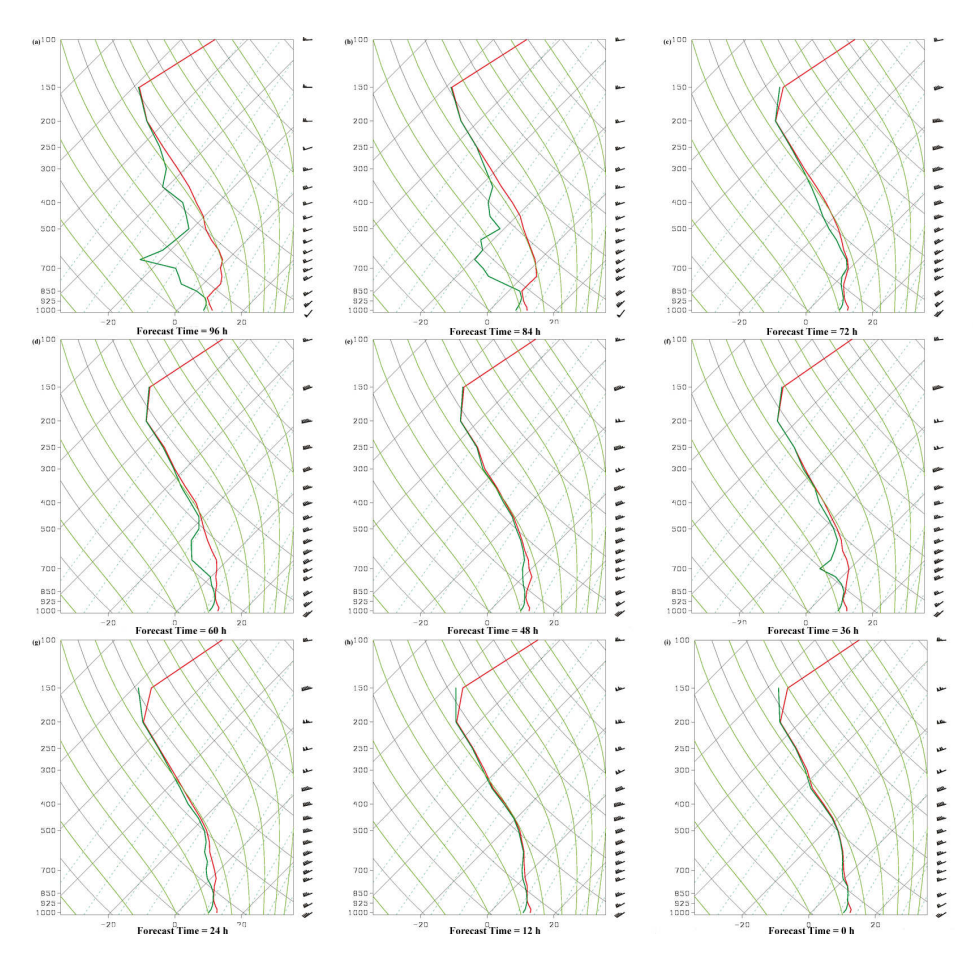


Figure 5.12: As in Fig. 5.9, but for GFS forecast soundings at St. John's (CYYT) with temperature (°C, red) and dewpoint (°C, green).

Chapter 6

Summary, Discussion, and Future Research

The primary objective of this thesis is to identify synoptic-scale dynamic and thermodynamic regimes and precursors associated with cool-season precipitation events at St. John's, Newfoundland. These results are designed to aid the local forecaster, particularly in the prediction of extreme precipitation events, when QPF is even more of an operational challenge. The work presented in the preceding chapters is summarized here, in addition to general conclusions and potential future research directions.

6.1 Climatology and Synoptic-Scale Characteristics of Cool-Season Precipitation Events at St. John's, Newfoundland, 1979-2005

In Chapter 2, a climatology of cool-season (October-April) precipitation events lasting 48 hours or less (1983 total events) is established for 1979-2005, at St. John's, Newfoundland and Labrador (CYYT). Using the calculated statistics of the climatology, events are partitioned into three precipitation event intensity categories (extreme, moderate, and light). The fifty median events in each category are then selected for composite analysis of three atmospheric mass fields: Sea-level pressure (SLP), 500 hPa height, and precipitable water (PW).

Composite and anomaly plots of SLP and PW show that the storm systems responsible for the precipitation event at St. John's originate farther south and east with increasing precipitation amount (e.g. extreme versus moderate). In the extreme cases, a negative SLP and PW anomaly are visible near the Gulf of Mexico up to 48 hours prior to the time of heaviest precipitation at St. John's. The moderate composite exhibits the widest range of initial anomalous cyclone locations, with a composite anomaly located in the Ohio Valley. The light cases originate in the upper midwest of the United States and, in combination with an overall weaker anomaly than the moderate and extreme composite, are consistent with what one would expect from an Alberta Clipper-type system. In summary, the track of the SLP anomaly becomes more zonal with decreasing precipitation amount, suggesting a more continental (thus, drier) storm track for systems that are responsible for smaller amounts of precipitation at St. John's.

Mid-tropospheric (500 hPa) composite and anomaly height plots show that a statistically significant anomalous 500 hPa ridge is evident on the west coast of the U.S. in the extreme and moderate composites, but not in the light composite. This precursor ridge is stronger and farther south in the extreme cases than in the moderate. In addition, downstream Rossby wave development initiated with the precursor ridge is more prevalent with increasing precipitation event amount; this is partially responsible for the stronger mid-tropospheric height anomalies present near St. John's around the time of heaviest precipitation. The downstream ridge is considerably stronger in the extreme cases than in the moderate or light composites, suggesting that both low-level warm-air advection and latent heat

release from extreme values of precipitation act to raise heights downstream of St. John's.

Finally, a climatology of near-surface (925 hPa) geostrophic and 10 m observed winds shows that winds at the time of heaviest precipitation at St. John's rotate cyclonically (from east to southwesterly) with decreasing precipitation amount. This finding is in accordance with the observation of more zonal storm tracks in the moderate and light composites than in the extreme. More importantly, although extremely rare in a climatological sense, easterly winds dominate at St. John's during extreme events, at the time of heaviest precipitation.

6.2 Synoptic Typing of Extreme Cool-Season Precipitation Events at St. John's, Newfoundland, 1979-2005

In Chapter 3, the fifty median events from each precipitation amount category defined in Chapter 2 are selected for further analysis, with a focus on the extreme events. This analysis is performed using two methods of manual synoptic typing. The first methodology partitions events into three categories (south, southwest, and west), using a five-day backward trajectory analysis to separate cases by air parcel origin. The second methodology utilizes time series of three commonly - used quasi-geostrophic (QG) forcing for ascent parameters (mid-tropospheric vorticity advection, low-tropospheric temperature advection, and low-tropospheric frontogenesis); this results in two categories of events (cyclone, and frontal). Composite and anomaly plots of SLP, 500 hPa height, and PW are then constructed for each synoptic type.

Applying the first methodology to the aforementioned extreme events, south cases (11 events) are found to be dominated by a downstream anomalous ridge (and corresponding anomalous sea-level anticyclone), which helps to initiate southerly geostrophic flow and moisture transport into St. John's. There is also a lack of a substantial anomalous upstream sea-level cyclone.

In contrast, the largest composite type - southwest cases (31 events) - shows evidence of synoptic-scale structures and precursors that are quite similar to the overall extreme composite presented in Chapter 2. That is, southwest cases generally involve a rapidly intensifying anomalous cyclone that develops along the U.S. gulf coast 48 hours prior to the maximum precipitation at St. John's and subsequently moves northeastward towards St. John's. As a result, the anomalous 500 hPa ridge downstream of St. John's intensifies as the anomalous cyclone approaches the station. This is due to low-level warm air advection and latent heat release from heavy precipitation ahead of the anomalous cyclone, as well as to downstream Rossby wave development observed in the extreme composite in Chapter 2.

Finally, the west trajectory composite (8 events) shows synoptic-scale structures that are substantially disparate from the other two types. Specifically, the relatively strong 500 hPa trough upstream of St. John's shows that while the upper-level dynamics are potent, there exists a lack of low-level baroclinicity and low static stability while the system remains over the continent. However, when the anomalous mid-tropospheric trough reaches the Atlantic Ocean, a rapidly

intensifying anomalous sea-level cyclone forms off the coast of Maine and propagates northeastward towards St. John's, as the negative 500 hPa and sea-level anomalies intensify due to baroclinic instability. It is also found that the extreme west cases show anomalously high PW values in the central plains of the U.S., 36-48 hours prior to the time of maximum precipitation at St. John's. It is suggested that this is a precursor signal to extreme precipitation events at St. John's, since it is not observed in the moderate or light west trajectory composite (presented in the online supplement to Chapter 3).

The second methodology of manual synoptic typing results in two classes of extreme events: cyclone (35 events) and frontal (11 events). Cyclone events are similar to the overall extreme composite detailed in Chapter 2, in that negative SLP and positive PW anomalies are visible along the U.S. gulf coast, 48 hours prior to the heaviest precipitation, and they proceed to move northeastward towards St. John's. Downstream Rossby wave development and enhancement of an anomalous mid-tropospheric ridge downstream of St. John's, due to low-level warm air advection and latent heat release, are also evident in the cyclone composite.

In contrast, the frontal composite is dominated by an anomalous midtropospheric ridge (and an associated anomalous sea-level anticyclone), located downstream of St. John's. This initiates strong southerly geostrophic flow and associated northward moisture transport near St. John's. Meanwhile, the anomalous upstream sea-level cyclone is substantially weaker than it is in the cyclone composite. The frontal composite also shows a northeast-southwest oriented quasi-stationary baroclinic zone situated near St. John's. Frontal cases are characterized by weak mid-tropospheric vorticity advection and low-level temperature advection in a low static-stability environment. Thus, it appears that much of the QG forcing for ascent at St. John's is caused by low-level frontogenesis in a warm, moist atmosphere. The frontal cases, while not climatologically frequent, are a prime example of extreme precipitation events associated with relatively benign synoptic-scale structures.

Composite soundings of the cyclone group show that the environment at St. John's is similar to what one would expect during the passage of typical mid-latitude cyclone or cold-core low. However, the vertical profiles of temperature and moisture during frontal events show a substantially elevated tropopause and are representative of a warm, moist, subtropical air mass that is not altogether common in the cool season at St. John's.

6.3 A Diagnostic Examination of Consecutive Extreme Cool-Season Precipitation Events at St. John's, Newfoundland in December 2008

In December 2008, consecutive extreme precipitation events at St. John's produced over 125 mm of precipitation over a span of six days. Chapter 4 presents a diagnostic examination of both events utilizing the manual synoptic typing methodologies outlined in Chapter 3, in addition to a detailed dynamic and thermodynamic analysis.

The first event, from 1200 UTC 7 December to 1200 UTC 9 December, produced 73.6 mm of precipitation at St. John's. Applying the synoptic typing defined in Chapter 3, it is found that this case is a southwest and cyclone event. Meteograms show that most of the precipitation falls while St. John's is located in the warm sector of a sea-level cyclone that approaches the station from the southwest. The sea-level cyclone rapidly intensifies (50 hPa in 36 hours), exceeding the "bomb" criterion of Sanders and Gyakum (1980), and the center passes just to the west of St. John's. The heaviest period of precipitation ends when a trailing cold front moves through the station, bringing cooler temperatures and lighter precipitation.

A synoptic analysis shows that the first event is marked by extremely high values of precipitable water - especially at the time of heaviest precipitation at St. John's - in the presence of strong QG forcing for ascent and weak static stability. Moreover, potential temperatures on the dynamic tropopause (DT) and 850 hPa equivalent potential temperature are comparable to values observed in the Gulf of Mexico, suggesting that an extremely warm and moist air mass is present at St. John's during the period of heaviest precipitation. Low values of the coupling index, a measure of bulk atmospheric stability (Galarneau and Bosart 2006), near St. John's support the hypothesis of weak static stability during the period of heavy precipitation. Observed soundings show a substantial shift in air mass between that in the warm sector of the cyclone and that behind the trailing cold front. Specifically, the tropopause descends approximately 200 hPa in six hours following the passage of the cold front. The column temperature and mixing ratio

exhibit steep declines as well. Finally, a cross-sectional analysis shows an area of convective instability near St. John's in the warm sector of the cyclone during the period of heaviest precipitation. Overall, the synoptic-scale structures observed for this event are consistent with the cyclone composite presented in Chapter 3.

The second event, from 0000 UTC 11 December-0000 UTC 13 December, results in 54 mm of precipitation at St. John's. Utilizing the manual synoptic typing methodologies defined in Chapter 3, it is found that this event is a southwest and frontal case. Meteograms show that the second event occurs in three stages: an initial warm stage, a subsequent cool stage following the passage of a cold-front, and a second warm stage following the northward retreat of the aforementioned cold front. The second warm stage concludes with the approach of a closed cyclone from the Gulf of Mexico. The majority of the precipitation from this event falls during the initial warm stage and cold frontal passage, with lighter amounts occurring near the end of the event.

A dynamic analysis finds that the environment is dominated by a downstream anticyclone, consistent with the results of the frontal composite in Chapter 3. It is also found that this case is associated with a quasi-stationary northeast-southwest oriented baroclinic zone situated near St. John's for the duration of the event. The event is marked by persistently high values of precipitable water in the presence of relatively weak QG forcing for ascent and moderate atmospheric stability. The QG forcing for ascent is shown to result almost entirely from large values of frontogenesis, while values of mid-

tropospheric vorticity advection and low-tropospheric temperature advection are near zero for the duration of the event. This event is remarkable in that the large-scale synoptic environment is relatively benign, considering the extreme amount of precipitation recorded. Observed soundings show an extremely high tropopause for the duration of the event, and suggest that the cool stage in the middle of the event is limited to the boundary layer. Overall, the dynamic and thermodynamic properties of this event are similar to those seen in the frontal composite in Chapter 3.

The two cases of extreme precipitation in December 2008 are examples of very disparate means to cause an extreme event at St. John's. While the first case is a classic example of a rapidly intensifying cyclone, the second case occurs in the presence of a relatively nondescript synoptic-scale environment. It is believed that the difference of ~20 mm of precipitation between the two events is related to the stronger values of quasi-geostrophic forcing for ascent and smaller stabilities (i.e. convective instability) observed in the first case. Using the climatology presented in Chapter 2, both events would rank among the top twenty precipitation events of the past three decades at St. John's, with the first event placing in the top 5.

6.4 Evaluation of Two Independent Operational Forecasts during Consecutive Extreme Cool-Season Precipitation Events at St. John's, Newfoundland in December 2008

In Chapter 5, an evaluation of two separate operational forecast systems is presented for the two extreme precipitation events in December 2008 that are detailed in Chapter 4. The first forecast system evaluated is the National Centers for Environmental Prediction (NCEP) Global Forecast System (GFS) model with a half-degree horizontal resolution. The second forecast system evaluated is the Environment Canada (Newfoundland Weather Office) operational forecasts, which are used as a proxy for the Environment Canada Global Environment Multiscale (GEM) model forecasts. Evaluations of precipitable water and precipitation forecasts are made for the period of precipitation at St. John's at forecasts lead times of up to four days (96 hours) for the GFS. A dynamic and thermodynamic analysis is also performed for forecasts that verify at the time of heaviest precipitation at St. John's (t=0 h). Environment Canada operational forecasts are evaluated at lead times of 1-2 days, since precipitation amount forecasts are not issued for longer lead times.

For the first event, it is found that the evolution of the GFS precipitable water forecasts at St. John's is generally accurate for all initialization times, although the model slightly underforecasts (~2-5 mm) amounts relative to the GFS analysis. In addition, a dynamic analysis shows that the model underforecasts the values of potential temperature on the DT at the time of heaviest precipitation at St. John's, for all initialization times except t=-12 h (after some precipitation has already fallen). This is likely due to the model not properly analyzing diabatic impacts of the precipitation during the early part of the event at St. John's until the t=-12 h initialization time. In combination with

inaccurate forecasts of the coupling index and intensity and position of the sealevel cyclone, particularly at earlier initialization times, it is clear that the model underestimates the intensity of the warm moist air mass on the eastern (warm sector) side of the cyclone. As a result of the above factors, the GFS vastly underpredicts (~15-20 mm) the precipitation at St. John's during the period of maximum precipitation; this error is consistent for all initialization times, including the t=-12 h initialization time; this suggests that even though the air mass around St. John's is more accurately predicted by the t=-12 h model run, the QPF is still too low.

In general, Environment Canada operational forecasts underforecast the amount of precipitation at St. John's by approximately 20 mm, at lead times of 24-36 hours. Moreover, a rainfall warning (25 mm or more in twelve hours) is not issued for St. John's until after 40+ mm of precipitation has already fallen in 16+ hours. This rainfall warning is issued in the middle of the heaviest twelve hours of precipitation at St. John's (0000-1200 UTC 8 December), during which 41 mm of precipitation is recorded. This finding implies that the GEM model also has trouble predicting the extremity of this event. While further work needs to be done to quantify the GEM forecasts, it is possible that diabatic-induced errors played a role in the under-predicted value of precipitation.

For the second event, the earliest initialization times of the GFS (t=-96 h and t=-84 h) greatly underestimate the precipitable water, which results a in QPF of near zero at St. John's. Later initialization times (t=-72 h to t=-60 h) capture

the evolution of the early part of the precipitable water and QPF, but fail to accurately predict the second warm stage, primarily due to poor prediction of a closed cyclone in the Gulf of Mexico. Medium-range initialization times (t=-60 h to t=-36 h) accurately represent the evolution of the precipitable water and precipitation, but are six hours too slow with both fields. It is not until the t=-24 h and t=-12 h initialization times that the GFS predicts evolutions of QPF and precipitable water that are similar to the observed values and analysis, respectively.

A dynamic analysis of the GFS forecasts shows that early initialization times (i.e. inaccurate precipitable water and QPF fields) are marked by poor representation of synoptic-scale structures in the vicinity of St. John's.

Specifically, at these early initialization times, the GFS produces a strong sealevel cyclone in northeastern Quebec that does not verify in the analysis. This leads to the bulk of the precipitation falling to the north of St. John's, which corresponds to the extremely poor QPF of the t=-96 h and t=-84 h initialization times. The t=-72 h and t=-60 h initialization times are marked by poor representation of a closed cyclone in the Gulf of Mexico, which leads to a failure to predict the aforementioned second warm stage.

A thermodynamic analysis shows that with the exception of the t=-96 h and t=-84 h initialization times, the thermodynamic environment at St. John's is relatively well forecasted. Forecasts that verify at t=0 h show a slight underforecast of potential temperature on the DT and 850 hPa equivalent potential

temperature, but the difference between forecasted and actual values is substantially smaller than is observed in the forecasts for the first event. This assertion is further confirmed by model forecast soundings.

In summary, the thermodynamic environment in the second event is more accurately forecast than in the first event, and errors in the QPF for the second event likely result from inaccurate timing and magnitude of ascent. Because the primary ascent-forcing mechanism in the second event is frontogenesis, small errors in the position or intensity of the quasi-stationary baroclinic zone can result in large QPF errors. In general, the GFS underpredicts the QPF at t=0 by ~5-10 mm in the t=-12 h and t=-24 h initialization times and shifts the timing of the heaviest precipitation by about six hours at medium-range (t=-72 h to t=-36 h) initialization times.

Environment Canada operational forecasts show that the second event is relatively well-predicted; over 80% of the observed precipitation is forecast in the 1-2 day lead times. This assertion corresponds with the relatively accurate QPF in the GFS at the t=-24 h and t=-12 h initialization times. It is suspected that as seen in the GFS, larger errors would be observed at longer lead times, in association with poor resolution of the aforementioned synoptic-scale features. In summary, the forecasts for the second event are substantially more accurate than those issued for the first event.

6.5 General Conclusions

The preceding chapters present synoptic-scale dynamic and thermodynamic structures and precursors associated with various classes and synoptic types of precipitation events at St. John's, Newfoundland. While the majority of precipitation events are associated with various intensities of sea-level cyclones, as one might expect, there is a significant subset of events that occurs under much more synoptically benign conditions. In general, the author hopes that the precursor synoptic-scale signals, in addition to the analyzed dynamic and thermodynamic properties of the atmosphere at and around St. John's during the various classes and types of precipitation events, can be utilized in the future by the operational forecaster, particularly in terms of aiding OPF.

6.6 Future Research Directions

In order for operational forecasters in the Atlantic Canada region to obtain the full value of this study, conceptual models and/or forecast decision trees that depict different types of precipitation events that one would expect to affect the region should be developed and implemented at local forecast offices. This is the logical and most important follow-up to this thesis.

In addition, it will be important to apply the methodologies of synoptic classification utilized for St. John's in this study to other stations in Atlantic Canada and across the country. Sisson and Gyakum (2004) have already performed a study for Burlington, Vermont, using similar foundations of the categorical separation of precipitation events defined here in Chapter 2. While St. John's is the location of the climatological maximum of precipitation events in

Atlantic Canada in the cool season, other stations in the region (e.g. Halifax, Nova Scotia and Fredericton, New Brunswick) are also prone to frequent and extreme precipitation events (Stewart et al. 1987). It would be beneficial to operational forecasters in the region to compare the synoptic-scale precursor signals, as well as dynamic and thermodynamic properties of the atmosphere associated with events at St. John's, with results from other stations in the region.

Further study of particular dynamical conclusions in this study is warranted, particularly with respect to the synoptic types discussed in Chapter 3. For example, the observation in the extreme west trajectory composite of anomalously high values of precipitable water in the central United States two days before the precipitation event at St. John's calls for further investigation. The author would like to add cases to the west trajectory group by extending the study forward and backward in time. It is suggested in this study that in order to get an extreme event with a continental-based west trajectory, air mass conditioning in the central United States might be a necessary condition. An investigation of a recent extreme precipitation event or events with west backward trajectories would be useful in investigating aforementioned dynamic and thermodynamic properties, preferably with a relatively high-resolution analysis. Finally, such an event could be dynamically and thermodynamically compared to a west event(s) that did not produce an extreme precipitation event at St. John's (i.e. a null case), in order to further investigate the mechanisms responsible for an extreme west trajectory precipitation event.

In terms of forecast evaluation, an objective evaluation should be made of the GFS forcing for ascent for MAG 1 and MAG 2; this would best be accomplished by a using an area-averaged representation of quasi-geostrophic ascent (e.g. Q-vector convergence). Doing this would eliminate the possibility of incorrect results due to the usage of a noisy model field such as vertical motion (ω). Additionally, there is a need to evaluate the actual GEM model output (without using proxies) as well as output from other operational forecast models (e.g. UKMET, ECMWF). In addition, it would be useful to examine ensemble prediction systems, such as the North American Ensemble Forecast System (NAEFS), and the NCEP GFS ensemble (GEFS), in order to assess the mean and variance for the case studies presented in Chapter 4. For example, one might ask if certain members of a particular ensemble were able to better handle the closed low circulation in the Gulf of Mexico during the second extreme event in Chapter 4.

An evaluation of different model (both deterministic and ensemble) forecasts for a larger number (e.g. five cool seasons) of extreme precipitation events at St. John's would allow for an assessment of any biases and tendencies that might be inherent to the model. Charles and Colle (2009a, b) completed a similar exercise for much of the North American continent using both the NCEP operational models and the NCEP Short-Range Ensemble Forecasts system (SREF), albeit with a focus on extratropical cyclones. A similar exercise for Atlantic Canada, with a focus on all extreme events (cyclone or otherwise), using both NCEP and Environment Canada GEM model output would be quite useful to

the modeling and forecasting community in aiding future prediction of these events.

Finally, it would be useful to extend the methodology of this work to the warm season (May-September) at St. John's and similar stations. Ralph et al. (2005) conclude that due to convective precipitation (which is notoriously difficult to accurately predict, both in location and intensity) in the warm season, QPF skill in the cool season can exceed that of the warm season by a factor of 2. Due to its location, convection at St. John's is not as important as it might be at other stations across Canada. However, an evaluation of the synoptic-scale structures and precursors associated with various classes of warm-season precipitation events would be a natural complement to this work, in addition to being insightful to the operational forecaster.

Bibliography

- Aguado, E., and J. E. Burt 2007: *Understanding weather and climate*. Pearson Prentice Hall, 562 pp.
- Atallah, E. H., J. R. Gyakum, P. A. Sisson, M. Kimball, and A. Roberge, 2005: Warm season extreme quantitative precipitation forecasting for the Burlington, VT region. Preprints, 21st Conference on Weather Analysis and Forecasting, Amer. Meteor. Soc., Washington, D.C.
- Banacos, P. C., and D. M. Schultz, 2005: The use of moisture flux convergence in forecasting convective initiation: Historical and operational perspectives *Wea. Forecasting*, **20**, 351-366.
- Bao, J. W., S. A. Michelson, P. J. Neiman, F. M. Ralph, and J. M. Wilczak, 2006: Interpretation of enhanced integrated water vapor bands associated with extratropical cyclones: Their formation and connection to tropical moisture. *Mon. Wea. Rev.*, **134**, 1063-1068.
- Bluestein, H., 1992a: *Synoptic-dynamic meteorology in midlatitudes: Volume I.* Oxford University Press, 431 pp.
- Bluestein, H., 1992b: *Synoptic-dynamic meteorology in midlatitudes: Volume II.* Oxford University Press, 594 pp.
- Bosart, L. F., 1980: Evaluation of LFM-2 quantitative precipitation forecasts. *Mon. Wea. Rev.*, **108**, 1087-1099
- Bosart, L. F., 1981: The Presidents' Day snowstorm of 18-19 February 1979: A subsynoptic-scale event. *Mon. Wea. Rev.*, **109**, 1542-1566.
- Bosart, L. F., and S. C. Lin, 1984: A diagnostic analysis of the Presidents' Day storm of February 1979. *Mon. Wea. Rev.*, **112**, 2148-2177.
- Bosart, L. F., and G. M. Lackmann, 1995: Postlandfall tropical cyclone intensification in a weakly baroclinic environment: A case study of Hurricane David (September 1979). *Mon. Wea. Rev.*, **123**, 3268-3291.
- Bosart, L. F., G. J. Hakim, K. R. Tyle, M. A. Bedrick, W. E. Bracken, M. J. Dickinson, and D. M. Schultz, 1996: Large-scale antecedent conditions associated with the 12-14 March 1993 cyclone ("Superstorm '93") over eastern North America. *Mon. Wea. Rev.*, **124**, 1865-1891.
- Brennan, M. J., and G. M. Lackmann, 2006: Observational diagnosis and model forecast evaluation of unforecasted incipient precipitation during the 24-25 January 2000 East Coast Cyclone. *Mon. Wea. Rev.*, **134**, 2033-2052.

- British Society of Geomorphology, 2009: Map of the North Atlantic. *British Society of Geomorphology*, 5 Jan. 2010, http://www.geomorphology.org.uk/pages/education/alevel/coldenvirons/Gulfstream.htm.
- Caplan, P. M., 1995: The 12-14 March 1993 Superstorm: Performance of the NMC global medium-range model. *Bull. Amer. Meteor. Soc.*, **76**, 201–212.
- Casati, B., and Coauthors, 2008: Forecast verification: Current status and future directions. *Meteorol. Appl.*, **15**, 3–18.
- Charles, M. E., and B. A. Colle, 2009a: Verification of extratropical cyclones within the NCEP operational models. Part I: Analysis errors and short-term NAM and GFS forecasts. *Wea. Forecasting*, **24**, 1173-1190.
- Charles, M. E., and B. A. Colle, 2009b: Verification of extratropical cyclones within the NCEP operational models. Part II: The short-range ensemble forecast system. *Wea. Forecasting*, **24**, 1191-1214.
- Dickinson, M. J., L. F. Bosart., W. E. Bracken, G. J. Hakim, D. M. Schultz, M. A. Bedrick, and K. R. Tyle 1997: The March 1993 Superstorm cyclogenesis: Incipient phase synoptic- and convective-scale flow interaction and model performance *Mon. Wea. Rev.*, **125**, 3041-3072.
- Dirks, R. A., J. P. Kuettner, and J. A. Moore, 1988: Genesis of Atlantic lows experiment (GALE): An overview. *Bull. Amer. Meteor. Soc.*, **69**, 148-160.
- Doswell, C. A. III, H. E. Brooks, and R. A. Maddox, 1996: Flash flood forecasting: An ingredients-based methodology. *Wea. Forecasting*, **14**, 560-581.
- Durran, D. R., and L. W. Snellman, 1987: The diagnosis of synoptic-scale vertical motion in an operational environment. *Wea. Forecasting*, **2**, 17-31.
- Emanuel, K. A., 1983: On assessing local conditional symmetric instability from atmospheric soundings. *Mon. Wea. Rev.*, **111**, 2016-2033.
- Estoque, M. A., 1957: An approach to quantitative precipitation forecasting. *J. Meteor.*, **14**, 50-54.
- Fischer, A. P., 1997: A synoptic climatology of Montreal precipitation. M.S. thesis, Dept. of Atmospheric and Oceanic Sciences, McGill University, 71 pp.

- Frakes, B., and B. Yarnal, 1997: A procedure for blending manual and correlation-based synoptic classifications. *Int. J. Climatol.*, **17**, 1381-1396.
- Fritsch, J. M., and Coauthors, 1998: Quantitative precipitation forecasting: Report of the eighth prospectus development team, U.S. weather research program. *Bull. Amer. Meteor. Soc.*, **79**, 285–299.
- Fritsch, J. M., and R. E. Carbone, 2004: Improving quantitative precipitation forecasts in the warm season. *Bull. Amer. Meteor. Soc.*, **85**, 955–965.
- Funk, T. W., 1991: Forecasting techiques utilized by the forecast branch of the National Meteorological Center during a major convective rainfall event. *Wea. Forecasting*, **6**, 548-564.
- Galarneau, T. J. Jr., and L. F. Bosart, 2006: An examination of the long-lived MCV of 10-13 June 2003. Preprints, *Severe Local Storms Symposium*, Atlanta, GA, Amer. Meteor. Soc., P1.32.
- Grumm, R. H., and R. Hart, 2001: Standardized anomalies applied to significant cold season weather events: Preliminary findings. *Wea. Forecasting*, **16**, 736-754.
- Gyakum, J. R., and K. J. Samuels, 1987: An evaluation of quantitative and probability-of-precipitation forecasts during the 1984-85 warm and cold seasons. *Wea. Forecasing*, **2**, 158-168.
- Gyakum, J. R., and E. S. Barker, 1988: A case study of explosive subsynoptic-scale cyclogenesis. *Mon. Wea. Rev.*, **116**, 2225-2253.
- Gyakum, J. R., 1991: Meteorological precursors to the explosive intensification of the QE II storm. *Mon. Wea. Rev.*, **119**, 1105-1131.
- Gyakum, J. R., D. Zhang, J. Witte, K. Thomas, and W. Wintels, 1996: CASP II and the Canadian cyclones during the 1989-92 cold seasons. *Atmos. Ocean*, **34**, 1-16.
- Gyakum, J. R., and R. E. Stewart, 1996: A multiscale analysis of a case of slow growth /rapid cyclogenesis during CASP II. *Atmos. Ocean*, **34**, 17-50.
- Gyakum, J. R., and P. J. Roebber, 2001: The 1998 ice storm—Analysis of a planetary-scale event. *Mon. Wea. Rev.*, **129**, 2983-2997.
- Harley, W. S., 1965: An operational method for quantitative precipitation forecasting. *J. Appl. Meteor.*, **4**, 305-319
- Hart, R. and J. Evans, 2001: A climatology of the extratropical transition of Atlantic tropical cyclones. *J. Climate*, **14**, 547–564.

- Hoskins, B. J., I. Draghici, and H. C. Davies, 1978: A new look at the ω-equation. *Quart. J. Roy. Meteor. Soc.*, **104**, 31-38.
- Huo, Z., D. Zhang, J. Gyakum, and A. Staniforth, 1995: A diagnostic analysis of the Superstorm of March 1993. *Mon. Wea. Rev.*, **123**, 1740-1761.
- Huo, Z., D. Zhang, and J. Gyakum, 1996: The life cyclone of the intense IOP-14 storms during CASP II. Part I: Analysis and simulations. *Atmos. Ocean*, **34**, 51-80.
- Jones, P. D., M. Hulme, and K. R. Briffa, 1993: A comparison of Lamb circulation types with an objective classification scheme. *Int. J. Climatol.*, **13**, 655-663.
- Kalnay, E., and Coauthors, 1996: The NCEP/NCAR 40-year reanalysis project. *Bull. Amer. Meteor. Soc.*, **77**, 437–471.
- Keyser, D., M. J. Reeder, and R. J. Reed, 1988: A generalization of Petterssen's frontogenesis function and its relation to the forcing of vertical motion. *Mon. Wea. Rev.*, **116**, 762-780.
- Knippertz, P., and J. E. Martin, 2007: A Pacific moisture conveyor belt and its relationship to a significant precipitation event in the semiarid southwestern United States. *Wea. Forecasting*, **22**, 125-142.
- Knowland, K. E., 2008: A study of the meteorological conditions associated with anomalously early and anomalously late openings of a Northwest Territories winter road. M.S. thesis, Dept. of Atmospheric and Oceanic Sciences, McGill University, 72 pp.
- Koch, S., M. DesJardins, and P. Kocin, 1983: An interactive Barnes objective map analysis scheme for use with satellite and conventional data. *J. Appl. Meteor.*, **22**, 1487–1503.
- Kocin, P. J., P. N. Schumacher, R. F. Morales, and L. W. Uccellini: Overview of the 12-14 March 1993 Superstorm. *Bull. Amer. Meteor. Soc.*, **76**, 165–182.
- Lackmann, G. M., and J. R. Gyakum, 1996: The synoptic and planetary-scale signatures over the Mackenzie River basin. *Atmos-Ocean*, **34**, 647-674.
- Lackmann, G. M., and J. R. Gyakum, 1999: Heavy cold-season precipitation in the Northwestern United States: Synoptic climatology and an analysis of the flood of 17-18 January 1986. *Wea. Forecasting*, **14**, 687-700.
- Ladd, J. W., and D. M. Driscoll, 1980: A comparison of objective and subjective means of weather typing: An example from West Texas. *J. Appl. Meteor.*, **19**, 691-704.

- Macdonald, K. A., M. Danks, and J. D. Abraham, 1988: A short-range forecasting experiment conducted during the Canadian Atlantic Storms Program. *Wea. Forecasting*, **3**, 1412-152.
- Martin, J. E., 2006: *Mid-latitude atmospheric dynamics*. John Wiley and Sons Ltd, 324 pp.
- Mekis, E., and W. D. Hogg, 1999: Rehabilitation and analysis of Canadian daily precipitation time series. *Atmos. Ocean*, **37**, 53-85.
- Mesinger, F., and Coauthors, 2006: North American Regional Reanalysis. *Bull. Amer. Meteor. Soc.*, **87**, 343–360.
- Meteorological Service of Canada, Environment Canada, 2003. PUBPRO: Manual of standard operational procedures for issuing public weather forecasts and warnings. Retrieved October 7, 2009, from http://www.msc.ec.gc.ca/msb/manuals/pubpro/index_e.cfm.
- Milrad, S. M., E. A. Atallah, and J. R. Gyakum, 2009a: Synoptic-scale characteristics and precursors of cool-season precipitation events at St. John's, Newfoundland, 1979-2005. *Wea. Forecasting*, **24**, 667-689.
- Milrad, S. M., E. A. Atallah, and J. R. Gyakum, 2009b: Synoptic typing of extreme cool-season precipitation events at St. John's, Newfoundland, 1979-2005. *Wea. Forecasting*, in press.
- Muller, R. A., 1977: A synoptic climatology for environmental baseline analysis: New Orleans. *J. Appl. Meteor.*, **16**, 20-33.
- Muller, R. A., and A. L. Jackson, 1985: Estimates of climatic air quality potential at Shreveport, Louisiana. *J. Climate and Appl. Meteor.*, **24**, 293-301.
- Nadeau, D., 2007: Impacts of synoptic atmospheric circulations and topographic conditions on sustained strong surface winds over southern Nunavut.
 M.S. thesis, Dept. of Atmospheric and Oceanic Sciences, McGill University, 129 pp.
- Novak, D. R., L. F. Bosart, D. Keyser, and J. S. Waldstreicher, 2004: An observational study of cold season-banded precipitation in Northeast U.S. cyclones. *Wea. Forecasting*, **19**, 993-1010.
- Novak, D. R., J. S. Waldstreicher, D. Keyser, and L. F. Bosart, 2006: A forecast strategy for anticipating cold season mesoscale band formation within eastern U.S. cyclones. *Wea. Forecasting*, **21**, 3-23.
- Olson, D. A., N. W. Junker, and B. Korty, 1995: Evaluation of 33 years of quantitative precipitation forecasting at NMC. *Wea. Forecasting*, **10**, 498-511.

- Overland, J. E., and T. R. Hiester, 1980: Development of a synoptic climatology for the Northeast Gulf of Alaska. *J. Appl. Meteor.*, **19**, 1-14.
- Ralph, F. M., and Coauthors, 2005: Improving short-term (0-48 h) cool-season quantitative precipitation forecasting. *Bull. Amer. Meteor. Soc.*, **86**, 1619-1632.
- Reap, R. M., 1972: An operational three-dimensional trajectory model. *J. Appl. Meteor.*, **11**, 1193-1202.
- Reuter, G. W., and M. K. Yau, 1990: Observations of slantwise convective instability in winter cyclones. *Mon. Wea. Rev.*, **118**, 447-458.
- Reynolds, D., 2003: Value-added quantitative precipitation forecasts. *Bull. Amer. Meteor. Soc.*, **84**, 876-878.
- Roberge, A., J. Gyakum, and E. Atallah, 2009: Analysis of intense poleward water vapor transports into high latitudes of western North America. *Wea. Forecasting*, in press.
- Roebber, P. J., and L. F. Bosart, 1998: The sensitivity of precipitation to circulation details. Part I: An analysis of regional analogs. *Mon. Wea. Rev.*, **126**, 437-455.
- Roebber, P. J., and J. R. Gyakum, 2003: Orographic influences on the mesoscale structure of the 1998 ice storm. *Mon. Wea. Rev.*, **131**, 27-50.
- Sanders, F., and J. R. Gyakum, 1980: Synoptic-dynamic climatology of the "bomb." *Mon. Wea. Rev.*, **108**, 1589-1606.
- Sanders, F., and L. F. Bosart, 1985a: Mesoscale structure in the Megalopolitan snowstorm of 11-12 February 1983. Part I: Frontogenetical forcing and symmetric instability. *J. Atmos. Sci.*, **42**, 1050-1061.
- Sanders, F., and L. F. Bosart, 1985b: Mesoscale structure in the Megalopolitan snowstorm of 11-12 February 1983. Part II: Doppler Radar Study of the New England Snowband. *J. Atmos. Sci.*, **42**, 1398-1407.
- Sanders, F., 1986: Explosive cyclogenesis over the west-central North Atlantic Ocean, 1981-84. Part II: Evaluation of LFM model performance. *Mon. Wea. Rev.*, **114**, 2207-2218
- Sheridan, S. C., 2002: The redevelopment of a weather-type classification scheme for North America. *Int. J. Climatol.*, **22**, 51-68.
- Sisson, P. A., and J. R. Gyakum, 2004: Synoptic-scale precursors to significant cold-season precipitation events in Burlington, Vermont. *Wea. Forecasting*, **19**, 841-854.

- Stewart, R. E., R. W. Shaw, and G. A. Isaac, 1987: Canadian Atlantic Storms Program: The meteorological field project. *Bull. Amer. Meteor. Soc.*, **68**, 338-345.
- Stewart, R. E., and N. R. Donaldson, 1989: On the nature of rapidly deepening Canadian east coast winter storms. *Atmos. Ocean*, **27**, 87-107.
- Stewart, R. E., C. A. Lin, and S. R. Macpherson, 1990: The structure of a winter storm producing heavy precipitation over Nova Scotia. *Mon. Wea. Rev.*, **118**, 411-426.
- Stewart, R. E., 1991: Canadian Atlantic Storms Program: Progress and plans of the meteorological component. *Bull. Amer. Meteor. Soc.*, **72**, 364-371.
- Uccellini, L. W., P. J. Kocin, R. A. Petersen, C. H. Wash, and K. F. Brill, 1984: The Presidents' Day cyclone of 18-19 February 1979: Synoptic overview and analysis of the subtropical jet streak influencing the pre-cyclogenetic period. *Mon. Wea. Rev.*, **112**, 31-55.
- Uccellini, L. W., D. Keyser, K. F. Brill, and C. H. Wash, 1985: The Presidents' Day cyclone of 18-19 February 1979: Influence of upstream trough amplification and associated tropopause folding on rapid cyclogenesis. *Mon. Wea. Rev.*, **113**, 962-988.
- Uccellini, L. W., 1986: The possible influence of upstream upper-level baroclinic processes on the development of the QE II storm. *Mon. Wea. Rev.*, **114**, 1019-1027.
- Wash, C. H., S. M. Heikkinen, C. Liou, and W. A. Nuss, 1990: A rapid cyclogenesis event during GALE IOP 9. *Mon. Wea. Rev.*, **118**, 375-391.
- Wernli, H., and H. C. Davies, 1997: A Lagrangian-based analysis of extratropical cyclones. I: The method and some applications. *Q. J. R. Meteorol. Soc.*, **123**, 467-489.
- Wernli, H., 1997: A Lagrangian-based analysis of extratropical cyclones. II: A detailed case study. *Q. J. R. Meteorol. Soc.*, **123**, 467-489.
- Wernli, H., S. Dirren, M.A. Liniger, and M. Zillig 2002: Dynamical aspects of the life cycle of the winter storm 'Lothar' (24–26 December 1999). *Q. J. R. Meteorol. Soc.*, **128**, 405-429.
- Whitaker, J. S., L. W. Uccellini, and K. F. Brill, 1988: A model-based diagnostic study of the rapid development phase of the Presidents' Day cyclone. *Mon. Wea. Rev.*, **116**, 2337-2364.
- Yau, M. K., and M. Jean, 1989: Synoptic aspects and physical processes in the rapidly intensifying cyclone of 6-8 March 1986. *Atmos. Ocean*, **27**, 59-86.

- Zhang, F., C. Snyder, and R. Rotunno, 2002: Mesoscale predictability of the "Surprise" snowstorm of 24–25 January 2000. *Mon. Wea. Rev.*, **130**, 1617-1632.
- Zishka, K. M., and P. J. Smith, 1980: The climatology of cyclones and anticyclones over North America and surrounding ocean environs for January and July, 1950–77. *Mon. Wea. Rev.*, **108**, 387-401.